Investigating Imaging Biomarkers of Neuroinflammation and Neurodegeneration in Rodent Models of Alzheimer's Disease

A thesis submitted to the University of Manchester for the degree of Doctor of Philosophy in the Faculty of Biology, Medicine and Health

2016

Aisling Chaney

School of Health Sciences

Table of Contents

List of Figures

List of Tables

List of abbreviations:

Aβ	Amyloid-beta
AchR	Acetylcholine receptor
AD	Alzheimer's disease
APP	Amyloid Precursor Protein
BP	Binding potential
^{11}C	Carbon-11
CC	Cingulate cortex
CD11b	Cluster of differentiation molecule 11B
CNS	Central nervous system
Cr	Creatine
CSF	Cerebrospinal fluid
Ctx	Cortex
EC	Entorhinal cortex
^{18}F	Flourine-18
FC	Frontal cortex
FDG	Flouro-deoxyglucose
FID	Free induction decay
GABA	γ-Aminobutyric acid
GFAP	Glial fibrillary acidic protein
Glu	Glutamate
Glx	Glutamate+glycine
GSH	Glutathione
GSI	γ secretase inhibitors
GSM	γ secretase modulators
^{1}H	Hydrogen proton
HAPCs	High amyloid pathology non-demented controls
HC	Hippocampus
Hypo	Hypothalamus
Iba1	Ionized calcium-binding adapter molecule 1
IL	Interleukin
LTP	Long term potenetiation

LPS	Lipopolysacharide
MAPs	Microtubule associated proteins
MC	Motor cortex
MCI	Mild cognitive impairment
mI	myo-Inositol
MRI	Magnetic resonance imaging
MRS	Magnetic resonance imaging
^{13}N	Nitrogen-13
NAA	N-acetylaspartate
NFT	Neurofibrillary tangle
NMR	Nucleur magnetic resonance
NOR	Novel object reconition
NSR	Novel smell recognition
^{15}O	Oxygen-15
PET	Positron emission tomography
PCr	Phosphocreatine
PiB	Pittsburgh compound B
PBR	Peripheral-type benzodiazepine receptor
ppm	Parts per million
PS	Presenilin
p-tau	Hyperphosphorylated tau
RF	Radiofrequency pulse
ROS	Reactive oxygen species
SUV	Standard uptake value
Str	Striatum
Taur	Taurine
TC	Temporal cortex
tCho	Total choline
TE	Echo time
TG	Transgenic
TH	Thalamus
TG_I	Transgenic infected
TG_NI	Transgenic non-infected

TNF	Tumor necrosis factor
TR	Repition time
TSPO	Translocator protein
VCAM-1	Vascular cellular adhesion molecule-1
WT	Wild type
WT_I	Wild type infected
WT_NI	Wild type non-infected
β^+	Positron
σ-1R	Sigma-1 receptor

Abstract

Submitted by Aisling Chaney to The University of Manchester for the for the degree of Doctor of Philosophy entitled "Investigating Imaging Biomarkers of Neuroinflammation and Neurodegeneration in Rodent Models of Alzheimer's Disease" 27/09/16

Alzheimer's disease (AD) is a progressive neurodegenerative disease resulting in alterations in memory, language, executive function and emotional behaviour. Although it can be characterised by symptoms, by the time they arise significant pathological alterations have already emerged in the central nervous system, namely increased amyloid plaques, neurofibrillary tangles and neuronal loss. Despite known pathological hallmarks the exact aetiology of AD is poorly understood and no current treatments are available. However, there is growing interest in the role of neuroinflammation in AD, with increases observed in the early stages of disease and with disease progression. Moreover, it has been suggested that peripheral inflammation can influence neuroinflammation and worsen neurodegeneration. Using Positron Emission Tomography (PET) and Magnetic Resonance Imaging (MRS) we can non-invasively measure biomarkers of neuroinflammation and degeneration allowing multi-modal investigation of its role in normal aging and AD.

Considering this the objectives of this study were to (i) Use PET and MRS to investigate neuroinflammatory and metabolite alterations in transgenic (TG) models of AD and their wildtype (WT) animals. (ii) Assess rates of cognitive decline in these models using memory based tests. (iii) Investigate relatively new TgF344AD rat as an AD model by characterising younger time-points than previously reported. (iv) Investigate the contribution of peripheral inflammation on AD progression.

PET and MRS imaging was carried out longitudinally in the APP_{swe}×$PS1_{de9}$ mouse. Neuroinflammation was confirmed *ex vivo* and cognitive ability was assessed by behavioural tests. Results revealed significantly increase hippocampal and thalamic neuoinflammation in old TG mice as assessed by [^{18}F]DPA-714 PET and supported by immunohistochemistry. Reduced neuronal marker N-acetlyaspartate was seen with age and was exacerbated in the TG mice. Accelerated cognitive decline was also seen in TG mice.

PET and MRS imaging was carried out at 6 and 12 months in the TgF344AD model, which expresses amyloid and tau pathology as well as neuronal loss. No cognitive decline was observed in TG rats; however increased anxiety behaviour was seen. Increased [^{18}F]DPA-714 PET was observed as an effect of gene in the thalamus at 6 months and the hypothalamus at 12 months. Increases in glutamate were seen with age in the TG rats but not the WTs. Increased inflammation and metabolite alterations were seen with aging.

The effect of peripheral urinary tract infection (UTI) on cognition and imaging out was assessed. Imaging was carried out prior to and after re-current UTI. Infection induced cognitive decline in infected TG but not WT rats. Infection had an increasing effect on hypothalamic neuroinflammation in WT rats but a decreasing effect on TG rats, which masked the original gene differences.

This thesis is set out in the alternative format with each experimental study represented as a chapter. Results in this thesis implicate neuroinflammation in AD development and progression. In addition, we report systemic infection-CNS interactions accelerating cognitive decline in AD and highlight the importance of understanding the effects of comorbidities in disease.

Declaration

No portion of the work referred to in the thesis has been submitted in support of an application for another degree or qualification of this or any other university or other institute of learning.

Copyright Statement

i. The author of this thesis (including any appendices and/or schedules to this thesis) owns certain copyright or related rights in it (the "Copyright") and s/he has given The University of Manchester certain rights to use such Copyright, including for administrative purposes.

ii. Copies of this thesis, either in full or in extracts and whether in hard or electronic copy, may be made **only** in accordance with the Copyright, Designs and Patents Act 1988 (as amended) and regulations issued under it or, where appropriate, in accordance with licensing agreements which the University has from time to time. This page must form part of any such copies made.

iii. The ownership of certain Copyright, patents, designs, trade marks and other intellectual property (the "Intellectual Property") and any reproductions of copyright works in the thesis, for example graphs and tables ("Reproductions"), which may be described in this thesis, may not be owned by the author and may be owned by third parties. Such Intellectual Property and Reproductions cannot and must not be made available for use without the prior written permission of the owner(s) of the relevant Intellectual Property and/or Reproductions.

iv. Further information on the conditions under which disclosure, publication and commercialisation of this thesis, the Copyright and any Intellectual Property University IP Policy (see http://documents.manchester.ac.uk/display.aspx?DocID=24420), in any relevant Thesis restriction declarations deposited in the University Library, The University Library's regulations (see http://www.library.manchester.ac.uk/about/regulations/) and in The University's policy on Presentation of Theses.

Acknowledgements

I would like to first and foremost thank my PhD supervisors Hervé Boutin, Steve Williams, Karl Herholz and my advisor Stuart Allan. If it wasn't for their support and understanding I would not have got this far in one piece. Thank you Hervé for calming me down and convincing me that "running off to the rainforest to be with the all the animals" probably isn't what it's cracked up to be and thank you Steve for putting up with me when jMRUI is acting the maggot and when my eyes start to glaze over when you talk about k space. Many thanks to graham who has helped me so much over the years and to all the radiochemistry people at WMIC, who were so professional and amazing you made my work a whole lot easier.

Karen Davies you have been my rock! Thanks you so much for the chats and laughs over the past few years. I don't think any MRI would happen without you around and if it did it'd be no craic. I would also like to thank, Duncan Forster, Alison Smigova and everyone else at the MRI lab, WMIC and the AV Hill. Duncan if I've learned anything from you it's that anything can be solved by a pint.

I would like to thank my friends Cathy, Colm, Cairns, Pritchard, Gav and Hil. You guys have made my free time albeit rare but amazing by providing emotional and alcoholic support in prosecco fuelled nights, expo lounge mornings and bento king evenings. I will never wall twerk and not think of you guys. I would also like to thanks my partner in crime Ian. You've really helped me through all of my degrees, put up with my moaning, stressing and occasional tears. Without you handing me food and coffee the last stretch of this PhD would not have been possible. I'm really looking forward to a life together that is thesis-free!

Finally, I would like to thank my family, mostly for putting up with my questionable decision to be a student for 9 years (sorry about that), but also for your constant support and understanding. I really appreciate the visits mainly to bring me Lyons tea and feed me. You're either really good at putting up with my skype moans or are really good at zoning them out. Either way, thank you.

Chapter 1. Introduction

1.1 Overview

Alzheimer's disease (AD) is the most common form of dementia, a group of debilitating and progressive neurodegenerative disorders, characterised by global deterioration of cognitive, intellectual and emotional function. Degeneration in AD typically begins in the basal forebrain and spreads to the hippocampus and then the rest of the cortex, producing clinical symptoms such as memory deficits, confusion and language difficulties. Dementia has become a grave international health problem with an estimated 46.8 million people with it worldwide (1). AD is the most common form of dementia representing approximately 60-70% of cases (2), and is the leading cause of dementia in the elderly. Currently, approximately 850,000 people in the UK live with dementia (1), costing the UK economy over £24 billion a year (3). The biggest risk factor for AD is age and as generations grow older the incidence of AD will continue to rise. It is estimated that over 1 million people in the UK will suffer from dementia by 2025 and 2 million by 2050 (1), causing a huge impact on families, society and the economy.

AD can be characterised by the pathological hallmarks extracellular amyloid beta (Aβ) plaques and intracellular hyper-phosphorylated tau neurofibrillary tangles (NFTs). However, the causative role of these hallmarks in disease development remains uncertain, and although their contribution is undoubted, it is clear that many other factors are involved in AD. It is increasingly recognised that inflammation plays an important role in the pathophysiology of AD (4-6), whether as cause or consequence is unclear, though recent genome-wide association studies point to the former (7). Inflammatory changes in the brain, such as microglial activation and increased cytokine expression, are seen post-mortem (8) and *in vivo* (9-11). However, with evidence of both beneficial and detrimental effects, the precise contribution of neuroinflammation to AD remains to be determined.

As a result of the idiopathic nature of AD, current treatment is restricted to symptomatic therapy that does not cure, prevent nor halt disease progression. Therefore, early diagnosis and management are essential. A huge unmet need exists to unravel the

mechanisms underlying AD and find robust non-invasive biomarkers, which can be exploited not only to aid the diagnosis and early detection of AD but also to develop new treatments and assess the efficacy of current and future therapies. As technology advances, more techniques emerge which can be utilised to help the risk-factors and pathophysiological mechanisms associated with AD, including inflammation. A major area that has had huge advances in the past few decades is the field of bio-medical imaging. Imaging provides a non-invasive method to obtain physiologically relevant information *in vivo* that can be used to better understand and diagnose many neurological disorders. Imaging permits a safe and translatable method of probing the mechanisms of AD and other diseases progression, and proves an indispensable tool at both a pre-clinical and clinical level. However, innovative multi-modal approaches are required to tackle this problem. Therefore the aim of this PhD is to investigate early markers of neuroinflammation and neurodegeneration in rodent models of AD.

This chapter will give an overview of AD and its known pathophysiology. It will also describe neuroinflammatory cells and their responses in health and disease, with a focus on the potential role of neuroinflammation and peripheral inflammation in AD progression. Modelling AD through rodent models of disease will also be covered. Finally, the principles behind the imaging methods positron emission tomography (PET) and magnetic resonance spectroscopy (MRS) and their contribution to AD research will be highlighted.

1.2 Alzheimer's Disease

AD is a progressive neurodegenerative disease associated with Aβ and NFT pathology. Regional and progressive neuropathological staging of Aβ plaques and NFTs in AD has been described by Braak and Braak (12). NFT pathology can be defined by 6 stages (I-VI), with stages I-II demonstrating NFT degeneration in transentorhinal cortex and the CA1 region of the hippocampus, stages III-IV see the progression of NFTs to the limbic areas including the amygdala, thalamus and the subiculum of the hippocampus, and in stages V-VI NFT pathology worsens in the mentioned areas and progresses to isocortical regions. Conversely, Aβ pathology begins in the isocortex. Aβ progression can be split into 3 stages (A-C). Stage A describes the development of plaques in the basal regions of the frontal, temporal and occipital cortices; stage B depicts the progression of plaques across the isocortex and hippocampus, with progression to subcortical regions. (12, 13).

Symptoms of AD typically manifesting over a period of years, with initial symptoms include short-term memory loss such as decline in factual and spatial memory, language difficulties such as finding the right words for objects, places or people, decline in executive functions such as decision making and planning, and changes in mood and behaviour such as increased anhedonia or irritability which may result in social withdrawal. These symptoms worsen as the disease progresses and additional symptoms such as loss of appetite, sleeping difficulties, altered perception and hallucinations may arise. AD is preceded by a prodromal phase known as mild cognitive impairment (MCI). People with MCI will not always progress to AD but all AD patients begin with MCI. Diagnosis of probable AD is dependent on clinical cognitive assessments and the presence of the amyloid pathology and reduced metabolism that can be assessed by PET imaging.

1.3 Neuropathological Hallmarks and Hypotheses in AD

The pathological hallmarks (Aβ plaques and NFTs) allow the characterization of AD and form the basis of the two main hypotheses, the amyloid hypothesis and the tau hypothesis. These have been a source of notable dispute within the scientific community and are still a matter of debate today.

1.3.1 Amyloid Pathology

Aβ plaques are a pathological hallmark of AD and an area of great controversy. They occur due to deposition of extracellular insoluble beta-amyloid, which is created upon dysfunction in Amyloid Precursor Protein (APP) processing. Many believe that Aβ is the trigger for AD with increased accumulation initiating inflammatory responses and causing neuronal death and cognitive decline. This is known as the amyloid hypothesis of AD and is associated with dysfunctional APP processing (14-16). Under normal conditions, APP is thought to be essential for neuronal survival including repair and growth, however when dysfunctional APP processing occurs a second pathway leads to the generation of a toxic form of APP. Enzymes called secretases fragment APP (Figure 1); α-secretase cleaves APP into APPsα and α-stub, which is fragmented further by γ-secretase to P3 a non-toxic neuroprotective protein. However, when β-secretase acts on APP it cleaves APPsβ and β-stub which is then fragmented by γ-secretase to $A\beta_{1-40}$ and $A\beta_{1-42}$, soluble and insoluble Aβ proteins respectively (17). These Aβ proteins are thought to be toxic and high levels can lead to detrimental effects. Insoluble $A\beta_{1-42}$ is sticky and can aggregate; therefore the formation of amyloid plaques is dependent on the ratio of $A\beta_{1-42}$ to $A\beta_{1-40}$.

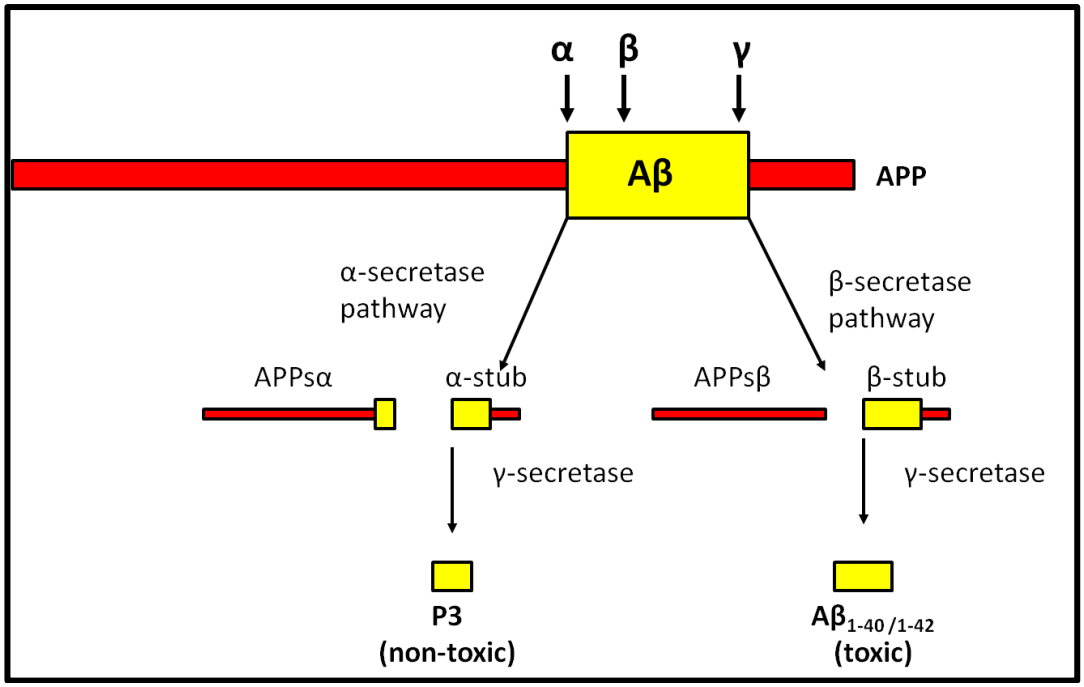

Figure 1 Schematic of APP Processing. APP processed via two pathways. Cleavage by α-, β- and γ-secretases leads to the production of either non-toxic P3 or toxic $A\beta_{1-40}$/$A\beta_{1-42}$. Adapted from Zhen *et al.* **(17)**

It was this plaque formation that was considered the driving force of the disease. In support of this theory, APP processing mutations, including mutations in the catalytic component of γ-secretases presenilin proteins (PS1 and 2), can also cause a predisposition to AD (14, 15). PS mutations are seen in inherited early onset AD. This early onset is known as familial AD (FAD) as it is associated with specific inheritable genetic mutations and constitutes approximately 5% of cases, whereas the other 95% are of idiopathic origin referred to as sporadic AD. FAD occurs before the age of 65 and can develop as early as 35, however sporadic AD occurs after the age of 65 and is thought to be of a more aggressive nature with faster disease progression (18). Although, the exact aetiology of these types may be different, they share the same symptoms and pathology such as Aβ plaques, NFTs and global neuronal loss; therefore investigation of inheritable forms of AD may help us gain a better understanding of this disease. Furthermore, transgenic rodent models of AD have been developed that express human APP, PS1 and PS2mutations and develop AD-like brain pathology (see section 1.7; animal models of AD). As amyloid plaques were considered the driving force behind AD this led to the idea of their removal and their elimination as the focus of much research. However, it is important to note that although plaques are found in neurodegenerative disorders they are also found in healthy

elderly populations as a consequence of normal aging, thereby suggesting that other mechanisms may be at play in AD aetiology and progression.

1.3.1.1 Vaccination studies and clinical trials

Vaccination studies were carried out in mice for active immunization against Aβ. Transgenic mice (Tg_{2576}) were injected with $A\beta_{1-42}$ plus adjuvant (19). This immunization was found not only to clear Aβ deposition in these mice but also ameliorated mild memory deficits. However, if treatment was disease modifying or not could not be confirmed as the model does not display neuronal death.

As a result of positive pre-clinical and safety studies a small-scale human phase I trial was carried out in a population of 24 AD patients. A single-dose of $A\beta_{42}$, named AN1792, was administered using adjuvant (QS21) to elicit an immunological response (20). No signs of intolerability were identified and AN1972 was assumed to be safe. A subsequent larger-scale trial was carried out in 74 patients using a multi-dose approach. Results were promising, immunization appeared to be well tolerated and good immune responses were reported in some patients (20). The apparent success of the first two Phase I trials led to the launch of a large international double-blind Phase IIa trial in October 2001 (21). This trial included 372 patients with probable AD from the USA and Europe who were randomly allocated to the placebo (72 patients) or AN1792 group (300 patients). The trial was to carry on for a year with immunization received at 1, 3, 6, 9, and 12 months and incorporated volumetric magnetic resonance imaging (MRI) and cognitive assessments. However, it had to be halted suddenly in January 2002 when symptoms of meningoencephalitis were reported in eighteen patients, all of which had received active immunization (21). Although administration was halted, follow-up on the patients was continued. A total of 59 out of the 300 responded to AN1792. These patients were positive for serum anti-AN1792 despite immunization being discontinued. Cognitive and disability tests did not reveal any significant improvement in responders compared to the placebo group. However, responders demonstrated a reduced decline in overall neuropsychological battery test scores, which included memory and learning tests. Furthermore, CSF tau was reduced in antibody responders (n=11) compared to placebo-administered patients.

However, it is important to note that these patients differed in CSF baseline from other responders and may not represent a reliable population sample (22). After this trial was discontinued, a report was published analysing post-mortem tissue of a 72 year old woman who passed away due to a pulmonary embolism a year after cessation of the trial (23). Post-mortem brain tissue was analysed and compared to that of non-immunized patients (n=7). Plaque deposition was significantly lower in the cingulate gyrus and temporal cortex of this immunized patient. Furthermore, phagocytic microglia were identified in areas with little or no plaques, and macrophage and leukocyte infiltration was also identified. It is important to note that the immunized case presented signs of meningoencephalitis and had uniform distribution of other non-AD related Aβ deposits (23). More recently a study by Serrano-Pozo *et al.* examined post-mortem hippocampal tissue of 5 patients immunized in the AN1792 Phase IIa trial and compared results with non-immunized AD patients and non-AD controls (24). Similar results were found with plaque density and neurite abnormalities decreased in immunized samples compared to non-immunized. Despite severe side effects in a group of patients in this trial, results displayed extensive amyloid plaque removal and indicated beneficial effects, however cognitive and long-term efficacy could not be assessed. Subsequent vaccines aimed to activate antibody responses that do not involve T cell activation but simply activate microglia to increase clearance of plaques. Passive immunization in AD mice models had shown positive results (25) and as a result a clinical trial involving Bapineuzumab, a passive antibody designed to attach to the N terminus of Aβ, was launched with the hope of amyloid clearance without T-cell activation and therefore avoiding the severe side effect of meningoencephalitis. Results were initially promising with an ascending dose trial with good tolerance and treatment completion rates (26). Interestingly, positive responses were identified in non-APOEε4 carrier patients who completed treatment. However, side effects were noted including oedema in approximately 10% of patients treated with Bapineuzumab. Furthermore, 18 month treatment revealed decreased amyloid plaque deposition compared to baseline and placebo treatment assessed by carbon-11-labelled Pittsburgh compound B (^{11}C-PIB) retention using positron emission tomography (PET) (27). However, 2 patients also demonstrated oedema. In August 2012 it was announced that Bapineuzumab would not progress any further. Many drugs are still in clinical trials including Solanezumab. However, further understanding of the molecular mechanisms of AD remains essential in the development of future efficacious treatments.

The amyloid hypothesis has been considered the most plausible, however therapeutics emerging as result of it have so far been unsuccessful. Moreover, accumulating evidence suggests that it is in fact the soluble form of Aβ that is the most toxic. Investigation of soluble Aβ has increased, perhaps as a result of the disappointing immunization results and a substantial body of evidence suggesting that plaque burden does not correlate with disease progression or severity (28, 29).

1.3.1.2 Soluble Amyloid

Soluble amyloid species also exist in AD. Recent evidence suggests that soluble Aβ may have a key role in the pathogenesis of AD and may be a more suitable biomarker of disease severity (30). A study by Lue *et al.* analysed entorhinal and frontal tissue of cognitively normal elderly controls, high amyloid pathology non-demented controls (HAPCs) and AD patients (31). Analysis revealed that HAPCs were not discriminated from AD patients using measures of insoluble Aβ, including plaque deposition, plaque deposition with and without cores or thioflavin fluorescent plaques. Although measures of insoluble Aβ could discriminate cognitively normal controls from HAPCs, soluble Aβ levels distinguished HAPCs from AD patients. Therefore, soluble amyloid load may be responsible for neurodegeneration in AD and may explain why plaque deposition is seen in normal aging without the presence of cognitive dysfunction and neurodegeneration. HAPCs displayed higher levels than cognitively normal controls, but levels were 80% lower than AD patients suggesting that soluble amyloid burden may be a good indicator of AD. Soluble amyloid has been shown to cause neurotoxic effects. Single intracerebroventricular injection of soluble oligomeric $A\beta_{25-35}$ in rats had detrimental AD-like effects on the brain (32). Six weeks after injection, cholinergic neuronal loss, hippocampal pyramidal loss, inflammation and memory deficits were evident. Furthermore, APP processing and tau phosphorylation were found to be altered after soluble Aβ injection, an effect which was not demonstrated upon scrambled-Aβ injection.

As studies have shown soluble Aβ to be neurotoxic, an obvious solution would be to reduce the concentration of soluble Aβ *in vivo*. A way of achieving this is through the use of γ-secretase modulators (GSMs). GSM-2 was found to selectively reduce soluble Aβ

in a 5month old Tg_{2576} mouse model of AD, with subsequent cognitive improvement (33). However, when plaques formed at a later stage in this model it appeared that GSM2 reduced soluble Aβ levels in 10 month old mice but not in 14 or 18month old. Further analysis revealed that in the oldest mice only newly formed soluble Aβ was reduced (34). The mechanisms behind this are not known. Nonetheless, cognitive function was improved at every age proving reducing soluble Aβ has beneficial effect.

GSMs and γ-secretase inhibitors (GSIs) are currently under investigation in clinical trials, however it is important to note that γ-secretase also cleaves many other proteins including Notch (35) and blocking its action could have adverse physiological effects. A phase III GSI clinical trial recently failed as it worsened cognitive decline. In addition, other neuronal dysfunction in the form of hyperactivity and calcium transients has been shown in neurons around plaques in animal models (36), however this is evident prior to plaque formation and therefore implicates soluble Aβ in its manifestation. Soluble Aβ appears to be associated with neuronal toxicity, dysfunction and cognitive decline and therefore its effect in the development of AD should be investigated further.

1.3.2 Tau Pathology

NFTs are another pathological hallmark of AD. They are constructed of aggregated hyper-phosphorylated tau protein which pairs with other threads of tau forming paired helical filaments. Tau is one of three microtubule associated proteins (MAPs) and exists in 6 isoforms in the human brain. Its main function is to bind to tubulin and promote the formation of microtubules. Microtubules are essential elements of the cytoskeleton necessary for maintaining structure and permitting transport. Under physiological conditions tau stabilises microtubules allowing normal neuronal function to occur, however when abnormal hyper-phosphorylated tau (ptau) occurs as in AD and other tauopathies, it inhibits microtubule formation (37). It has been suggested that a number of damaging factors act together to cause the phosphorylation of tau. These include Aβ oligomers, oxygen free radicals and iron overload. It is hypothesized that over time these factors cause hyperphosphorylation in tau resulting in NFTs and degeneration (Figure 2) (38). Furthermore, it has also been suggested that upon neuronal death the hyper-

phosphorylated tau is released from cell bodies and causes further damage by promoting microglial activation and release of pro-inflammatory mediators such as TNFα, IL-6 and IL-1β (38) . In addition, abnormal tau sequesters normal tau and other MAPs resulting in the collapse of the neuronal transport system. It is this damage that is thought to cause neurodegeneration with loss of function ensuing. The tau hypothesis encompasses the idea that abnormal tau protein is the main contributor to the disease cascade. In support of this, tau in AD brains have been found to be 3-4 times more phosphorylated than tau found in healthy brains. NFTs have been identified in the entorhinal cortex of normal aging brains, however in AD NFTs seem to appear in the entorhinal cortex and spread to the hippocampus and cortex, correlating with the pattern of neurodegeneration (39, 40). NFT load correlates better with cognitive decline and disease severity than Aβ load (41) and CSF tau has been found to increase from healthy elderly controls to MCI patients and from MCI patients to probable AD patients (42). Furthermore, MCI patients scoring higher in the clinical dementia rating scale exhibited higher tau levels than lower scoring MCI patients, suggesting that this measurement of tau is a reliable marker of cognitive dysfunction. Hampel *et al.* found cerebrospinal fluid (CSF) tau to correlate to hippocampal atrophy in 22 probable AD patients independent of disease severity and duration, suggesting that tau may not be a marker of disease severity but could be used to track hippocampal degeneration in AD. No effect was seen with total tau levels indicating that the atrophy is not a result of an overall change in tau levels but is specific to hyper-phosphorylation (43).

Abnormal tau NFTs are thought to be toxic to neurons, however as with amyloid, more recent studies have suggested that soluble p-tau is the cause of neurotoxicity (44). A mouse model expressing transgenic tau which could be supressed upon doxycycline administration was created by Santacruz *et al.* (45). Cognitive function and NFT load was assessed in this model before and after tau suppression. Cognitive function declined in these transgenic mice by 2.5 months, which was shown to be tau-dependent. Doxycycline administration reversed this effect and tau pathology did not progress. However, when doxycycline was given to 4 month old mice it improved cognitive function and stopped neuronal loss but did not stop the accumulation of NFTs, suggesting that NFTs are not sufficient to cause cognitive dysfunction and neuronal death. Another mechanism must be at play, perhaps the action of neurotoxic soluble forms of tau. A follow-up study using this model found the presence of two tau dimers (140 and 170 kDa) suggested to be made of

two 55kDa Tau or two 64kDa P-Tau proteins respectively (46). These tau species were found in the soluble and insoluble fractions, although the 140kDa was predominantly found in the soluble fraction whereas the 170kDa species was predominantly found in the insoluble fraction. Interestingly, the 170kDa form presented a strong AT8 immunoreactivity, known to detect hyper-phosporylated and pathogenic P-Tau, whereas the 140kDa specie did not. Overall this suggested that the 170kDa dimers come from larger hyper-phosphorylated and pathological aggregates. A significant correlation was identified between the levels of P-Tau 64kDa and 140/170kDa species in the insoluble fraction and cognitive decline in this model and another model of tauopathy (JNPL3). Considering these and the previous result from Santacruz *et al.*, the authors hypothesized that tau may be most toxic when it is in intermediate sized aggregates consisting of the smaller multimers. Furthermore, tau140 was found to be present early in disease and at low levels prior to cognitive dysfunction suggesting that a clinical threshold may exist leading to memory impairment.

On the other hand, uncertainties remain whether tau dysfunction directly leads to neurodegeneration in AD. Tau mutations found on chromosome 17 are associated with frontotemporal dementia and parkinsonism (FTD-17) (47), however no direct tau-associated genetic link has been made to AD. This supports the idea of Aβ being the driving force of AD. Although Aβ burden can be observed in normal subjects, Aβ pathology contributes to Tau hyperphosphorylation and it is appears to be Tau that cause the neuronal loss. Therefore there is a trigger than causes Aβ to become pathological and cause Tauopathy in some subjects but not others. Nonetheless, preventing mutant tau aggregation has shown beneficial effects and the role of tau in neurodegeneration should be investigated further.

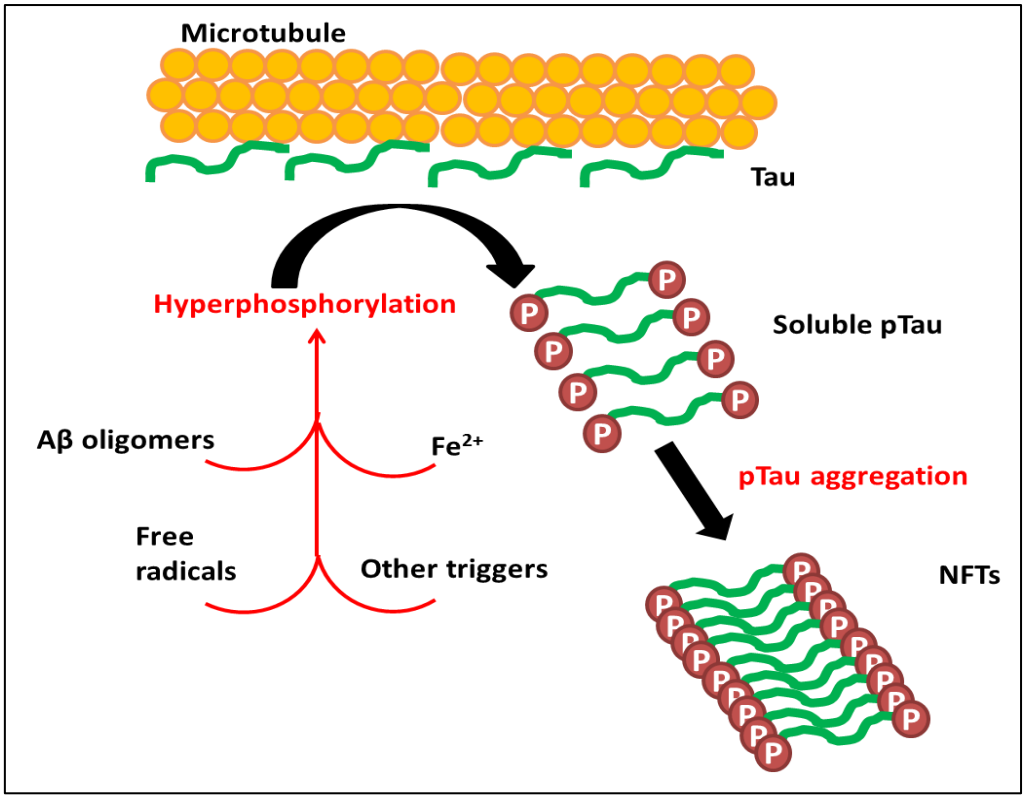

Figure 2 Neurofibrillary tangle formation.

1.4 Neurotransmitter Dysfunction

Neurotransmitter dysfunction is also heavily reported in AD, with the cholinergic system thought to be the worst affected. The cholinergic hypothesis suggests that the cognitive dysfunction that occurs in AD is a direct result of loss of cholinergic neurons to key areas. Cholinergic neurons are targeted early on in the disease starting at the basal forebrain and spreading up to the hippocampus causing severe neuronal loss in language and memory areas. Acetylcholine is an essential neurotransmitter in the brain and has a major role in regions associated with memory and learning such as the hippocampus. This region is also targeted early in AD. In addition, it has been reported that there is an interaction between acetylcholine receptors (AChR) and Aβ. It has been suggested that the α7 AChR which is found in the hippocampus binds Aβ and may cause different levels of toxic effects depending on the different amyloid aggregates in interacts with (48). This led to the idea of cholinesterase inhibitors as therapeutics agents in AD. Galantamine, a reversible cholinesterase inhibitor was shown to significantly attenuate cognitive and global dysfunction in AD patients after 6 months administration in comparison to placebo (49). This effect remained evident after 12 months without adverse effects. However, these patients were suffering from mild to moderate dementia and although enhancing cholinergic function can improve cognitive function in these cases, no evidence suggests it presents any beneficial effects in severe cases or importantly that it delays disease progression.

Glutamate (Glu) dysfunction has also been reported in AD with disruption causing adverse effects including excitotoxicity. Excitotoxicity has been implicated in many neurological disorders and is thought to be a key contributing factor in neurodegeneration (50). Excitotoxicity occurs as a result of excessive and/or persistent neuronal release of excitatory amino acids, namely Glu. This causes over-activation of Glu receptors, which can cause ATP-dependent Glu transporters to act in reverse. This further increases Glu levels, altering calcium concentrations and leads to the activation of various enzymes resulting in neuronal dysfunction, oxidative stress and apoptosis. Mitochondrial dysfunction, defined as impaired electron transfer, is associated with excitotoxicity and oxidative stress and has also been implicated in dementia (51). Oxidative stress occurs due to an imbalance between the production of reactive oxygen species (ROS) and the

antioxidant defences, causing damage to lipids, proteins and DNA. Most ROS formation occurs during various biological processes particularly mitochondrial energy production, and is necessary for many physiological mechanisms such as cellular responses and signal transduction (52). The ability to produce energy in the form of ATP comes as a result of the electron transport chain, consisting of five enzymatic complexes on the inner mitochondrial membrane. Although this is an essential process, it results in the production of ROS such as superoxide (O_2·-) and hydrogen peroxide (H_2O_2). Disturbance to any of the five complexes can compromise the function of the electron transport chain causing oxidative damage (53).

The sigma-1 receptor (σ-1R) has been shown to modulate some of the major neurotransmitter systems of the CNS including cholinergic and glutamatergic. Furthermore, the σ-1 system has been linked to memory and cognition with σ-1 ligands acting as powerful anti-amnesiacs (54). Reduced receptor density has been reported in hippocampal tissue and prefrontal, temporal and occipital lobes of AD patients (55) and selective σ-1R ligands have been shown to attenuate memory deficits observed in mice models of AD and protective against amyloid toxicity (56, 57). Marrazzo *et al.* found that selective σ-1R compounds PRE-084 and (–)MR-22 could block Aβ-induced neuronal death in cultured cortical rat neurons. This effect was significantly inhibited by σ-1R antagonist NE-100, but it did not affect Aβ-induced damage alone. Interestingly, donepezil another acetylcholinesterase inhibitor also binds to the σ-1R. Moreover, a σ-1R antagonist (BD1047) can inhibit its protective action (58), indicating that donepezil's neuroprotective action works through the σ-1R. Moreover, when donepezil was administered alongside Aβ, memory impairments that would manifest with Aβ alone did not become apparent. These results support the involvement of the neurotransmitter dysfunction in AD symptom and pathology development.

More recently, GABA abnormalities have been highlighted in AD, with GABA dysfunction demonstrated by a reduction in GABAergic neurons (59) and altered levels in an AD transgenic model (60). Therefore, assessing neurotransmitter levels with disease progression and their effect on other aspects of disease is of great importance in AD research.

Accumulating evidence suggests oxidative stress, mitochondrial dysfunction and excitotoxicity play a contributing role in the pathophysiology of AD. Neurotransmitter dysfunction seems to be implicated in these problems and should therefore be investigated as targets for progression and therapeutic intervention.

1.5 Neuroinflammation in AD

1.5.1 Microglia

For many years the central nervous system (CNS) was considered an immuno-privileged organ; however we now know this is not the case. Microglia are the resident immune cells of the CNS. They constitute approximately 10% of cells in the nervous system and play a key role in surveillance of the brain (61). They typically exist in a ramified state monitoring the brains environment, however in response to certain stimuli they can become activated and morphologically change into an amoeboid-like state. In this state there is an up-regulation of cytokines and chemokines, of which some can be cytotoxic. Microglia are the first line of defence and this activation is necessary for removal of infections, microorganisms and debris.

Neuroinflammation is increasingly linked to many neurological disorders and much evidence supports its involvement in AD. Under physiological conditions microglia are neuroprotective, having a key role in phagocytosis and neurotrophin release, their activation is implicit to maintaining a healthy brain environment. However, upon activation they also produce pro-inflammatory cytokines, particularly interleukin-1α (IL-1α), interleukin-1β (IL-1β) and tumor necrosis factor-α (TNF-α) resulting in an inflammatory response (62). IL-1α and TNF-α cause the up-regulation of cell adhesion molecules on microglia such as intracellular adhesion molecule-1, vascular cell adhesion molecule-1 and leucocyte functional antigen-1. Activated microglia also synthesise proteolytic enzymes such as Cathepsin B causing destruction to the extracellular matrix and neuronal dysfunction (63). Normally inflammation resolves itself and contributes to the healing process, but sometimes this is not the case and it can become chronic (pathologic and self-sustaining) inflammation. Excessive amount of excitotoxins such as glutamate can also be released. Therefore, if prolonged (i.e. chronic) activation occurs it can have detrimental effects on brain function due to excessive or persistent release of cytotoxic factors. This persistent over-activation has been implicated in many neurodegenerative disorders including AD.

In AD a link to neuroinflammation is supported by the observation that activated microglia surround amyloid plaques in AD pathology (64). Traditionally, microglia were assumed to be either in a pro- or anti-inflammatory state, however recent evidence suggests that their activation is not as simplistic. Microglial activation has proven to be an intricate and complex mechanism triggered by multiple environmental stimuli and it is more likely that there is a continuum of functional states possible depending on environment (61, 62, 65). Whether microglial cells are a contributing factor to disease progression in AD or can actually be beneficial in AD is still a matter of great debate. Nonetheless, much evidence implicates microglia activation and inflammation in AD pathophysiolology and investigation into their role in AD is essential.

Microglia activation is thought to be initiated by Aβ and tau species, and seems to be a key underlying pathological mechanism of AD. Although the mechanism remains elusive, results consistently suggest Aβ causes an inflammatory response. It has been reported that pre-fibrillar $A\beta_{1\text{-}42}$ is more effective than fibrillar $A\beta_{1\text{-}42}$ at eliciting a TNF-α response *in vitro* (66). This early pre-fibrillar soluble $A\beta_{1\text{-}42}$ microglia activation suggests that there may be a specific time period prior to plaque formation that causes a large immune response. This supports evidence demonstrating that plaque formation is not the sole cause of AD and different Aβ species may produce varying microglial activation with their respective cytokine profiles.

1.5.1.1 Cytokines

Cytokines are small signalling proteins, which are synthesised and released by a number of cells including neurons, microglia, astrocytes and peripheral immune cells to elicit a response after insult or injury. These cytokines can be pro-inflammatory such as IL-1α, IL-1β and TNF-α, or anti-inflammatory such as IL-4, IL-10 and IL-13. In AD, activated microglia produce pro-inflammatory cytokines to promote cytotoxic and inflammatory responses. This is thought to be triggered through Aβ stimulation of nuclear factor kappa-B and subsequent mitogen-activated protein kinase and extracellular signal-regulated kinase pathways, which can regulate phosphorylation, secretase activity and apoptosis (67). Elevated pro-inflammatory cytokines and reduced anti-inflammatory

cytokines have been reported in the CNS and periphery of AD patients (68, 69). This further supports the role of inflammation in AD and suggests that a balance between pro- and anti-inflammatory cytokines may be needed to prevent neuronal damage and disease.

IL-1 is a considered a major contributor to the immune response in AD. With increased serum levels of both IL-1α and IL-1β reported in both AD and MCI patients (70). Blocking IL-1 receptors has been shown to improve water maze and contextual fear conditioning test performance in a triple transgenic mouse model displaying Aβ and tau neuropathology, suggesting that IL-1 could be a major contributor to cognitive deficits seen in AD (71). Furthermore, other pro-inflammatory cytokines were significantly reduced and tau and amyloid pathology were significantly and mildly affected respectively, suggesting a major modulatory role of IL-1. Mice with increased levels of IL-1β and S100B (a calcium binding protein indicative of astrocyte activation (72)) have shown exacerbated damage in response to intracerebroventricular injection of human $A\beta_{1-42}$ (73) suggesting that baseline neuroinflammation may also have a role in disease development. IL-1 has also been shown to increase acetylcholinesterase activity, emphasising its detrimental effects. In addition, it forms a feedback loop increasing microglial activation and eliciting further IL-1 production. Similarly, TNF-α is another pro-inflammatory cytokine with a major role in the inflammatory process. Like IL-1, TNF-α is also produced by glia and promotes further release of pro-inflammatory cytokines exacerbating the inflammatory response(69). Hence, initiating a vicious cycle of cytokine release, microglial recruitment and activation causing extensive neurodegeneration can occur as a result of cytokine action and resulting damage signals sent from neurons (Figure 3).

It is important to note that cytokines are not purely deleterious but are thought to be expressed in low concentration in the healthy brain where they have roles in normal functioning. Cytokine receptors are found in the hippocampus where they appear to play a role in memory formation. Evidence suggests that IL-1β influences memory (74), its receptors are found in the hippocampus where it also has a role in synaptic plasticity (75). Long-term potentiation (LTP), an important process in synaptic plasticity and memory consolidation, upregulates IL-1β messenger ribonucleic acid. Furthermore, application of

IL-1 receptor antagonist impairs LTP. Therefore at the right levels cytokines can be beneficial. On the other hand, a recent study by Chakrabarty *et al.* found that anti-inflammatory cytokine IL-4 increased plaque load in in mice (76). This may be viewed as an exacerbation of plaque burden due to decreased microglial clearance as has been suggested by the authors, however it does not necessarily increase the severity of the disease as shown by previous plaque burden correlation studies. It is likely that appropriate levels of cytokines are beneficial but alterations in their levels may result in dysfunction.

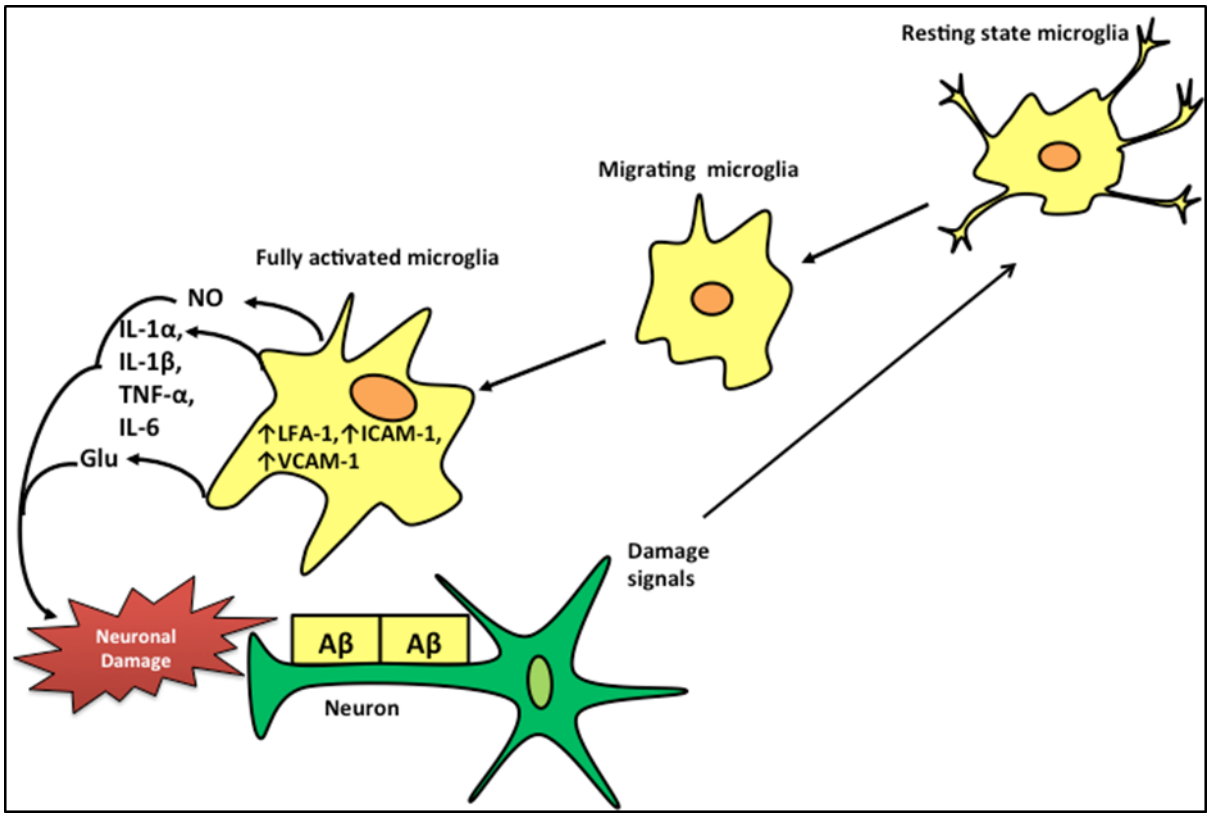

Figure 3 Summary of microglia activation and cytokine release in AD

1.5.2 Astrocytes and Astrogliosis

Astrocytes are the most abundant glial cell in the brain and were originally thought to be merely the structural support cells of the CNS (77). However, in recent years it has emerged that astrocytes play a crucial role in neuronal survival. In addition to structurally stabilising neurons, astrocytes have been shown to communicate with the vasculature, release neurotrophic factors such as growth hormones and like microglia they respond to

injury by morphological changes and upregulation of cytokines and chemokines (78). They provide metabolic support during periods of increased neuronal activity by converting glucose into lactate for neuronal use and store energy in the form of glycogen. Astrocytes and neurons are involved in the glutamate-glutamine cycle, a mechanism allowing the replenishment of Glu independent of the Krebs' cycle. Astrocytes express excitatory amino acid transporters allowing the influx of Glu after release from neurons. Glu is then converted to glutamine via glutamine synthase and is stored in the astrocytes acting as an inactive reservoir of Glu. This is an important and crucial mechanism as it prevents the over-activation of Glu receptors and hence helps prevent excitotoxicity, another major contributor to degeneration (79). Astrocytes have also been shown to uptake other molecules such as GABA, lysine and taurine emphasizing their role in glial-neuronal transmission. Furthermore, astrocytes are a source of glutathione (GSH) for neurons (80, 81). GSH is the most prevalent anti-oxidant in the brain. It is a tripeptide crucial for the prevention of damage caused by circulating reactive oxygen and nitrogen species, hence preventing oxidative stress and excitotoxicity. It depletion has been associated with many neurological disorders and has been suggested as a novel therapeutic target (82). Astrocytes also have other beneficial functions, which contribute to brain homeostasis, such as extracellular potassium buffering, mediation of brain pH and provide communication between cells and blood flow (77). Therefore, impairments to the functioning of astrocytes could be detrimental to neuronal survival.

Astrocyte modifications are known to occur in AD, which could contribute to neurotransmitter dysfunction, oxidative stress and neuronal death. Astrogliosis is accepted to be triggered by Aβ and has been identified in both human tissue (83) and animal models of AD (84, 85). Interestingly, hippocampal tissue of a triple transgenic mouse model of AD revealed astrocyte atrophy from 6 months of age, a stage prior to plaque accumulation which may account for some of the early symptoms of AD. However, upon plaque formation (between 12 and 18 months) astrocytic hypertrophy was identified in astrocytes surrounding plaque cores with significantly larger surface areas and volumes than those not encompassing plaques (84). This result is somewhat in contradiction to the previous studies reporting overall astrogliosis in AD; however it does support Aβ causing astrogliosis and suggests that astrocyte behaviour is more complex and may be of a site- and stage-specific nature. Furthermore, these astroctyes that have undergone astrogliosis

have been shown to help clear plaque deposition, demonstrated by intracellular accumulation of Aβ and neuronal debris, which is absent in the atrophic astrocytes (86). This has been demonstrated within the entorhinal cortex of AD brains and has also shown that astroctyes can undergo lysis producing astrocytic plaques (83). In addition to causing gliosis, Aβ deposition has also been found to elicit calcium responses in astrocytes. Cultured astrocytes from rat cortices were shown to induce intracellular calcium transients and spontaneous intercellular calcium waves upon Aβ treatment (85), indicating that Aβ has a direct effect on astrocyte function. Calcium is a signalling molecule and can have a variety of effects in many pathophysiological mechanisms including glutamate release and transmission and may cause further neuronal damage.

Astrogliosis around senile plaques seems to be a pathophysiological characteristic of AD and may represent a contribution to neurotransmitter dysfunction and oxidative stress. Moreover, as gliosis appears to occur subsequent to plaque deposition, it has the potential to be used as a biomarker for AD diagnosis.

1.6 Peripheral Inflammation and AD

More recently, there is a growing body of evidence suggesting that peripheral infection and inflammation can influence neuroinflammation, and that this can affect the progression of neurodegenerative diseases including AD. The pro-inflammatory changes induced in microglia seen in neurodegenerative diseases have been termed "microglia priming". This refers to the state in which microglia are more likely to exhibit exaggerated responses to further stimuli after previously been innervated by pathology such as Aβ and tau species (87). Therefore in the presence of neurodegeneration, subsequent infection may result in exacerbated and maladaptive neuroinflammation leading to more rapid neurodegeneration and disease progression. In fact many pre-existing comorbidities that are considered risk factors for AD are known to increase basal systemic inflammation, including obesity, diabetes and heart disease (88-91). In support of this, it has been shown that AD patients that experienced 1 or more systemic infection event (e.g. respiratory infection) had increased TNF-α levels and accelerated cognitive decline compared to AD patients without systemic infection events over a 6 month time period (6). Basal TNF-α levels also affected cognitive decline, with higher initial levels causing a 4 fold increased rate of cognitive decline compared to those with low basal TNF-α levels, suggesting that both systemic inflammatory events and basal TNF-α levels can negatively affect cognitive ability in AD patients. Systemic infections in AD patients have shown increased serum levels of IL-β, which were shown to associated with accelerated cognitive decline (92). In addition, long-term treatment with non-steroidal anti-inflammatories, particularly ibuprofen, has been found to reduce the risk of AD onset (93). It may be that the pathology already present in neurodegenerative diseases such as AD and its associated neuroinflammation described previously may be intensified upon peripheral stimulation, leading to increased disease progression and severity. It has been shown that multiple forms of systemic infection can stimulate new neurodegenerative pathology or exacerbate existing neurodegeneration (94). It has been suggested that some aspect of neurodegeneration in AD or AD pathology itself may prime microglia for a more exacerbated response to further infection. Increased inflammatory markers have also been reported in MCI patients and were even able to discriminate between MCI subtypes (95). More recently Bu et al demonstrated that serum positivity for bacterial and viral infections more prevalent in AD and were significantly associated with higher levels of serum $A\beta_{40}$,

$A\beta_{42}$ and total Aβ, further supporting the role of peripheral immune system-CNS communication in neurodegenerative disease development (96). Overall infectious burden from common infections including chlamydia pneumoniae, Helicobacter pylori, cytomegalovirus and herpes simplex viruses 1 and 2 were also found to be associated with memory decline in a stroke-free population (97).

In parallel to human findings, peripheral inflammation such as lipopolysaccharide (LPS) injection (98, 99), polyinosinic-polycytidylic acid injection (100) or pulmonary infection (101) has been shown to worsen neuroinflammation, pathology and cognitive performance in mouse models of disease. Mc Manus *et al.* assessed the effect of respiratory infection on young (4 months) and older (10 months) $APP_{swe}\times PS1_{\Delta e9}$ mice (101). Significant pathology emerges at 6 months in this model therefore the effect of pre- and post- pathology could be investigated. Respiratory infection resulted in increased peripheral cell infiltration, neuroinflammation and amyloid pathology in the old APP×PS1 mice compared to non-infected old TGs and both WTs infected and non-infected. The increased microglial and astroglial activation and amyloid plaque deposition seen in older APP×PS1 mice was significantly exacerbated in the cortex and hippocampus of infected APP×PS1 mice, as was soluble amyloid levels, indicating that peripheral infection in older mice with existing pathology can have a negative effect on disease severity.

Overall it is evident that there is interplay between peripheral inflammation and neuroinflammation which has a significant role in AD progression, however little is known about the exact contribution. Therefore more research is warranted in this field.

1.7 Animal Models of AD

Animal models of AD are used in fundamental research to investigate specific mechanisms and pathways, and to gain a better understanding of the disease as a whole. Although no model can fully represent the human condition, their use in pre-clinical research is essential. Every model has both advantages and limitations, and knowing these allows for correct interpretation and translation of results.

The most common types of AD models *in vivo* are genetically modified murine models, which express known human mutations present in early onset AD. Mutations in APP and its processing have been identified in early onset AD, therefore mouse models have been developed which express these mutations. Moreover, models have been developed that can express multiple mutations. Both APP and PS1 mutations can be expressed in the same mouse leading to amyloid pathology that is not seen with single mutations. Importantly, these double transgenic (TG) mice generate AD-like pathology, including amyloid plaques, increased inflammation and progressive cognitive decline. Some of the most widely used AD TG models and the emergence of pathology and cognitive decline are summarised in Table 1. These models differ in the age of onset of AD-like pathology and cognitive decline, and in the rate of disease progression. Therefore, it is implicit to understand AD development in a chosen model to construct an appropriate experimental design. The PDAPP mouse is one of the early models of AD and expresses a single APP_{V717F} mutation leading to the development of amyloid pathology by 6 months of age (102) and cognitive deficits appearing from 4 months of age (103). Other single APP mutations have also been used. For example, the APP23 mouse has the $APP_{K670M/N671L}$ mutation, also known as the Swedish mutation on a C57BL/6 background and develops sparse Aβ plaques by 6 months, which increase with age (104). This results in cognitive deficits visible by 3 months of age in the Y maze (103). However, when this mutation is on a different background strain as in the TG_{2576} mouse (B6 mixed background) amyloid pathology does not appear until 9 months of age (105). Moreover, the APPl/s mouse has this same Swedish mutation with an additional London mutation (APP_{717l}) and develops amyloid pathology from 3 months of age (106), making it a more attractive model to investigate AD-like pathology in a shorter time-frame. Similarly, double APP and PS1 mutation mice are used to generate mice that develop pathology at an earlier age. For example the APP_{swe}×$PS1_{\Delta e9}$ mouse is a popular TG AD model that displays high $A\beta_{42}$ levels (107), progressive amyloid deposition from 4 months of age and

cerebral amyloid angiopathy (108). Similarly the TASTPM mouse model expressing the $APP_{KM594/5NL}$ and $PS1_{M146V}$ mutations develops Aβ pathology by 3 months of age and cognitive deficits by 6 months of age (109). These animal models are valuable in the investigation of the role of amyloid in AD; however a major problem with these models is the lack of tau pathology and neuronal loss. As of yet, no tau mutation has been linked to AD, hence tau mutations present in frontotemporal dementia are expressed in TG mice to investigate the role of tau in neurodegeneration as seen in the triple transgenic (3xTG) mouse model. The 3xTG mouse model incorporates the amyloid mutant APP (K670N/M671L), PSN mutant (PS1M146V) and tau mutant (TauP301L) and develops amyloid pathology, tauopathy and increased neuroinflammation (110). It is important to note that as no tau mutation has been identified in human AD, using this model to investigate the mechanisms of disease development may not truly represent the clinical tauopathy observed in clinical AD.

Strain	Species	Mutation	Cognitive deficits	Deficit Type	Aβ pathology	Tau pathology
PDAPP	Mouse	APP_{V717F}	4months	Reference /working memory	6months	N/A
APPl/s	Mouse	$APP_{K670M/N671L, V717l}$	5months	Recognition memory	3months	N/A
APP23	Mouse	$APP_{K670M/N671L}$	3months	Working memory	6months	N/A
TG_{2576}	Mouse	$APP_{K670N,M671L}$	3months	Working memory	9months	N/A
TASTPM	Mouse	$APP_{KM594/5NL}$ $PS1_{M146V}$	6months	Object recognition	3months	N/A
APP_{swe}×$PS1_{\Delta e9}$	Mouse	$APP_{KM594/5NL}$, $PS1_{\Delta e9}$	6months	Reference /working memory	4months	N/A
3×TG	Mouse	$APP_{K670N/M671L}$ $PS1_{M146V}$ Tau_{P301L}	3months	Reference /working memory	6months	12months
McGill-R-Thy1-APP	Rat	$APP_{K670N/M671L}$ APP_{V717F}	3months	Reference /working memory	6months	N/A
TgF344AD	Rat	$APP_{KM594/5NL}$, $PS1_{\Delta e9}$	15months	Reference /working memory	6months (soluble) 16months (plaques)	6months (soluble) 16months (tangles)

Table 1 Summary of commonly used transgenic animal models and the emergence of their pathology and cognitive decline.

.

Until recently only mouse models were available, but in recent years multiple rat models have been generated. The early genetic rats generated by Echeverria *et al.* using the single Swedish and Indiana mutations or a double mutant with an additional PS1 mutation on a Wistar background were not ideal as they only precipitated inter-neuronal amyloid deposition and no Aβ plaques were formed (111). An increase in tau kinase activity was observed in the hippocampus but no tau pathology was reported. Folkesson *et al*. developed a rat model with the APP_{swe} mutation, with increased exctracellular Aβ depositions but they were sparse and diffuse (112). Flood *et al.* later developed a rat model that developed Aβ-like plaques however only some developed dense cores which was found to be related to low levels of soluble Aβ. The McGill-R-Thy1-APP transgenic rat model developed by Leon *et al.* has shown great promise (113). This model expresses human AβPP751 and displays full amyloid pathology with Aβ accumulation evident by 1 week postnatal, significant cognitive impairments and extracellular plaques by 6 months. Another rat model has been developed by *Cohen et al.*, this TG model (TgF344-AD) expresses a double amyloid mutation (APP_{swe}×$PS1_{\Delta e9}$), yet develops amyloid pathology, tauopathy, reactive gliosis, neuronal loss and cognitive decline (114). This is the only model that encompasses the full range of AD-like pathology as a result of amyloid mutation alone, and highlights the importance of this protein and its pathways in the manifestation of AD. Increased soluble Aβ, Aβ plaques, interneuronal Aβ and CAA is observed in this model with age. Moreover the soluble Aβ oligomers were significantly increased compared to those found in the PSAPP mouse with the same constructs and were seen to be abundant prior to plaque formation at 6 months. With the APP and PS1 mutation this model not only develops amyloid pathology but also develops age dependent increases in p-tau that aggregate in to structures resembling NFTS with subsequent neuronal loss. Age-dependent increases in neuroinflammation arise from 6 months, which is in parallel to increased soluble amyloid and tau pathology, further supporting the role of neuroinflammation in the early stages of disease development. In addition, TgF344-AD rats have many advantages over traditional mouse models of AD. For example as it only uses AD relevant mutations it may be argued that it more accurately models the human case. Moreover, there are many experimental advantages in using rat TG models than mouse, including larger brain size, which is particularly relevant in imaging allowing for better anatomical localisation and resolution, and potentially richer behavioural displays permitting more accurate cognitive assessment. Therefore these models may reveal

findings not previously possible with mice models of AD. On the other hand pathology and cognitive decline emerge early in the mouse models due to decreased lifespan. This is advantageous in research as it allow the investigation of more studies quicker and cheaper.

When using animal models it is important to note that many differences exist between murine models and the human condition. Fundamental physiological, pharmacological, anatomical and genetic differences exist between animal models and humans, resulting in limitations in the translation from bench to bedside. A prime example of low translatability would be in the amyloid immunization studies. Positive effects of clearance were seen in animal models and no adverse effects were noted (19, 25). However, severe side effects or lack of efficacy were observed in human patients causing cessation of several trials (20). Furthermore, the heterogeneity of human AD is vast with varying clinical history, age of onset and severity. The factors above cannot be replicated in animal models of AD and controversy exists over their use being of clinical relevance. Moreover, approximately 95% of AD is idiopathic and current animal models utilise known genetic mutations in APP and PSs, accounting for less than 5% of cases. On the other hand, it can be argued that animal models have provided us with important information on the pathophysiology of many diseases that would not have been generated using any other method, and will continue to do so in the coming years. However, the development and use of improved pre-clinical animal models is essential in elucidating unknown pathways and mechanisms.

1.8 Positron Emission Tomography Principles

PET is a powerful 3-dimensional functional imaging technique that allows the visualization of biological processes and can measure blood flow, metabolism (glucose, protein) and receptor density and their localization *in vivo*. However, the anatomical capabilities of this imaging modality are lacking in comparison with computed tomography and MRI. PET can therefore be used in conjunction with these imaging modalities, resulting in highly detailed images containing both anatomical and functional information. PET involves the production of positron (β+) emitting radionuclides such as ^{11}C, ^{13}N, ^{15}O, ^{18}F, which are utilised to radiolabel many compounds and ligands without modifying their properties. Tracking of these radiolabelled compounds through the body allows early detection of functional abnormalities prior to anatomical changes, such as degeneration or disease.

1.8.1 Annihilation and Detection

Radionuclides emit particles as a result of an unstable amount of protons and neutrons. Emission of β+ occurs due to excess protons in the outer shell and results in the conversion of a proton to a neutron while also releasing a neutrino and can be described as follows where p is proton, n is neutron and v is neutrino (115);

$$p = n + \beta^{+} + v$$

Within a tissue the β+ will only travel a few millimetres undergoing deflections from atomic electrons. It will slow down when its energy decreases and will collide with an electron forming positronium. A β+ is the anti-particle of an electron and when they collide they create pure energy in the form of two anti-parallel 511KeV γ rays in a process known as annihilation (Figure 4a). These rays are capable of penetrating the tissue and can be detected by the PET scanner through coincidence detection. When the γ rays hit the detectors the events can be restricted to certain line of response (LOR). Multiple events

will occur allowing the origin of the event to be located. Coincidence is acquired using a time frame window where the two rays are detected within certain thresholds. This coincidence can be true, random and scattered (Figure 4b). True coincidence is when the rays are detected without interacting with the surrounding matter and represent a true LOR. However, a scattered coincidence can occur due to a process known as Compton scattering. This occurs when one of the rays interacts with a lower energy atom transferring an amount of energy to it and causing it to eject an electron. The γ ray will continue and be detected creating a false LOR with a lower energy. Random events can also be paired to give a false LOR. This occurs when two independent events occur and hit the detectors within the given time window. In addition the energy can be absorbed by the tissue and not reach the detectors thereby reducing signal and sensitivity, this is the attenuation. True coincidence detection is the only data that gives accurate information on the localization of the events, therefore it is implicit that attenuation, scatter coincidence and random coincidence are considered by applying the appropriate correction. A computed tomography (CT) scan of the region of interest can be carried out to create and attenuation map of the tissue being investigated. CT attenuation coefficients are applied to the raw PET data to generate a more accurate image essential for quantification.

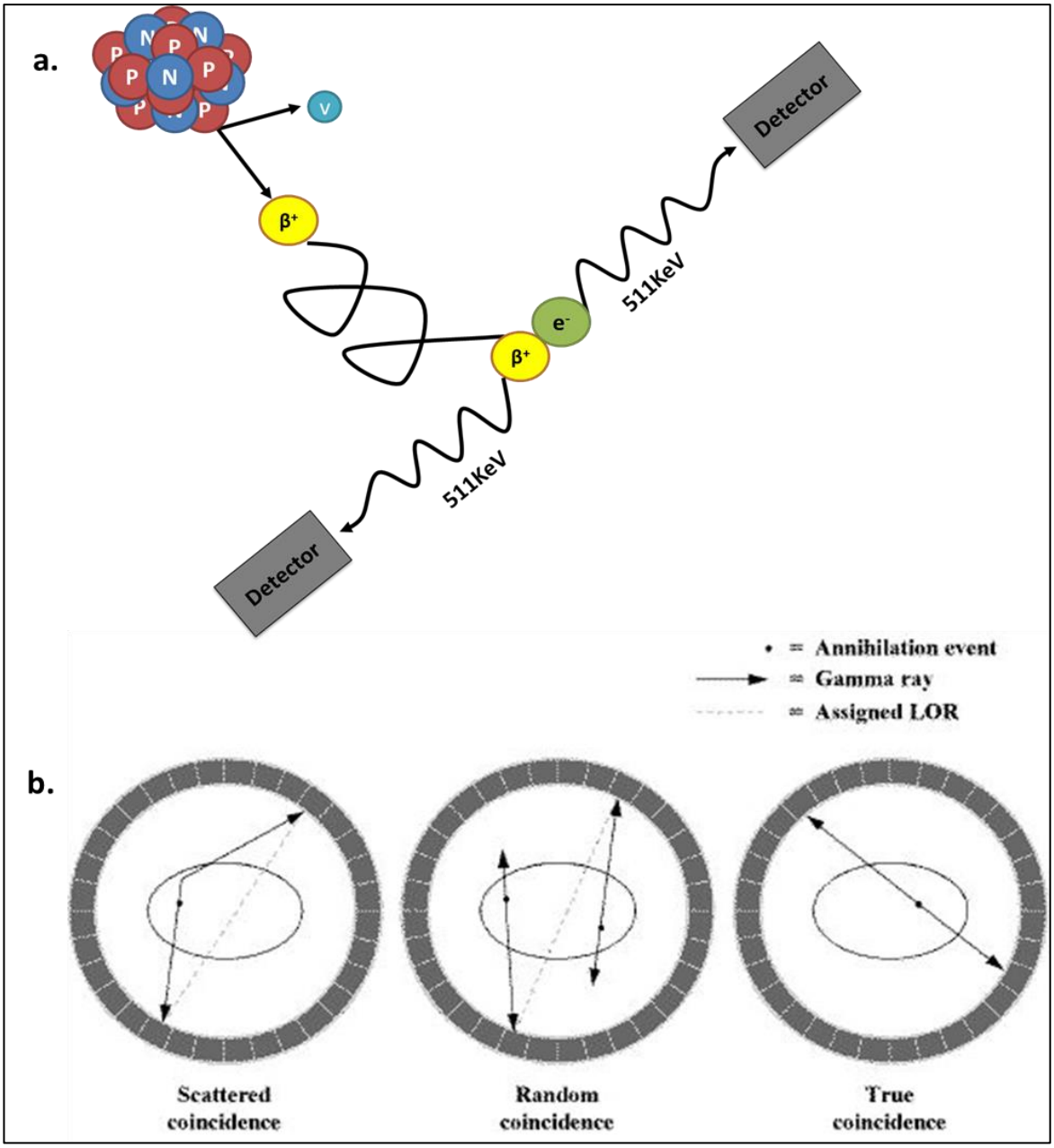

Figure 4 Schematic of positron annihilation (a) and different types of coincidence detection (b). Pictures adapted and sourced from *http://depts.washington.edu/nucmed/IRL/pet_intro/intro_src/section2.html*

1.8.2 Radiotracer half-life and production

Radioisotopes are generated via a cyclotron, which accelerates a proton and shoots it into a target gas to generate a radioactive isotope. Positron emitting isotopes can label a large number of compounds by replacing the C, N, O or F with the radioactive version. Once the compound of interest is labelled a small quanitity is injected into the subject and the annihilation events are detected and converted to a PET image. The small amount of tracer used is what makes PET safe. These radiolabelled molecules will interact with their targets *in vivo* allowing the quantification of the PET signal by referencing the binding potential (BP) or standard uptake value (SUV) in the region of interest (ROI).

The release of β^+ is termed as radioactive decay which decreases with time. This will occur randomly in a sample; however the general rate of decay is dependent on the half-life ($t_{1/2}$) of the isotope. The half-life is defined as the time it takes for the sample to decay to half of its original activity and is unique to different isotopes. This activity at a given time (A_t) can be described mathematically as follows and is related to the decay constant (λ), where A_0 is the activity at time 0.

$$A_t = A_0 e^{-\lambda t}$$

The decay constant is related to the half-life of a radionuclide as follows;

$$\lambda = \frac{0.693}{t_{1/2}}$$

^{11}C and ^{18}F are the most commonly used radionuclides. The $t_{1/2}$ of ^{11}C is approximately 20 minutes and ^{18}F is 110 minutes. A lower $t_{1/2}$ means that the radioactivity decays faster and is measureable for a shorter period of time restricting experimental times and design therefore radionuclides with a longer $t_{1/2}$ are preferred when possible, making ^{18}F a more sought after nuclide to introduce.

PET imaging in AD PET imaging can be used to investigate various biomarkers in AD including glucose metabolism, amyloid plaques and neuroinflammation.

1.9 PET in AD

PET can be used to asses various biological markers in AD including glucose metabolism, amyloid pathology and neuroinflammation. This section will briefly describe glucose and amyloid imaging and give a detailed description neuroinflammation imaging including the rationale of its use and a summary of pre-clinical and clinical findings.

1.10 [^{18}F]fluoro-2-deoxy-D-glucose (FDG) Imaging

In AD multiple fundamental processes are affected such as metabolism in the form of glucose consumption. The most common PET radioligand is [^{18}F]FDG, a glucose analogue, which can be used to analyse glucose metabolism throughout the body, including the CNS. It is highly used in oncology and has also been used to identify AD in the brain as a reduction in cerebral glucose metabolism is typically observed in human AD (116), whereas reports in animal models of AD are inconsistent with increased, decreased and similar levels of FDG uptake observed (117-121). A multi-centre study demonstrated 93% sensitivity and specificity in the identification of mild to moderate probable AD from normal aging in a large cohort using FDG PET (122). Furthermore, areas of reduced metabolism associated with normal aging and those associated with AD did not overlap greatly, and impairments in glucose metabolism were found to be proportional to dementia severity. However, it can be argued that reduced glucose metabolism is a feature of many neurological diseases. It is seen in other forms of dementia and although the regions of change may be indicative of AD it may not be specific to it. Therefore, FDG PET may be a good indicator of clinical dementia but is not sufficient for definitive diagnosis.

1.11 Amyloid imaging

PET is also used to image amyloid *in vivo*. Much effort has been focused on this area and a substantial amount of radioligands that identify Aβ have been developed including ^{18}F-Florbetapir (also known as AV-45) (123, 124), [^{18}F]Florbetapen (125), [^{18}F]FDDNP and PiB. PiB is currently the most commonly used tracer for Aβ. Successful identification of probable AD patients has been demonstrated using this compound (126) with increased retention evident in frontal, cortical, parietal, occipital and striatal regions (127). However, identification of patients with MCI appears more difficult. Forsberg *et al.* found no significant difference in PiB retention between MCI patients and healthy controls (128), but MCI patients that went on to develop AD revealed higher retention than both non-converters and healthy controls. This indicates that a high PiB retention may predict progression to AD. Conversely, PiB retention was not found to correlate with plaque load in a TG APP×PS1 (APP Tg2576 (K670N/M671L) mice crossed with M146L PS1 mice) mouse model (129). Extremely low retention was observed despite histology revealing extensive amyloid deposition. This result highlights the uncertainty of PiB's binding characteristics. Other issues with amyloid imaging include non-specific white matter retention, the inability to visualise individual plaques and that amyloid imaging is not sufficient for AD diagnosis (130). Amyloid deposition is not related to cognitive function and is therefore not indicative of symptom severity. It is important to note that amyloid plaques are present in normal aging and looking at soluble amyloid may provide further information. In fact, a clear obstacle in the field of amyloid imaging is that current tracers do not distinguish between soluble and insoluble Aβ. It could also be argued that imaging plaques is not an effective way of tracking AD progression, as in addition to it not correlating well to severity, by the time of high deposition the sensitivity of the technique may become low. Specific imaging of tau may correlate better to disease severity, as has been the case with *in vitro* measurements, however no accurate method currently exists. More sophisticated PET radiotracers must be developed in order to tackle these problems. However, amyloid imaging is beneficial in the assessment of efficacy of drugs which aim to clear Aβ deposition (27), and is an important technique to be used alongside other methods which aid diagnosis.

1.12 Neuroinflammation Imaging

Amyloid and tau deposition are well characterised in both human AD and in mouse models of disease, however the pattern of neuroinflammation remains elusive. This could be partially attributed to the fact that investigating neuroinflammation *in vivo* has proven difficult. However, with the use of PET imaging, quantification of microglial activation *in vivo* has been available for some time. The translocator protein (TSPO) is used as a target for neuroinflammation tracers and has been around for some years. Here I will describe the biology of TSPO and pre-clinical and clinical findings using TSPO PET.

1.12.1 The Translocator Protein (TSPO)

TSPO, formerly known as the peripheral-type benzodiazepine receptor, is an 18kDa protein located on outer mitochondrial membranes. This protein is involved in the synthesis of neurosteroids and cholesterol transport (131). TSPO is highly expressed in the periphery but expression in a healthy human brain is low and restricted to mainly to glia (132). Moreover, evidence suggests that this protein is involved in neuronal survival and neuroinflammation, and has been associated with the neuropathology of many disorders including AD (133). TSPO is expressed on microglia and is up-regulated upon microglial activation suggesting that it may play a role in microglial response and hence a role in the modulation of neuroinflammation. A rat model of neuronal degeneration involving quinolinic acid injection, which stimulates N-methyl-D-aspartate receptors and results in excitotoxicity, neuronal death and neuroinflammation, has been used to demonstrate increased microglial and astrocytic TSPO expression (134, 135). These studies have also shown that TSPO agonists exert neuroprotective effects. N-[(2r)-Butan-2-Yl]-1-(2-Chlorophenyl)-N-Methylisoquinoline-3-Carboxamide (PK11195), a TSPO antagonist, has been shown to decrease the degree of microglial activation, reduce pro-inflammatory mediators IL-1β, TNFα and IL-6, and reduce oxidative lipid and deoxyribonucleic acid damage (134). However, application of PK11195 did not alleviate astrocytic reactivity, suggesting that TSPO may selectively modulate microglia activation. Neuroprotective effects have also been shown with other TSPO ligands in the latter model of degeneration (135), a model of motor-neuron degeneration (136) and a model of kainic acid induced neuronal loss (137) demonstrating a reproducible therapeutic effect. Moreover, Ro5-4864

another TSPO ligand has been shown to ameliorate pathology in a 3xTG mouse model of AD. Repeated Ro5-4864 injection resulted in reduced Aβ pathology, neuroinflammation as well as improved working memory in this model (138).

Upon microglial activation, TSPO undergoes several changes including increased expression and polymerization leading to the formation of possible multiple binding sites (132). Further investigation needs to be put into understanding the significance of its multiple binding sites, as their functions remain unclear and represent a major problem preventing therapeutic and diagnostic exploitation. However, TSPO remains a promising target representing a modulatory system that links neurotransmitter dysfunction, excitotoxicity and inflammation, all of which appear to be crucial processes in AD pathophysiology.

This specific upregulation of TSPO on microglial can be exploited to image neuroinflammation *in vivo*. Radiotracers have been developed that allow the introduction of radionuclides onto TSPO ligands. As levels are low in healthy brains but appear to be elevated during microglial activation, it's expression may be a good indicator of inflammation severity and hence has been a viable target to image neuroinflammation using PET.

1.12.2 TSPO PET in Clinical AD

PK11195, a potent TSPO antagonist, has been ^{11}C-labelled for use in PET and has shown good correlation to microglial activation (139-141) with increased PK11195 binding correlating with increased CD68 staining in human AD tissue (141). Increased [^{11}C]PK11195 binding has been shown in AD patients *in vivo* (9, 10, 142). A study by Edison *et al.* investigated [^{11}C]PK11195 uptake in 13 AD patients and found increased uptake in areas associated with AD pathology including striatum, frontal, occipital, temporal and parietal regions as well as the anterior and posterior cingulate and whole cortex (10) compared to healthy controls. However, no significant increases in PK11195 uptake were identified in the hippocampus. [^{11}C]PiB imaging to assess amyloid load was also carried out to assess amyloid plaque levels in these subjects. PiB uptake also increased in AD in all areas including the hippocampus and thalamus. In addition, an inverse correlation was observed between PK11195 uptake and MMSE scores, implicating neuroinflammation in cognitive function and disease severity. No such correlation was found with PiB uptake. Similarly, Yokokura *et al.* found that PK11195 binding was significantly increased in AD patients in medial frontal and parietal cortex and left temporal cortex (142). A negative correlation was also identified in MMSE scores and left regions of the brain including the hippocampus, ACC, precuneus and MFC. However no correlations were identified between PiB and PK11195 uptake. In contrast, other studies have found that PK11195 was not increased in AD or MCI patients compared to controls (143, 144). Schuitemaker *et al.* reported no significant differences in PK11195 uptake between AD or amnesic MCI patients and healthy subjects using an ROI approach (144). Furthermore no correlation was found between cognitive scores and PK11195 uptake. However, small clusters of increased binding were observed within the parietal lobe of AD patients but not in prodromal or healthy participants, suggesting that inflammation in AD may be a highly conserved process with subtle increases. Wiley *et al.* reported that AD patients displayed a two fold increase in PiB retention compared to control subjects in regions associated with amyloid pathology but no differences in PK11195 retention was observed between any diagnostic groups or within PiB positive or negative groups and no correlation was found with PK11195 uptake in amyloid rich areas (143). MCI also appears to be hard to distinguish from healthy controls, with reports of increased (145) and unchanged PK1195 uptake and no correlation of PK11195 or PiB uptake with cognitive scores (143). A recent review by Hommet *et al.* evaluated 6 studies which investigated the

link between neuroinflammation and amyloid load by either [^{11}C]PK11195 or [^{11}C] C-deuterium-L-deprenyl (DED) (binds to monoamine oxidase B in astrocytes) and PiB PET in AD and came to the same conclusions (146). There was no correlation between PK11195 and PiB, however there was a correlation in the one study that looked at [^{11}C]DED and PiB suggesting that astrocyte activation may be directly related to plaque load but microglial activation may work independently via a different mechanism such as through soluble Aβ or tau as previously discussed. In contrast, a more recent follow up study by Fan *et al.* investigating [^{11}C]PK11195, [^{11}C]PiB, and [^{18}F]FDG uptake as well as correlations between these at a voxel level in AD patients and healthy controls showed that [^{11}C]PK11195 uptake was positively correlated with amyloid load and negatively correlated with glucose metabolism in the AD cohort (147). In addition, the regions with increased [^{11}C]PK11195 uptake at baseline differed from the regions affected upon follow up, which is line with the theory that neuroinflammation can change with disease progression.

Overall there are contradictory results in terms of neuroinflammation in AD patients *in vivo* using PET. However this could be down to the difficulties with its use. Although PK11195 is currently the most widely used TSPO tracer there are many limitations to its use due to its high non-specific binding, leading to a poor signal to noise ratio and modelling issues (148, 149). Considering this, [^{11}C]PK11195 is not an ideal tracer and makes it difficult to detect subtle inflammatory changes, hence the need to develop more sensitive tracers is essential. Much effort has been put into this and many second generation tracers have been developed that possess higher affinities than [^{11}C]PK11195 such as [^{18}F]-FEPPA (150) [^{11}C]DAA1106 (151), [^{11}C]DPA-713 (152), [^{18}F]DPA-714 (153-155), [^{18}F]GE-180 (156, 157) and [^{11}C]PBR28 (158, 159). However, the identification of multiple binding sites on TSPO for these 2nd generation tracer has somehow limited a more generic use of these TSPO radio-ligands. This was first identified when [^{11}C]PBR28 ligand was tested in 12 human subjects (159). Two of these subjects did not display any specific binding and a high variability in signal was evident between subjects. It was later discovered that these differences in binding characteristics were due to the TSPO polymorphisms (rs6971) (160) leading to the TSPO binding site being either of high affinity or low affinity (161), with subjects displaying high affinity, low affinity or both high and low affinity alleles resulting in a mixed affinity. Therefore, genotyping is

essential for the quantification of TSPO using these new ligands. Kriesl *et al.* investigated TSPO binding in AD, MCI and control subjects using PBR28 and observed a significant increase in PBR28 uptake in AD patients compared to MCI and control subjects in cortical regions including prefrontal, inferior parietal, superior, medial and inferior temporal and occipital regions (162). When subjects were stratified by genotype into high and mixed affinity, uptake was increased in the parietal cortex in high affinity AD patients compared to both high affinity MCI and healthy subjects. Whereas, mixed affinity AD patients had a significant increase in uptake compared to healthy subjects but only a trend towards significance was reached compared to MCI patients. No differences were found between MCI and healthy subjects, suggesting that increased inflammation is a specific characteristic in the progression of MCI to AD. Yasuno *et al.* investigated [^{11}C]DAA1106 binding in AD, MCI and healthy subjects with a five year follow up (163). Mean BP values were significantly increased in AD and MCI patients in all regions including prefrontal, parietal and occipital regions as well as the cingulate cortex, striatum and thalamus, but no significant differences in BPs were identified between MCI and AD patients. No correlation was found between psychological scores and BP values in any region. The five-year follow up revealed that all the MCI patients that had significantly increased [^{11}C]DAA1106 uptake compared to controls developed dementia. This result further supports the role of microglial activation in the manifestation of AD and proves TSPO imaging useful in tracking AD progression.

Although there are contradictory results from TSPO imaging and correlations with PK11195 uptake and cognitive ability, further investigation into TSPO as a marker for neuroinflammation and its role in AD development is needed. Furthermore, as increased TSPO binding was found in the majority of studies and no association was found with PiB uptake it suggests that neuroinflammation may work independently of Aβ plaque load and have an earlier role to play in the disease. Development of and correlation with better tau and soluble amyloid tracers may help to resolve this.

1.12.3 TSPO PET in Pre-clinical Models of AD

[^{11}C]PK11195 imaging has also been carried out pre-clinically in mouse models of AD. Rapic *et al.* have shown [^{11}C]PK11195 uptake to be significantly increased in the whole brain as well as the cortex, hippocampus and cerebellum of 15 months old APP_{swe}×$PS1_{\Delta e9}$ mice compared to WT, however this did not remain significant after multiple comparisons (164). Although increased microglia activation around amyloid plaques was demonstrated by immunohistochemistry in the TG mice by 12.5 months, no difference in [^{11}C]PK11195 PET was evident at 13 months of age. Therefore this tracer may not be sensitive enough to pick up subtle microglial changes in this mouse model of AD. Hence [^{11}C]PK11195 may not be an ideal tracer investigating inflammation in AD pre-clinically. In contrast, Venneti *et al.* found increased PK11195 binding in the same mouse model at 16-19 months but not at the earlier age of 13-16 months (141). This coincided with increases in Iba-1 staining in 16-19 months but not in 13-16 months, suggesting that PK11195 can detect increases in microglial activation in contrast to Rapic *et al.* However, this could be at least partly explained by the broader age gap in the time-points.

The TSPO polymorphism does not occur in animals and therefore new tracers with improved kinetics and affinities can be used pre-clinically to investigate microglial activation. Pre-clinical use of PET has many advantages over its use in a clinical research setting including confirmation of results by *ex vivo* means and correlation with other *ex vivo* modalities (e.g histology, immunohistochemistry). This can be exploited to explore the relationship between AD pathology and neuroinflammation. Increased [^{18}F]GE-180 uptake (a novel TSPO tracer (156)) was found in the hippocampus of 26 month old APP_{swe}×$PS1_{\Delta e9}$ mice compared to wildtype (WT) mice and young 4 month old TG mice, demonstrating that both normal aging and disease have an effect on microglial activation (165). These results were supported by increased GE-180 binding in *ex vivo* autoradiography and increased TSPO immunoreactivity, reinforcing its use as a good TSPO tracer *in vivo*. Similarly, increased uptake of an alternative TSPO tracer, [^{18}F]PBR06, was observed *in vivo* in the cortex and hippocampus of APPl/s mice compared to WT mice at 16 months of age, which was supported by *ex vivo* autoradiography and CD68 staining (166). However, *ex vivo* analysis revealed that there

was also an increase in [^{18}F]PBR06 uptake and CD68 staining at 9-10 months that was not detected using PET analysis *in vivo*. These results indicate that either [^{18}F]PBR06 or TSPO PET was not sensitive as a tracer or as a technique to pick up subtle neuroinflammatory changes earlier in disease. However it must be noted that investigations in mouse are limited by the spatial resolution of the scanner, which is a limitation of pre-clinical imaging however confirmation of results can be done *ex vivo*. Autoradiography has also been used to investigate the relationship between neuroinflammation and amyloid or tau pathology. Ji *et al.* looked at [^{18}F]FEDAA1106 uptake in brain slices of an amyloid (APP23 mouse) and tau (PS19 mouse) pathology model of AD (167). Increased [^{18}F]FEDAA1106 uptake was found in the hippocampus and entorhinal cortex of the amyloid model at 20 months and the tau model at 9 months of age. A co-localisation of GFAP and TSPO staining in close proximity to both Aβ pathology in the APP23 mouse was observed, however CD11b (cluster of differentiation molecule 11B; microglial marker) positive cells displayed very low levels of TSPO expression. The opposite was seen in the PS19 tau model, with TSPO co-localising well with CD11b positive cells but not with GFAP (glial fibrillary acidic protein; astrocyte marker) positive cells suggesting that tau and amyloid pathology may alter neuroinflammation status differently via activation of different glial cells. Increased [^{3H}]DAA1106 was also found *ex vivo* in the hippocampus and cortex of the P301S tau model as early as 3 months of age and prior to tau pathology becoming evident at 6 months in this model (168), reinforcing the role of neuroinflammation in the early stages of both tau and amyloid pathology manifestation.

Multiple tracer studies have been performed pre-clinically to investigate the relationship between neuroinflammation and other characteristics of disease. Sérriere *et al.* investigated amyloid and pathology and neuroinflammatory status in the APP_{swe}×$PS1_{\Delta e9}$ mouse model using [^{18}F]DPA-714 and [^{18}F]AV-45 (amyloid tracer) uptake at 6, 9, 12, 15 and 19 months of age. Increased [^{18}F]AV-45 binding was observed in TG mice as early as 9 months of age in the cortex but not until 19 months in the hippocampus (169). Increased [^{18}F]DPA-714 appeared after increased amyloid pathology at 12 and 19 months of age in the cortex and hippocampus respectively. There was a positive correlation between TSPO and amyloid imaging at the 19 months suggesting that as pathology progresses, neuroinflammation worsens. Furthermore, amyloid imaging correlated with glial immunoreactivity *ex vivo* and TSPO imaging correlated with amyloid staining *ex vivo*. In

contrast, Brendel *et al.* found increased neuroinflammation and metabolism in the PS2APP model prior to significant amyloid pathology in a triple tracer study using [^{18}F]GE-180, [^{18}F]FDG and [^{18}F]Florabetaben (117). A small but significant 9% increase in [^{18}F]GE-180 uptake was observed in the TG compared to WT mice at 5 months of age, which continued and reached a 25% increase by 16 months of age. A significant increase in [^{18}F]Florabetaben was not observed until 13 months of age indicating that a small increase in basal neuroinflammation may precede pathology development, which is exacerbated after significant plaque burden is observed. Increased [^{18}F]FDG occurred from 5 months and peaked at 13 months. A strong correlation was found between [^{18}F]GE-180 and [^{18}F]Florabetaben uptakes. This indicated that there is a relationship between neuroinflammation and plaque load and is in line with results found by Serriere *et al.* in the $APP_{swe}\times PS1_{\Delta e9}$ model. However, it does not explain the early spike in neuroinflammation, but it is possible that this could be initiated by soluble amyloid or another unknown mechanism.

TSPO and amyloid PET has also been used to assess treatment action. Maeda *et al.* used [^{18}F]FEDAA1106 and [^{11}C]PiB to assess the effects of anti-amyloid treatment in the APP23 mouse (170). Treatment with anti-Aβ antibody showed decreases in [^{11}C]PiB and increases in [^{18}F]FEDAA1106 uptake in the TG mice, indicating that the treatment successfully reduced amyloid burden and was associated with increased neuroinflammation. These types of studies can give insight in to the mechanisms of disease and support the role of pre-clinical PET imaging in neurodegenerative research.

Despite contradictory PET results being reported on whether neuroinflammation precedes amyloid pathology, IHC analysis *ex vivo* suggests that neuroinflammation occurs earlier than is detectable with current PET tracers. More longitudinal and multimodal studies with *ex vivo* and PET analysis in parallel are warranted to investigate this further. Nonetheless, it is evident that neuroinflammation has a role to play in AD and further research into this topic is needed to get a better understanding of the mechanisms of action and their contribution to AD.

1.13 Magnetic Resonance Principles

MRI is a sophisticated imaging technique based on the principles of nuclear magnetic resonance (NMR), which refers to the ability of certain nuclei in the presence of a magnetic field and subject to a radiofrequency pulse to couple with an external detector coil and induce a detectable electrical signal. This can be exploited in the body to create images using hydrogen protons (^{1}H) from water. NMR describes a phenomenon whereby certain nuclei possess a spin that in the presence of an applied magnetic field (B_0) will generate a small magnetic moment. These nuclei possess a spin due to an odd number of protons and neutrons, which in turn generates a small internal magnetic field called a magnetic moment (μ). In the presence of an applied B_0, μ will spin at an angular momentum (L) that is constant and depends on the unique gyromagnetic ratio (γ) of the nuclei (171).

$$\mu = \gamma L$$

In absence of B_0, these spins will point randomly in different directions, but in the presence of an applied B_0 these spins can be described as a quantum superposition of two energy states; parallel high energy and anti-parallel low energy states (Figure 5a). The probablility density distribution across an ensemble of spins will ensure that a slight majority will always be in the low energy state creating a net magnetization in the direction of the B_0. The protons also experience a torque under an applied B_0, which is relative to the magnetic field strength, where T is torque (172).

$$T = B_0 \times \mu$$

Under an applied torque the angular momentum can change, therefore the protons precess at a specific angular frequency dependent on B_0 strength. This is called the Larmor frequency (ω_0) and can be defined by the following equation;

$$\omega_0 = \gamma B_0$$

To elicit an MR signal, energy in the form of a radiofrequency (RF) pulse is applied at the Larmor frequency while in the presence of a magnetic field. The γ value for hydrogen is 42.65MHzT^{-1} (173), therefore for example at a field strength of 7 Telsa the Larmor frequency is approximately 300Hz. When this is applied the net magnetisation is tipped by 90° into a transverse plane. This 'transverse' magnetisation will start to precess about the B_0 field, inducing an electromagnetic field in the detector coil and generating an MR signal (174). This is known as the classical description of NMR, however quantum mechanics is needed to quantify the difference in energy states and describe the relationship between the spins and electromagnetic waves (172). In quantum mechanics the direction of L is defined by the spin angular momentum number (I), where h is Planck's constant (electromagnetic energy constant) (171).

$$\mu = \gamma L = \gamma \left(\frac{h}{2\pi}\right) I$$

I is ½ for protons and with an applied B_0 there exists 2I+1 values for I. Hence, there are only 2 energy states available for protons (±½). We can calculate the energy difference using the following equation;

$$\Delta E = \gamma \left(\frac{h}{2\pi}\right) B_0$$

The distribution into high and low energy states is determined by the field strength and sample temperature and is given by the Boltzmann equation;

$$\frac{Nhigh}{Nlow} = e^{\Delta E/\mathrm{kBT}}$$

where N_{high} and N_{low} are the numbers in the high and low energy levels, k_B is the Boltzmann constant and T is body temperature. The difference between the two energy states defines the net magnetisation. Nuclei possessing this characteristic include Hydrogen (^{1}H), Carbon-13 (^{13}C) and Phosphorus-31 (^{31}P). The net magnetization (M_0) is very small, with 4 extra protons in the anti-parallel direction for every 1 million protons (at 1.5T), however due to its abundance in the body in the form of water; ^{1}H can be used to generate a strong signal. The MR signal is created when this net magnetization is tipped into the transverse plane perpendicular to the B_0. This is done by applying a 90° RF pulse at Larmor frequency, creating a rotating magnetic field (B_1) in the transmit coil (Figure 5b). The nuclear magnetization M_0 will commence to precess about the B_1 field until the pulse is turned off. A 90^0 pulse is applied for long enough to rotate M_0 into the transvers plane. The subsequent precession of M_0 in the transverse plane creates a detectable voltage in the receiver coil, which only quantifies magnetization in this plane. When the RF pulse is turned off the magnetisation returns to equilibrium. This is known as relaxation and occurs in two forms; spin-lattice relaxation (T1) and spin-spin relaxation (T2) (Figure 5c-d). T1 relaxation is defined as the time that it takes for the longitudinal magnetisation (M_z) to return to equilibrium. This occurs due to energy loss from the protons to the surrounding tissue and results in return of the magnetisation to M_0. Whereas, T2 is defined as the process by which the transverse magnetisation (M_{xy}) decays. When proton spins interact with each other their magnetic moment affects the strength of the B_0 on the other protons. As protons interact with each other they begin to dephase and the signal diminishes. T1 decay occurs rapidly, whereas T2 relaxation takes a longer time. Therefore, T1 times for a given tissue are always longer than T2 times (Figure 5e). The MR signal is acquired as free induction decay (FID) as the protons quickly dephase and is converted to a spectrum via a Fourier transformation (Figure 6a).

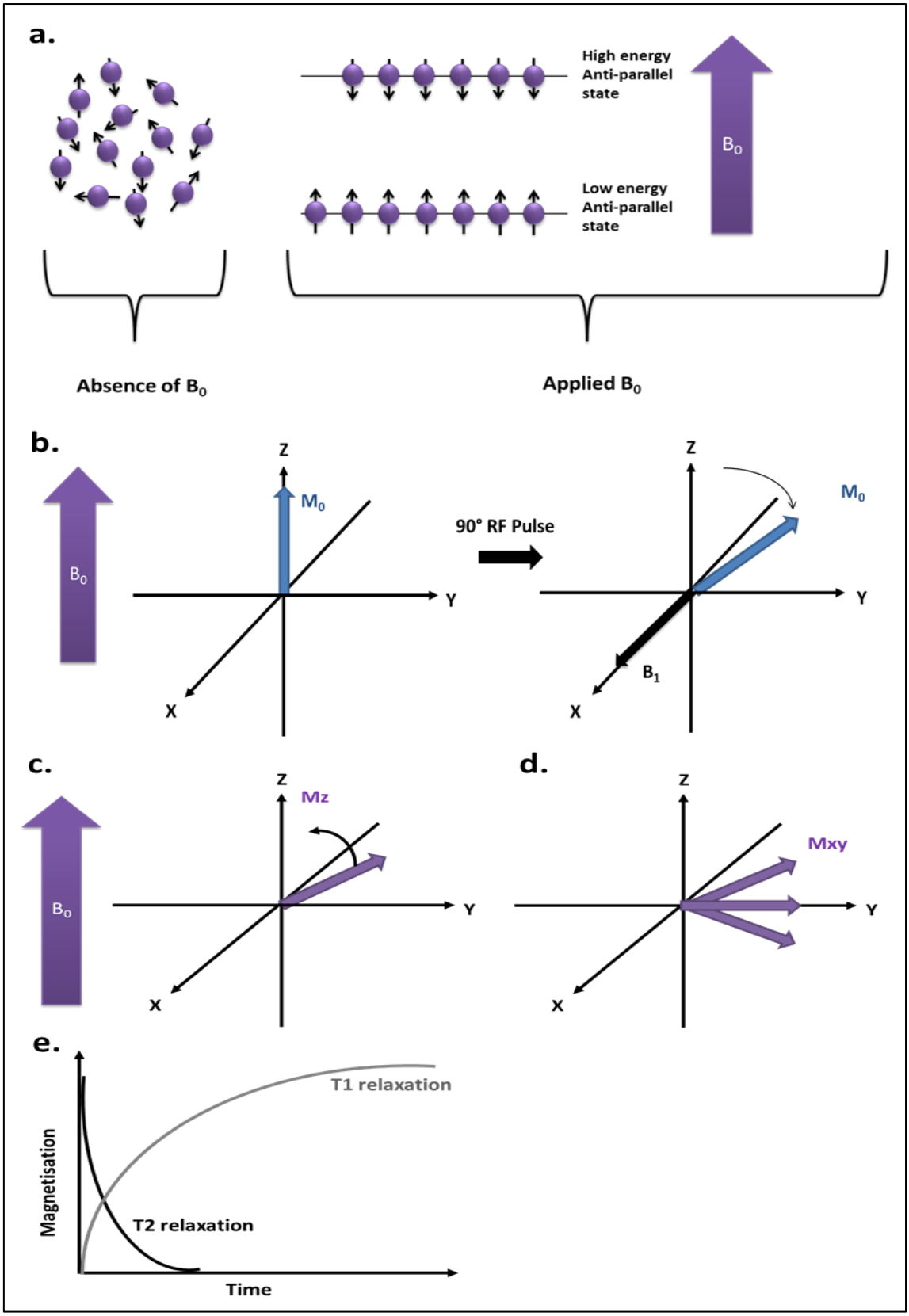

Figure 5 Behaviour of protons in the presence and absence of an applied magnetic field (B_0) **(a)**. Protons are split into low energy and high energy states in the presence of a B_0, creating a net magnetisation M_0 in the direction of the B_0. When the protons are hit with an RF pulse the M_0 is tilted **(b)**. When the RF pulse is turned off the magnetisation returns to equilibrium through T1 and T2 relaxation **(c-e)**. Illustration adapted from Mc Robbie (173).

1.14 MRS

Analysis of structural MRI images allows the quantification of various parameters including cerebral volume and has been used to aid diagnosis of many disorders including AD (175-177). However, it could be argued that by the time significant decline in the volume of some brain structure such as the hippocampus is observed in AD, it may be too late to improve prognosis as a substantial amount of damage has already occurred. Moreover, atrophy is due to neuronal degeneration, a characteristic present in all neurodegenerative disorders and hence not AD-specific. As a result other imaging modalities such as MRS are being utilized in AD research in the search for more specific abnormalities. MRS is also a non-invasive imaging method allowing the detection of subtle biochemical changes *in vivo*. It works on the same principles of MRI but exploits protons in metabolites rather than water, allowing the safe detection and identification of molecular changes prior to anatomical or disease manifestation. MRS can investigate small areas of the brain, allowing for direct analysis of specific anatomical regions. A three-dimensional pixel, called a voxel, is placed on a region of interest using a structural MR image. Spectroscopy is then carried out for this voxel only and produces a spectrum of metabolites that are detected in that region. Metabolites are represented as distinct peaks in a spectrum (Figure 6b). Every metabolite has a unique set of peaks due to the amount of ^{1}H atoms and their environment. The amplitude of the peaks will rise with increasing concentration, enabling quantification. This technique can be of particular importance as it allows the safe detection and identification of molecular dysfunction in affected areas during disease progression and prior to anatomical or disease manifestation.

1.14.1 Chemical Shift and Spin-Spin Coupling

The distinct peaks produced by metabolites are a result of the unique chemical environment of each proton within a molecule. This is described by two parameters known as the chemical shift and spin-spin coupling.. These parameters are fixed for each metabolite and are not affected by field strength.

If all nuclei resonated at the same frequency (Larmor frequency) we would not be able to resolve them. However the resonance frequency also depends on the chemical

environment of the nuclei resulting in a chemical shift. The chemical shift is the difference in resonance frequency of nuclei due to differences in molecular environments. The resonance frequency of a given metabolite is determined by the shielding effect of surrounding nuclei (172). This will be characteristic due to the different chemical environments experienced within each molecule and will result in distinct resonances on a spectrum (i.e the frequency at which the peaks will appear on the spectra). Each nucleus of an atom is surrounded by a cloud of electrons that in the presence of an applied $B_{0,}$ generate an internal magnetic field opposing the main field. This creates a shielding effect, whereby the electron cloud shields the nucleus from the full effect of the applied B_0 (178). The effect to which the nucleus is shielded can be expressed as follows;

$$B = B_0(1 - \sigma)$$

Where B is the magnetic field experienced by the nucleus and σ is the shielding parameter (178). The chemical shift experienced by a given molecule will depend on its chemical structure as neighbouring atoms on the same element affect the shielding for a given nucleus. Different molecules will have distinct numbers of nuclei within different chemical environments and therefore will result in a characteristic chemical shift. The chemical shift is expressed in parts per million (ppm) and is defined as follows;

$$\sigma = \frac{v - v_{ref}}{v_{ref}} \times 10^6$$

where v is the frequency of a given molecule and vref is that of a reference molecule or peak. The methyl resonance of NAA is often used as a reference for MRS in the brain in vivo (172).

The chemical shift determines the resonance frequency of the molecule but splitting of the representative peaks is determined by spin-spin coupling, also known as scalar or J coupling. This splitting of peaks occurs due to the magnetic interactions between

neighbouring nuclei through valence electrons in the chemical bonds (172). A given spin will be surrounded by up and down neighbouring spins, which will result in a weak additional magnetic field in that spin location. This will have either a positive or negative effect depending on if the spins are in parallel with or anti-parallel to the B_0. Therefore, at the chemical shift frequency of a metabolite there will be two responses, one that is slightly above and one that is slightly below the chemical shift. This effect splits the resonance peaks into several peaks on a spectrum which represent the chemically distinct responses due to the spin-spin interactions within the molecule. The constant for each bond is known as the coupling constant (J) and is expressed in Hz (179). The splitting pattern of a resonance is usually symmetrical (e.g. a doublet 1:1 or a triplet 1:2:1) due to equal up and down states and is based on the number of possible outcomes of spin states of neighbouring nuclei. For example if a given proton is affected by one adjacent proton it will split into a doublet relative to the J constant of that bond due to the two possible spin states. Whereas if there are two adjacent protons there are four possible spin states and the resonance will split into a triplet (1:2:1). Spin-spin coupling is not affected by external factors such as field strength; however a homogeneous field is required in order to resolve the peaks.

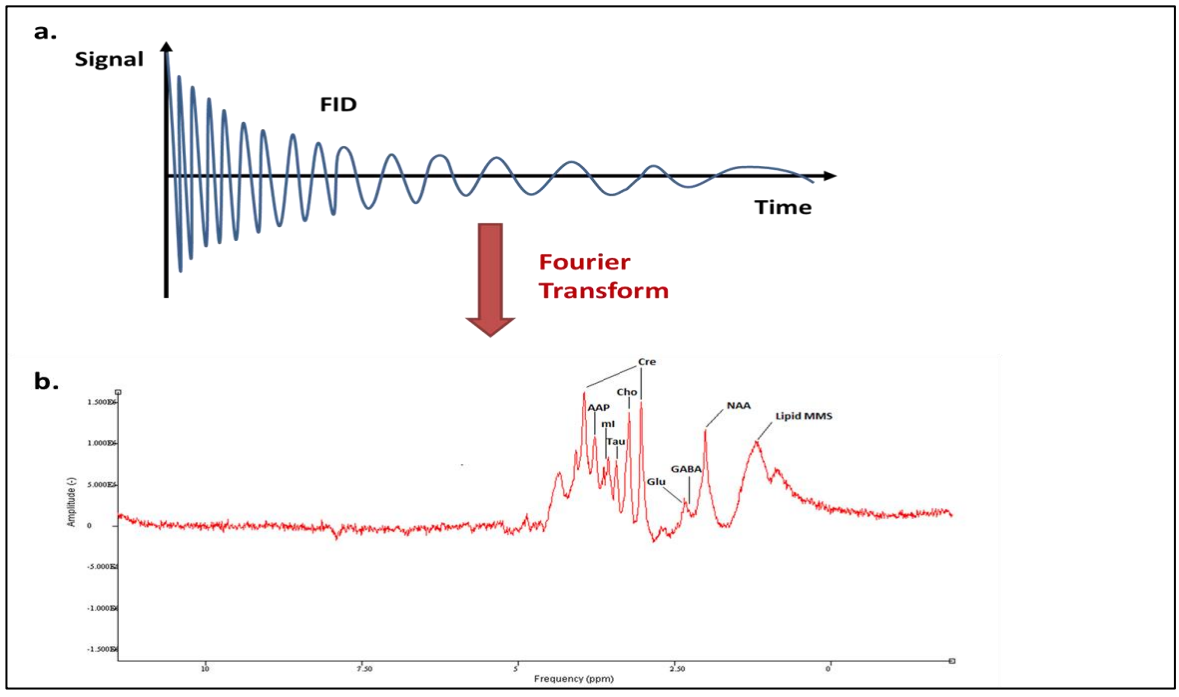

Figure 6 MR signal output visualisation as free induction decay (FID) **(a)**. Example of a MRS spectrum once a fourier transform is applied **(b)**.

1.14.2 Point Resolved Spectroscopy

Point resolved spectroscopy (PRESS) is an MRS acquisition sequence based on spin-echo. It is able to generate spectra with high signal to noise ratios in a short space of time and is used regularly *in vivo*. As described above, applying an RF pulse at the resonance frequency allows the magnetisation to flip into the transverse plane and an MR signal can be acquired. The length and strength of the RF pulse determines how far the M_0 is flipped, therefore by doubling the time or strength of the 90° pulse we can generate a 180° pulse. By applying this additional 180° RF pulse the nuclei spins can be flipped allowing the protons in the different energy levels to dephase in the opposing direction and come back into phase forming a spin echo (180). With PRESS, a second 180° RF pulse is given to refocus the initial echo while also applying a gradient in each direction with each pulse (Figure 7). A gradient allows the selective excitation of a slice in a particular plane and is applied in the x plane for the initial 90° excitation pulse, and in the y and z plane for the subsequent 180° refocussing pulses. The FID signal is only collected after the last 180° pulse allowing selective excitation of a defined region of interest. The echo time (TE) is defined as the time between the 90° and the height of the echo signal. In PRESS the point at which the first echo is generated is TE1 and the final signal echo is TE2. The signal captured depends on the relaxation times of the metabolites; therefore the TE of the sequence can be adjusted to investigate metabolites of interest.

As described earlier T1 relaxation is the process by which the net magnetisation (M_z) returns to its original equilibrium state and T2 relaxation is the decay of the M_{xy} magnetisation. Upwards from 15 metabolites can be quantified *in vivo* using MRS, however it is important to consider the relaxation times of the metabolites when creating a MRS sequence. Different metabolites have different T1 and T2 relaxation times and the acquisition parameters will depend on these times. For example N-acetylaspartate (NAA) has a T1 of 1674ms and a T2 of 294.3ms at 9 Tesla (172). Therefore, to ensure you get a high signal to noise ratio, a TR longer than 1674ms and TE shorter than 294.3ms should be used. The long TR will allow enough time for the magnetisation to return to equilibrium prior to the next pulse and the short TE will allow for acquisition prior to T2 decay.

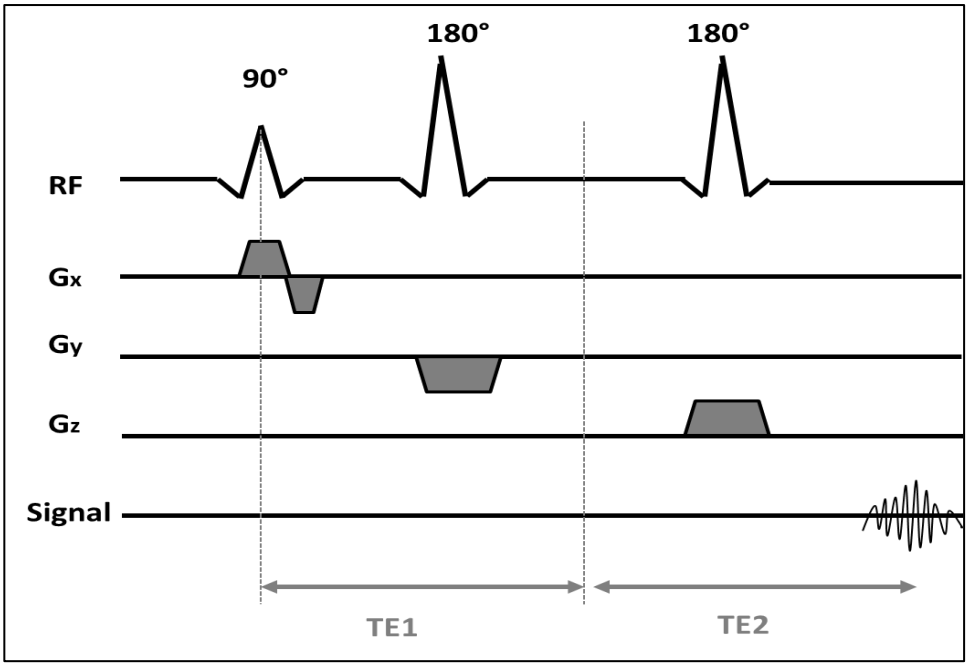

Figure 7 Example of a PERSS sequence. (RF: radiofrequency, Gx, y, z: 3 dimensional readouts for each plane, TE: echo time). Illustration adapted from Mc Robbie (173).

1.14.3 Water Suppression

As water is abundant in brain tissue, the water signal needs to be supressed in order to observe the metabolite peaks within the spectrum. In order to do this the water signal must be selectively excited within the voxel and the protons dephased, thereby supressing the signal picked up by the coil. An example of such a sequence is CHESS (chemical shift selective water suppression), which involves a 90° excitation pulse and a homogeneity spoiling gradient as described by Haase *et al.* (181). However, the VAPOR (volume localized, solvent attenuated, proton NMR) sequence can also be used which includes three RF pulses associated with three low energy gradients to specifically supress the water signal (182).

1.14.4 Metabolites

The main brain metabolites detected in MRS are N-acetylaspartate (NAA), myo-Inositol (mI), glutamate (Glu), taurine (Taur), creatine + phosphocreatine (Cr) and total choline [choline+ phosphocholine+glycerophosphoscholine] (Cho). NAA is considered a

neuronal marker and therefore decreasing levels are suggestive of neuronal dysfunction or death (183). Whereas mI has been suggested to be a glial specific marker and increasing levels are indicative of microglial activation or gliosis (184), mI also has a role in cell growth and as an osmolite. Although more recent studies have not found any association between mI and neuroinflammation, a correlation to amyloid burden has been found (185). These inconsistencies question the role of mI and further investigation is needed. Cr is known to be involved in energy storage as phosphocreatine is involved in the generation of adenosine triphosphate and is suggested to be a neuromodulator affecting the function of neurotransmitters such as GABA post-synaptically (186). Cr levels are generally considered stable; hence MRS data are often expressed as a ratio of Cr. Choline is needed for the production of the neurotransmitter acetylcholine and the cell membrane component phosphatidylcholine. It has been suggested that Taur has a variety of functions including a role in osmoregulation, neurotransmitter regulation and neuroprotection (187). Taur has been shown to protect against excitotoxicity induced damage by endoplasmic reticulum stress (188) and amyloid (189) and is therefore thought to be protective in AD. By measuring Glu we can also directly see how the NT system is being affected in specific areas. Glu is the main excitatory transmitter in the brain and is associated with various processes including learning and memory. Therefore alterations in Glu may be indicative of cognitive dysfunction in AD.

1.14.5 MRS in Clinical AD

In recent years, the use of MRS to research the mechanisms behind many disorders has increased. Increased mI/Cr levels have been consistently reported in different brain regions of AD patients including temporal lobe (190), posterior cingulate (185, 191-193), hippocampus (193, 194) and parietal grey matter (195). As mI is a suggested glial marker, an increase in mI levels is indicative of elevated gliosis. In addition, these areas are associated with early AD pathology and support the role of neuroinflammation in the early staged of AD development. In contrast, decreased NAA/Cr levels have been reported in the same regions (185, 194-196) as well as the frontal lobe of AD patients (190). Decreased NAA is indicative of neuronal death and/or dysfunction and has been shown to correlate with some specific cognitive tests including delayed word recall of a learned list and delayed praxis (194). These results are in line with the progressive pathology and neuronal deterioration seen in AD. Murray *et al.* (185) found that increased mI/Cr levels in the posterior cingulate of AD patients were not associated with microglia but were positively associated with Aβ burden, whereas decreased NAA/Cr levels were negatively associated with burden, suggesting mI as a marker of Aβ rather than neuroinflammation.

A similar case has been reported in MCI patients, with increased mI/Cr and decreased NAA/Cr levels reported in the hippocampus and cingulate (191, 193, 197). This is in line with regions that are targeted early in AD and reinforces the theory that increased neuroinflammation and decreased neuronal function may lead to AD manifestation. mI/Cr levels have been shown to predict a progression to AD with a 70% sensitivity and 85% specificity (197) and discriminate between amnesic and non-amnesic MCI (198). In contrast, Foy et al. investigated hippocampal metabolite concentrations in healthy controls, mild AD and MCI subjects (194). Significantly lower levels of NAA were seen in AD patients compared to control subjects and MCI subjects. Although there was a trend indicating a difference between NAA levels in MCI and normal subjects, this was not significant.

MRS is also able to detect some neurotransmitters and help identify abnormalities such as those observed in glutamate. Glu dysfunction has been recognised in AD and

decreased Glu or Glu +glutamine (Glx) have been reported in the posterior cingulate of AD patients (193, 199). Decreased Cr and increased Cho levels have also been reported in AD and MCI patients that convert to AD (191, 194), therefore providing a further means of discrimination between AD and healthy aging.

It has also been suggested that MRS can be utilised to help differentiate between different forms of dementia. For example Griffith *et al.* examined metabolite concentrations in AD, Parkinson Disease Dementia and healthy older subjects (200). AD patients revealed significantly lower levels of NAA/Cr and higher levels of Cho/Cr and mI/Cr than healthy controls, supporting the results of previous studies. PDD patients also revealed decreased NAA/Cr, however these patients displayed significantly lower Glu/Cr levels compared to AD allowing metabolic differentiation. MRS has also been used to differentiate between AD and subcortical ischemic vascular dementia (193).

These results indicate that both mI/Cr and NAA/Cr levels can be used to identify those with MCI and AD from a normal aging population and other dementias, although discrimination using Glu, Cho, Cr or between MCI and AD is less conclusive. However, this may be down to factors such as different analysis methods or diagnostic criteria used between these studies.

1.14.6 MRS in Pre-clinical Models of AD

MRS has been carried out in various animal models of AD with results reflecting the clinical situation. Decreased hippocampal and cortical levels of NAA, Glu and increased levels of mI have been shown in various animal models of AD (201-204). However, results are less consistent in terms of metabolite change and age of alterations than in clinical AD.

Chen *et al.* found significantly increased hippocampal/frontal mI/Cr ratio from 3 months of age and decreased NAA/Cr from 5 months of age in the APP_{swe}×$PS1_{\Delta e9}$ mouse model. Both effects increased with age (205). In a subsequent study Chen *et al.* replicated these results and a decrease in Glu/Cr levels at 5 months was also observed (203). Moreover, the mI increase occurs prior to plaque development (108) or cognitive decline in this model and before the NAA decrease was observed in this study. Therefore, mI abnormalities seem to manifest prior to major symptom onset or neuronal damage, indicating neuroinflammation as a crucial player in the early events of AD. However, it is important to note that metabolic alterations appear to not only differ between AD models but also between studies. Other studies did not report significant NAA/Cr reduction in this model until later ages. Jansen *et al.* reported decreased NAA/Cr levels at 12 months of age, with no alterations in mI or any other metabolite evident (206). Similarly, Xu *et al.* also found decreased NAA/Cr levels to be the only metabolite alteration in this model. This effect emerged at 16 months of age and was associated with hippocampal CA3 pathology (207). Marjanska *et al.* observed decreased NAA/Cr levels at 16 months in the same model, as well as decreased Glu/Cr and increased mI/Cr at that age (201).

Metabolite alterations are consistently reported in different models of AD. Decreased NAA/Cr levels and Glu/Cr ratios were found in the PS2APP mouse model at 20 and 12 months respectively (208). Decreased NAA and Glu levels were found to positively correlate with plaque load in the frontal cortex in this model. However, no differences in mI or any other metabolite were observed. Dedeoglu *et al.* found significantly decreased NAA, Glu and glutathione (major antioxidant in the brain) in the frontal cortex of TG_{2576} mice (209). They did not report increased mI levels, however they did see increased Taur.

It has been suggested that Taur in rodents acts similar to mI in humans and that may account for lack of effect on mI. In contrast, a significant effect of genotype has been shown for mI in other models of AD with significantly increased levels in TG compared to WT mice (204, 210, 211). Oberg *et al.* found increased hippocampal mI levels in an $APP_{swe}xPS1_{PS1M146L}$ model of AD as early as 2.5 months (204). Similar to the study by Chen *et al.* in a different double APPxPS1 mouse model, this mI alteration preceded NAA and Glu reductions which appeared at 6.5 months of age suggesting neuroinflammation is a key factor in future neuronal death or dysfunction. Yang *et al.* found that increased mI levels in hippocampal and cortical regions of TG_{4510} mice. Results were supported by increased GFAP and Ionized calcium binding adaptor molecule 1 (Iba1; microglial marker) staining; demonstrating up-regulated astrocyte and microglia activation and supporting increased mI levels as an indicator of gliosis. Decreased NAA and Glu ratios were also seen but were not statistically significant. This model is a tau mutation model, hence these results suggest that tau can also initiate an inflammatory response but alone may not be enough to cause neuronal death in this model. Nonetheless, it strengthens the link between neuroinflammation and AD pathology and emphasizes the role of neuroinflammation in AD development. Forster *et al.* demonstrated a significant negative correlation between cognitive function, as assessed by Y-maze, and mI levels in TG mice. Better scores were associated with lower levels of mI (210), suggesting that high levels of mI may have a negative effect on cognitive performance. Significantly decreased NAA levels and increased Cr levels were also reported. In a previous study Forster *et al.* carried out NMR *in vitro* using ^{1}H-NMR and did not find significant changes in NAA levels between TG and WT mice (212). However, they did find that genotype had a significant effect on mI, with increased levels found in TG mice at all time points except 3 months. This effect was independent of age and indicates that it is a persistent characteristic of AD. This study used whole brain extractions, which may be masking regional effects and may explain why no significant difference was observed in NAA. On the other hand it emphasizes the extent of change observed in mI as a significant effect was recognised globally. Similar to the human case, mI has been suggested to be an early indicator of AD-like pathology in AD animal models. Recently, a MRS study was conducted using a new transgenic rat model (McGill-R-Thy1-APP rats) (60). Decreased mI levels were found in the dorsal hippocampus at 3 months compared to WT rats. However, by 9 months of age mI levels were significantly increased, resulting in higher levels of mI than WT at this age. However,

by 12 months no differences in mI levels were identified in the TG rats compared to the WT, indicating that neuroinflammation response may be more complex than originally thought and neuroinflammatory status may change prior to and during disease manifestation and progression. This is line with many views as discussed previously. In addition, increases in tCho have also been reported in an APP×PS1 (KM670/671NL× PS1 M146L) mouse model (213). Although no decreases in NAA or mI were reported, it is in line with what has been seen in the clinical situation and is also seen in other disorders which may affect membrane stability such as cancer and brain injury.

MRS has also been used pre-clinically as an outcome measure for therapy efficacy. MRS was carried out in TG_{2576} mice prior to and after one of two Aβ passive immunization treatments or vehicle treatment. TG mice displayed increased levels of mI with age compared to WT mice. Both immunization treatments in these TG mice decreased Aβ levels and prevented mI levels from increasing at the same rate as the vehicle treated TG mice (214). A protective effect was also seen on mI levels by ibuprofen treatment in the 3xTG mouse model (215). Ibuprofen treatment prevented increases in mI levels at 6 months and decreases in NAA levels at 17 months which were seen as an effect of aging in this model. NAA level attenuation by ibuprofen was also shown in a PSAPP mouse model, however no effect on mI was observed (216).

The contrasting reports may be down to a variety of factors including differences in numbers of animals, models used, gender and methods of acquisition and quantification. Nonetheless, despite some inconsistencies it is evident that metabolite concentrations represent a good output to look at AD progression. Decreased NAA and increased mI levels are consistently reported in both clinical and preclinical studies. Although, some mI reports are contradicting further investigation into its role in AD and proof of its link to neuroinflammation is still lacking. In depth longitudinal studies using MRS and correlating outcomes to measurements *ex vivo* such as glial activation, amyloid concentration and neuronal integrity markers at each disease stage are needed in order to validate MRS results at a cellular level and get a better understanding of the correlation between mI and neuroinflammatory status as well as the link with NAA and other metabolite levels.

1.15 Summary

AD is a devastating neurodegenerative disease. Its incidence continues to grow each year representing a global socioeconomic problem. Elucidation of its development and mechanisms involved is a hot topic in neuroscience research. However, despite great effort and many hypotheses brought forth, the exact pathophysiology remains elusive. Molecular abnormalities are likely to precede cognitive symptoms and identification of such early biomarkers would not only aid disease management but would also supply therapeutic targets for future research. Therefore, investigation into clinically relevant AD-specific biomarkers is imperative.

It has become apparent that AD is a complex multifactorial disease with many contributing factors. Accumulating evidence suggests that neuroinflammation has a pivotal role in AD pathophysiology, however to what extent and if this can change with disease state remains unclear. Advances in bio-medical imaging have made it possible to image neuroinflammation and neurodegeneration in rodent models of AD. New technologies such as that of bio-medical imaging should be used to probe the mechanisms of AD and help assess and develop new therapeutics. Measuring microglial activation in vivo in AD would help understand the importance of inflammation in this disease. Investigation may identify important inflammatory patterns helping us to gain a more in depth knowledge of molecular mechanisms and could present as potential diagnostic biomarkers. Furthermore, it could also be used to assess the efficacy and specificity of anti-inflammatory therapies. However, further investigation into the binding sites of the TSPO is implicit for reliable and accurate assessment. It is important to note that microglial activation is not specific to AD as neuroinflammation is also present in other neurological disorders, nonetheless increased regional neuroinflammation may represent a good biomarker for early diagnosis in conjunction with other specific biomarkers such as [^{11}C]PIB or other tracers for PET amyloid imaging and cognitive and psychological testing. In recent years advances have been made in our understanding of microglial biology with their origins being redefined and functions being reviewed (62). We know that microglia are very dynamic cells that adapt rapidly to their microenvironment but much regarding their functions remains to be resolved. Hence, further investigation into their functions and triggers is warranted. Using imaging techniques to investigate their behaviour in diseases such as AD will help to give

us a better understanding of microglial function *in vivo* and pave the way for future anti-inflammatory therapies in neurodegenerative disease.

1.16 Hypotheses and Aims

Considering the above review of the literature, we hypothesise that AD animals will develop cognitive decline at a faster rate than age-matched WT animals and that *in vivo* imaging markers of neuroinflammation and neurodegeneration within regions associated with AD pathology (e.g. cortex and hippocampus) will allow discrimination between TG and WT animals. In addition, we also expect imaging alterations to be identifiable in more regions and at earlier disease states in the TgF344AD rats than are currently seen in TG mice models. Furthermore, we hypothesise that recurrent peripheral inflammation will drive disease progression in AD with earlier cognitive decline and increased neuroinflammation in TG animals. Therefore, the overall aim of this project is to investigate neuroinflammatory and metabolite markers of AD progression in rodent models using PET and MRS. In order to achieve this the following objectives were set out:

- Use non-invasive imaging methods to characterise neuroinflammatory and metabolite differences with AD progression in the $APP_{swe}/PS1_{\Delta e9}$ mouse and TgF344AD rat model.
- Assess rates of cognitive decline in these models using memory based behavioural tests.
- Investigate the use of the TgF344AD rat as a model for identifying early markers of AD by characterising younger time-points than previously reported.
- Investigate the contribution of peripheral inflammation on AD progression using neuroinflammatory and metabolite markers.
- Assess the ability of *in vivo* TSPO PET and MRS to identify neuroinflammatory and neurodegenerative changes specific to AD that allow the discrimination of AD models from WT animals.

1.17 Papers and Contributions of authors

Paper 1-" Longitudinal investigation of neuroinflammation and metabolite profile in the APP_{swe}×$PS1_{\Delta e9}$ transgenic mouse model of Alzheimer's disease".

Chaney A., Bauer M., Bochicchio D., Smigova A., Kassiou M., Davies K, Williams S., Boutin H.

Chaney A carried out the MRS and PET imaging and analysis, as well as all behavioural tests and analysis.

Bauer M re-ran the PET results with an up-dated MRI template.

Bochicchio D carried out the immunohistochemistry.

Kassiou M provided the precursor for PET imaging.

Smigova A and Davies K provided laboratory support for PET and MRS respectively.

Chaney A , Williams S and Boutin H contributed to the writing and editing of the paper.

Paper 2-" Longitudinal investigation of Neuroinflammatory and Neurodegenerative status of the TgF344-AD rat model of Alzheimer's disease".

Chaney A., Smigova A., Kassiou M., Davies K., Williams S., Boutin H

Chaney A carried out the MRS, PET, behavioural tests and all analysis.

Kassiou M provided the precursor for PET imaging.

Smigova A and Davies K provided laboratory support for PET and MRS respectively.

Chaney A , Williams S and Boutin H contributed to the writing and editing of the paper.

Paper 2-" Effect of recurrent Urinary Tract Infection on Disease Progression in the TgF344-AD rat model of Alzheimer's Disease".

Chaney A, Sharp A, Burges E, Davies K, Smigova A, Warn P, Williams S, Boutin H

Chaney A carried out the MRS, PET, behavioural tests and all analysis.

Sharp A, Burges E and Warn P were involved in administering and planning of the infection.

Kassiou M provided the precursor for PET imaging.

Smigova A and Davies K provided laboratory support for PET and MRS respectively.

Chaney A , Williams S and Boutin H contributed to the writing and editing of the paper.

Chapter 2 (Paper 1)

Longitudinal investigation of neuroinflammation and metabolite profile in the APP_{swe}×$PS1_{\Delta e9}$ transgenic mouse model of Alzheimer's disease

Chaney A., Bauer M., Bochicchio D., Smigova A., Kassiou M., Davies K, Williams S., Boutin H.

Longitudinal investigation of neuroinflammation and metabolite profile in the APP_{swe}×$PS1_{\Delta e9}$ transgenic mouse model of Alzheimer's disease.

Chaney A.[1], Bauer M.[2], Bochicchio D.[1], Smigova A.[1], Kassiou M.[3], Davies K.[1], Williams S.[1], Boutin H.[1,4].

[1]Faculty of Biology, Medicine and Health, School of Health Sciences, University of Manchester, Manchester, M13 9PT, UK

[2] Medical University Vienna, Department of Clinical Pharmacology, Waehringer Guertel 18-20, 1090 Vienna, Austria.

[3] School of Chemistry, University of Sydney, NSW 2006 Australia.

[4] Wolfson Molecular Imaging Centre, Faculty of Biology, Medicine and Health, University of Manchester, Manchester, M20 3LJ, UK.

Corresponding Author:

Dr Hervé Boutin,

Wolfson Molecular Imaging Centre,

27 Palatine Road, Manchester, M20 3LJ, UK

Email: herve.boutin@manchester.ac.uk

Tel: +44 1612750078

Fax: +44 161 275 0003

Abstract

Neuroinflammation has become a hot topic in research with an increasing amount of evidence linking it to many neurological disorders including Alzheimer's disease. Although it is evident that neuroinflammation has a role to play, the exact contribution to disease manifestation and/or progression remains to be fully understood. Therefore, a need exists to find new innovative ways of investigating neuroinflammation in both health and disease. Here we investigate neuroinflammatory and other neurodegenerative changes in parallel with cognitive decline in the $APP_{swe} \times PS1_{\Delta e9}$ transgenic mouse model of Alzheimer's disease. Transgenic (TG) mice were compared to C57BL/6 wild type (WT) mice at 6, 12 and 18 months of age. Neuroinflammation was investigated by measuring TSPO expression using [^{18}F]DPA-714 positron emission tomography and myo-Inositol levels using ^{1}H magnetic resonance spectroscopy. Neuronal and cellular dysfunction was investigated by looking at other metabolites such as N-acetylaspartate (NAA), choline containing compounds, taurine and glutamate using MRS. Cognitive decline appeared from 12 months in the TG mice as assessed by working memory tests. A significant increase in [^{18}F]DPA-714 uptake was seen in the hippocampus and cortex of 18 months old TG mice when compared to age matched wild-type mice and 6 months old TG mice. No overall effect of gene was seen on metabolite levels; however a significant effect of age and a significant gene × age interaction was observed on NAA with TG mice demonstrating significant reductions in NAA that were not significant in WT mice. In addition, age resulted in glutamate and choline changes. Therefore we can conclude that increased neuroinflammation and a faster rate of cognitive decline are observed in TG animals, whereas NAA alterations occurring with age are exacerbated in the TG mice. These results support the role of neuroinflammation and metabolite alteration in AD and in aging.

Key words: Alzheimer's disease, neuroinflammation, positron emission tomography, magnetic resonance spectroscopy.

Introduction

Alzheimer's disease (AD) is the most common form of dementia, a group of debilitating and progressive neurodegenerative disorders. AD has become a huge socio-economic burden due to an increased aging population and despite vast research the exact mechanisms leading to its' manifestation remains unclear. AD is defined pathologically by amyloid plaques (Aβ), neurofibrillary tangles (NFTs) and neuronal loss (12); however the exact aetiology of this disease remains elusive. Hence, a need exists to find viable biomarkers of disease progression that can help to aid diagnosis and track the efficacy of current and future therapeutic interventions.

It has become evident that it is likely that AD is a multifactorial disease associated with complex neuronal and neuroinflammatory alterations (5, 69, 87, 217, 218). In particular, there has been an increasing interest in the role of neuroinflammation in the manifestation of neurodegenerative disorders including Alzheimer's disease. Although the exact contribution of neuroinflammation is unclear, much evidence implicates it in AD pathophysiology. Activated microglia have been shown to surround amyloid plaques (219) *ex vivo* and increased inflammatory cytokine expression is observed post-mortem in brain and *in vivo* in the serum and CSF of AD and MCI patients (69, 70, 220-222). In addition, treatments which reduce pro-inflammatory cytokines have been shown to improve memory performance (223, 224), suggesting increased inflammation could contribute to memory impairments seen in AD.

Specific and sensitive techniques to assess neuroinflammation *in vivo* are fundamental to our understanding of the impact it has in AD. Hence, much effort has been put into developing non-invasive imaging methods to quantify neuroinflammation. The discovery of translocator receptor (TSPO) expression on glial cells has enabled the generation of TSPO radio-ligands to image neuroinflammation *in vivo* using positron emission tomography (PET). TSPO expression is low in the CNS but increases during neuroinflammation (132, 133). PK11195, a TSPO ligand, has been successfully labelled with ^{11}C and has shown good correlation to microglial activation *ex vivo* (141), however contradictory reports exist regarding the detection of neuroinflammation in AD using [^{11}C]PK11195 TSPO imaging. Some studies have demonstrated increased [^{11}C]PK11195

binding in AD and mild cognitive impairment patients (10, 142), whereas others have reported no differences in any regions between patients and age matched controls (143, 144). Short half-life, low signal to noise ratio, high non-specific binding and modelling issues may have contributed to these contradictory results (148, 149), hence new generation tracers with improved affinities and kinetics such as [^{18}F]DPA-714 (153-155, 225) have been developed to assess TSPO expression.

Similarly, magnetic resonance spectroscopy (MRS), an MR imaging method that allows the detection of metabolite profiles *in vivo*, can also be used to investigate neuroinflammation through measurement of myo-Inositol (mI) levels. mI has indeed been suggested to be a glial specific marker (184) indicative of increased gliosis. Although increased levels of mI have been repeatedly reported in AD patients and subjects with mild cognitive impairment in regions associated with degeneration in AD (185, 190-195), evidence suggests that mI does not necessarily correlate with increased microglial activation *ex vivo* (185, 226) and may be more directly associated with plaque load. MRS can measure other metabolites of interest affecting neuronal function including N-acetylaspartate (NAA), glutamate (Glu), taurine (Taur), total choline (tCho) and creatine (Cr). NAA is a neuronal marker (183) and decreases in its levels are consistently reported in AD patients (185, 190-196), suggesting neuronal dysfunction or death. Moreover, mI and NAA levels have been shown to be correlated with Aβ burden (185, 227) and performance in some cognitive tasks (194, 195), implicating both in AD pathology and disease severity.

Although, the majority of AD cases are sporadic (approximately 95%), so far most of the animal model use transgenes present in the inheritable familial form. Nevertheless, these models give us insight in to the pathological mechanisms underlying AD. Hence, here we used the human double mutation APP_{swe}×$PS1_{\Delta e9}$ mouse model to investigate inflammatory and neuronal integrity biomarkers as indicators of disease progression using MRS, PET, immunohistochemistry and cognitive assessment.

A longitudinal study was conducted in male TG APP_{swe}×$PS1_{\Delta e9}$ and WT C57BL/6 mice to investigate neuroinflammation using PET, neurochemical profile using MRS and

cognitive function using several behavioural assessments. This was done with the aim of characterising inflammatory, metabolite and cognitive differences between TG and control animals with age. We hypothesised that there would be increased neuroinflammation (demonstrated by increased DPA-714 uptake and mI levels), neuronal dysfunction (decreased NAA levels) and cognitive decline with age in the TG compared to WT mice.

Methods

Animals

Male and female TG $APP_{swe\times}PS1_{\Delta e9}$ mice with a C57BL/6 background and WT C57BL/6 mice were acquired from the Jackson laboratory (Bar Harbor, Maine, USA) at 8 weeks of age, some of the males were used in the study while the other male and females were used to set up breeding colonies in house. All mice were kept in the Biological Sciences Unit in the University of Manchester. Animals were housed in individually ventilated cages in groups of 2-5 in a 12h:12h light and dark cycle with environmental enrichment and 24h access to food and water. In total, 22 male WT and 21 TG male mice were used in this study. 8 WT and 10 TG were measured repeatedly for MRS (2 WT and 5 TG of these were bred in house), however a total of 18 WT and 15 TG (5 WT and 7 TG of these were bred in house) mice were used non-repeatedly in the PET assessment. This was as a result of 4 TGs and 2 WTs dying of unknown causes, and one WT was excluded after abnormal brain morphology was noticed during MR imaging. Older mice died during anaesthesia from 9 months of age (3 TGs and 3 WTs) in the PET. In addition n=3 for both TG and WT were used for *ex vivo* analysis for 6 and 12 months. The scanning animals were used for *ex vivo* at 18 months. All animals were cognitively assessed. All experiments were carried out in accordance with the Animal Scientific Procedures act 1986.

Study Design

The study design is set out in Figure 1. Mice underwent behavioural testing and imaging at 6, 12 and 18 months of age. Experiments began at 6 months of age due to the development of detectable amyloid pathology from this age in this model (107). PET and MRS imaging was carried at least one week apart to allow the animals to rest in between anaesthesia. Immunohistochemistry was carried out on separate animals at 6, and 12

months. The imaging animals were culled and used for *ex vivo* at 18 months of age. A week gap was given between imaging and behavioural experiments to allow animals to recover of potential stress and limit interference between experiments. All experiments were carried out between 9am and 5pm. All behaviour was carried out during the light phase at the same time of day for each time-point. For all behavioural tests the animals were placed in the testing room for 30 minutes prior to the beginning of the experiment to allow for habituation to the testing environment.

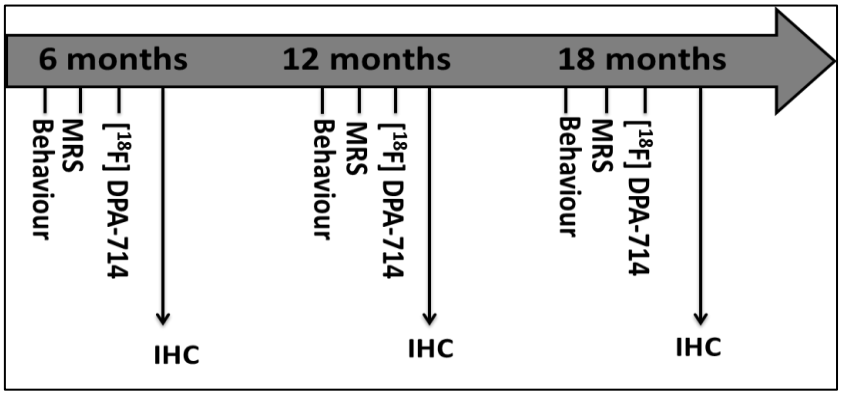

Figure1 Experimental study design. Behaviour was carried out at 3, 6, 9, 12 and 18 months. MRS and PET were carried out at 6, 12 and 18 months.

Behaviour

Novel Object and Smell Recognition Tests

Novel object recognition (NOR) utilizes the natural behaviour of rodents to explore novelty to test non-associative working memory (228). Animals were subjected to two days of habituation and one day of testing (Figure 2a). Habituation involved the mice exploring an empty arena (30cm diameter, 21cm height) for 5 minutes and was carried out in a random order within the same timeframe each day. Test day consisted of two phases (Figure 2b). In phase 1 the mice explored two identical unfamiliar objects for 10 minutes. They were returned to their home cage and a 1 hour delay was implemented before phase 2. In phase 2 a novel object replaced one of the familiar objects. The mice were given 4 minutes to investigate both objects and the time investigating the novel and familiar was recorded. Total time exploring the objects was calculated and results were expressed in terms of percentage of exploration. In between trials all objects and areas were cleaned with 70% ethanol to remove any scent of the previous mouse which may alter results. Novel smell recognition (NSR) also utilizes the natural exploration of novelty to test working memory in rodents through olfaction. The experimental design is the same as the

NOR, however there is a delay of 3 minutes and instead of objects it uses scent balls filled with cotton wool and half a millilitre of a certain scent such as vanilla, almond, orange or lemon (Figure 2c). For both tests a video recorder was placed above the arena and was surrounded by blackout screens. Tests were recorded and analysed later to ensure the mice behaved naturally. Time spent investigating left and right identical objects/smells in phase 1 was assessed by t-tests to ensure there was no side bias. Time spent exploring the novel and familiar objects in phase 2 was used to generate a discrimination index (DI), which was defined as the novel minus the familiar time divided by the total time. This resulted in values ranging from -1 to +1. A minus value indicated more time spent with the familiar, a positive value indicated more time investigating the novel and a zero value indicated equal time investing both. A two-way ANOVA was carried out to compare the performance in the groups with age.

Y-maze spontaneous alteration task

The Y-maze spontaneous alteration task utilizes the natural exploratory behaviour of rodents to assess spatial learning and short-term memory function. A black Perspex maze with 3 arms labelled with A, B, C and different visual cues at the end of each arm was used (Figure 2d). The mice were allowed to explore, while entries within the arms were recorded over an 8 minute period. Partial entries were excluded; entries were only valid if the whole body of the mouse entered the arm. Successful alternation was determined by consecutive entries into the 3 arms in any order. Analysis was carried out by calculating overlapping triplet sets to determine working memory function, and total number of arm entries to examine exploratory behaviour. The percentage number of alternation defines the success of the task and was calculated as the number of successful triplets divided by the total entries minus two.

Behaviour to predator and non-predator urine

A Y maze with either predator or non-predator urine at the end of each arm was used to assess the general olfaction ability of 12 month old WT and TG mice. The maze had no visual cues and the same dimensions as the spontaneous alternation task. Vented containers were injected with one millilitre of bobcat, fox and rabbit urine and were placed at the end of each arm. Mice were allowed to explore the maze for 8 minutes and time (in

seconds) spent in each arm was quantified. Time spent in the middle of or rearing on the side of the maze was not counted. Both bobcats and foxes are predators for mice, whereas rabbits are not, hence an increased amount of time in the arm containing rabbit urine would be expected in mice with intact olfaction.

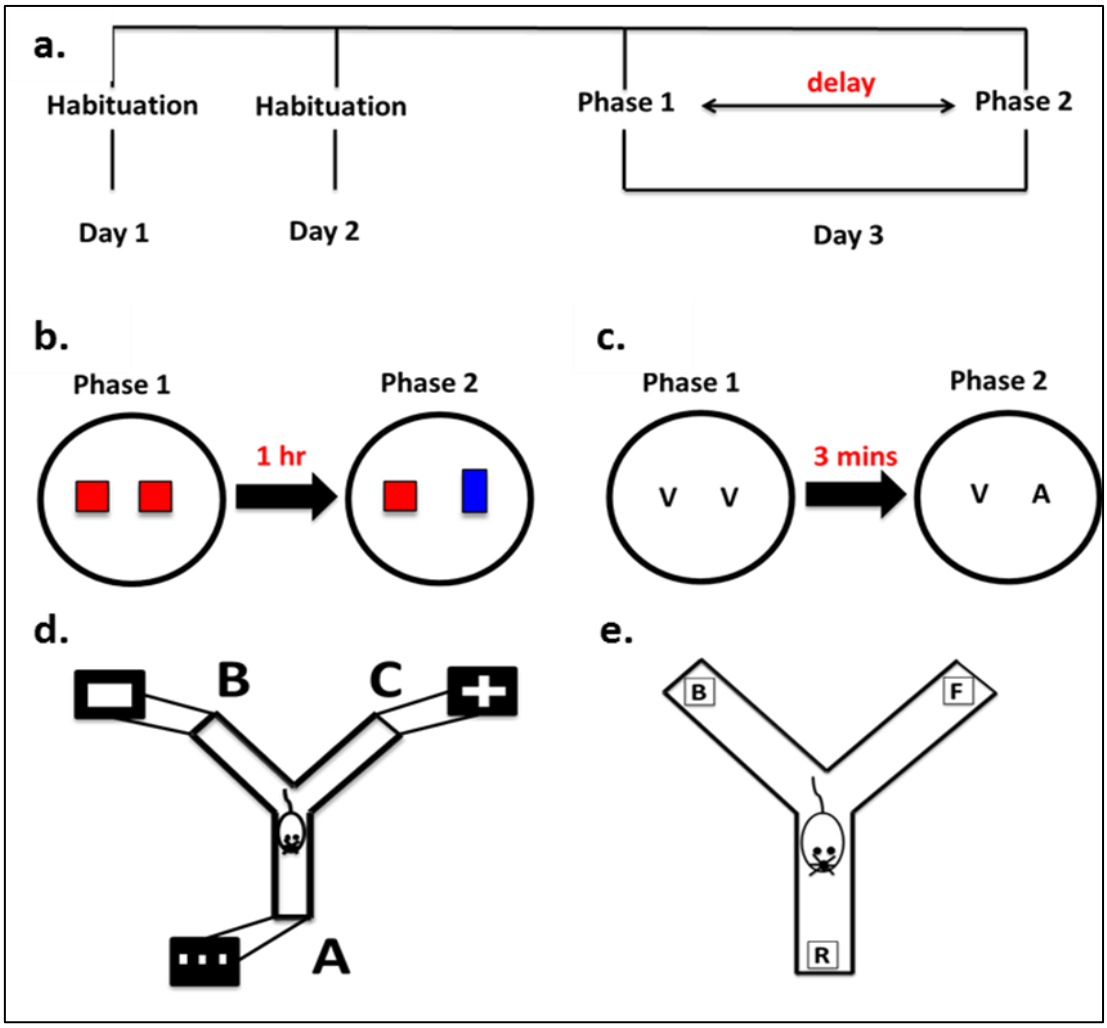

Figure 2 Outline of behavioural methods. Novel test experimental design included 2 days of habituation and 1 day of testing **(a)**. The novel object recognition test consisted of 2 identical plastic objects in phase 1 replaced by one novel object in phase 2 **(b)**. The novel smell test contained identical scents replaced by a novel in phase 2 **(c)** [V= vanilla, A=almond]. Percentage alternation was assessed using Y-maze labelled A, B and C with visual cues at the end of each arm **(d)**. Sense of smell was assessed using a Y-maze with different predator and non-predator urine [B=bobcat, F= fox, R=rabbit].

[^{18}F]DPA-714 PET

Neuroinflammation was investigated using the TSPO tracer [^{18}F]DPA-714. [^{18}F]DPA-714 was produced as previously described (225). Animals were anesthetised, cannulated (via tail vein) and injected with approximately 10MBq of [^{18}F]DPA-714. Respiratory rate and temperature were monitored constantly throughout the experiment and body temperature was maintained through the use of a heating and fan module controlled by the rectal probe via the interface of the BioVet® system (m2m Imaging Corp., Cleveland, OH, USA). Images were acquired on a Siemens Inveon® PET-CT scanner using a 60 minutes dynamic acquisition. CT scans were performed prior to PET acquisition to obtain the attenuation correction factor. The time coincidence window was set to 3.432 ns and levels of energy discrimination to 350 keV and 650 keV. List mode data from emission scans were histogrammed into 16 dynamic frames (5 × 1 min; 5 × 2 mins; 3 × 5 mins and 3 × 10 mins) and emission sinograms were normalised, corrected for attenuation, scattering and radioactivity decay and reconstructed using an OSEM3D protocol (16 subsets and 4 iterations) into images of dimensions 128 (transaxially) ×159 (axially) with 0.776×0.776×0.796mm voxels.

Dynamic PET images were analysed using Brainvisa and Anatomist software (http://brainvisa.info/web/index.html). CT images were resampled to fit the PET space (128×128×159) and were used to define the skeleton and brain volume of each animal. The PET images segmented using the local means analysis method and the organ mean time activity curves were corrected for partial volume effect as previously described (153, 229, 230). The correction method combined the geometric transfer matrix (GTM) method and the regions of interest (ROI)-opt method. The mask brain volume determined on the CT image was co-registered in Brainvisa with a MRI mouse brain template, from the Waxholm space created by Johnson *et al* (231). This MRI mouse brain template was used to create 4 brain ROIs (all cortical areas, whole hippocampus, other subcortical regions and cerebellum) large enough to be accurately quantified based on the spatial resolution of the PET scanner (Figure3 a-c). Data are expressed as uptake values normalised to the cerebellum and body weight (NUV_{cb}).

Magnetic Resonance Spectroscopy Acquisition and Analysis

Animals were anesthetised using isoflurane (3% induction and 1-2% maintenance) and medical oxygen at a rate of 2L/min. Respiratory rate and temperature were monitored constantly throughout the experiment. MRI and MRS were conducted using a 7 Tesla Magnex scanner (Agilent Technologies, Oxford Industrial Park, Yarnton, Oxford, UK) connected to a Bruker Biospec Avance III console (Bruker Biospin Ltd, Banner Lane, Coventry, UK). MRI was used to carry out an initial pilot scan allowing visualisation of the positioning of the mice in the scanner and ensuring correct head placement of the mice. An anatomical FLASH (Fast Low Angle SHot) MRI sequence (9 slices, 2 averages, 0.5mm inter-slice distance) was carried out giving cross-sectional images of the brain, which was used to locate the hippocampus for voxel placement. A PRESS (Point REsolved SpectroScopy) sequence (232) was applied to allow the position of the voxel for shimming ($4.5x4.5x4.5mm^3$). The shim voxel was positioned on the hippocampus and an automatic shim algorithm based on 'FASTMAP' (233) was used to estimate B_0 inhomogeneity and adjust 1st and 2nd order shimming accordingly (Bruker). Prior to acquisition a VAPOR (volume localized, solvent attenuated, proton NMR) sequence was carried out to supress the water signal (182). Spectroscopy was acquired using a PRESS sequence (TR 2500ms, TE 20ms, 512 averages) using a $2.5x4.5x3mm^3$ voxel that covered the hippocampus and the most dorsal part of the thalamus (Figure 3d).

A metabolite basis-set was simulated using NMRScope in the jMRUI version 5 software package. This allows the generation of metabolite signals via theoretical simulation based on chemical shift information. Metabolites included in the basis-set were as follows; N-acetylaspartate (NAA), glutamate (Glu), myo-Inositol (mI), creatine (Cre), GABA, scyl-Inositol (Scy-I), glutamine (Gln), taurine (Tau) and choline containing compounds (tCho) which consisted of choline, glycerophosphocholine and phosphocholine combined (Cho + GPC + PC). Peaks at 0.9 and 1.3ppm were included to model lipid/macro-molecules. Another additional peak was added at 3.76ppm to cover the detection of α-protons of amino acids (AAP) not otherwise included in the basis set. These additional peaks were added to help with spectral fitting as significant residual signal had previously been found at these resonances (210). An example spectrum *in vivo* with labelled metabolites is shown in Figure 3e. Metabolites were simulated using strong

coupling simulation and the same parameters as acquisition (TE20ms, sampling interval 0.25ms, 2048pts, 300MHz).

Spectra were pre-processed by applying a time circular shift and a HLSVD (Hankel Lanczos Singular Values Decomposition) filter to supress the residual water signal. HLSVD uses a black-box quantitation method to estimate the water signal and subtracts it from the acquired spectra (234). This was performed by manually highlighting the water peak and applying the filter. In vivo metabolite concentration was measured using the jMRUI version 5 algorithm QUEST (235). QUEST compiles the metabolite theoretical signals into a basis-set, and then fits the signals to the in vivo spectra, allowing detection and measurement. QUEST was run without background handling. Results were referenced to Cr. Referenced data was used to compare metabolite levels in WT compared to TG mice. WT and TG metabolite profiles were examined including and excluding GABA in the basis-set.

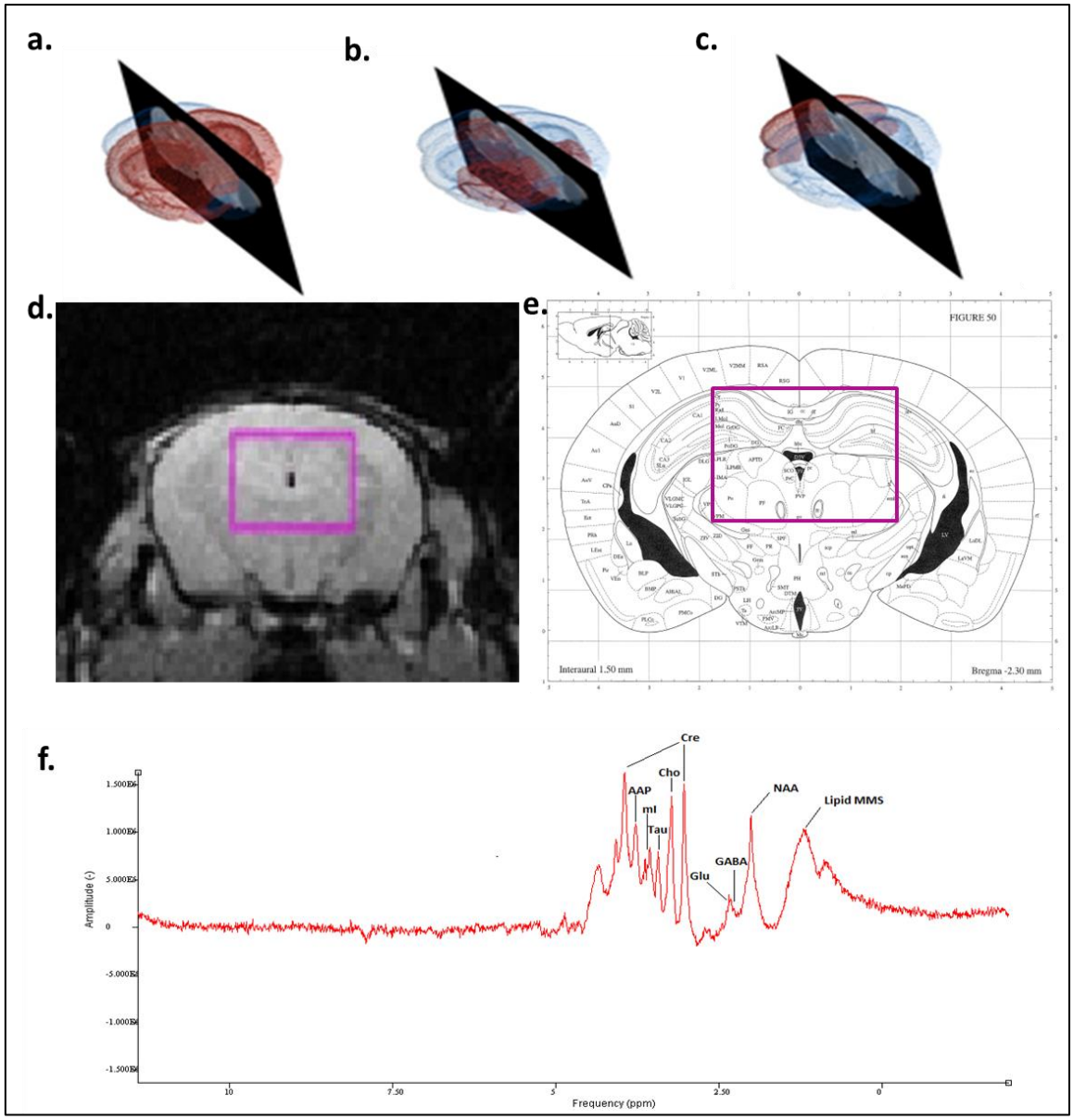

Figure 3 The whole brain was segmented into the hippocampus and cortex **(a)**, other subcortical **(b)** and cerebellum **(c)** regions of interest for PET quantification using a modified version of the Waxholm space template (231). The MRS voxel was centred at bregma -2.30mm according to the Paxinos mouse brain atlas and encompassed hippocampal and thalamic regions **(d-e)**. Example of an i*n vivo* MRS spectra with the main metabolites highlighted **(f)**. AAP-amino acid proton, mI-myo-Inositol. Tau-taurine, Cho-choline containing compounds, Cre-creatine, Glu-glutamate, GABA- gammaAminobutyric acid, NAA-N-Acetylaspartate, Lipid MMS- lipid macromolecules.

Immunohistochemistry

Immunohistochemistry was carried out on TG and WT animals (n=3-5) to visualise CD11b (microglial marker), GFAP (astroctyic marker), TSPO, 6E10 (Aβ marker), SVA2 (synaptic vesicle marker), MAP2 (microtubule marker) and NeuN (neuronal marker). Animals were culled by CO_2 and cervical dislocation. The brains were collected, quickly snap frozen using isopentane and stored at -80°. Brains were sectioned at 20µm using a cryostat (Leica CM3050s, Leica Biosystems Nussloch GmbH, Germany). Each series began at the frontal brain and finished at the cerebellum. Sections were fixed at room temperature with 4% paraformaldehyde for 10 min before being washed 6 times for 5 minutes in phosphate buffered saline (PBS) and incubated for 30 minutes in 2% normal donkey serum and 0.1% Triton X-100 in PBS to permeabilize and block non-specific binding. TSPO, 6E10 and neurogranin immunohistochemistry required an extra step of antigen retrieval done by incubating the slides in 10mM citrate buffer at 90°C for 20min and then washed 2 × 3min in PBS. Primary antibody incubation was carried out overnight at 4°C with one of the following primary antibodies in 2% normal donkey serum and 0.1% Triton X-100 in PBS; rat anti-mouse CD11b (AbD Serotec (MCA711), 1:1000), rabbit anti-mouse TSPO (Abcam (EPR5384), 1:250), rabbit anti-mouse GFAP (DAKO (Z0334), 1:1000), mouse anti-human 6E10 amyloid (BioLegend (803001) 1:1000), rabbit anti-mouse SV2A (Abcam (ab32942) 1:500), chicken anti-mouse MAP2 (Abcam (ab5392), 1:1000), rabbit anti-mouse NeuN (Abcam (ab177487), 1:500), rabbit anti-mouse Neurogranin (Abcam (ab23570), 1:500). Sections were washed 3 times for 10 minutes with PBS and incubated with one of the following secondary antibodies for 2 hours at room temperature in 2% normal donkey serum and 0.1% Triton X-100 in PBS; Alexa Fluor 594 nm Donkey anti-rat IgG 1:500 (for CD11b), Alexa Fluor 488nm Donkey anti-rabbit IgG 1:500 (for TSPO, GFAP, SV2A), Alexa Fluor 594nm Donkey anti-mouse IgG 1:500 (for 6E10), Alexa Fluor 488nm Goat anti-chicken. The sections were washed a further 3 times and a coverslip was applied using Prolong™ anti-fade kit (Molecular Probes, Invitrogen). An extra step for antigen retrieval using citrate buffer was carried out for SV2A and neurogranin. Double staining was carried out for CD11b+TSPO, CD11b+GFAP and 6E10+TSPO and to allow the visualisation of microglia and astrocytes with TSPO expression and Aβ burden. Double staining was also carried out for MAP2+NeuN to look at neuronal density and synaptic markers. Single staining was carried out for SVA2. Images of the hippocampus and cortex were collected between bregma -

2.06mm and -2.30mm on a Olympus BX51 upright microscope using a 4×/0.13, 10×/0.30 or 20×/0.50 UPlanFLN objectives and captured using a Coolsnap ES camera (Photometrics) through MetaVue Software (Molecular Devices). Specific band pass filter sets were used to prevent bleed through from one channel to the next. Images were then processed and analysed using ImageJ (http://rsb.info.nih.gov/ij).

Statistical analysis

The data were statistically analysed using GraphPad Prism version 5.04. Data are expressed as mean ± SD. Paired *t* tests were used to determine differences in exploration in phase 1 of both the NOR and NSR tests and alteration in the Y maze. Two way analysis of variance (ANOVA) were carried out to test the effect of strain and age on DI, metabolite and [^{18}F]DPA-714 levels in WT and TG mice with post-hoc analysis using Dunnet's and Sidak's tests. Main effects were considered significant if $p \leq 0.05$. Interactions were deemed significant if $p \leq 0.1$.

Results

Behavioural Analyses

To test whether non-associative working and recognition memory was affected at different ages, Y maze and novel recognition tests were carried out. No significant differences were seen in the exploration of identical objects on the left and right in phase 1 of the NOR (Figure 4a). TG and WT mice display similar positive DI results at 6 months suggesting a preference for the novel in both groups at this age. A two-way ANOVA of DI revealed a significant gene × age interaction (Figure 4b, $p=0.0225$). Multiple comparisons revealed a significant decrease in DI values in TG mice compared to WT mice at 12 months of age suggesting increased cognitive decline in TGs at this time-point.

In the NSR no side bias was seen in the exploration of identical scents on the left and right in phase 1 demonstrated by so significance in paired t tests (Figure 4c). A two-way ANOVA of DI results did not reveal any significant effects of interaction of gene or age (Figure 4d). High variation was seen in these animals from 12 months onwards, therefore the ability of the mice to smell was tested at this age. In the smell test neither WTs nor TGs spent significantly more time in the arms containing rabbit urine compared to fox or bobcat urine (Figure 4e) indicating olfactory dysfunction from at least 12 months of age.

WT and TG mice performed well in the Y maze at 6 months of age with no significant differences seen in the percentage of successful alternation between arms in TG when compared to WTs (Figure 4f), suggesting no memory deficit at this age. However, at 12 and 18 months of age the WT mice perform better than the TG mice with significantly increased percentages of successful alternation achieved in the WT group compared to TGs, indicating decline in working memory from 12 months of age in the TGs.

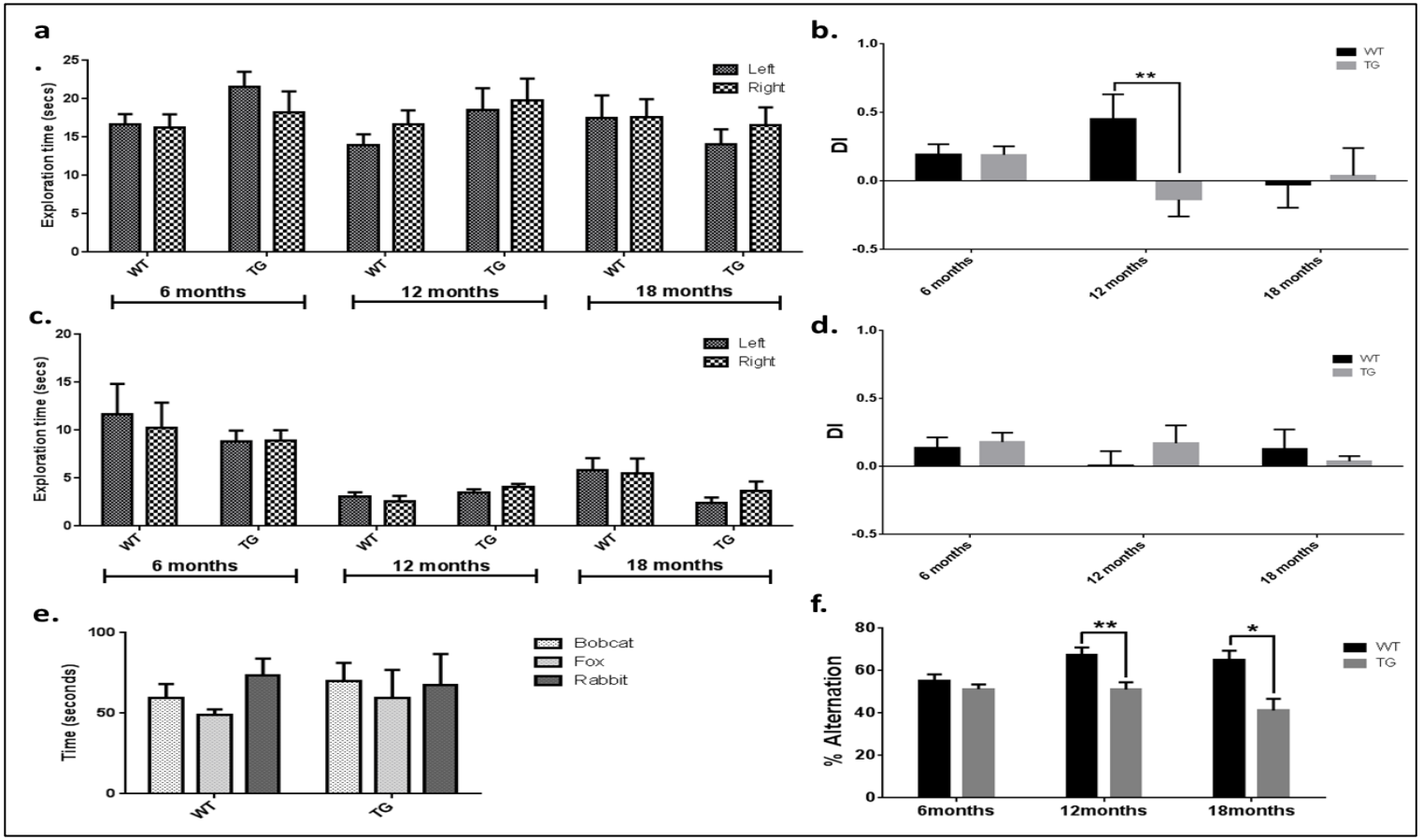

Figure 4 Exploration times of right and left objects in phase 1 of the NOR and NSR **(a&c).** Discrimination index of exploration of the novel and the familiar in phase 1 and 2 (WT n=11, TG=15 at 6 months, WT n=6, TG=9 at 12 months, WT n=6, TG=6 at 18 months) **(b&d)** Time spent in the presence of predator and non-predator urine (n=4) **(e)**. Alternation in the Y-maze demonstrated decreased working memory in TG mice compared to WT mice from 12 months of age **(f)**. Results are shown as mean±SEM. Statistical analysis was performed using t-tests and two-way ANOVAs.

In vivo [^{18}F]DPA-714 significantly increases as a result of AD-like pathology and age

To assess neuroinflammation differences between APP_{swe}×$PS1_{\Delta e9}$ and WT mice [^{18}F]DPA-714 NUV_{cb} was compared at 6, 12 and 18 months in the hippocampus and cortex ROI and the subcortical ROI (Figure 5a). A two-way ANOVA revealed a significant effect of gene (p=0.02) and age (p=0.03) on [^{18}F]DPA-714 uptake in the hippocampus and cortex, and an effect of age only for the other subcortical regions (p=0.0008). Multiple comparisons analysis revealed that hippocampal and cortical [^{18}F]DPA-714 NUV_{cb} was significantly increased in 18 when compared to 6 month old TG mice (Figure 5b, +7%, p=0.03) and when compared to age-matched WT (+7%, p=0.04). This effect was not significant in the WT mice. A significant increase in [^{18}F]DPA-714 uptake was also seen with multiple comparisons in other subcortical regions of 18 months old TG mice when compared to 6 months old TG mice (Figure 5c, +14%, p=0.002). The same trend was observed in the subcortical regions of WTs but was not significant (**Figure**Figure 5c, p=0.058).

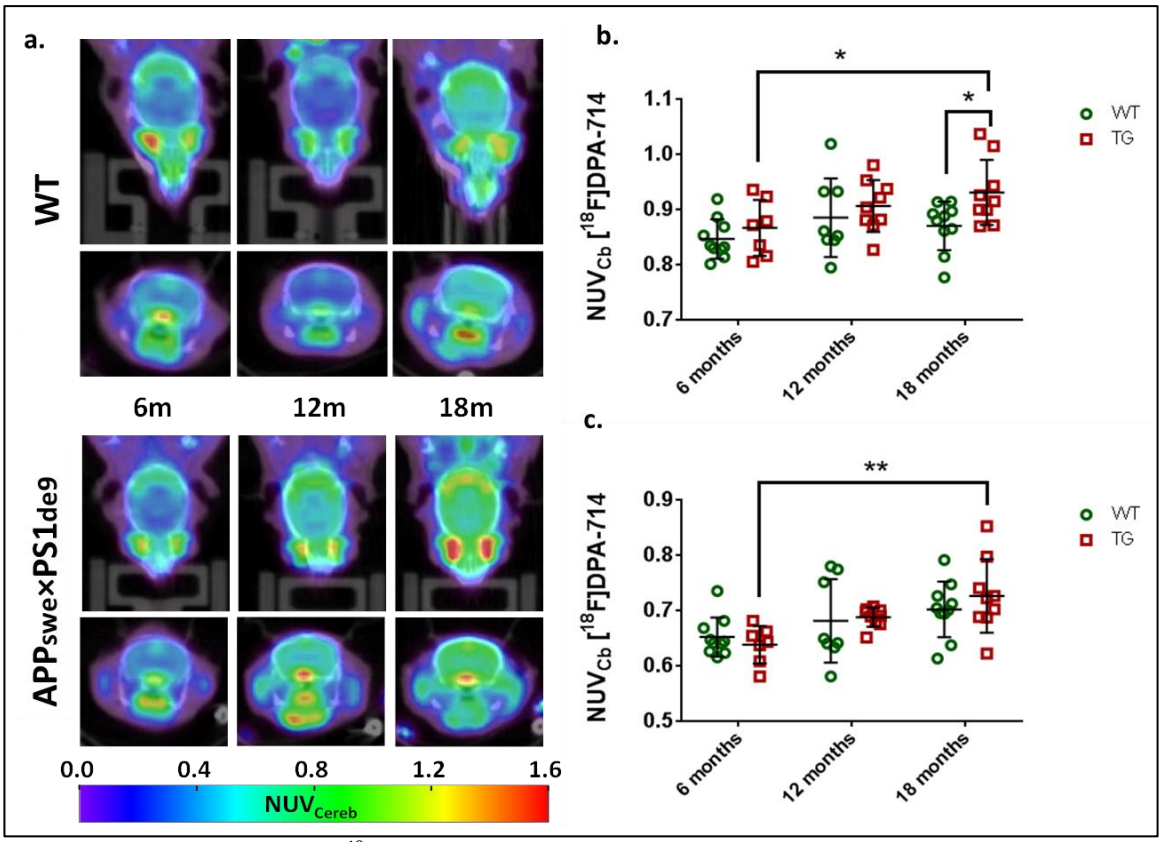

Figure 5 PET images showing [^{18}F]DPA-714 uptake in WT and APP_{swe}×$PS1_{\Delta e9}$ mice at 6 (WT n=10, TG=7), 12 (WT n=8, TG=9) and 18 months (WT n=10, TG=9) of age **(a)**. NUV_{cb} values in the hippocampus and cortex **(b)** and other subcortical regions **(c)**. Results are expressed as mean±SD. Statistical analysis was performed using two-way ANOVA followed by Sidak and Dunnet's post hoc analysis (*p≤0.05, **p≤0.01).

Metabolite profiles of APP_{swe}×$PS1_{\Delta e9}$ and WTs are affected by age

Single voxel MRS was repeated in the same cohort of TG and WT mice at 6, 12 and 18 months of age in a voxel that encompassed the hippocampus and the most dorsal part of the thalamus (Figure 6a). No significant differences were seen in Cr concentration referenced to water at any age group for either WT or TG mice (Figure 6b), allowing metabolite data to be expressed as a Cr ratio.

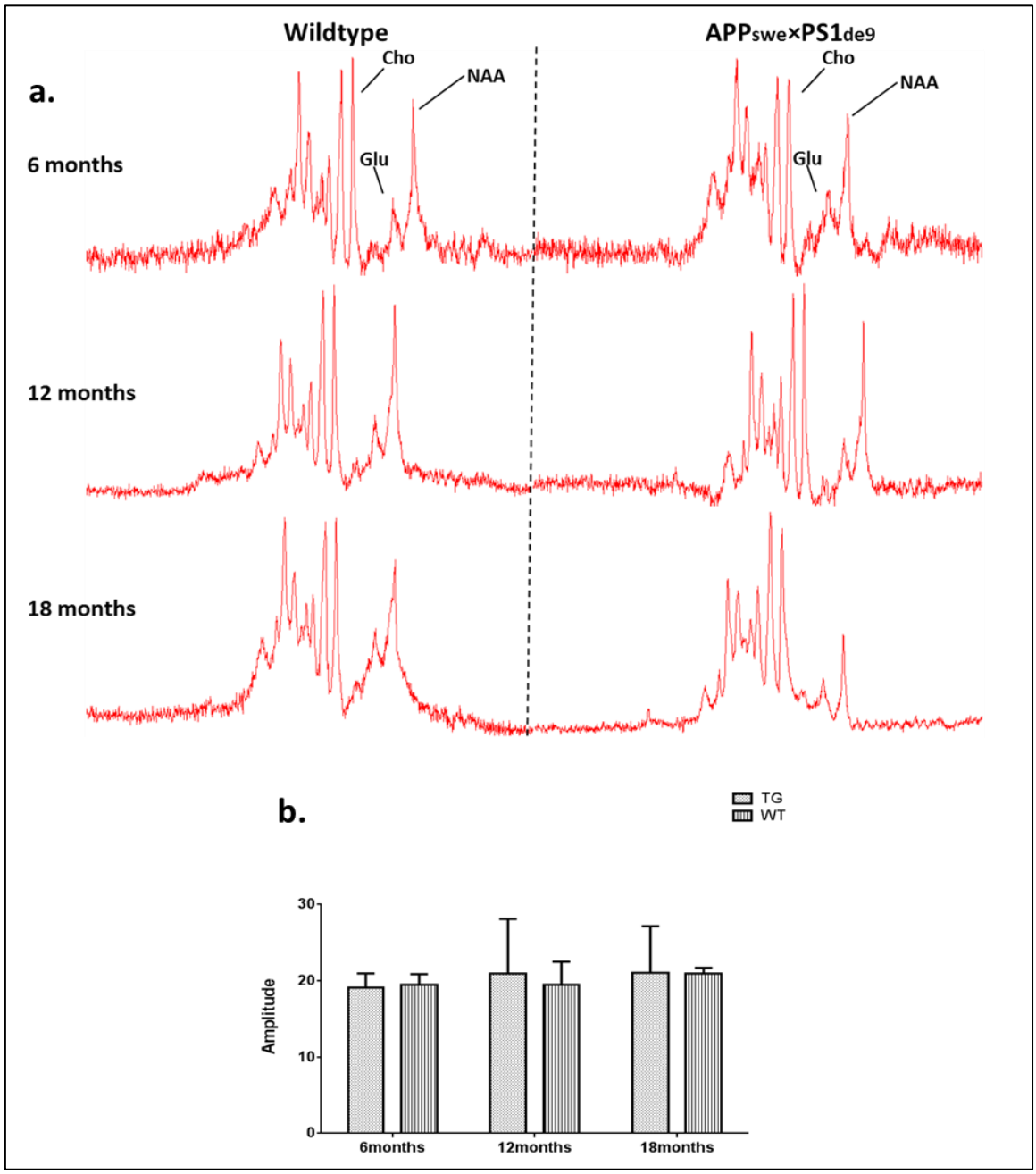

Figure 6 Example spectra from WT and TG mice at 6, 12 and 18 months **(a)**. Reduced Glu/Cr levels were seen in old WT mice. No differences were observed in the Cr concentration (mean±SD) referenced to water **(b)**. Statistical analysis was performed using two-way ANOVA.

The two-way ANOVA revealed an overall significant effect of age and a significant gene × age interaction (p=0.0866) on hippocampal and thalamic NAA levels (p=0.0006). NAA levels were significantly lower in 18 months TG mice (-58%, Figure 7Figure b, p≤0.0001) when compared to 6 months TG mice using multi-comparisons analysis. This effect was seen in the WT (-20%) but was not significant *post hoc*. A significant effect of age but not of gene or interaction was observed on Glu (p=0.0003) and tCho (p=0.0016) levels. This resulted in reduced Glu (-53% average across groups from 6 to 18 months) and increased tCho (+71% average across groups from 6 to 18 months) levels with age.

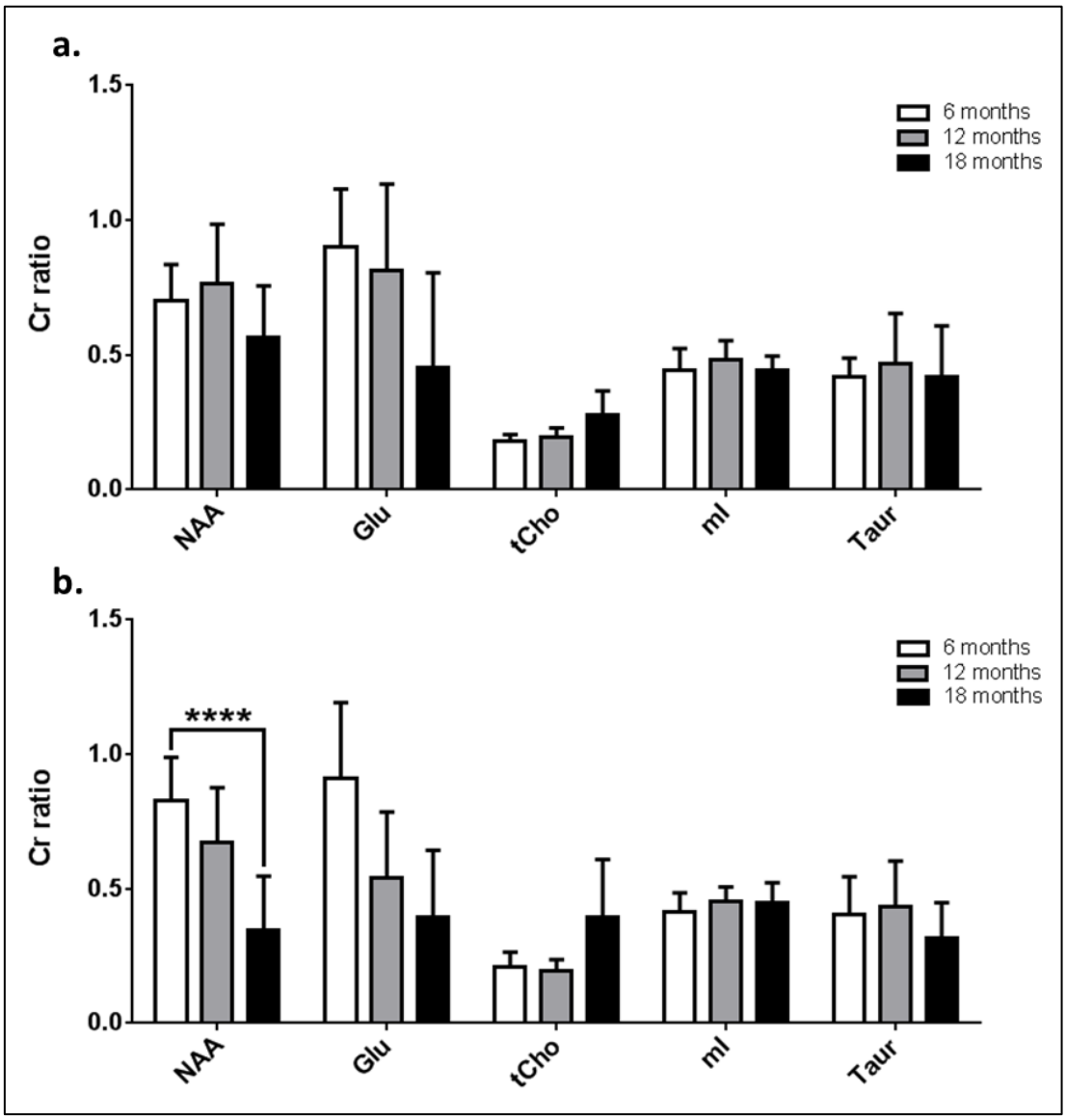

Figure 7 Metabolites expressed as creatine ratios in WT (n=6) **(a)** and TG (n=8) **(b)** mice at 6, 12 and 18 months of age. Results are shown as mean±SD. Statistical analysis was performed using two-way ANOVA followed Dunnet's *post hoc* analysis. (versus 6 month TG ****p≤0.0001)

Immunohistochemistry

Immunohistochemistry was carried out to qualitatively assess neuroinflammation, Aβ burden and neuronal integrity. Double staining for TSPO and CD11b revealed an increase in both proteins with age in the hippocampus (Figure 8a) and cortex (Figure 8b) of the TG. Arrows indicate regions of high TSPO and CD11b staining. In the TG there was regional co-expression of TSPO and CD11b in the hippocampus from 12 months of age, whereas this was evident from 6 months of age in the cortex. TSPO staining was only visible in the vessels of WT animals in both regions. No CD11b staining was evident in the WTs at any age. Double staining for TSPO and Aβ pathology revealed similar results. An age dependent increase was seen in Aβ burden in both the hippocampus (Figure 9a) and cortex (Figure 9b) of TG mice. Aβ staining was sparse at 6 months but increased with age revealing a heavy burden by 18 months. TSPO and 6E10 demonstrated good regional co-expression at 6 and 12 months in the cortex of TG mice, indicating increased microglial activation around Aβ plaques. No Aβ staining was evident in the WT mice at any age. No differences were seen in double staining for MAP2 and NeuN between TG and WT mice or with age in the hippocampus or cortex (Figure 10a-b). Similarly, no differences were revealed with single staining for SV2A and neurogranin (Figure 11a-b), indicating that neuronal death could not be detected in this model.

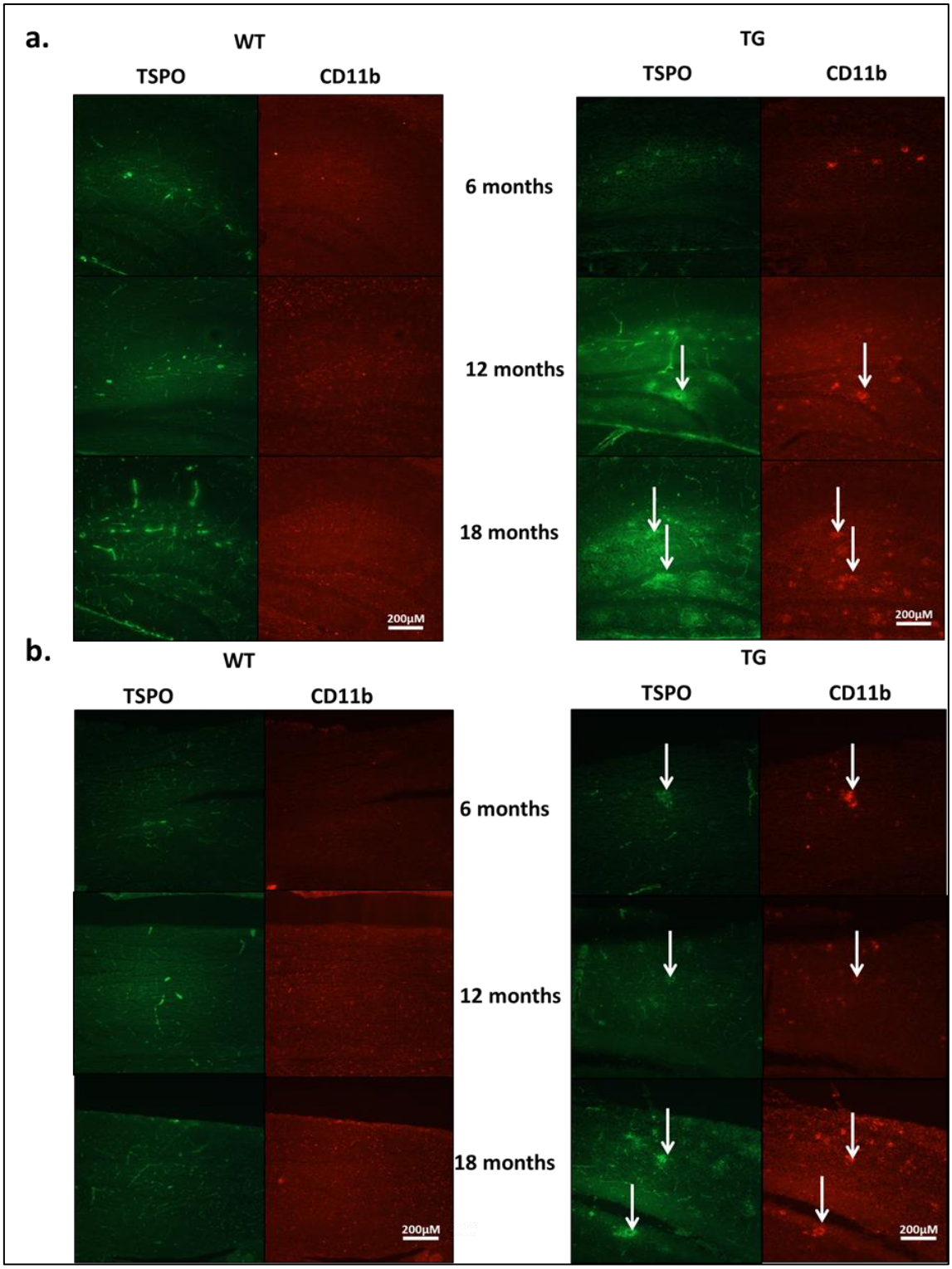

Figure 8 Immunoreactivity of CD11b (red) and TSPO (green). Representative images of double staining in the hippocampus **(a)** and cortex **(b)** of WT and $APP_{swe} \times PS1_{\Delta e9}$ mice at 6, 12 and 18 months of age. Pictures were taken at 10x magnification between bregma -2.06mm and -2.30mm.

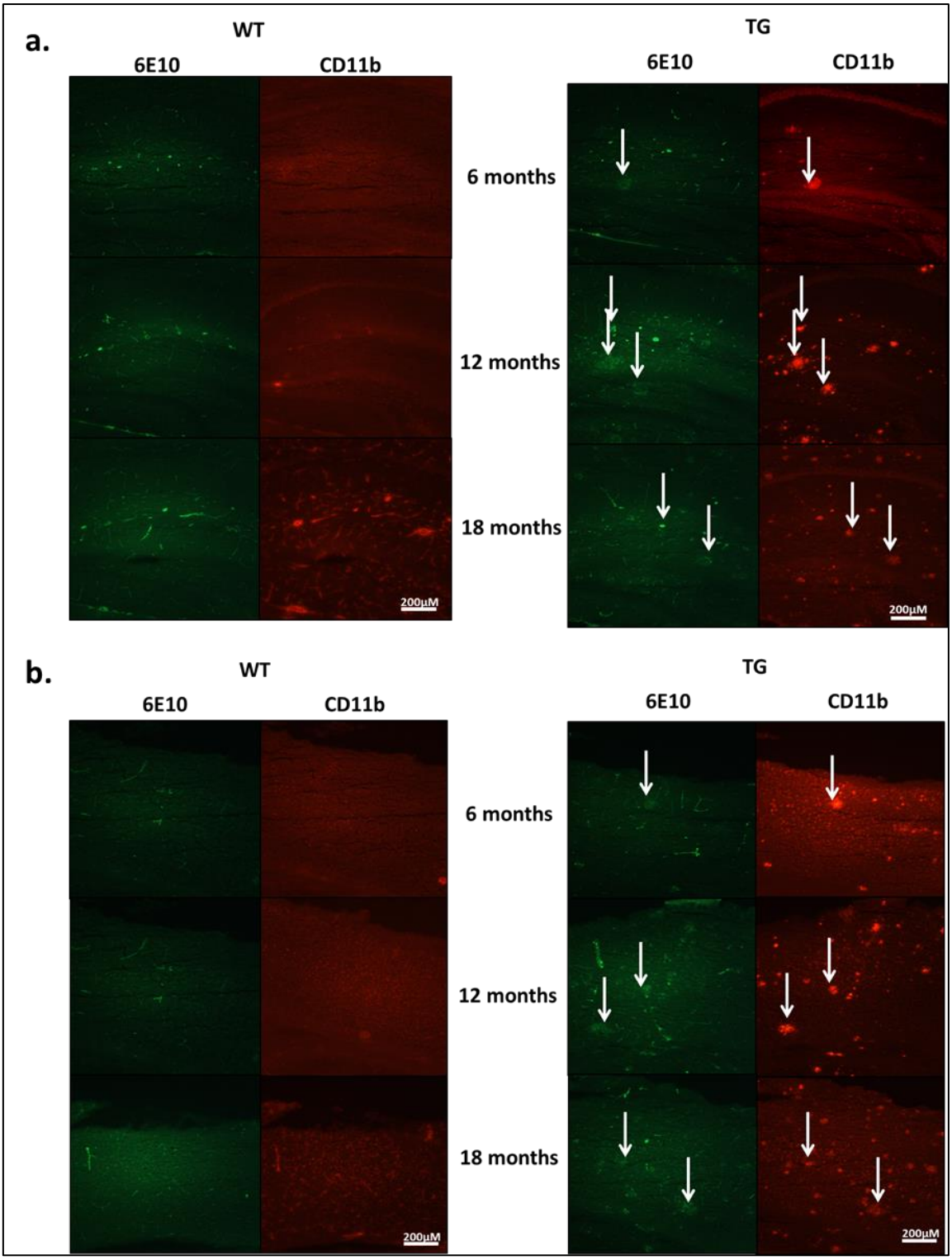

Figure 9 Immunoreactivity of Aβ (red) and TSPO (green). Representative images of double staining in the hippocampus **(a)** and cortex **(b)** of WT and APP_{swe}×$PS1_{\Delta e9}$ mice at 6, 12 and 18 months of age. Pictures were taken at 10x magnification between bregma -2.06mm and -2.30mm.

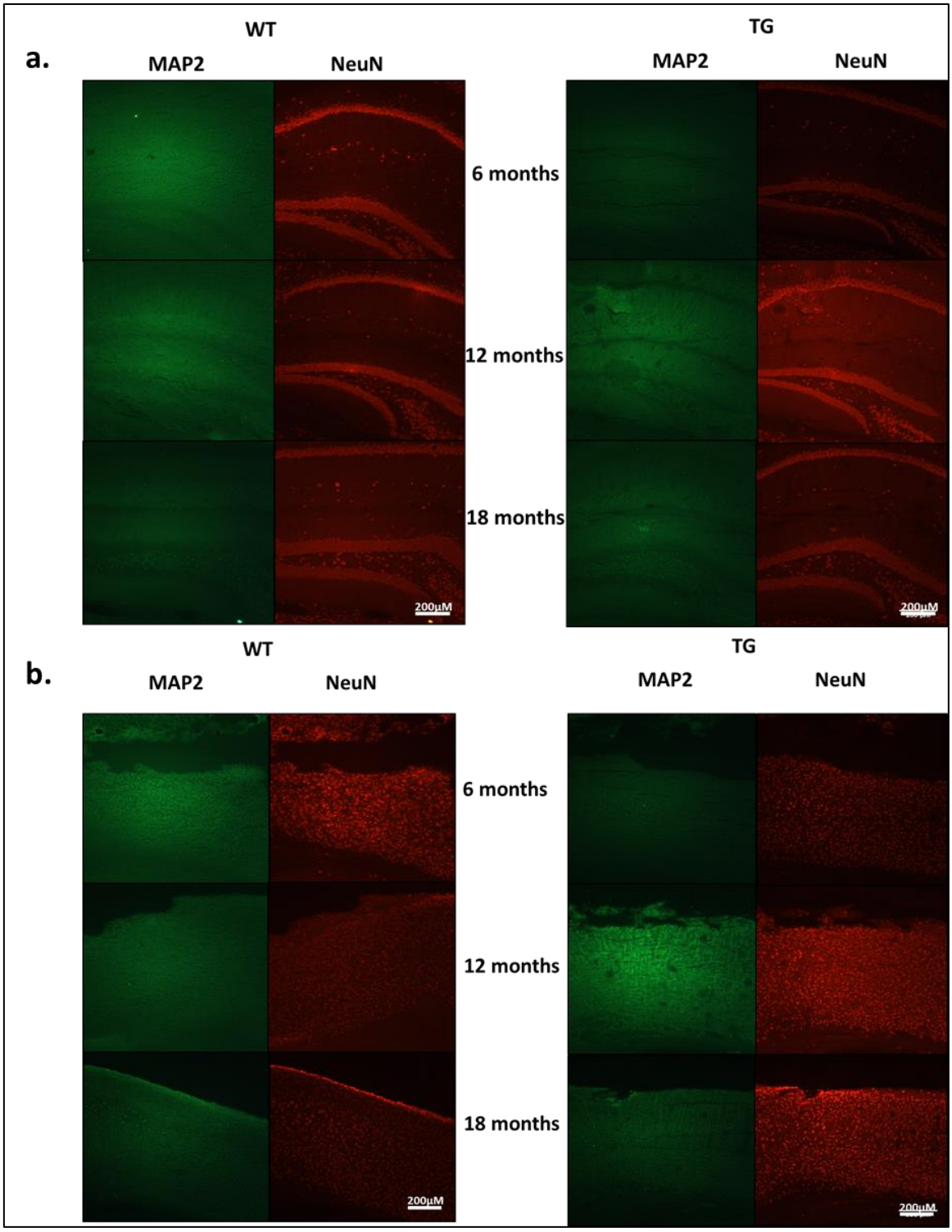

Figure 10 Immunoreactivity of MAP2 (green) and NeuN (red). Representative images of double staining in the hippocampus **(a)** and cortex **(b)** of WT and APP_{swe}×$PS1_{\Delta e9}$ mice at 6, 12 and 18 months of age. Pictures were taken at 10x magnification between bregma -2.06mm and -2.30mm.

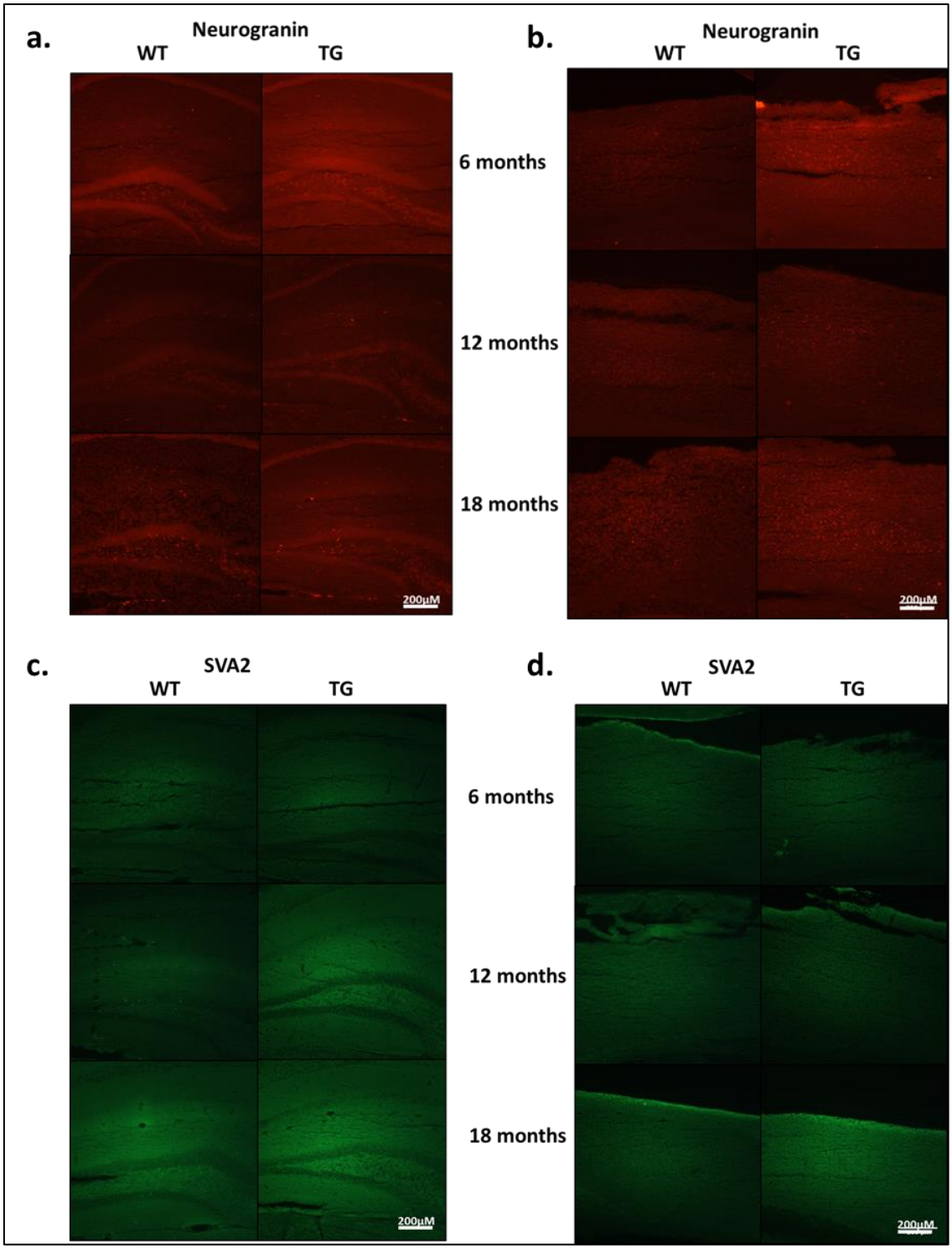

Figure11 Immunoreactivity of SV2A (green) and neurograinin (red). Representative images of single SV2A staining in the hippocampus **(a)** and cortex **(b)** and neurogranin staining in the hippocampus **(c)** and cortex **(d)** of WT and APP_{swe}×$PS1_{\Delta e9}$ mice at 6, 12 and 18 months of age. Pictures were taken at 10x magnification between bregma -2.06mm and -2.30mm.

Discussion

Cognitive assessment

TG mice displayed deficits in non-associative recognition memory and working memory from 12 months of age in this model. Intact working memory prior to this was expected as significant pathology is not manifested until 6 months of age in this animal model (107, 108), hence their cognitive ability should match that of the WT mice. Previous studies have also found that at an early time-point TG AD mice display good cognitive performance in a variety of memory based tests. In line with our result, the APP_{swe}×$PS1_{\Delta e9}$ model has been shown to perform well in the Morris water maze at 3 and 5 months, with no cognitive deficits evident until 8 months of age, whereas the memory of WT mice remains intact at 8 months (203, 206). It has also been shown that other models of AD have an intact memory at an early age that declines over time (103, 236). We found that WT mice retained memory later than TGs in the NOR and Y maze. WTs demonstrated good working memory in old age, with a higher percentage of alternation in the Y-maze compared to TG at 12 and 18 months. However, no effects were seen in the NSR and high variation was observed from 12 months. We hypothesised that these animals may have altered olfaction by this age and therefore carried a smell test using predator and non-predator urine. Exposure to predator (bobcat and fox) and non-predator (rabbit) urine in a Y-maze revealed that neither group spent significantly more time in any arm. An increased amount of time in the arm with non-predator urine would be expected in mice with intact olfaction; hence this result suggests that both WTs and TGs have a decreased sense of smell from 12 months of age and the variation seen from this age may be down to reduced olfaction rather than memory induced. Nonetheless, cognitive decline occurs with age in these TG mice, which is in support of our working hypothesis that cognitive performance decreases with age at a faster rate in the TG mice compared to the WT.

Neuroinflammatory status

Here we present increased neuroinflammation as an effect of AD-like pathology and age. Increased [^{18}F]DPA-714 NUV_{cb} was found in the hippocampal and cortical region of old TG mice compared to WT mice. This increase was only statistically significant at 18 months of age despite increased Aβ, GFAP and CD11b immunostaining evident from 12 months of age. Serriere *et al* 2015 investigated [^{18}F]DPA-714 uptake in the same mouse

model at 6, 9, 12, 15 and 19 months of age and revealed increased neuroinflammation from 12 months of age (169). NUV ratios referenced to the cerebellum were increased in the cortex of TG mice at 12 and 19 months and in the hippocampus at 19 months of age. In our analysis methods, we pooled both of these areas as one region as both regions present AD pathology and because the size of the pooled ROI is more compatible with the resolution of μPET imaging with our scanner (~1.6mm). Therefore, by pooling the hippocampus and cortex into a single ROI, we may have masked the possible effect in each region, and hiding the increased neuroinflammation that appears earlier in the cortex. This is in line with what we observed in the immunohistochemistry results, with increased CD11b and TSPO co-localisation occurring in the cortex earlier than in the hippocampus in this model. Although a significant increase is seen with age in [^{18}F]DPA-714 uptake in the other subcortical regions, no significant differences were found when comparing TG to WT at any age, which is line with other reports and the lack of pathology in these areas. Increases in TSPO expression have been found in other models of AD (117, 166, 167) and in human AD (69, 70, 220, 221), indicating that elevated neuroinflammation is a consistent characteristic of this disease.

We also report significant increases in [^{18}F]DPA-714 uptake with age in the hippocampal-cortical and subcortical ROIs. Multiple comparisons analysis revealed that this increase only remained significant in the TG group suggesting that the effect is driven by the TG data. Increased neuroinflammation was observed in old TG mice compared to young TG mice in the hippocampal and cortical ROI, which is in line with the *ex vivo* data revealing progressive amyloid, GFAP and CD11b staining as well as TSPO expression in these regions. Increased [^{18}F]DPA-714 uptake was also demonstrated in the other subcortical regions of TGs revealing an increase in neuroinflammation with age that appears to be independent of amyloid pathology as these regions have little to no burden. However, a trend towards significance was observed in the WTs in the subcortical ROI, suggesting that neuroinflammation in these regions may increase as a result of normal aging. Our results are in agreement with previous reports showing a significant effect of both age and gene on TSPO PET in the same model using [^{18}F]GE-180 (165). Increased [^{18}F]GE-180 uptake was seen in the hippocampus of old TGs compared to age matched WTs and young TG and WT mice. In addition increased [^{18}F]GE-180 uptake was also seen in the whole brain of old TGs compared to young TGs. This age effect was replicated in

WT mice with significant increases in uptake from young to old mice in both hippocampal and whole brain, implicating both normal aging and AD pathology on neuroinflammatory status. Increased neuroinflammation has also been observed as an effect of aging in both humans (237-239) and in the WTs of other described AD models (117). Altogether, our results further support previous findings that age can significantly alter microglial responses, which are modified further in the presence of neurodegenerative diseases such as AD.

Metabolite Profile

Metabolites were represented as Cr ratios in this study as Cr concentrations remained constant in both TG and WT mice at each age. This has been previously reported in this model (206), however it was important to assess this as elevated Cr levels have previously been reported in a different mouse model of AD (TASTPM) *in vivo* at an early age (210) and at a later age using brain extractions *in vitro* (240).

In contrast to previous reports we did not observe an overall effect of gene on any metabolite in this study including mI levels, despite observing increased neuroinflammation in TG mice with PET in addition to *ex vivo* methods. This lack of agreement between neuroinflammatory status and mI results questions mI as a putative marker for gliosis. In support of this, no alterations in mI levels were found in the same model by *Jansen et al* (206) or in similar studies of the TG_{2576} (209) and PS2APP (208) mouse models. In a clinical study mI was found to be associated with amyloid pathology and not neuroinflammation (185), therefore it is possible that mI levels more closely represents amyloid load. On the other hand we have extensive amyloid burden in this model without seeing mI alterations. These results are in contrast to many other reports demonstrating increased mI levels and decreased NAA in clinical AD (185, 192-194, 241) and AD models (201-205, 210, 211, 214-216). *Chen et al* reported significantly higher mI/Cr levels in the $APP_{swe}\times PS1_{\Delta e9}$ compared to WT mice as early as 3 months of age (205). However this voxel included a large proportion of cortical as well as hippocampal regions. In our and in previous results inflammation and plaques appear first and more frequently in cortical regions than hippocampal regions which may account for this, however we did not access this at 3 months of age in this study and it is possible that there

is an increase in mI that occurs early in this model that we may have missed as they reported increased hippocampal GFAP staining from 3 months of age without the presence of amyloid pathology. However increased inflammation and amyloid pathology has previously been reported from 6 months with further increases with age. This study also reports reduced NAA/Cr from 5 months of age. In contrast, other studies did not report significant NAA/Cr reduction in this model until later ages. Jansen *et al* reported decreased NAA/Cr levels at 12 months of age, with no alterations evident in any other metabolite or at the earlier age of 8 months (206). Xu *et al* illustrated reduced hippocampal NAA/Cr from 16 months, which was associated with increased pathology in this region (207). Jack *et al* found decreased NAA/Cr, Glu/Cr and increased mI/Cr in a different APPxPS1 model (APPswe-PS1M146L) with increasing age in a voxel encompassing the hippocampus and cortex (202). Though, they took these mice to a greater age than in this study and only saw acceleration in mI levels in the TG at a later age of 20 months. Nonetheless, increased mI and decreased NAA levels have been shown in the TASTPM (210), PSAPP (216), APPxPS1 (201, 204), and 3xTG (215) mouse models of AD suggesting that they may be good markers of disease in these models. Although we did not get an overall effect of gene on NAA levels in this study, we do see a significant effect of aging and a significant gene × age interaction. This resulted in a significant decrease in NAA from 6 to 18 months in the TG mice that was not significant in the WT mice using multiple comparisons. This suggests NAA levels are influenced by both age and gene and although reduced NAA appears to be a normal effect of aging, this effect is accelerated in the TG mice. This underlines the importance of understanding the effects of normal aging on brain metabolites or other potential biomarkers, as in this instance the age effect is most likely confounding the possible detection of a gene effect by the two-way ANOVA. Reductions in NAA with age have been reported previously in this model. Xu *et al* found a significant decrease in hippocampal NAA/Cr in 16 month APP_{swe}×$PS1_{\Delta e9}$ TG mice compared to younger TG mice. In agreement with our findings this effect was not seen in the WT mice. A similar effect of age on NAA levels has also been shown in a 3xTG mouse (215).

We also report age to have a significant effect on Glu and tCho levels without the presence of a gene effect or an interaction. Glu levels were decreased and tCho levels increased in both WT and TG mice. This result suggests that these effects are a result of normal aging in this strain. In contrast, reduced Glu and increased tCho have been reported

in mouse models of AD (201-204, 208, 209, 213, 216) and in the clinical situation (191, 193, 194, 199, 200).

Ex vivo Aβ pathology was sparse in young TG mice with increasing burden by 12 months and abundant plaque by 18 months, which is line with many previous reports in this model (107, 108, 242). Similarly low levels of CD11b, GFAP and TSPO staining were evident in the hippocampus and cortex of TG mice at 6 months of age which increased with age. Good co-localisation was observed between CD11b and TSPO immunostaining in the cortex and then later in the hippocampus. Similarly, good co-localisation was seen between TSPO and Aβ burden in the cortex of TG mice suggest increased glial activation around Aβ plaques. Similarly, strong astrogliosis was detected around microglial cells which were found only around Aβ plaques supporting the presence of both astrocytes and microglia around Aβ plaques. Microglia are known to surround plaques in human AD and have been shown to co-localize with pathology in AD models further supporting the role of neuroinflammation in AD. In contrast to our results, Ji *et al* did not find co-expression of CD11b and TSPO in the APP23 mouse model, but found co-localisation of GFAP and TSPO which were in close proximity to amyloid plaque staining (167). Whereas in a tau mouse model they found the opposite with some CD11b positive cells expressing TSPO but not GFAP positive cells, suggesting the tau and amyloid pathology may alter TSPO expression differently *in vivo* (206). TSPO expression was only visible in the vessels in WT animals. TSPO has been reported to exist in vessels and is not abnormal (243).

We did not identify any reductions in neuronal, synaptic vesicle or microtubule markers in this study. This is in line with previous reports (206) and suggests that APP mutations are not sufficient to cause neuronal loss that is observed in human AD and models with tau abnormalities. On the other hand amyloid pathology was enough to induce cognitive decline. This lack of congruency could be explained by many factors. Perhaps we are assessing the wrong neuronal/synaptic markers or the changes may be extremely specific regionally or as a result of changes in specific neuronal population (e.g cholinergic) not detectable using markers such as neurogranin or MAP2.

Conclusions

It has become evident that Alzheimer's disease is a complex multi-factorial disease in which neuroinflammation plays a pivotal role. In support of this, we report increased neuroinflammation in the form of increased [^{18}F]DPA-714 uptake and reduced neuronal function in the form of accelerated NAA reductions in the APP_{swe}×$PS1_{\Delta e9.}$ These results support the role of neuroinflammation and metabolite alteration in the pathogenesis of AD. We also show that TSPO PET can detect changes in neuroinflammation within this mouse model, however not as early as is detected using ex vivo techniques. Although TSPO PET is a viable imaging technique to study AD in animal models, the current restrictions due to resolution and brain size in mice hamper earlier detection. Moving to larger species such as rats may address this.

Acknowledgements

This research was supported by the European Union's Seventh Framework Programme (FP7/2007-2013) under grant agreement n°HEALTH-F2-2011-278850 (INMiND). The authors wish to thank all the personnel of the WMIC, especially Dr Michael Fairclough, Ms. Lidan Christie, Mr Michael Green, Mr Jamil Gregory, Ms. Carol Brough and Ms. Gemma Chapman for facilitating the study. We would also like to thank Dr Jack-Auty and Rebecca Montacute who were responsible for breeding some of the mice used in this study.

Conflicts of Interest

All authors report no conflict of interest.

Chapter 3 (Paper 2)

Longitudinal investigation of Neuroinflammatory and Neurodegenerative status of the TgF344-AD rat model of Alzheimer's disease.

Chaney A., Bochicchio D., Smigova A., Kassiou M., Davies K., Williams S., Boutin H.

Longitudinal investigation of Neuroinflammatory and Neurodegenerative status of the TgF344-AD rat model of Alzheimer's disease

Chaney A.[1], Bochicchio D.[1], Smigova A.[1], Kassiou M.[2], Davies K.[1], Williams S.[1], Boutin H.[1,3].

[1]Faculty of Biology, Medicine and Health, School of Health Sciences, University of Manchester, Manchester, M13 9PT, UK

[2] School of Chemistry, University of Sydney, NSW 2006 Australia.

[3] Wolfson Molecular Imaging Centre, Faculty of Biology, Medicine and Health, University of Manchester, Manchester, M20 3LJ, UK.

Corresponding Author:

Dr Hervé Boutin,

Wolfson Molecular Imaging Centre,

27 Palatine Road, Manchester, M20 3LJ, UK

Email: herve.boutin@manchester.ac.uk

Tel: +44 1612750078

Fax: +44 161 275 0003

Abstract

Current amyloid mouse models of Alzheimer's disease (AD) are useful but not ideal as they are missing essential characteristics of clinical AD pathology such as spontaneous Tau fibrils and neuronal loss, hence there has been a drive to create new models that develop full AD-like pathology. The transgenic (TG) TgF344-AD rat has been reported to develop amyloid plaques, neuroinflammation, neuronal loss and cognitive decline, but also neurofibrillary tangles despite only expressing APP and PS1 mutations, in an age dependent manner similar to that seen in clinical AD. Hence, this model appears to be appropriate for the investigation of the early mechanisms of AD such as neuroinflammation, neuronal dysfunction and cognitive deficits. Here we investigate these parameters using [^{18}F]DPA-714 positron emission tomography (PET) and magnetic resonance spectroscopy (MRS) at 6 and 12 months as well as behavioural assessments at 3, 6, 9 and 12 months of age. No significant cognitive decline was observed in these animals by 12 months in the novel object recognition test; however increased anxiety-like behaviour was seen at 9 and 12 months in the TG rats in the social interaction test. Increased neuroinflammation as assessed by PET was observed in the TG rats in the hypothalamus (+23%) and thalamus (+23%). Increased hypothalamic Glu levels were identified in TG rats that was not seen in age matched WT rats. Increased neuroinflammation was seen as an effect of age in the cingulate cortex, frontal cortex, somatosensory cortex and striatum Effects of aging were seen on N-acetylaspartate, glutamate, choline and taurine. Here we show evidence of increased neuroinflammation in the TgF344-AD rat, which precedes known plaque deposition as well as alterations in neuroinflammation and metabolite profile as a result of normal aging.

Key words: Alzheimer's disease, animal models, positron emission tomography, magnetic resonance spectroscopy.

Introduction

Alzheimer's disease (AD) has become a major health problem and a better understanding of the pathophysiology is urgently needed. An unmet need exists for robust early markers of disease than can aid early diagnosis and treatment development. An effective way to advance the knowledge and understanding of a disease is to investigate its progression within a living organism. This is done for various diseases through the use of pre-clinical animal models. Clinical AD pathology is characterised by progressive deposition of amyloid plaques (Aβ), neurofibrillary tangles (NFTs), neuronal loss and increased neuroinflammation, however animal models of disease are generally limited to displaying certain aspects of AD. Genetically modified mouse models are commonly used in AD research allowing the investigation and confirmation of markers of disease induced by familial AD mutations. This is integral to our understanding of the mechanisms underlying disease as the use of preclinical models allows confirmation of results ex vivo that is not plausible in the clinical situation. Although they have many benefits, they are not ideal models as they do not display all the neuropathological characteristics seen in the clinical situation. Mouse models expressing mutations associated with familial AD such as the APP_{swe}×$PS1_{\Delta e9}$ model used in Chapter 2 develop AD-like amyloid pathology such as age dependent increases in senile plaque deposition, soluble and insoluble $A\beta_{40}$ and $A\beta_{42}$, and cerebral amyloid angiopathy (CAA) (102, 105, 107-109, 244). Increased neuroinflammation and cognitive decline is also seen in these models (245, 246). In addition, the amyloid pathologies observed are structurally similar to those seen in clinical AD; hence these models are beneficial in gaining a better understanding of amyloidogenic pathways such as amyloid induced neuroinflammation and memory loss. However, these models do not develop neuronal loss or NFTs without the integration of tau mutations that are associated with frontotemporal dementia as no tau mutations have been found for AD. Although, some amyloid models have been reported to express increased hyperphosphorylated tau, this does not develop into tau aggregates similar to NFTs (247, 248). This could be as a result of an inability of mouse tau to aggregate or perhaps human amyloid pathology cannot induce tau pathology in these mice models. As tau is suggested to drive neuronal loss this also results in models without this characteristic. This lack of concordance with the clinical situation may be in some part responsible for the low success in translatability of AD therapies. A good example of this would be the amyloid

vaccination studies, where TG mice underwent active immunization against Aβ. Mice displayed positive results with good Aβ clearance, immune responses and tolerability (19). However, when immunization studies were brought to clinical trials they had to be halted at phase III due to symptoms of meningoencephalitis observed in probable AD patients (249).

Considering this, there is a need for improved animal models of disease as currently available mouse models do not replicate the human situation fully. More recently transgenic AD rat models have been developed. Rat models of disease are desirable as the larger brains are beneficial for neuroimaging research. Rats generally express richer behavioural phenotypes than mice which is beneficial for cognitive assessment. Early genetic rat models were unsuccessful in precipitating extracellular amyloid plaques (111) or had low diffuse pathology not comparable to AD (112). The APP×PS1 rat model generated by Flood *et al* displayed dense fibrillar plaques, phosphorylated tau in close proximity to plaques and overall Aβ levels similar to those observed in the equivalent mouse model (250). Similarly, the McGill-R-Thy1-APP model generated by Leon *et al* displayed complete AD-like amyloid pathology, cognitive deficits and increased neuroinflammation (113), however neither reported neuronal loss or NFT-like tau pathology. A new model, the TgF344-AD rat, described by Cohen *et al* (114) demonstrated an age-dependent progressive amyloid pathology including plaque deposition, CAA, inter-neuronal and soluble amyloid as shown by immunohistochemistry, ELISAs, western blots and confocal microscopy, in regions associated with and at levels comparable to that observed in clinical AD. Moreover, NFT-like tau pathology as well as neuronal loss and neuroinflammation were reported providing full AD-like pathology. In this study Cohen *et al* characterised this model at 6, 16 and 26 months of age. Increased $A\beta_{40}$ and phosphorylated tau were reported as early as 6 months with plaque and NFT deposition by 16 months. Finally, increased microglial and astrocyte activation were detected as early as 6 months of age. Hence this model seems to be a good candidate to investigate early markers of AD. Here we investigate earlier time-points in this model than previously described, with a focus on investigating neuroinflammation and degeneration markers using PET and MRS at 6 and 12 months. Neuroinflammation can be assessed by exploiting the increased expression of the TSPO receptor by activated microglia with PET imaging and has also been reported to be linked to *myo*-inositol (mI) levels assessed by

MRS, hence we wanted to assess whether the early increased cellular inflammation reported in this model can be quantified by these non-invasive methods. Neurodegeneration can also be assessed using MRS by measuring the neuronal marker N-acetylaspartate (NAA), the neurotransmitter glutamate (Glu) as well as other metabolites such as choline-containing compounds (Cho), creatine + phosphocreatine (Crn) and taurine (taur). We aim to further characterise the model using imaging at 6 and 12 months of age as well as assessing cognitive abilities at 3, 6, 9 and 12 month of age. To our knowledge this is the first study to assess neuroinflammation and metabolite profile using these methods in this rat model of AD.

Methods

Animals

Two male and female wild-types (WT) Fisher and TgF344-AD with the APP_{swe} and $PS1_{\Delta e9}$ mutations were purchased from Prof T. Town lab (University of Southern California) and were set up as breeding pairs in house at the Biological Services Unit in the University of Manchester. A total of 11 male TGs and 10 male wild-types Fisher rats (WTs) were originally chosen for the imaging and behaviour studies. However, 1 TG was found dead at 5 months of age. Therefore, 10 TGs and 10 WTs were used to repeatedly measure imaging and behavioural outcomes. These were chosen based on cognitive performance at 3 months of age. Rats had high anxiety levels and low locomotor activity, therefore rats that expressed the most exploratory behaviour at this age were chosen for continued behavioural assessment and imaging. Handling of these animals was increased to reduce anxiety behaviour with the tester. All animals were housed in groups of 2-4 in cages with individual ventilation, environmental enrichment and constant access to food and water. A 12:12 hour cycle of light and dark was used, with light from 7am until 7pm. All experiments were carried out in accordance with the Animal Scientific Procedures Act 1986, following internal ethical review at the University of Manchester.

Study Design

The study design is set out in Figure 1. Cognitive assessment was carried out at 3, 6, 9, and 12 months, whereas imaging was carried out at 6 and 12 months of age. These time-points were chosen as only 6, 16 and 26 month time-points have previously been

investigated in this model, and resulted in huge pathology progression from 6 to 16 months of age (114). Therefore we wanted to investigate more frequent early time-points. A minimum gap of a week was given between anaesthetising animals for imaging and conducting behavioural tests. Imaging experiments were carried out during the light phase, however behavioural assessments begun at the end of the dark phase (5-6 am) as the rats were shown to be more active and express exploratory behaviour at this time.

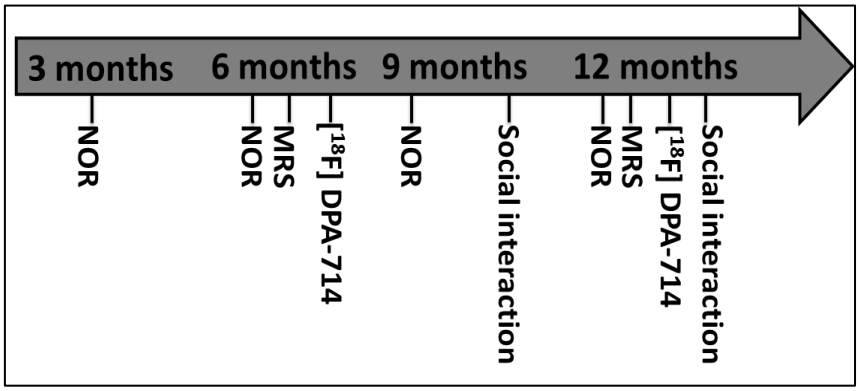

Figure 1 Experimental study design involved behavioural time-points at 3, 6, 9 and 12 months of age and imaging time-points at 6 and 12 months of age. NOR – novel object recognition behavioural test

Behaviour

The Fisher strain was found to be highly anxious, therefore animals were extensively handled every day for a minimum of 3 days prior to behavioural testing (3 weeks of handling was given for the first two time-points and was reduced to 3 days by 12 months). Animals were initially habituated to the test arena with littermates for 30 minutes the day prior to the 3 and 6 month tests. This became unnecessary as they were tested more frequently in the same arena.

Novel Object Recognition Tests

Novel object recognition (NOR) test was carried out in WT and TG rats at 3, 6, 9 and 12 months of age to assess short-term non-associative working memory (228). All NOR tests were carried out at the end of the dark phase (5am-7am) in 3% light. A square Plexiglas arena (52 × 52 × 31 cm) with black walls and a white floor, and an overhead camera were used for the test environment. All tests were recorded and analysed later to

allow for natural behaviour. The NOR test involved a 3 minute acquisition phase, 3 minute delay and a 3 minute retention phase (Figure 2a). During the acquisition phase animals were exposed to two identical objects (such as a metal can or plastic bottle, which are easily cleanable and do not retain scents when washed with 70% ethanol), and time spent exploring the left and right objects was quantified. The delay phase involved putting the rats into individual unfamiliar cages. The retention phase involved a novel object being switched with one of the familiar objects from the acquisition phase, and time spent exploring the novel and familiar objects was quantified. This time was used to quantify the discrimination index (DI) for each animal, which is expressed as the novel minus the familiar time divided by the total time giving values ranging from -1 to +1. A minus value indicated more time spent with the familiar, a positive value indicated more time investigating the novel and a zero value indicated equal time investing both. In addition, total exploration times in the acquisition phase and retention phase were quantified to assess the amount of time interacting with the objects in both WT and TG rats as this strain has been shown to show low motor activity in males as well as high anxiety. An exploration time of each side in the acquisition phase was assessed to ensure there was no side bias. Arenas and objects were cleaned with 70% ethanol between trials. Three different objects were rotated as the familiar and novel objects and the side that contained the novel object alternated for each rat with every time-point. A threshold was set for minimum exploration to be included in discrimination analysis with animals spending less than 2 seconds total exploration time excluded as well as animals that displayed same side bias (greater than 65%) in both phases.

Social Interaction Test

A Social Interaction test was used to assess anxiety-like behaviour (251) in the WT and TG rats at 9 and 12 months of age. This test was carried out in the end of the dark phase in 45% light. The rat being tested was marked with a non-toxic black marker on its back to allow discrimination from the conspecific animal. All rats were age and weight matched to avoid dominant and fighting behaviour. Arenas were cleaned with 70% ethanol between trials to remove any scents left by the previous rats which may alter their behaviour. A test rat and an unfamiliar wildtype conspecific rat were placed in the behaviour arena for ten minutes with an inanimate object (e.g. metal can or plastic bottle) in the centre (Figure 2b). Behaviour during this period was recorded by an overhead

camera for analysis post-test. Time spent sniffing, following and avoiding the con-specific animal as well as exploring the central object were quantified and were defined as follows:

Sniffing behaviour: Active sniffing of the conspecific's snout or parts of the body including the tail and anogenital region.

- Avoiding: Immediate avoidance upon approach of the con-specific animal by turning or moving away.
- Following: Following the con-specific animal around the arena by actively moving after the con-specific rat.
- Exploring: Actively exploring the central object by sniffing and interacting with it. Time spent against or on the object but with snout faced in a different direction was not counted.

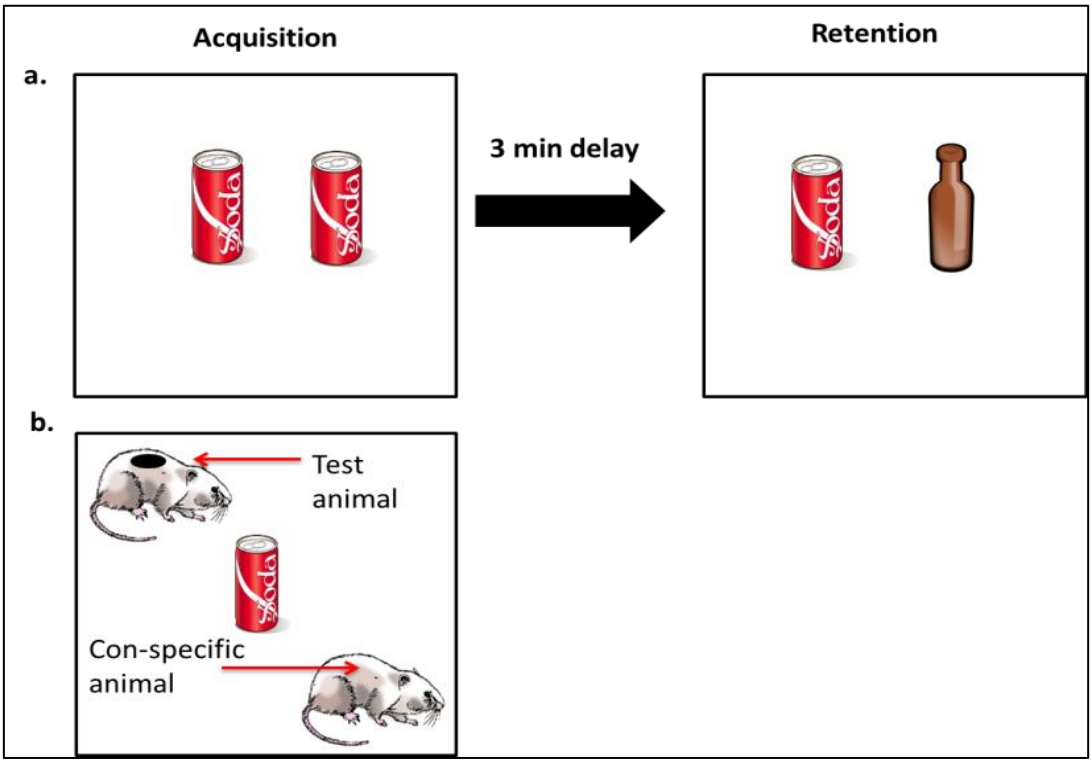

Figure 2 Experimental layout of the NOR **(a)** and social interaction **(b)** tests.

[^{18}F]DPA-714 PET acquisition and Analysis

TSPO tracer [^{18}F]DPA-714 was used to assess neuroinflammatory status in WT and TG rats at 6 and 12 months of age. ^{18}F]DPA-714 was synthesized as previously described (225). DPA-714 precursor and cold reference were kindly donated by Prof. Michael Kassiou. Animals underwent anaesthesia (1-2% Isoflurane and 2L/min oxygen), tail vein cannulation and [^{18}F]DPA-714 injection (approximately 30mBq). For all scans, 280µl of tracer followed by a 220µl saline flush were injected using Cole-Parmer Syringe® Touchscreen Control pumps at a rate of 1ml/min in a single bolus over 30s to ensure steady delivery of the tracer. Imaging was carried out on a Siemens Inveon® PET-CT scanner. CT scans were carried out prior to PET and were used to obtain attenuation correction information and provide anatomical data for the PET images. Respiratory rate and temperature were monitored constantly throughout the experiment and body temperature was maintained through the use of a heating and fan module controlled by the rectal probe via the interface of the BioVet® system (m2m Imaging Corp., Cleveland, OH, USA). A 60 minute dynamic PET protocol was used for acquisition starting with tracer injection. The time coincidence window was set to 3.432 ns and levels of energy discrimination to 350 keV and 650 keV. List mode data from emission scans were histogrammed into 16 dynamic frames (5 × 1 min; 5 × 2 mins; 3 × 5 mins and 3 × 10 mins) and emission sinograms were normalised, corrected for attenuation, scattering and radioactivity decay and reconstructed using the methods previously described in chapter 2 (OSEM3D protocol: 16 subsets and 4 iterations, image dimensions: 128^2 (transaxially) ×159 (axially) with 0.776×0.776×0.796mm voxels). Skeletal and brain regions were defined manually in the PET images using Brainvisa and Anatomist software and the different regions of interest (ROI) were quantified by applying a rat MRI template adapted from Schwarz *et al* (252). ROIs included; entorhinal cortex (EC), cingulate cortex (CC), motor cortex (MC), somatosensory cortex (SA), frontal cortex (FC), temporal cortex (TC), hippocampus (HC), thalamus (TH), hypothalamus (Hypo) and striatum (ST). Data are expressed as Standardised Uptake Values of the PET tracer, normalised to the cerebellum (NUV_{cb}).

Magnetic Resonance Spectroscopy Acquisition and Analysis

To assess metabolite profile, single voxel MRS was performed in the HC (2x9x3mm^3), TH (2.5x8x3mm^3), Hypo (2x3x3mm^3) and cortex (Ctx,1.2x3x3mm^3) in TG and WT rats at 6 and 12 months of age. Isoflurane (1-2%) and oxygen (2L/min) were used to anesthetise and maintain rats. Structural MRI (Fast Low Angle SHot: 9 slices, 2 averages, 0.5mm inter-slice distance) and MRS were carried out as described in Chapter 2 using a 7 Tesla magnet (Agilent Technologies, Oxford Industrial Park, Yarnton, Oxford, UK) interfaced to a Bruker AVANCE III spectrometer (Bruker Spectrospin, Coventry, UK). In brief, FASTMAP (233) was used to shim a 10mm^3 region encompassing the planned voxels. The VAPOR method was used for water suppression and a PRESS (Point REsolved SpectroScopy) (232) sequence (TR 2500ms, TE 20ms) was carried out (182). For large ROIs (HC and TH), 128 averages were performed in PRESS and for smaller ROIs (Hypo and Ctx) 512 averages were acquired. Data were processed and analysed using QUEST in jMRUI as previously described. The basis-set was generated in the same way as Chapter 2 using the acquisition parameters and included; NAA (N-acetylaspartate, Glu (glutamate), mI (*myo*-Inositol), Cr (creatine), Taur (taurine), tCho (choline and phosphocholine, glycerophosphocholine), glutamine (Gln), GABA, and Scy-I (scyllo-Inositol). Peaks at 0.9, 1.3ppm and 3.76ppm were included to model macro-molecules and α-amino acid protons that have been previously observed in brain MRS of rodents (210). Metabolites are expressed as amplitude of institutional units relative to water.

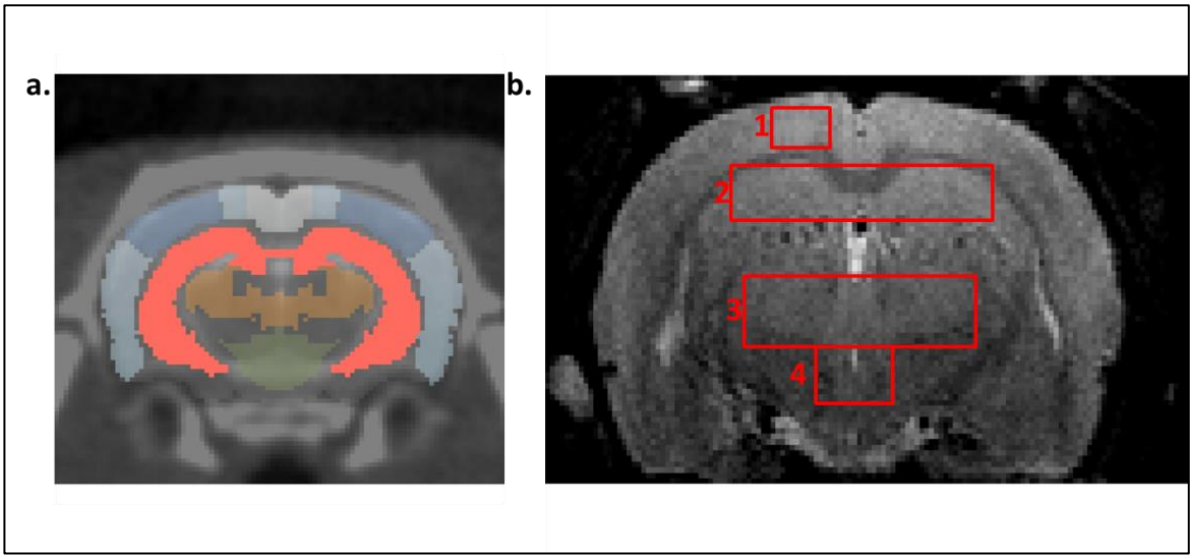

Figure 3 Regions of interest for PET and MRS analysis. MRI mask adapted from *Schwarz et al* (252) for PET quantification **(a)**. FLASH MRI image indicating voxel placement for MRS acquisition **(b)** in the 1: Cortex, 2:Hippocampus, 3: Thalamus and 4: Hypothalamus.

Statistical analysis

The data were statistically analysed using GraphPad® Prism™ for Windows (v6.04, GraphPad Software, Inc., San Diego, California USA). Behavioural data were expressed as mean±SEM. Paired *t*-tests were used to determine differences in raw exploration times of the left and right, and familiar and novel objects in the NOR. Shapiro-Wilk normality test was carried out raw exploration times to assess side bias and depending on the normality of the distribution either *t*-tests or Wilcoxon tests were used. PET and MRS data are expressed as mean±SD. Two-way analysis of variance (ANOVA) was used to assess the effect of gene and age and possible interaction on total exploration times, DI, metabolite and [^{18}F]DPA-714 levels in WT and TG. If a significant effect and/or interaction were found by the 2-way ANOVA. Interactions were considered significant if $p<0.1$. For all other statistical analyses, the significance level was $p<0.05$.

Results

Behaviour

NOR test

The NOR test was carried out at 3, 6, 9 and 12 months of age to compare the cognitive abilities of WT and TG rats with age. The Fisher strain has previously been shown to have high anxiety (253) and males have shown low locomotor activity (254), therefore we also measured the level of total exploration of objects in both phases of the test and side of exploration. Preference for objects on a particular side of the arena was assessed by carrying out *t*-tests on raw exploration times of sides in the acquisition phase. No significant differences were identified between the exploration of the left and right objects in the acquisition phase with either group at any age (Figure 4c), allowing investigating of cognition without side bias. Age and gene had a significant effect on total exploration times in both the acquisition ($p \leq 0.0001$ and $p=0.0384$ respectively) and retention ($p \leq 0.0001$ and $p=0.0384$ respectively) phases (Figure 4a-b). Using multiple comparisons a significant decrease was seen in total exploration time in TG rats when compared to the WT rats in the acquisition ($p \leq 0.05$) and retention ($p \leq 0.05$) phases at 3 months of age (Figure 4a and 4b). Decreased exploration times were also seen with age in both WT and TG rats. Decreased exploration times were seen in WT rats at 6, 9, and 12 months when compared to 3 months in the acquisition phase ($p \leq 0.0001$ for all) and at 9 and 12 months in the retention phase ($p \leq 0.0001$ for both). Similarly, TG rats also showed decreased exploration times at 9 and 12 months when compared to 3 months in the acquisition phase ($p<0.001$ and $p<0.01$, respectively) and the retention phase ($p<0.05$ for both). These results suggest that locomotor activity is reduced in young TG rats compared to WT rats and in both with age.

The raw exploration times were converted to a DI between -1 and +1. A negative result indicated preference towards the familiar, a zero result indicates no preference and a positive result shows preference towards the novel. A two-way ANOVA revealed no significant effects of age, gene or interaction age×gene (Figure 4e). Therefore this result suggests that there is no cognitive difference between groups at any age.

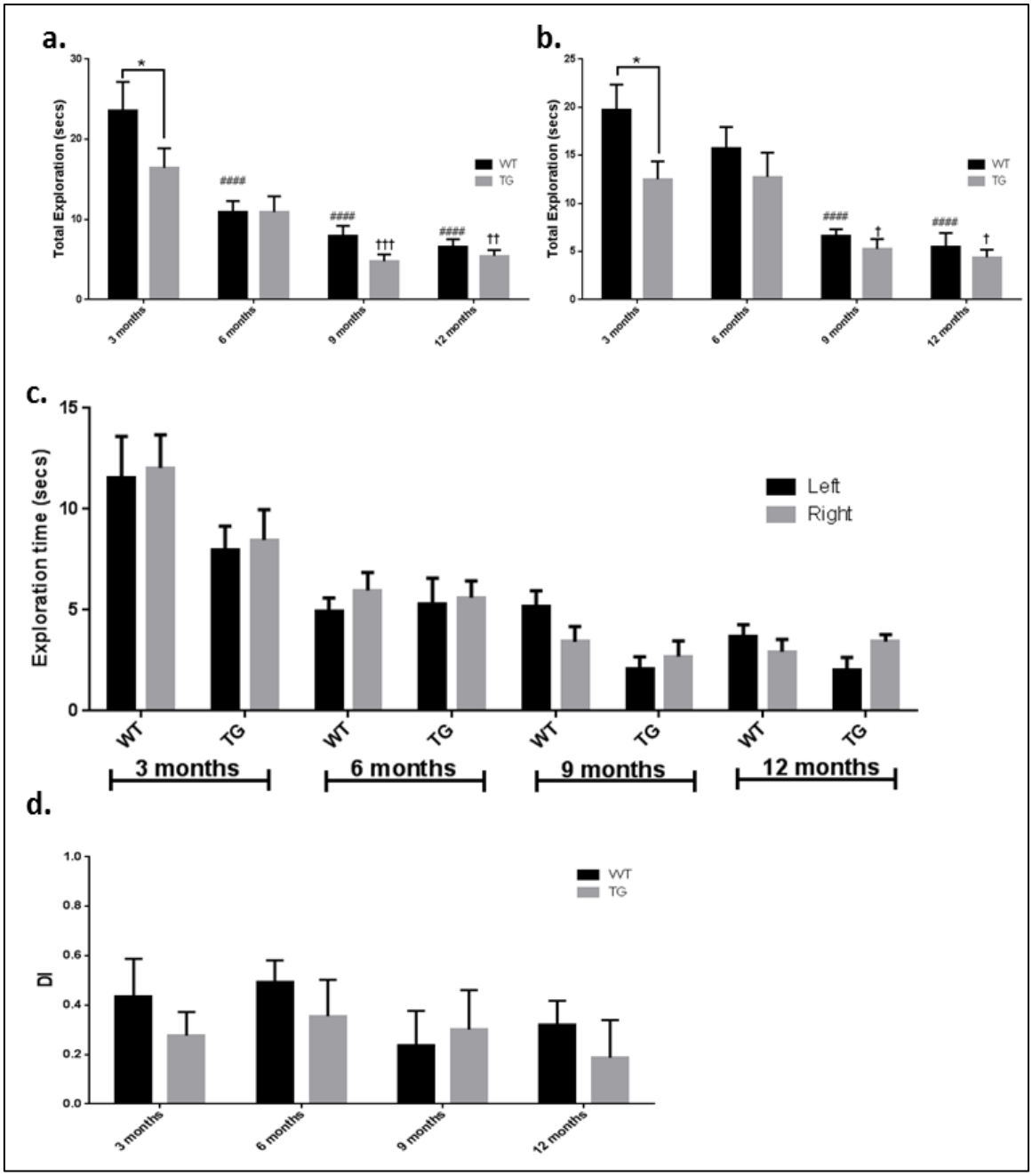

Figure 4 NOR results. Total exploration time in the acquisition **(a)** and retention phases **(b)**. Exploration of left and right objects in the acquisition phase **(c)**. Discrimination index revealed no cognitive differences between WT and TG animals at these ages (WT n=11 and TG n=9 at 3 and 6 months, WT n=9 and TG n=7 at 9 months, WT n=8 and TG n=8 at 12 months) **(d)**. Results are shown as mean±SEM. Statistical analysis was performed using two-way ANOVA followed by Sidak post hoc analysis for total exploration times and DI. All results are shown as mean±SEM. Paired t-tests were performed to assess side bias at all time-points (*TG versus WT, # versus 3 months WT, † versus 3 months TG,*p≤0.05, **p≤0.01, ***p≤0.001, ####p≤0.0001, †p≤0.05, ††p≤0.01, †††p≤0.001)

Social interaction

Anxiety-like behaviour was assessed at 9 and 12 months by investigation sniffing, avoiding, and following behaviour of a con-specific WT animal matched for age and weight (Figure 5). Exploration of a central object was also assessed. A two-way ANOVA revealed a significant effect of gene on sniffing behaviour (Figure 5a, p=0.0021) with TG rats spending less time sniffing and interacting with con-specific animals compared to WT at both ages. No effect of age or interaction was found on this behaviour.

A significant effect of age (Figure 5d, p=0.0043) and a significant gene × age interaction (p=0.0874) was seen in exploring behaviour. Multiple comparisons revealed a significant decrease in exploring behaviour from 9 to 12 months of age in the WT group (p≤0.01). This effect was not significant in the TG rats. No significant effects were observed on avoidance or following behaviour (Figure 5b-c).

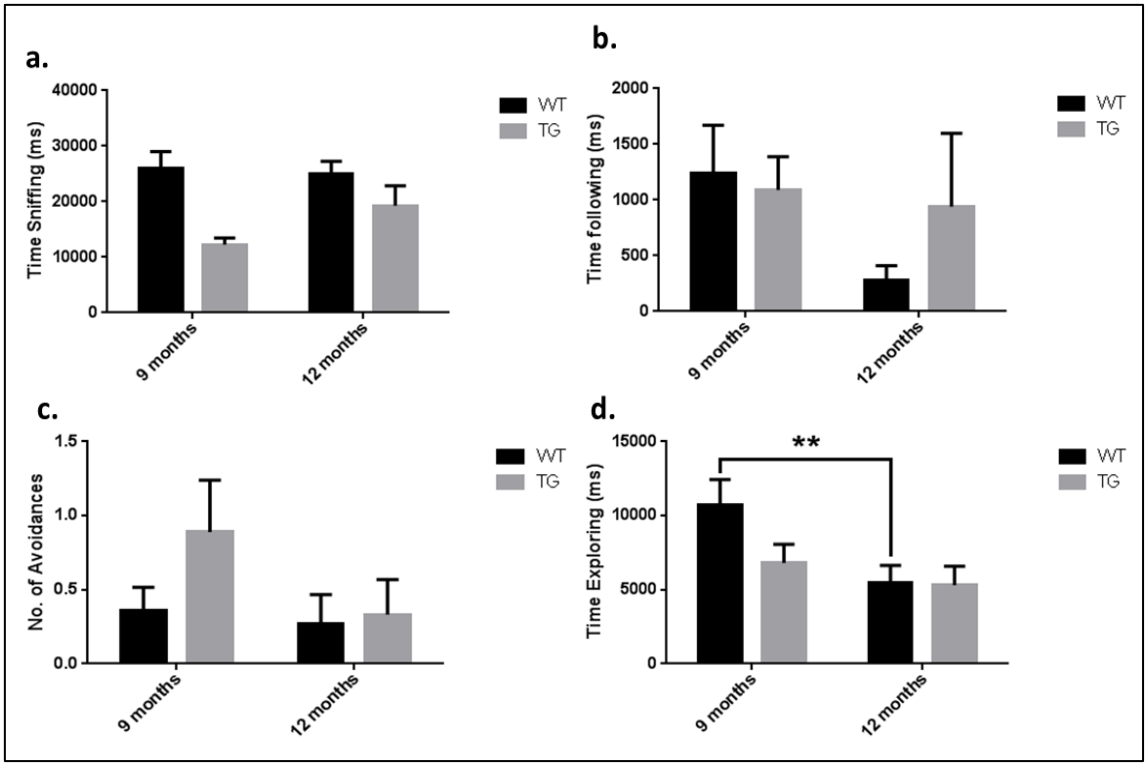

Figure 5 Social interaction analysis assessed differences in sniffing **(a)**, avoiding **(b)**, following **(c)** and exploring **(d)** behaviour of WT (n=11) and TG rats (n=9). Time spent sniffing was reduced in TG compared to WT rats. Time spent exploring an object was reduced in the WT group from 9 to 12 months. Results are shown as mean±SEM. Statistical analysis performed using two-way ANOVA followed by Sidak post hoc analysis (**p≤0.01).

[^{18}F]DPA-714 PET

[^{18}F]DPA-714 PET was carried out to assess neuroinflammation in TgF344-AD and WT rats at 6 and 12 months of age (Figure 6-7). The two-way ANOVA revealed that gene had an overall significant effect on NUV_{cb} values in the TC with increased [^{18}F]DPA-714 uptake seen in the TG compared to WT rats (Figure 7e, p=0.0316) but there was no effect of age or interaction was seen in this region and this was not significant with *post-hoc* analysis. There was also a trend to increase for NUV_{cb} values as an effect of gene in the CC (Figure 7a, p=0.078) and HC (Figure 7f, p=0.087) of TG rats but were not significant.

[^{18}F]DPA-714 uptake in the Hypo (Figure 7g) revealed a significant effect of age (p=0.009) and a significant gene × age interaction (p=0.0667). Multiple comparison tests revealed a significant increase in [^{18}F]DPA-714 uptake in 12 month old TG rats when compared to 12 month old WT rats (+23%, $p<0.05$) and to 6 month old TG rats ($p<0.01$, +24%). There were no significant changes between age groups in WT rats.

Similarly, a significant effect of age (Figure 7h, p=0.0002) and a gene × age interaction (p=0.033) was observed in the TH, Sidak post hoc test revealed a significant increase in [^{18}F]DPA-714 uptake in TG rats compared to WT rats at 6 months (+13%, $p<0.05$) using multiple comparisons. A significant increase in [^{18}F]DPA-714 uptake was also seen in the TH of the WT rats from 6 to 12 months (+23%, $p\leq0.001$), There was no significant changes with age in the TG rats.

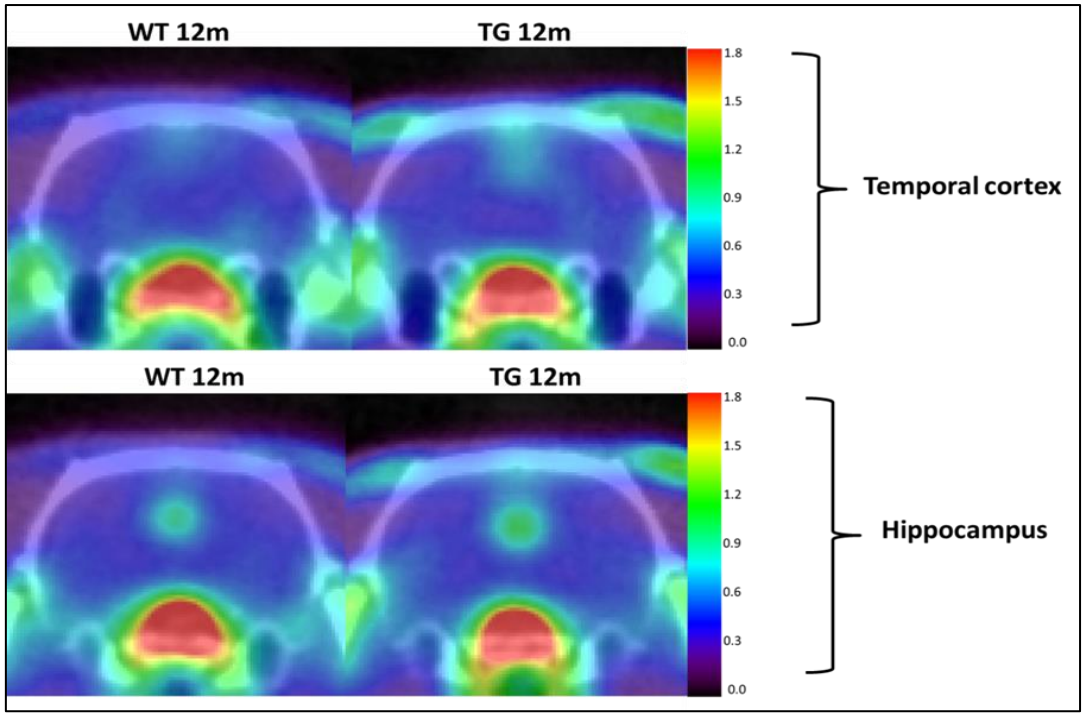

Figure 6 PET [^{18}F] DPA-714 SUV sum image (20-60min post-injection) in temporal cortex **(a)** and hippocampus **(b)** of TG and WT mice at 12 months.

A significant effect of age but no gene effect or interactions were observed on [^{18}F]DPA-714 NUV_{cb} values in the CC (Figure 7a, p=0.0317), FC (Figure 7c, p=0.0283), SC (Figure 7e, p=0.0181) and Str (Figure 7i, p=0.004). An average increase in [^{18}F]DPA-714 uptake across age groups of 8% (Figure 7a), 15% (Figure 7c), 7% (Figure 7e) and 12% (Figure 7i) was seen in these regions respectively.

No overall main effects of gene or age were observed in the MC, however a significant gene × age interaction was identified (Figure 7d, p=0.0357). WT rats displayed increased [^{18}F]DPA-714 uptake with age (+6%), whereas TG rat display decreased [^{18}F]DPA-714 uptake with age (-5%). No effects were significant after multiple comparisons.

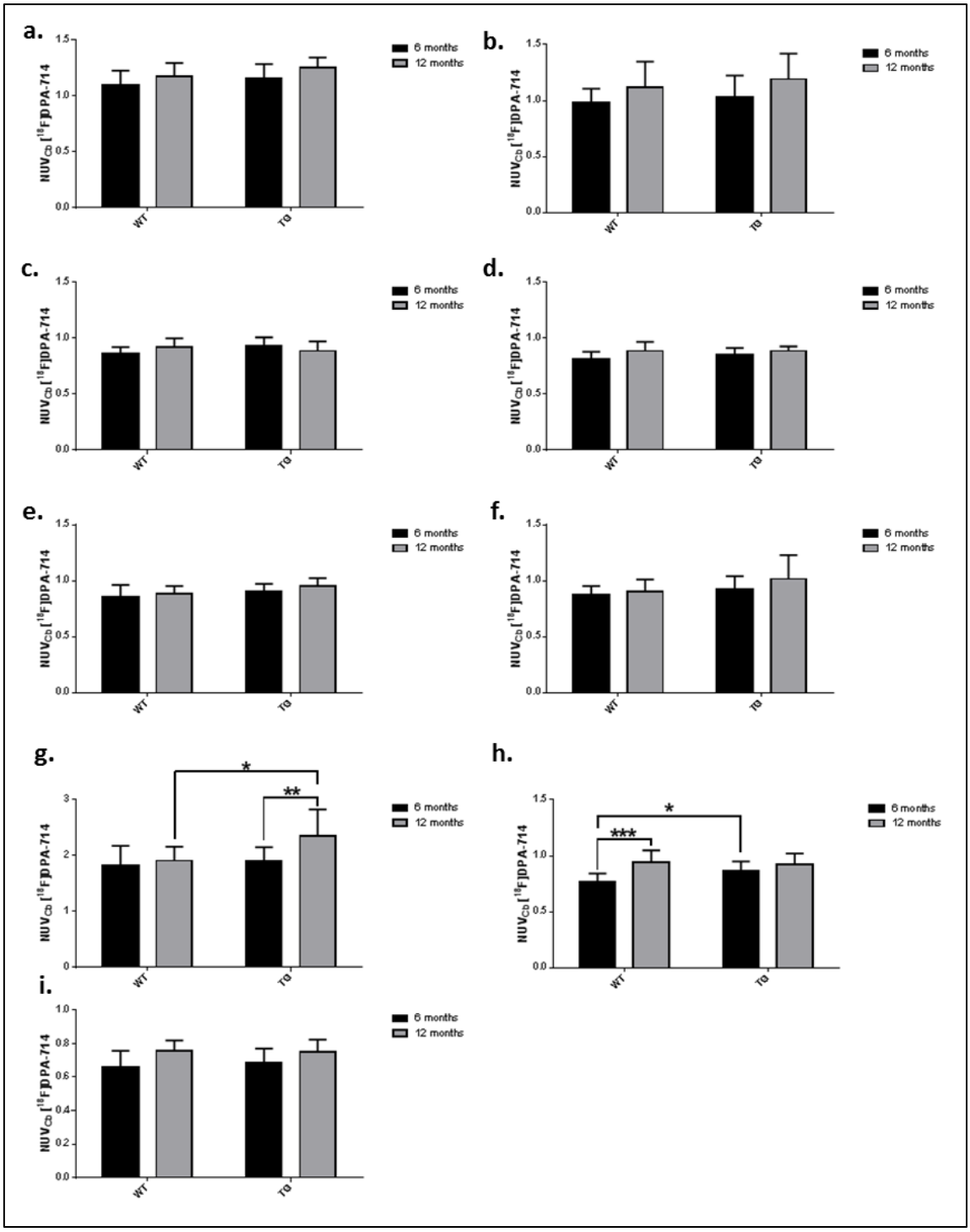

Figure 7 Analysis of [18F]DPA-714 NUVcb values in WT and TG (n=10 for both groups) rats in the cingulate cortex **(a)**, frontal cortex **(b)**, motor cortex **(c)**, somatosensory cortex **(d)**, temporal cortex **(e)**, hippocampus **(f)**, hypothalamus **(g)**, thalamus **(h)**, and striatum **(i)** at 6 and 12 months of age. Results are shown as mean±SD. Statistical analysis was performed using a two-way ANOVA followed by Sidak's post hoc analysis (*$p<0.05$, **$p<0.01$, ***$p<0.001$). Results are shown as mean±SD.

MRS

Examples of MRS spectra obtained from the HC, TH, Hypo and Ctx are shown in Figure 8. MRS was carried out to assess metabolite profile in the HC, TH, Hypo and Ctx with a focus on NAA, mI, Glu, tCho, Cr, and Taur levels (Figure 9).

Two-way ANOVAs did not reveal any significant effects of gene in any region with any metabolite, however a significant effect of age ($p=0.049$) and an age × gene interaction ($p=0.064$) were found in Glu levels in the Hypo (Figure 9e). This resulted in the TG rats demonstrating a significant increase in Glu ($p\leq0.05$) from 6 to 12 months in this region (+28%) using multiple comparisons, whereas changes in the WT were negligible (<1%).

No significant effect of age or gene was seen on mI levels in any region, although an age × gene interaction was found in the TH (Figure 9c, $p=0.0913$) and Hypo ($p=0.0977$). In the TH this resulted in WT rats demonstrating increased mI levels and TG rats demonstrating decrease in mI levels with age. The opposite was found for the Hypo with decreasing mI levels evident with normal aging in the WT and increased levels evident in the TGs. Similarly, no effects of gene or age were observed for Cr, however an age × gene interaction ($p=0.0778$) was observed in the Hypo with increased Cr levels in TG rats and decreased levels observed in the WT rats at 12 months. No effects were significant for either metabolite using multiple comparisons.

No other metabolites displayed a significant effect of gene or an interaction in any region using two-way ANOVAs; however age had a significant effect on other metabolites in all regions. NAA levels decreased from 6 to 12 months in the HC ($p=0.0153$, -15% average across groups) and TH ($p=0.0003$, -12% average). Similarly, tCho levels were also decreased age in the TH ($p=0.0057$, -10% average), Hypo ($p=0.0006$, -10% average) and Ctx ($p=0.0225$, -12% average). Age had the opposite effect on Glu and Taur levels. Glu levels were increased with age in the TH ($p=0.0088$, +18% average) and Ctx ($p=0.0007$, +30% average). Taur levels were increased with age in the Hypo ($p=0.0025$, +41% average) and Ctx ($p=0.049$, +21% average).

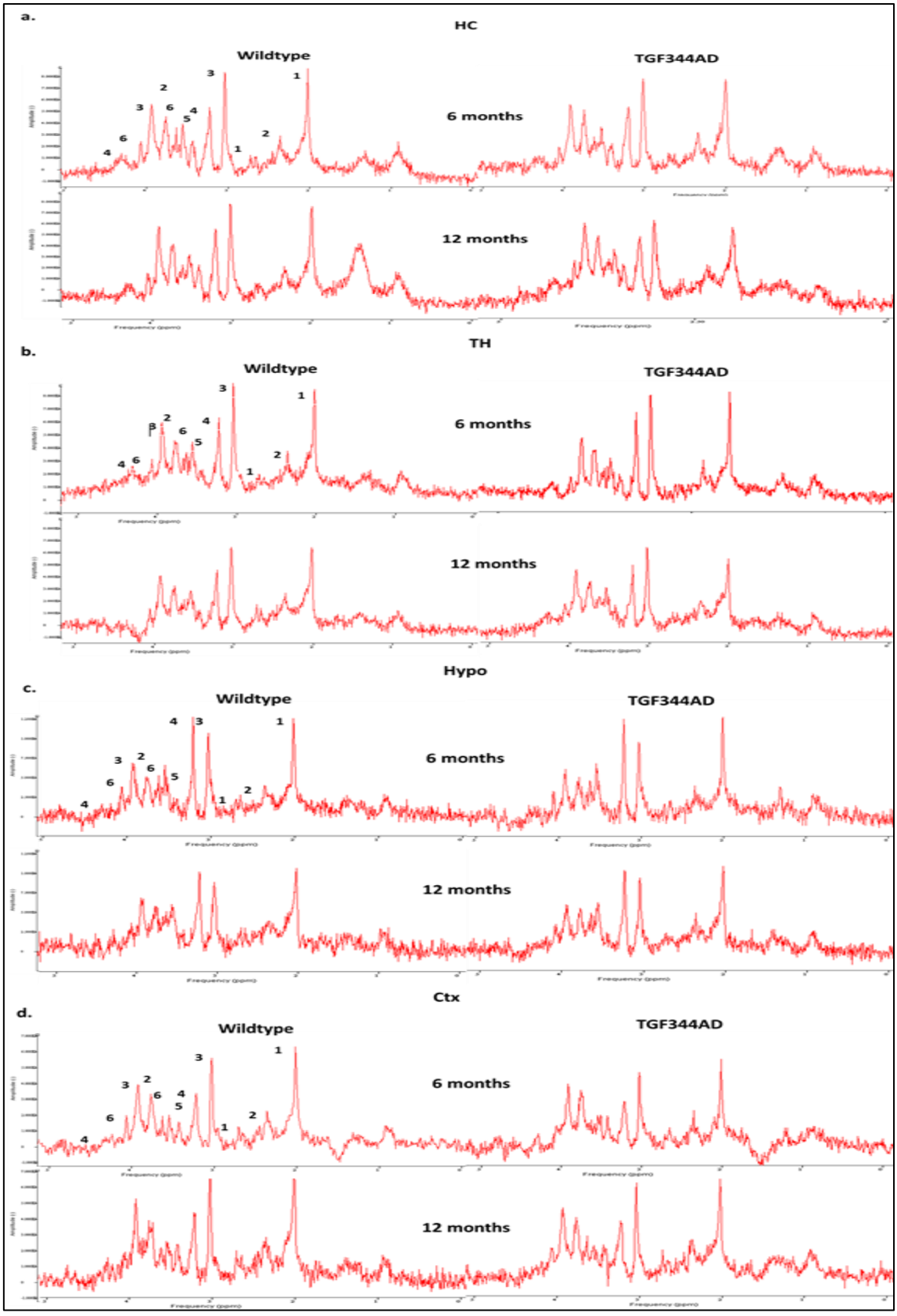

Figure 8 Examples of MRS spectra obtained from WT and TG rats at 6 and 12 months in the HC **(a)**, TH **(b)**, Hypo **(c)** and Ctx **(d).** The multiple peaks of metabolites of interest are labelled as 1:NAA, 2:Glu, 3:Cr, 4:tCho, 5:Taur, 6:mI. Representative spectra were shown based on average NAA levels for each group.

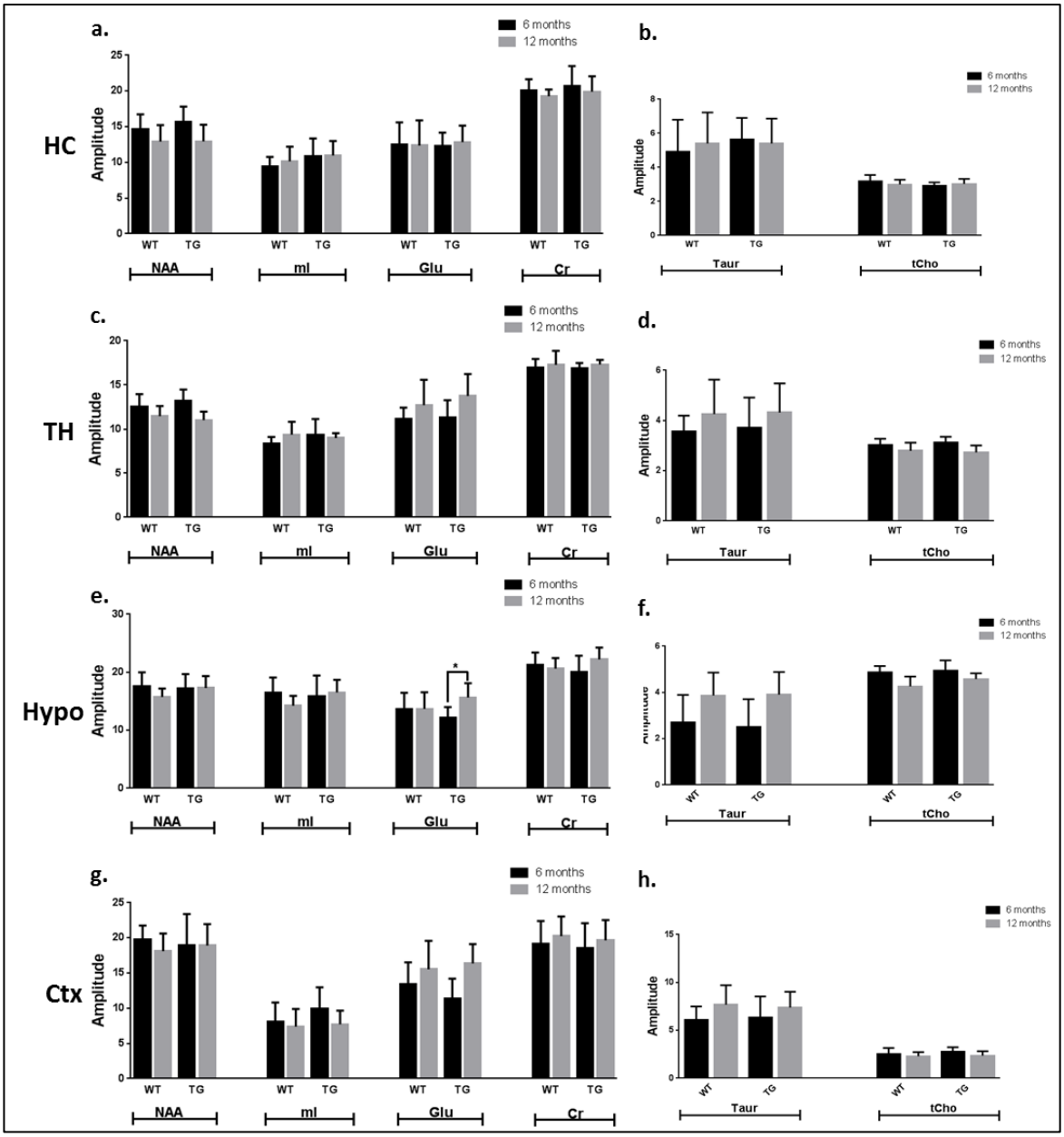

Figure 9 Metabolite profiles of WT and TG rats at 6 and 12 months (n=10 for both groups) in the hippocampus **(HC, a-b)**, thalamus **(TH, c-d)**, hypothalamus **(Hypo, e-f)** and cortex **(Ctx, g-h)**. Glu levels in the Hypo significantly increase in TG rats but not WT rats from 6 to 12 months. Statistical analysis was performed using a two-way ANOVA followed by Sidak's post hoc analysis (*$p<0.05$). Results are shown as mean±SD.

Discussion

The TgF344-AD model expresses all the physiological characteristics seen in clinical AD and therefore represents an ideal pre-clinical animal model for identifying early imaging biomarkers of neuroinflammation and degeneration. Here we characterise genetic and age effects of neuroinflammation via [^{18}F]DPA-714 PET, metabolite profile via MRS and cognitive abilities via the NOR test.

Young TgF344-AD do not have cognitive decline but do show increased anxiety

Cognitive deficits in the TgF344-AD model have been previously reported from 15 months in the Barnes maze and from 24 months using NOR (114). However no results for younger ages in the NOR were reported. Here, we assessed NOR at the earlier time-points of 3, 6, 9 and 12 months of age. Total time spent exploring objects was significantly affected by gene and age in both phases, with lower times seen in TG compared to WT rats at 3 months and exploration times reducing with age in both groups. The early hyperactivity observed was previously reported in this model (114). Although the overall exploration times are low in this study, reduced locomotor activity especially in males has been reported previously in this strain (254). Here we show that this effect is exacerbated in 3 month old TG rats but with both groups displaying low exploration in later time-points. Nonetheless no side bias was found and a two-way ANOVA of DI data did not reveal any significant effects of gene or age, suggesting there is no significant cognitive decline in these rats compared to WT rats at these ages. In addition all DI results were positive for each group suggesting that all groups show increased preference for the novel. This is in line with cognitive deficits occurring later in this model, however subsequent time-points between 12 and 24 months should be investigated.

As increased anxiety has been shown in this strain previously (253), we hypothesized the low exploration times seen in the NOR by the Fisher strain and exacerbated in the TG rats may be a result of increased anxiety-like behaviour, hence the social interaction test was carried out at 9 and 12 months in the same animals. Indeed, decreased sniffing behaviour was observed in the TG rats. A lower level of sniffing is indicative of decreased active social interaction and hence increased anxiety like

behaviour. No significant effect of gene was seen on exploration behaviour, however a significant effect of age and an age×gene interaction were observed. Significantly reduced exploration was observed in WT rats at 12 months compared to 9 months, whereas TG rats had low exploration times at both ages but were not significantly different from WTs. Increased anxiety like behaviour has also been reported in a mouse model of AD with the same APP_{swe}×$PS1_{\Delta e9}$ mutations (206) as assessed by open field and has been reported as an early symptom in human familial AD (255), suggesting that it may be a behavioural characteristic associated with AD.

[^{18}F]DPA-714 PET detects neuroinflammatory alterations in the TgF344-AD rat

Evidence suggests that neuroinflammation has an integral role to play in AD development and with reports of increased neuroinflammation early in clinical AD and MCI as well as in pre-clinical models of AD, hence it is a hot topic in AD research. Increased neuroinflammation was detected as early as 6 months of age in this TgF344-AD rat. Cohen *et al.* reported increases in area positive for IBA1 (microglia) immuonreactivity of 36% and 44% of TG compared to WT rats in the CC and HC respectively (114). Increases of 16% and 12% in the CC and HC were also found for GFAP (astrocyte) staining. Hence, we wanted to investigate if we could detect these and any other regional increases in neuroinflammation using [^{18}F]DPA-714 PET.

A significant effect of gene was found in the TC, with increased [^{18}F]DPA-714 NUV_{cb} values observed in TG rats. Increased neuroinflammation has been previously reported in the temporal lobe of AD patients (10, 142, 147, 162, 256) and is in line with early amyloid deposition (12) and atrophy in this region in AD (257). In addition, a trend for increased neuroinflammation was demonstrated by increased mI in the TC using *in vitro* MRS in a 3×TG mouse model expressing amyloid and tau pathology (215). No effect of age or interactions were seen in the TC suggesting that increased [^{18}F]DPA-714 uptake in this region is specific to the TG animals and provides a means of discriminating them from the WT rats at any early age prior to extensive plaque and NFT load. Furthermore it supports the idea that neuroinflammation may be an early contributor in AD development. Further *ex vivo* investigation in to glial activation, neuronal integrity and pathology burden in this region will help to understand the mechanisms underlying this. Increases in

[^{18}F]DPA-714 uptake were also observed in the CC and HC of TG rats but were not statistically significant (p=0.078 and p=0.087 respectively) suggesting that the significant increase in microglial activation reported by Cohen et *al* (114) is not detectable at 6 or 12 months using [^{18}F]DPA-714 PET in our cohort. Neuroinflammation was reported to increase dramatically with age in these regions of the TgF344-AD rat at 16 and 26 months, therefore it is possible that [^{18}F]DPA-714 PET will be able to significantly detect these changes at later time-points. Neuroinflammatory increases in AD patients using TSPO PET have been reported in the cingulate cortex (9, 163), as well as the hippocampus (147, 256) although some reports in this region are conflicting (10).

A significant increase in [^{18}F]DPA-714 uptake was seen in the TH of TG rats at 6 months age compared to age matched WT rats suggesting an early AD-specific change. However a significant increase in [^{18}F]DPA-714 was also seen from 6 to 12 months in the WT rats. An increase with age was also seen in the TG rats but was not significant. In support of this, a recent study found increases in [^{11}C](R)PK11195 in the thalamus of AD patients versus elderly controls and younger subjects (238). Increases in binding potential of [^{11}C](R)PK11195 were also seen in the young versus old healthy controls but were not significant. Pathology burden and glial cell activation in this area has not been investigated in this model. Hence *ex vivo* confirmation of these results is needed. Nonetheless these results suggest that increased neuroinflammation in the thalamus is an effect of both aging and AD. A significant increase in [^{18}F]DPA-714 uptake was also observed in the Hypo of TG rats at 12 months of age compared to WT rats, providing further regional alterations to distinguish TG and WT animals. A significant increase was also observed from 6 to 12 months in both groups but the increase with age is significant in the TG rats and not the WT rats (+24% compared to +5%), suggesting that the aging effect is exacerbated in the TG model. Although studies investigating the Hypo in AD are few in comparison to other regions such as the HC or cortex, there are reports of Aβ plaques, NFTs and neuronal loss in this region in AD patients (258). In addition, decreased glucose consumption and Hypo volume has been reported in the early stages of AD (258-261). Furthermore, the Hypo is essential for many homeostatic functions such as sleep and metabolism that are affected in AD. Dysfunction in the hypothalamic-pituitary-adrenal and hypothalamic-pituitary-thyroid axes have been reported in AD patients and in AD models of disease (reviewed by Ishii *et al* (258)). Similarly, decreased thalamic volume (262) and glucose consumption (261) has

also been reported in AD suggesting that these areas are also involved in AD development and providing regions of interest for further investigation.

An age × gene interaction is also observed in the MC but no overall main effects, with [^{18}F]DPA-714 uptake increasing with age in the WT and decreasing with age in the TG rats. These results suggest that the neuroinflammation in this region evolves differently between the groups with both gene and age influencing the neuroinflammatory status, but the differences are too small to be detected as an overall effect.

[^{18}F]DPA-714 PET detects normal aging in TgF344-AD and WT rats

No significant increases were seen in [^{18}F]DPA-714 for any other region as an effect of gene, however multiple effects were seen as an effect of age in these animals. Increased [^{18}F]DPA-714 NUV_{cb} values observed in 12 month versus 6 month old animals in the CC, FC, SC, and Str. No interactions were observed in these regions suggesting that the increases in [^{18}F]DPA-714 uptake are a result of normal aging in the Fisher strain between these time-points. Increased neuroinflammation as assessed by TSPO PET has been shown in healthy older subjects (237, 239)as well as in WT animals and is in line with suggested theories of increased microglial activation with age.

Investigation of neuroinflammation using MRS

Neuroinflammation status was also assessed by investigating mI levels using MRS. mI levels have been reported to be indicative of gliosis (184) with increased levels reported in clinical AD (185, 190-195) and in various amyloid induced animal models (203, 205, 210, 216), although reports in animal models are quite inconsistent (see Chapter 1). No significant overall effects of gene or age on mI levels were observed in any region at the age investigated in this study. This is in line with no mI alterations found in the APP_{swe}×$PS1_{\Delta e9}$ mouse model in our study in chapter 2 as well as a previous report on the same model (206). However, a significant age × gene interaction was observed for mI levels in the TH and Hypo. Although no significant effects were seen *post hoc* it showed mI levels increasing with age in the TH of WT rats but TG rats displayed a small decrease in mI levels in the TH. On the other hand, the opposite effect is seen in the Hypo with mI levels decreasing with normal aging in the WT rats but increasing slightly in the TG rats.

This result matches the interaction results we observed in these regions with [^{18}F]DPA-714 PET suggesting that these markers progress differently between the groups. The Ctx voxel encompasses the MC region, however we did not observe any significant effects of mI in this region or in the TH as was reported with PET. Further investigation is needed to confirm if mI is a good indicator of inflammatory status.

Investigation of neurodegeneration in TgF344-AD rats using MRS

No significant effects of gene were found for any metabolite in any gene in this study. However a significant increase in hypothalamic Glu levels were observed in TG rats at 12 months of age that was not mirrored in the WT group. This result suggests that genotype influences Glu levels in this region and is in contrast to our results in chapter 2 and previous reports depicting reduced Glu in AD models (201, 203, 204, 208, 209, 216) and in the clinical situation (193, 199). However it is important to note that we investigated early time-points in this study. Extensive neurodegeneration was previously reported from 16 months of age and therefore Glu levels may be elevated prior to increased pathology burden. Nonetheless it highlights a significant change in the TGs that is not seen in the WTs and supports the PET results found in this region, therefore providing an additional non-invasive means of discrimination between WT and TG animals at 12 months.

A significant age × gene interaction was also identified for Cr in the Hypo with increased levels in the TG group and decreased levels in the WT group. This suggested that Cr levels are influenced by gene over age however no results were significant after multiple comparisons. This is in contrast to what is observed in clinical AD with increased Cr levels reported in AD patients compared to healthy controls (194).

Neuronal loss was reported previously in this TG model with 29% and 39% decrease in the CC and HC from 6 to 16 months of age compared to WT. We did not observe any age by gene effects for NAA levels in any region at 6 or 12 months. However, age significantly reduced NAA in both groups from 6 to 12 months in the HC and the TC indicating that increased neuronal loss or dysfunction in these regions is a part of normal aging. We reported decreased NAA as an effect of age in the APP_{swe}×$PS1_{\Delta e9}$ mouse model

in chapter 2 and this effect has also been reported in the 3×TG mouse model of AD (215). Similarly age significantly affected Glu, tCho and Taur levels. tCho levels were decreased from 6 to 12 months in the TH, Hypo and Ctx, Similarly Glu levels were increased in the TH and Ctx, and Taur was increased in the Hypo and Ctx. These effects were seen as a result of age alone and without a gene effect or interaction, hence alterations in these regions are indicative of normal aging.

Metabolite profile has previously been investigated in the HC of a different rat model of AD, the McGill-R-Thy1-APP rat, which expresses full AD-like amyloid pathology (113). Intraneuronal Aβ is evident in this model from 1 week old with plaque deposition and neuroinflammation evident from 6 months old. Decreased mI levels were observed in the HC of this model compared to WT at 3 months of age; however mI levels in the TGs changed with age demonstrating increased levels at 9 months and similar levels by 12 months of age (60). Decreased Glu and tCho were also reported at 3 months of age, which remained significantly lower at 9 months but similar levels were shown at 12 months. NAA level were decreased in this TG rat at 12 months. We did not see similar results in our rat model; however this could be explained by the fact that this model is an accelerated model with pathology arising from a very early age. Further time-points in the TgF344-AD rat may reveal similar results.

Limitations

As there is currently no *ex vivo* immunohistochemistry to investigate the pathology load at this time we cannot confirm whether the changes observed are as a result of gene expression in the TG rats or whether they are pathology driven. Future work should look at characterising the pathology at early time-points such as the ones used in this study.

Conclusion

Here we report [^{18}F]DPA-714 PET and MRS results for the first time in young TgF344-AD and WT rats prior to known amyloid plaque and NFT deposition. Increased neuroinflammation was identified in the TH and Hypo of TG rats at 6 and 12 months respectively using [^{18}F]DPA-714 PET. In addition, overall increased neuroinflammation

was seen in the TC of TgF344-AD rats. Increased Glu levels in the Hypo were seen in the TG rats at 12 months providing further means of discriminating AD in this model. These results provide specific effects in the TG animals that can be used to discriminate them from WTs. Investigation into the involvement of these regions in AD is lacking and therefore further research is required. No significant neuronal loss was identified between WT and TG rats at these time-points. Further imaging time-points are needed to investigate if neurodegenerative differences are quantifiable by non-invasive *in vivo* imaging. *Ex vivo* analysis should also be carried out in the TC to confirm *in vivo* imaging results.

Acknowledgements

This research was supported by the European Union's Seventh Framework Programme (FP7/2007-2013) under grant agreement n°HEALTH-F2-2011-278850 (INMiND). The authors wish to thank all the personnel of the WMIC, especially Dr Michael Fairclough, Ms. Lidan Christie, Mr Michael Green, Mr Jamil Gregory, Ms. Carol Brough and Ms. Gemma Chapman for facilitating the study.

Conflicts of Interest

All authors report no conflict of interest.

Chapter 4 (Paper 3)

Effect of recurrent Urinary Tract Infection on Disease Progression in the TgF344-AD rat model of Alzheimer's Disease.

Chaney A[1], Sharp A[2], Burges E[2], Davies K[1], Smigova A[1], Warn P[2], Williams S[1], Boutin H[1].

Effect of re-current Urinary Tract Infection on Disease progression in the TgF344-AD rat model of Alzheimer's Disease.

Chaney A[1], Sharp A[2], Burges E[2], Davies K[1], Smigova A[1], Warn P[2], Williams S[1], Boutin H[1]

[1]Faculty of Biology, Medicine and Health, University of Manchester, Manchester, M13 9PT, UK

[2]Evotec (UK) Ltd., Williams House, Manchester Science Park, Lloyd Street North, Manchester M15 6SE, UK

Corresponding Author:
Dr Hervé Boutin,
Wolfson Molecular Imaging Centre,
27 Palatine Road, Manchester, M20 3LJ, UK
Email: herve.boutin@manchester.ac.uk
Tel: +44 1612750078
Fax: +44 161 275 0003

Abstract

It is accepted that neuroinflammation is a characteristic of Alzheimer's disease (AD), however more recently it has been suggested that peripheral infection can also drive neuroinflammation and influence pathology burden and cognitive decline in AD. In addition, increased infectious burden has been found in AD patients. Urinary tract infection is a common infection amongst the elderly in hospitals. Hence, the primary aim of this study was to investigate the effect of recurrent urinary tract infection on cognitive, neuroinflammatory and neuronal markers in the transgenic (TG) TgF344-AD compared to wild-type (WT) Fisher rats. This was carried out using behavioural assessments, [^{18}F]DPA-714 positron emission tomography (PET) and magnetic resonance spectroscopy (MRS). As a secondary aim we looked at the effect of age. Here we report evidence for effects of peripheral infection effects on central nervous system measurements in WT and TG rats. Re-current UTI infection resulted in cognitive decline in TG but not WT rats.. Infection also affected metabolite levels in WT and TG rats with significantly increased total choline levels (tCho) in the cortex and trends for increased hypothalamic N-acetylaspartate (NAA) and decreased hippocampal creatine (Cr) were also observed. However, [^{18}F]DPA-714 PET appeared to be differentially affected by infection in WT and TG rats in the hypothalamus, this was mirrored by altered *myo*-inositol (mI) levels in the same region. Increased [^{18}F]DPA-714 PET NUV_{cb} values and mI were seen in WT infected rats, whereas decreased [^{18}F]DPA-714 PET NUV_{cb} values and mI were seen in TG infected rats. TG rats could be discriminated from WT rats by uptake and increased hypothalamic NAA levels. Increases in [^{18}F]DPA-714 PET was observed as an effect of normal aging in multiple areas. Similarly, regional alteration in NAA, tCho, Glu, Cr and Taur were observed; although the evidence suggested that aging effects on NAA and tCho may be exacerbated in the TG groups.

Key words: Alzheimer's disease, Urinary tract infection, peripheral inflammation, positron emission tomography, magnetic resonance spectroscopy.

Introduction

It has become increasingly evident that neuroinflammation has a significant role to play in neurodegenerative diseases such as Alzheimer's disease (AD). It has also been suggested that systemic inflammation can accelerate neurodegeneration and worsen symptoms in AD (263). Clinical studies have shown relationships between systemic inflammation and AD, with increased plasma and serum levels of pro-inflammatory cytokines such as TNF-α, IL-1β, IL-6 observed in patients with AD (70, 96, 221, 264) and mild cognitive impairment (MCI) (95). In addition, many risk factors for AD and reported co-morbidities result in higher basal levels of inflammation such as heart disease, stroke, diabetes and obesity (88-91). Various studies have shown that higher levels of inflammatory cytokines were associated with a worse cognitive outcome and viral and bacterial infectious burden has been shown to cause memory decline in non-demented and stroke-free populations (97), but importantly such infections have been shown to be more frequent in AD patients (96) potentially aggravating the disease. Indeed, increased peripheral IL-1β levels have been shown to result in subsequent cognitive decline in AD (92) and increased IL-6 levels have been associated with reduced hippocampal volume in healthy subjects and suggested to be a contributor to cognitive deficits (265). Moreover, systemic infections have been shown to lead to increased peripheral TNF-α levels resulting in accelerated cognitive decline when compared to patients without systemic infection (6).

Peripheral infection has also been to shown to affect AD in pre-clinical animal models. Respiratory infection has been shown to directly increase microglial and astroglial activation, T cell infiltration and amyloid plaque deposition in the APP_{swe}×$PS1_{dE9}$ mouse (101). This also resulted in increased TNF-α, IL-1β and IL-6 mRNA expression in the cortex of these animals. Similarly, peripheral LPS challenge has been shown to increase pro-inflammatory cytokine mRNA expression, microglial activation and cognitive decline in an animal model of prion disease (266, 267), providing further evidence of peripheral immune – central nervous system communication.

It has been suggested that microglia in neurodegenerative disorders such as AD are primed as result of the disease pathology (94, 263). It has also been suggested that

increases in peripheral pro-inflammatory cytokines such as IL-6 and TNF-α IL-1β can result in microglial priming and increased neuroinflammation (263). In addition, normal aging causes elevated peripheral and neuro-inflammatory responses (268). Hence, when elderly patients with neurodegenerative diseases experience systemic infection they produce an exacerbated maladaptive neuroinflammatory response resulting in further neurodegeneration and accelerated disease progression. Considering this, recurrent peripheral infection may be a serious risk factor for both the development of AD and accelerated AD progression.

Infection in patients with AD is common (269) and urinary tract infection (UTI) has been shown to be among the most common reasons for hospital admission in AD patients and importantly is more prevalent than in healthy controls (270). Hence, in this study we aim to investigate the effect of recurrent urinary tract infection on cognitive abilities, neuroinflammation and neuronal function in the TgF344-AD model. We conducted this study in early time-points prior to known Aβ plaque and neurofibrillary tangle deposition to assess if increased inflammation can accelerate disease progression in these animals. We hypothesise that recurrent systemic infection will result in accelerated cognitive decline in the TG rats and increased neuroinflammation and neuronal dysfunction. We aim to assess this by the novel object recognition test, [^{18}F]DPA-714 PET and MRS. UTI was administered to WT and TG rats at 8 and 11 months of age. Cognitive assessments were carried prior to (3 and 6 months) and after each subsequent infection (9 and 12 months). Imaging was performed before any infection at 6 months and after two bouts of UTI at 12 months of age. The social interaction test was also carried out as high anxiety-like behaviour was found in this strain (see Chapter3).

Methods

Animals

Two male and female wild-types (WT) Fisher and TgF344-AD rats with the APP_{swe} and $PS1_{\Delta e9}$ mutations were purchased to Prof T. Town lab (University of Southern California) (114) and were set up as breeding pairs in house at the Biological Services Unit in the University of Manchester. A total of 21 TGs and 21 WTs male rats were chosen for the imaging and behaviour study and were split randomly into 4 groups based on the fact that infection had to be done on a box basis; WT and TG infected and non-infected (WT/TG_I/NI). However, 2 TG rats were found dead prior to infection and 1 WT in the infected group became ill and was culled at 12 months. Therefore, 10 WT_NI, 10 WT_I, 10 TG_NI and 9 TG_I were used to investigate DPA-714 PET and metabolite profiles. All animals were housed as described in chapter 3 and all experiments were carried out in accordance with the Animal Scientific Procedures act 1986, with local ethical review at the University of Manchester.

Study Design

The study design is set out in Figure 1a. Urinary tract infection was administered to the WT and TG infection groups at 8 and 11 months of age. Behavioural assessment was carried out prior to (3 and 6 months) and after (9 and 12 months) UTI. Similarly, imaging was carried out prior to infection at 6 months and after 2 rounds of UTI administration at 12 months of age. All imaging was carried out during the light phase (7am-7pm), however behavioural assessments were carried out during the dark phase (5-7am) in a room with low lighting. A minimum of a week was given between behavioural tests and imaging modalities.

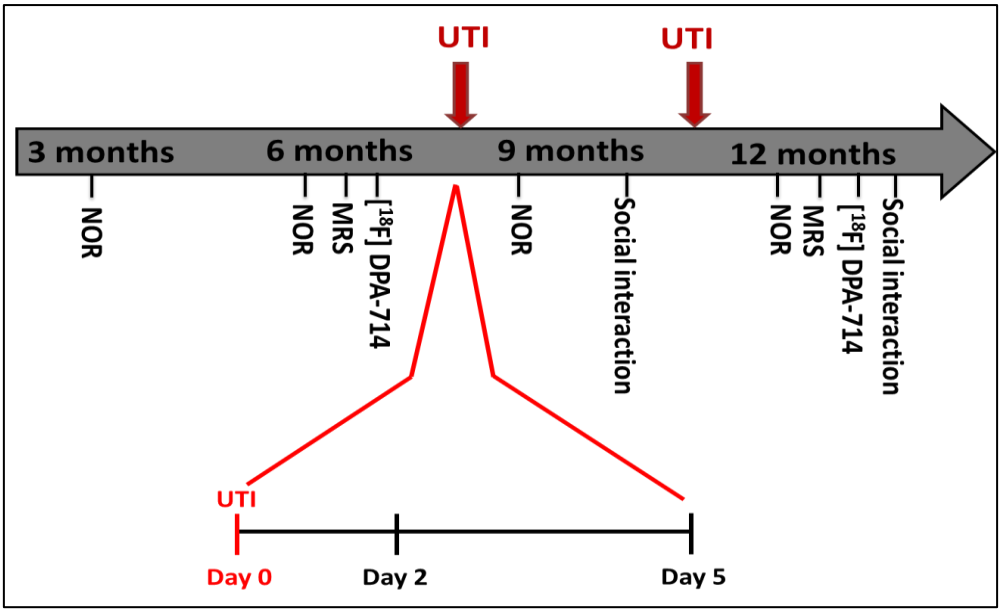

Figure 1 Study design to investigate recurrent UTI on behavioural and imaging outcomes. Behavioural assessments were carried out at all time-points. Baseline imaging was acquired at 6 months. UTI was administered at 8 and 11 months of age. Imaging was repeated post-infection at 12 months. Urine was collected at day 2 and 5 to confirm infection.

Urinary tract infection

UTI was administered to the WT_I and TG_I groups at 8 and 11 months of age using *Escherichia coli* (*E. coli*) UTI89 at a concentration of 1.3 x 10^9 cfu/mL. *E. coli* were stored as 1.02x10^{11} cfu/mL in 15% glycerol and were thawed rapidly and brought to the correct concentration using sterile phosphate buffered saline prior to infection. Rats were anaesthetised and infected with 0.1mL of *E. coli* UTI89 by inserting a catheter (polyethylene tubing covering 30-G hypodermic needles) into the urethra and injecting the inoculum into the bladder. Prior to infection buprenorphine 0.03mg/kg was used and the animals' bladders were emptied by gently pressing on the abdomen to release any bladder content. Infected animals were placed into clean cages and were monitored for 3 days for signs of illness. Urine samples were taken 2 and 5 days post infection to confirm infection levels (Figure 1b). Urine was plated on CLED agar plates and incubated at 37°C for 18-24hrs after which colony forming unit (CFU) counts were performed. Counts were scored 0, 0.5, 2, 3, or 4 based on the following classification of CFU counts in the below table.

0	0- Zero colonies
0.5	+- Scanty growth <5 cfu
2	+ Scanty growth <20 cfu
3	++- >20 cfu
4	+++- Confluent growth

Table 1 UTI was confirmed using CFU counts scored from 0 to 4.

Behaviour

As increased anxiety was seen in Chapter 3 and previous studies, all animals were extensively handled and habituated to the test arena with littermates prior to behavioural testing to reduce anxiety.

Novel Object Recognition Tests

Novel object recognition (NOR) test was carried out at 3, 6, 9 and 12 months of age in the four groups as previously described in Chapter 3 (228). In brief, the animals were placed in a test arena in 3% light and were exposed to two identical objects in the acquisition phase. One object was replaced by a novel object in the retention phase. Exploratory behaviour was recorded for 3 minutes in both phases using an overhead camera. A three minute delay was used between phases where the rats were in an empty unfamiliar cage. Results were expressed as total exploration times, time investigating each object and side and discrimination index (DI). Total exploration times were analysed to assess the active investigation with each group. The time spent exploring the two identical objects on each side in the acquisition phase was assessed per group to ensure there was no side bias that could affect the results in the retention phase. The DI was calculated to measure the amount of time spent investigating the novel and familiar in the retention phase. The DI is defined as subtraction of the time spent exploring the novel and the familiar object, divided by the total time. A minus value demonstrates increased time spent exploring the familiar object, zero value indicates no preference and a positive value demonstrates an increased amount of time exploring the novel object. A threshold was set for minimum exploration to be included in discrimination analysis with animals spending less than 2 seconds total exploration time excluded as well as animals that displayed same side bias (greater than 65%) in both phases. NOR behaviour was analysed at three different time-frames; (i) prior to any infection at 3 and 6 months, (ii) after one UTI administration at 9 months and (iii) after two rounds of infection at 12 months of age.

Social Interaction Test

Social interaction test was carried out in all groups at 9 and 12 months of age to assess anxiety-like behaviour (251). The test was performed as previously described in chapter 3. In brief, a test rat was exposed to an unfamiliar WT conspecific rat for 10 minutes in 45% light, which is age, weight and infection status matched. An inanimate object is placed in the centre of the arena and the time spent sniffing, following and avoiding the conspecific animal as well as the time exploring the object were recorded.

[^{18}F]DPA-714 PET Acquisition and Analysis

[^{18}F]DPA-714 was produced using the method previously described by James *et al.* (225). [^{18}F]DPA-714 PET was carried out in WT and TG rats at 6 months prior to infection (n=20 for WT and n=19 for TG) and in infected and non-infected groups after two rounds of UTI at 12 months of age (n=10 for WT_NI, n=10 for WT_I, n=10 for TG_NI and n=9 for TG_I). PET acquisition and analysis was performed as previously described in Chapter 3. In brief, animals were anaesthetised and an average of 30mBq of [^{18}F]DPA-714 was injected into each rat via the tail vein at a rate of 1ml/min in a 30s bolus. Dynamic PET was carried out and images were reconstructed using OSEM3D, analysed in BrainVisa and Anatomist and quantified using an adapted MRI template (252). The following regions of interest (ROI) were chosen for quantification; entorhinal cortex (EC), cingulate cortex (CC), motor cortex (MC), somatosensory cortex (SA), frontal cortex (FC), temporal cortex (TC), hippocampus (HC), thalamus (TH), hypothalamus (Hypo) and striatum (ST). All data were corrected for body weight and expressed as standard uptake values normalised to the cerebellum (NUV_{cb}) for each animal.

Magnetic Resonance Spectroscopy Acquisition and Analysis

Single voxel MRS was performed prior to infection at 6 months of age (n=20 for WT and n=19 for TG) and after infection at 12 months of age (n=10 for WT_NI, n=10 for WT_I, n=10 for TG_NI and n=9 for TG_I).MRS acquisition was performed in the HC, TH, Hypo and cortex (Ctx) as described in chapter 3 using a 7 Tesla magnet (Agilent Technologies, Oxford Industrial Park, Yarnton, Oxford, UK) interfaced to a Bruler AVANCE II console (Bruker Spectrospin, Coventry, UK). In brief, animals were

anaesthetised and a structural MRI scan (Fast Low Angle SHot) was used to allow voxel placement, followed by FASTMAP shimming to ensure field homogeneity, VAPOR water suppression and a PRESS sequence for spectral acquisition (TR 2500ms, TE 20ms). Spectra were processed and quantified as previously described in Chapter 3 using QUEST in jMRUI and the same basis-set which included; NAA (N-acetylaspartate, Glu (glutamate), mI (*myo*-Inositol), Cr (creatine + phosphocreatine), Taur (taurine), tCho (choline and phosphocholine, glycerophosphocholine), glutamine (Gln), GABA, scyllo-Inositol (Scy-I), amino acid proton at 3.76 ppm and macromolecules at 0.9, 1.3 ppm. Metabolites are expressed as amplitude of institutional units relative to water.

Statistical analysis

GraphPad® Prism™ for Windows (v6.04, GraphPad Software, Inc., San Diego, California USA) was used for all statistical analyses. For behavioural data the 3-6 (prior infection), 9 (after 1 infection) and 12 (after 2 infections) months data were treated separately. Two-way analysis of variance (ANOVA) was carried out on total exploration times and DI for each group. Paired *t*-tests were carried out to assess whether there was side preference in the acquisition phase. For imaging outcomes unpaired *t*-tests were carried out on 6 month data to assess differences in WT and TG rats prior to pathology or infection.. Shapiro-Wilks normality test was carried out to assess Gaussian distribution on raw left and right exploration times. Mann-Whitney was carried out if data were not normally distributed. To assess the effect of infection and gene a two-way analysis of variance (ANOVA) were performed, with post-hoc analysis using Sidak's multiple comparisons test. A two way ANOVA was also employed to look at the effects of age and group. Significance was set at $p \leq 0.01$ for interactions and at $p \leq 0.05$ for all other analyses.

Results

Urinary Tract Infection

UTI was confirmed by assessing urine samples plated on CLED agar plates at day 2 and 5 post-infection. Both WT and TG displayed positive infection at 7 and 11 months (Figure 2a-b). No significant differences were observed between the level of infection seen in the WT and TG rats.

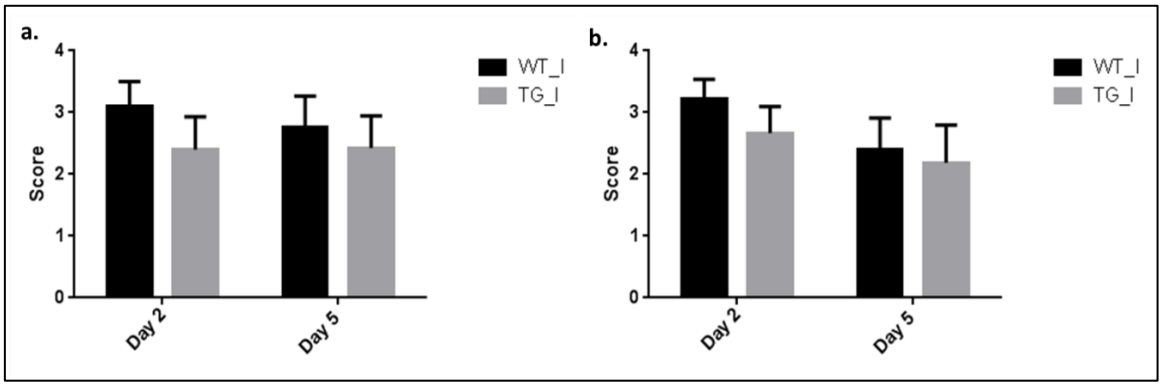

Figure 2 CFU scores confirming UTI infection at 7 **(a)** and 11 **(b)** months of age in WT (n=10) and TG (n=9) rats. Results are shown as mean±SD

Behaviour

To assess the cognitive abilities of WT and TgF344-AD rats at 3-6, 9 and 12 months with and without infection, the NOR was carried out.

NOR test prior to Infection

To investigate cognition in WT and TgF344-AD rats prior to UTI, NOR was assessed and at 3 and 6 months of age. No significant differences were identified between the exploration of the left and right objects in the acquisition phase at either time-point (Figure 3g), allowing investigating of cognition without side bias. A significant effect of age (Figure 3a, $p \leq 0.0001$) and a significant age × gene interaction ($p=0.0725$) was found for total exploration times in the acquisition phase. A trend for an effect of gene was found for the acquisition phase ($p=0.0622$) was also observed. Using multiple comparisons a significant decrease was seen in total exploration time in WT rats with age ($p \leq 0.0001$) and retention ($p \leq 0.05$) phases at 3 months of age. A significant effect of age (Figure 3d, $p=0.0314$) and gene ($p=0.0238$) was seen in the exploration times of the retention phase

with significantly lower exploration times seen in TG compared to WT rats at 3 months ($p<0.05$). Average DI results were positive suggesting a preference for the novel object (Figure 3j). However, the two-way ANOVA of DI data did not show any significant differences between groups or with age suggesting that at these ages the TG rats do not display cognitive decline compared to age matched WT rats.

NOR test after one round of UTI

To investigate cognition after a single round of peripheral infection (UTI), NOR was assessed in the WT and TG infected and non-infected groups at 9 months of age. No groups displayed any side preference in the acquisition phase (Figure 3h). A significant effect of gene was seen on the total exploration times in the acquisition phase (Figure 3b, $p\leq0.0082$) and the retention phase (Figure 3e, $p\leq0.0238$) with TG rats demonstrating lower times in both phases. No effect of infection or gene × infection was found therefore this result is suggestive of decreased locomotor activity in TG rats compared to WT irrespective of their infection status. All groups displayed a positive average DI results indicative of a preference for the novel object (Figure 3k). No significant differences were seen as a result in DI results of either infection or gene using a two-way ANOVA suggesting no differences in cognition between groups regardless of infection.

NOR test after re-current UTI

NOR was also assessed at 12 months of age after two rounds of UTI. As with all the other time-points no side bias was seen in the acquisition phase (Figure 3i). No significant effects of infection or gene were seen on total exploration times in either the acquisition or retention phase (Figure 3c&f). A two-way ANOVA of DI results revealed a significant effect of both infection (Figure 3l, $p=0.0254$) and gene ($p=0.0258$). Multiple comparison analysis demonstrated significantly reduced DI values in the TG_I group compared to both TG_NI ($p<0.05$) and WT_I groups ($p<0.05$) (Figure 3i), suggesting that re-current peripheral infection is sufficient to cause increased cognitive decline in TG rats.

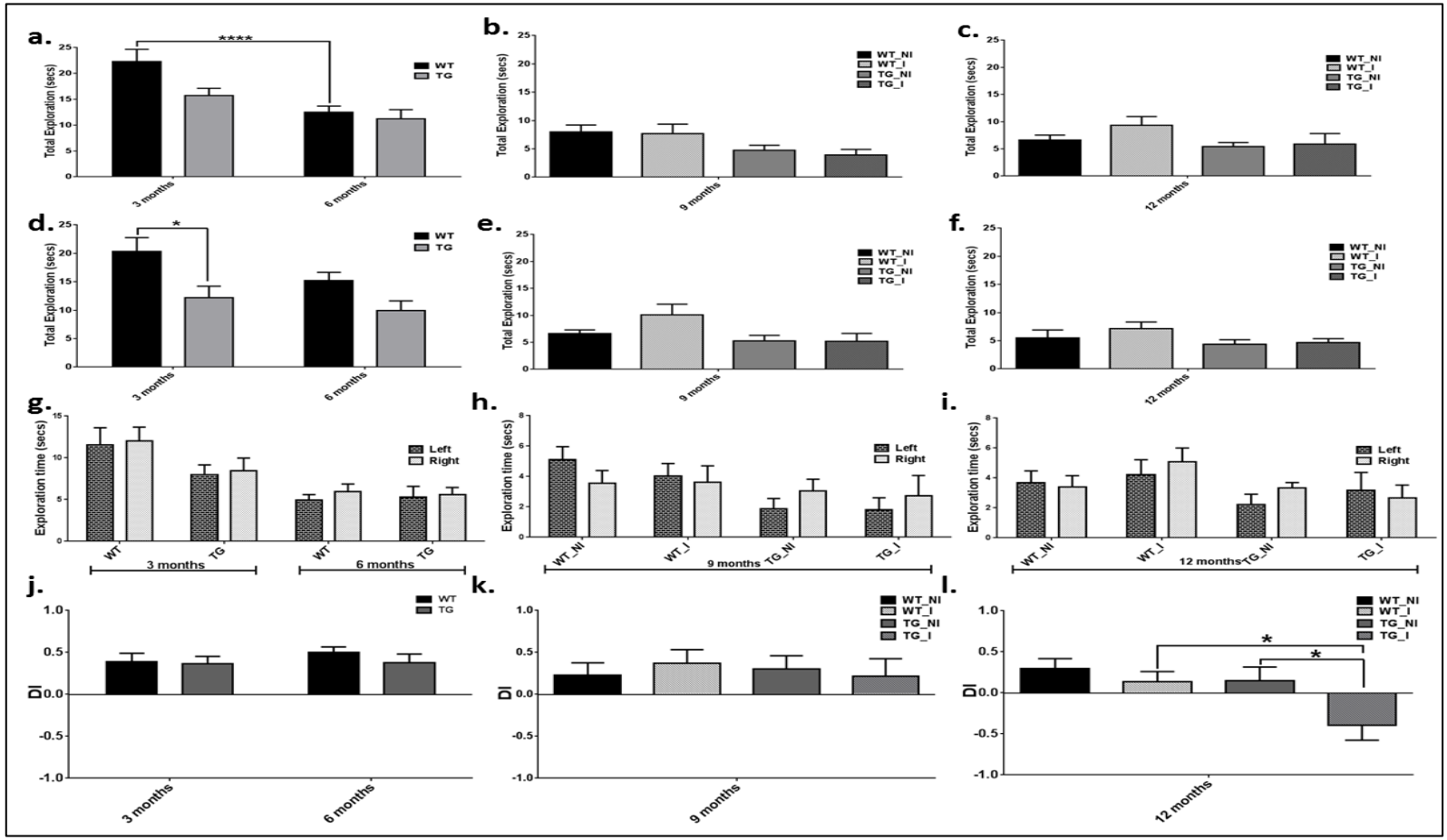

Figure 3 NOR results were assessed prior to infection (3-6 months, n=19 and 17 for WT and TG), after one round of infection (9 months, n=, 9, 7, 8, 5 for WT_NI, WT_I, EG_NI and TG_I) and after two UTI (12 months, n=, 8, 8, 9, 5). Total exploration times in the acquisition **(a-c)**, and retention phase **(d-f)** were assessed. Side preference **(g-i)** was investigated using paired t-tests. Preference for novel and familiar objects was expressed as DI **(j-l)**. Results are shown as mean±SEM. DI and total exploration were assessed by a two-way ANOVA followed by Sidak post hoc analysis for total exploration times and DI for each data group (*p≤0.05, ****p≤0.0001).

Social interaction test

The increased lack of exploration seen in the TG rats was suspected to be due to increased anxiety-like behaviour, therefore the social interaction test was carried out on the same animals from at 9 and 12 months of age. No effect of infection or interaction gene × infection was seen on any anxiety-like behaviours at any age, however a significant effect of gene was seen at both 9 and 12 months on sniffing behaviour ($p \leq 0.0001$, $p=0.0202$, Figure 4a-b), with lower times seen in TG groups. At 9 months of age, a significant effect of gene was also seen on avoidance ($p=0.0309$) and exploring ($p=0.0008$) behaviour with decreased exploration times and increased numbers of avoidances displayed by TG rats (Figure 4c&e). No effects were seen on these behaviours at 12 months of age (Figure 4d&h) and no effects were seen on following behaviour at either age (Figure 4e&f). Overall, these results suggest that TG rats display enhanced anxiety-like behaviour compared to the already anxious WT rats.

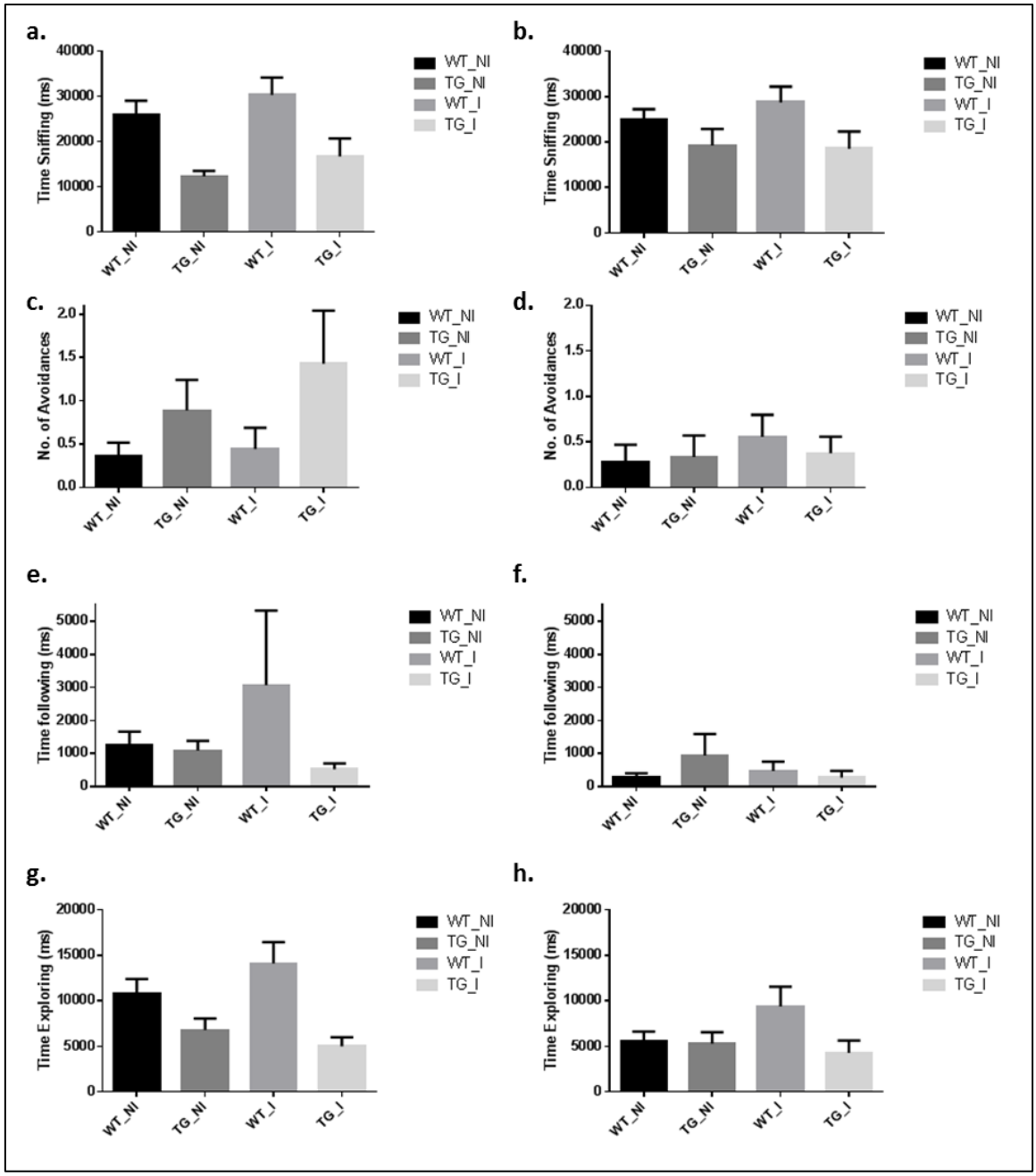

Figure 4 Social interaction revealed increased anxiety in TG rats. This tests assessed sniffing **(a)** and **(b)**, avoiding **(c)** and **(d)**, following **(e)** and **(f)** and exploring behaviour **(g) (h)** at 9 **(a, c, e, g)** and 12 **(b, d, f, h)** months of age. Results are shown as mean ±SEM. Statistical analysis was performed using a two-way ANOVA.

[^{18}F]DPA-714 PET prior to infection at 6 months

To investigate the effect of recurrent UTI on neuroinflammation, [^{18}F]DPA-714 PET was carried out prior to any infection in WT and TG rats at 6 months and after two bouts of infection at 12 months of age. PET imaging at 6 months of age revealed significant effects of gene with increases in NUV_{cb} values seen in the CC (7%, p=0.0057), MC (10%, p=0.0011), TC (6%, p=0.029), TH (14%, p≤0.0001), and Str (6%, p=0.0261) of TG rats compared to WT (Figure 5a).

Effect of infection on [^{18}F]DPA-714 PET at 12 months

At 12 months of age the groups were split into infection and no infection and the effect of infection and gene were assessed in each region using a two-way ANOVA (Figure 5b). No overall significant effects of infection were found on [^{18}F]DPA-714 NUV_{cb} values, however a significant gene × infection interaction was seen in the Hypo (Figure 5c, p=0.0319). This resulted in [^{18}F]DPA-714 uptake increasing in WT rats and decreasing in TG rats, however these effects were not significant using multiple comparisons. A trend for a significant effect of infection (p=0.06), in addition to a significant effect of gene (p=0.0007) was observed on [^{18}F]DPA-714 uptake in the TC. Although the post-hoc tests did not reveal any differences between groups, the two-way ANOVAs revealed a significant effect of gene alone in the HC (p=0.0235), with an average increase of 12% in [^{18}F]DPA-714 uptake seen in TG rats across groups regardless of infection. A trend for increased [^{18}F]DPA-714 uptake in the CC (p=0.058) and the EC (p=0.066) with an average increase in TG rats of 8% and 6% respectively.

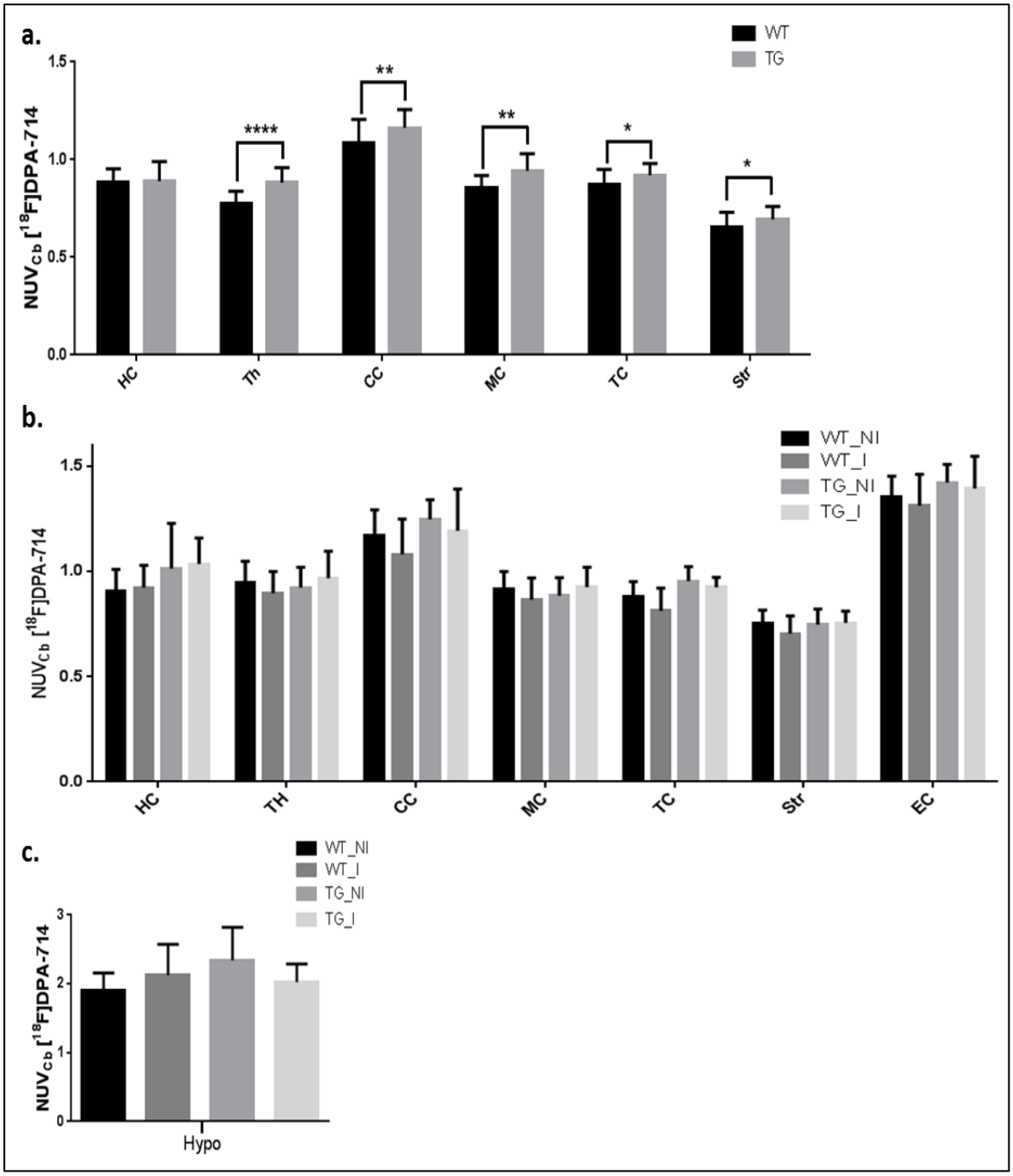

Figure 5 NUV_{cb} [^{18}F]DPA-714 uptake values were assessed in TG (n=19) and WT (n=20) rats prior to infection at 6 months **(a)** and after two bouts of UTI at 12 months (n=10, 10, 10 and 9 for WT_NI, WT_I, TG_NI andTN_I) **(b)** in the hippocampus (HC), thalamus (TH), cingulate cortex (CC), motor cortex (MC), temporal cortex (TC), striatum (Str), entorhinal cortex (EC) and hypothalamus (Hypo) **(c)**. Results are shown as mean±SD Statistical analysis performed using unpaired t-tests for 6 month data and using a two-way ANOVA 12 month data. (** $p \leq 0.01$, **** $p \leq 0.0001$).

Effect of age on [^{18}F]DPA-714 PET

To assess the evolution of neuroinflammation with age across groups the 6 month WT and TG groups were split into the 4 groups (WT_NI, WT_I, TG_NI and TG_I) seen at 12 months. A two-way repeated-measures ANOVA of group and age revealed a significant effects of age only on [^{18}F]DPA-714 NUV_{cb} values in the CC (Figure 6a, p=0.002), FC (Figure 6b, p=0.0004), SC (Figure 6c, p=0.0219), HC (Figure 6e, p=0.0004), Hypo (Figure 6f, p=0.0032), TH (Figure 6e, p<0.0001) and Str (Figure 6h, p=0.0002). Increased uptake was seen in all regions from 6 to 12 months of age (+5% in CC, +15% in FC, +4% in SC, +9% in HC, +11% in Hypo, +13% in TH, +10% in Str average across all groups). No interaction was seen in these effects therefore these alterations are indicative of normal aging in this strain.

A group effect (p=0.0039) and an age × group interaction (p=0.0481) were found in the TC (Figure 6c). This resulted in age causing increases in non-infected groups (+2% in WT and +6% in TG) and decreases in infected groups (-8% in WT and -1% in TGs) and is in line with the infection × gene interaction observed in this region at 12 months. A group effect (p=0.0187) was also seen in the TH (Figure 6g). This resulted in larger increases in WT groups compared to TG groups with age and is in agreement with TGs having higher basal [^{18}F]DPA-714 NUV_{cb} values at 6 months.

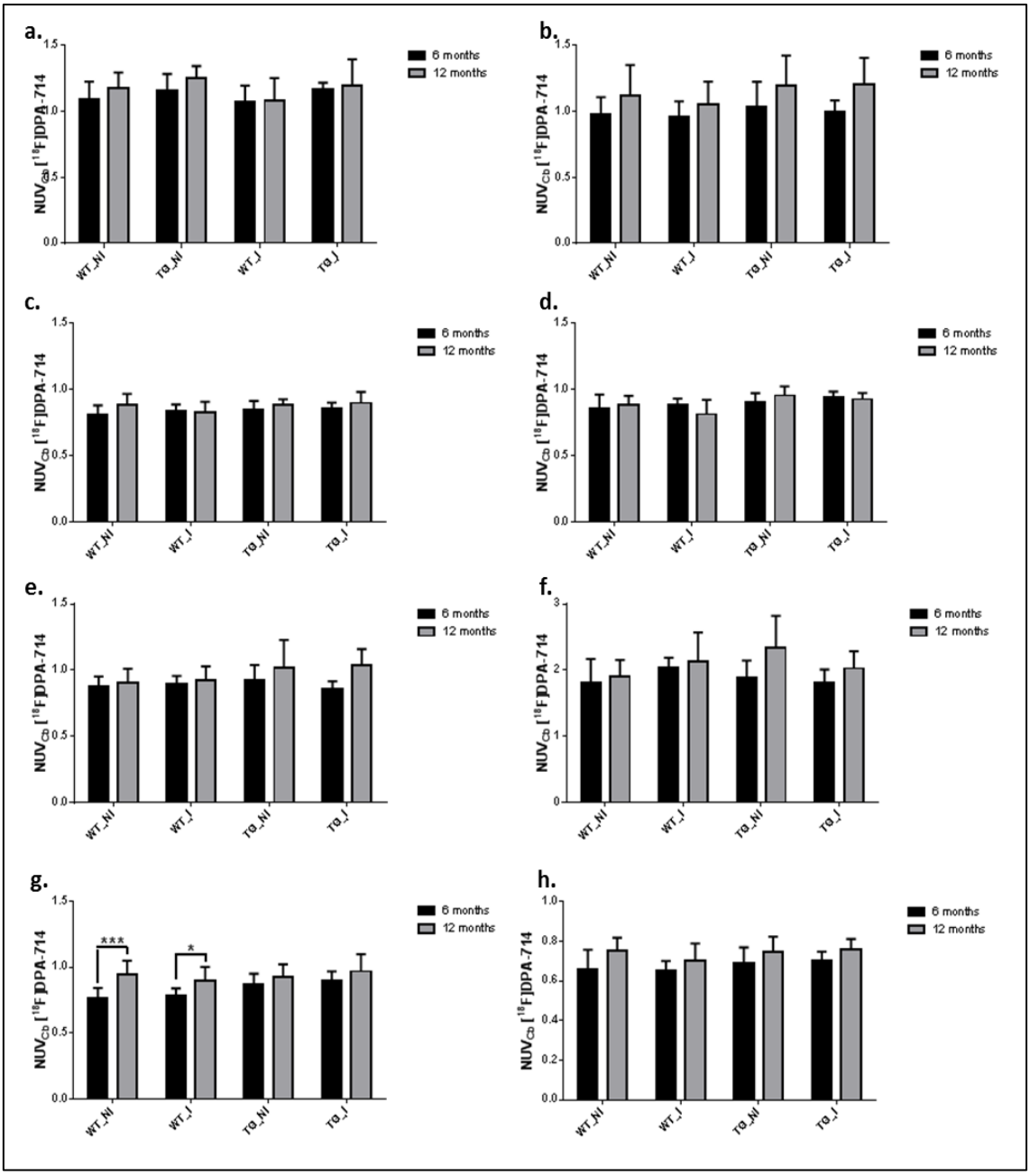

Figure 6 Effects of age on [^{18}F]DPA-714 NUV_{cb} values from 6 to 12 months of age ((n=10, 10, 10 and 9 for WT_NI, WT_I, TG_NI andTN_I) in the cingulate cortex **(a)**, frontal cortex **(b)**, somatosensory cortex **(c)**, temporal cortex **(d)**, hippocampus **(e)**, hypothalamus **(f)**, thalamus **(g)** and striatum **(h)**. A significant increase in WT groups was seen in the thalamus that was not significant in the TG groups after multiple comparisons. Results are shown as mean±SD Statistical analysis performed using a two-way ANOVA followed by Sidak post hoc analysis. (* $p \leq 0.05$, **** $p \leq 0.0001$).

Metabolite profile prior to infection at 6 months

Metabolite profiles in WT and TG rats were assessed prior to any infection at 6 months of age using *t*-tests (Figure 7). A significant increase in mI levels in the HC (p=0.0167, +14%). and TH (p=0.043, +10%). Similarly, increased NAA levels (p=0.0214, +8%) were also observed in the TH of TG rats at this age.

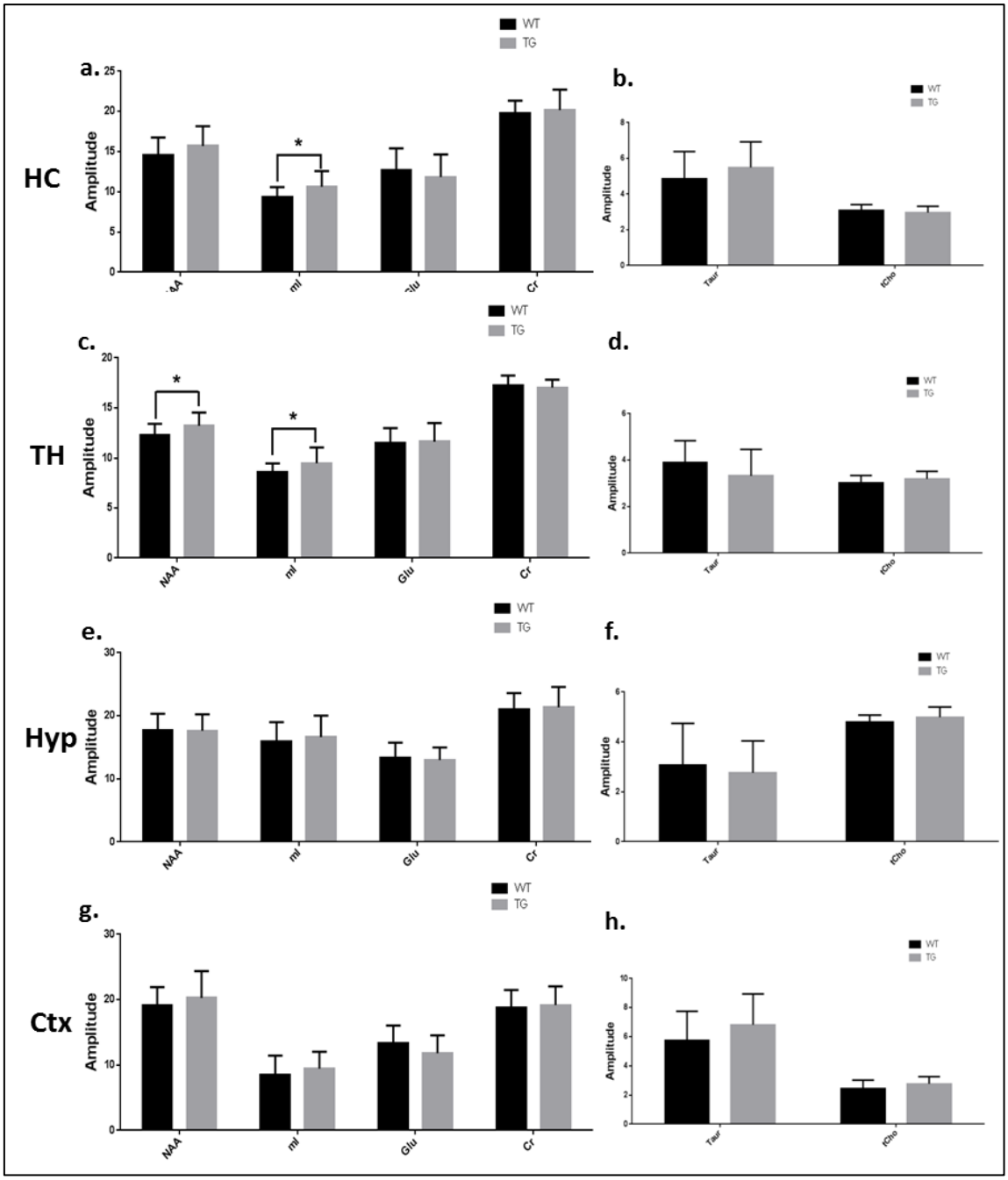

Figure 7 MRS metabolite profiles at 6 months of WT (n=20) and TG (n=19) rats in the hippocampus **(HC, a-b)**, thalamus **(TH, c-d)**, hypothalamus **(Hypo, e-f)** and cortex **(Ctx, g-h)**. Results are shown as mean±SD. Statistical analysis performed using unpaired t-tests corrected for multiple comparisons.

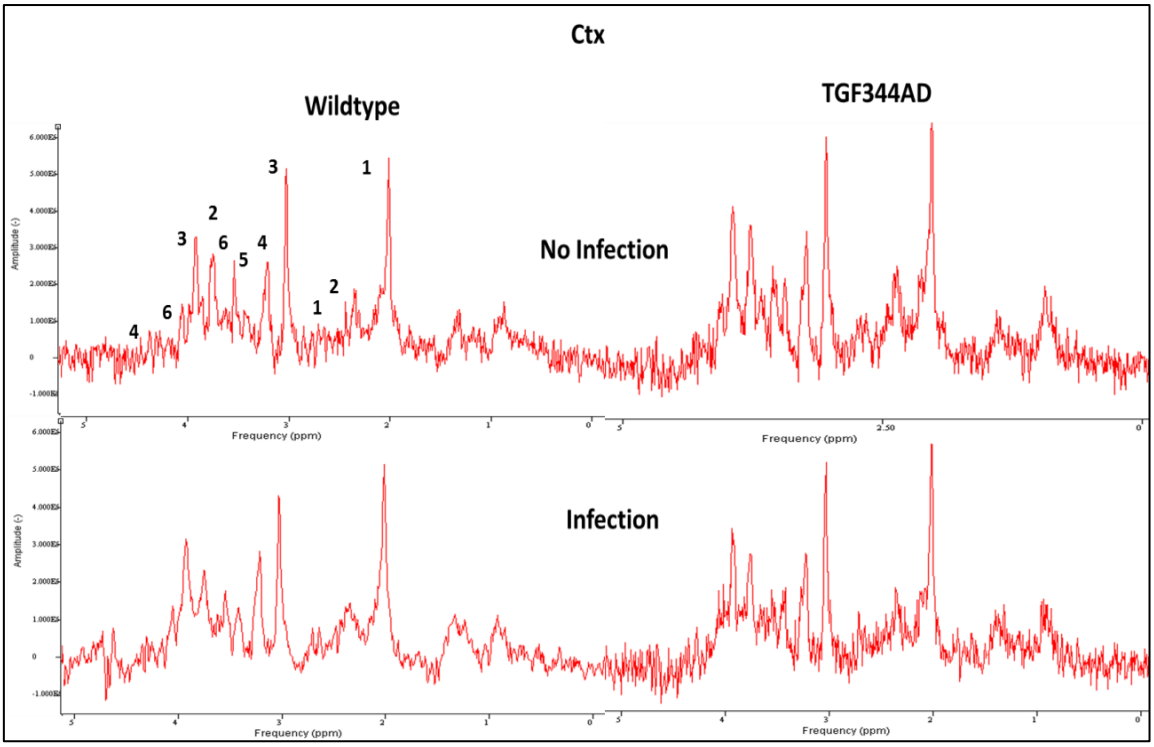

Figure 8 Examples of MRS spectra obtained in the cortex (ctx) from WT and TG rats at with and without infection at 12 months of age. The multiple peaks of metabolites of interest are labelled as 1:NAA, 2:Glu, 3:Cr, 4:tCho, 5:Taur, 6:mI. Representative spectra were shown based on average NAA levels for each group.

Metabolite profile as an effect of infection at 12 months

At 12 months of age the effect of UTI and gene on metabolite profile was assessed (Figure 7). A significant infection × gene interaction (Figure 9, p=0.0825) as well as a significant effect of gene (p=0.0488) was observed on mI levels in the Hypo. A significant increase was seen in TG_NI versus WT_NI (Figure 9e, +16%, p<0.05) that was not significant in TG_I versus WT_I (+1%). Hence, peripheral infection in these animals resulted in an increase in mI in the WT and a decrease in mI in the TG rats in this region that masked the gene effect seen in the non-infected groups.

A two-way ANOVA revealed a significant effect of infection (Figure 9h) but no gene effect or interaction on tCho levels in the Ctx, with increased tCho levels demonstrated with infection in both groups (+14% average across WT and TG) compared to non-infected gene matched animals. An effect of infection that was just outside of significance (p=0.0506) and a significant effect of gene (p=0.0332) was observed on NAA in the Hypo (Figure 9e). This resulted in increased levels seen in the TG compared to WT rats in both infected and non-infected groups (+8% average in TG versus WT infected and non-infected combined), however infection appears to further increase NAA levels in this region (+7% average in infected versus non-infected WT and TG combined). A trend for infection was also seen on Cr levels (Figure 9a, p=0.0525) with decreased levels of Cr seen in infected versus non-infected groups (+5% average). No other metabolite effects were identified as a result of infection.

Metabolite profile as an effect of gene at 12 months

Gene but not infection had a significant effect on Glu (p=0.0493) and tCho (p=0.022) levels in the Hypo, with increased levels of both seen in TG groups compared to WT groups at 12 months (Figure 9e-f). A 14% and 11% increase was seen in TG Glu in the non-infected and infected groups and an 8% and 5% increase in TG tCho was measured in the non-infected and infected groups respectively. No other significant differences were seen at this age in any region.

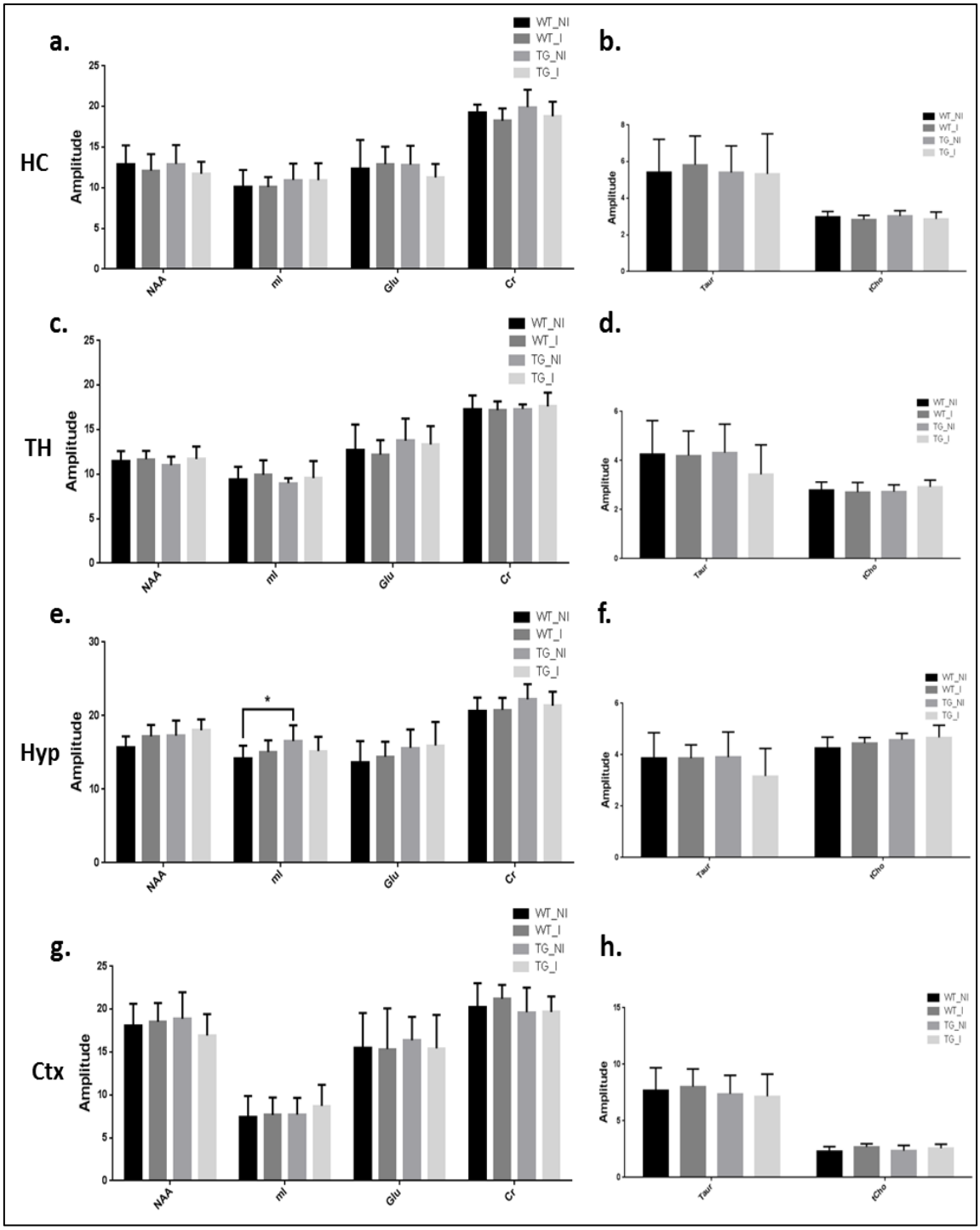

Figure 9 Metabolite profiles of WT and TG non-infected and infected rats at 12 months (n=10, 10, 10 and 9 for WT_NI, WT_I, TG_NI andTN_I) in the hippocampus **(HC ,a-b)**, thalamus **(TH, c-d)**, hypothalamus **(Hypo, e-f)** and cortex **(Ctx, g-h)**. Results are shown as mean±SD. Statistical analysis performed using a two-way ANOVA followed by Sidak post hoc analysis. (* $p \leq 0.05$).

Metabolite profile as an effect of age

To assess the effect of age across the different groups, the 6 month data was split into the treatment groups for 12 months and a two-way ANOVA for age and group was carried out for each metabolite (Figure 10). A significant effect of age (Figure 9b, $p \leq 0.0001$) as well as a significant age × group interaction ($p=0.0432$) was observed on NAA levels in the TH (Figure 10b, $p \leq 0.0001$) and Ctx (Figure 10c, $p=0.0241$). NAA levels were reduced in all groups at 12 compared to 6 months of age but were only significant in the TG groups (-17% in TG_NI, $p \leq 0.0001$ and -11% in TG_I, $p \leq 0.05$) with post hoc analysis. NAA in the Ctx was also effected by age (Figure 10c, $p=0.0241$) and a significant age × group interaction ($p=0.0628$), with a significant decrease using multiple comparisons only evident in the TG_I group (-22%, $p \leq 0.01$). A significant effect of age but not of group or age × group interactions was observed on NAA levels in the HC (Figure 10a, $p \leq 0.0001$), with decreases observes in all groups with age (-18% average across groups).

Two-way ANOVAs revealed a significant effect of age only on different metabolites. Age significantly affected Glu levels in the TH (Figure 10d, p=0=0048, +12% average), Hypo (Figure 10e, p=0.0069, +12% average) and Ctx (Figure 10f, p=0.0002, +25% average), with increased Glu levels observed across all groups from 6 to 12 months in these regions. Similarly, Taur levels were also significantly increased with age in the Hypo (Figure 10l, p=0.0051, +22% average) and the Ctx (Figure 10m, p=0.0033, +29% average). Age had a significant effect on Cr levels with reduced levels seen with age in the HC (Figure10j, p=0.0354, -5% average) and increased levels seen in the Ctx (Figure 10k, p=0.0476, +7% average) with reduced levels seen across groups. tCho levels were decreased with age in the TH (Figure 10g, $p \leq 0.0001$, -10% average) in all groups. No effects of group or interactions were found for any of the above effects, suggesting these changes are due to normal aging in this strain.

Some effects of group were observed but supported the previous results of gene and infection effects. A significant effect of age (Figure 10h, $p \leq 0.0001$) and group ($p=0.0391$) was seen on tCho levels in the Hypo. Age resulted in a decrease in tCho levels in all groups (-12% in WT_NI, -7% in TG_NI, -6% in WT_I and -7% in TG_I). This was significant using multiple comparisons in the WT_NI group ($p \leq 0.01$). This group effect

can be explained by higher levels observed in TG groups at 12 months and support the gene effect seen on tCho levels in this region at 12 months. A significant age × group interaction was observed for tCho in the Ctx (Figure 10i, p=0.0278). Decreased tCho levels were observed in the WT_NI, TG_NI and TG_I groups from 6 to 12 months but WT_I displayed increasing levels. This is in agreement with the significant effect of infection on tCho levels in this region at 12 months.

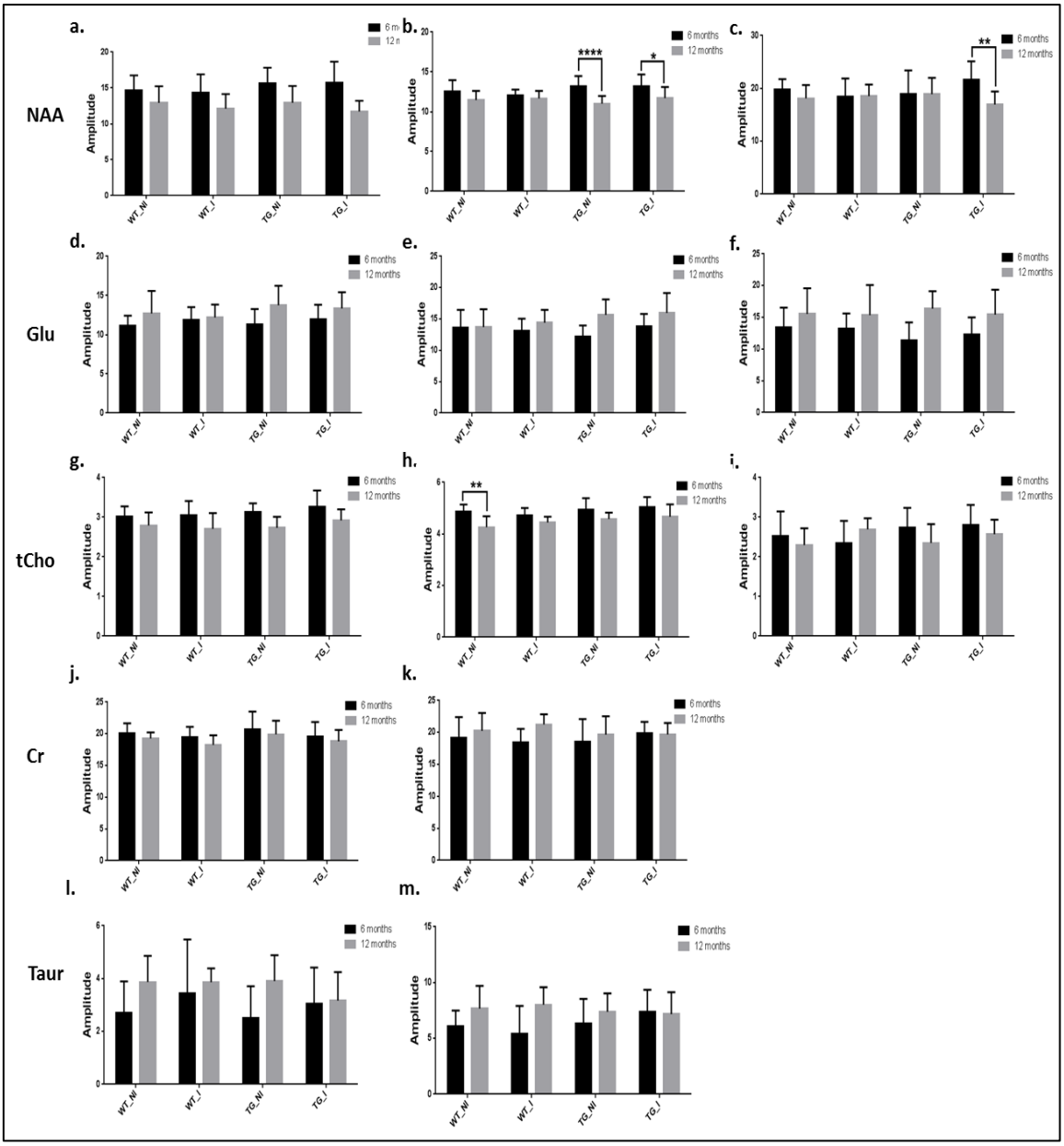

Figure 10 Assessment of age on metabolite levels from 6 to 12 months (n=10, 10, 10 and 9 for WT_NI, WT_I, TG_NI andTN_I). NAA levels decreased with age in the hippocampus **(a)**, thalamus **(b)** and cortex **(c)**. Glu levels were increased in the thalamus **(d)**, hypothalamus **(e)** and cortex **(f)**. tCho levels decreased in the thalamus **(g)** and hypothalamus **(h)**. A significant interaction was seen in tCho levels in the cortex **(i)**. Cr levels decreased with age in the hippocampus **(j)** and increased in the cortex **(k)**. Taur levels increased in the hypothalamus **(l)** and cortex **(m)**. Results are shown as mean±SD. Statistical analysis performed using a two-way ANOVA followed by Sidak post hoc analysis. (* $p \leq 0.05$, ** $p \leq 0.01$, **** $p \leq 0.0001$).

Discussion

Infection induced cognitive decline in TG rats

NOR was assessed prior to infection at 3 and 6 months, and after each UTI at 9 and 12 months of age. The differences observed in total exploration times in this study mirror what we see in Chapter 3. Activity in the WT rats decreased with age. Similarly significantly lower exploration times are seen in TGs at this age however this was also seen in Chapter 3 and is most likely down to increased anxiety in the TG rats. Reduced times were seen in TG groups compared to WT groups at 9 months of age but were not significant post-hoc. No significant differences are observed at 12 months. Infection did not affect the exploration times in either WT or TG rats with infected versus non-infected groups displaying similar exploration times. This is beneficial for assessment of the NOR as infection does not induce a sickness-like behaviour resulting in reduced locomotion and exploration. Despite early differences in total exploration this did not hinder the TG rats showing positive preference for the novel object as shown by positive DI values prior to infection at 3 and 6 months. Similarly at 9 months of age all groups displayed poditive DI values and no significant differences were observed in performance between groups. This result suggesting that neither gene expression nor a single dose of peripheral infection is sufficient elicit cognitive decline in TG or WT rats. Conversely at 12 months of age we observed a significant decreased in DI values in the infected TG rats compared to both non-infected TG rats an infected WT rats. This result demonstrated that recurrent UTI infection can elicit cognitive decline in the TG group that is not seen in the TG groups without infection. This is in line with previous reports suggesting that increased peripheral inflammation can lead to a worse cognitive outcome in AD (6, 92, 266). In addition it also demonstrates a difference between WT and TGs as UTI was not sufficient to drive cognitive decline in the WT group.

As the Fisher strain has been previously been found to be anxious and show low exploration times by us in Chapter 3 and by previous studies we investigated anxiety-like behaviour using the social interaction test in both WT and TG rats. In line with findings in Chapter 3, anxiety-like behaviour was exacerbated in TG compared to WT rats, with TGs displaying increased active avoidances of the conspecific animal as well as reduced

amount of time sniffing and interacting. Reduced exploring of a central object was also observed which mirrors what was seen in the NOR. Infection did not cause any differences in anxiety behaviour for either group. Overall this suggests that TG rats have a tendency to show increased anxiety like behaviour compared to WT rats, but this is not affected by re-current UTI.

Increased [^{18}F]DPA-714 uptake in 6 month old TgF344-AD rats

Significantly increased [^{18}F]DPA-714 NUV_{cb} values were observed in the CC, MC, TC, TH, and Str of TG rats compared to WT. These alterations occur prior to reported Aβ plaque and NFT pathology reported in this model; however increased p-tau and $A\beta_{40}$ were reported (114). This result implicates neuroinflammation as an early driver of disease in AD and supports the idea of soluble amyloid and tau causing toxic effects. In this study we observed increased in more regions that in Chapter 3. This may be explained by the fact that we have a larger n number in this study (n=20/19 versus n=9/10) and are looking at the effect at a specific age here not across ages. Nonetheless this analysis shows gene-specific increased regional inflammation in this model.

Altered [^{18}F]DPA-714 uptake as an effect of infection

Infection did not have an overall significant effect on [^{18}F]DPA-714 uptake in any region, however a trend for reduced [^{18}F]DPA-714 uptake was seen for infection ($p=0.0624$) in the TC. In addition, a significant gene × infection interaction was seen in the Hypo with infection resulting in increased [^{18}F]DPA-714 uptake in WT infected group but decreased values in the TG infected group. Hypothalamic inflammation is known to occur after peripheral infection and is associated with sickness behaviour such as decreased appetite (271). Additionally, the hypothalamus has the highest level of pro-inflammatory cytokine receptors in the brain (272) and may be activated dues to increased plasma cytokine levels as a result of infection. Furthermore it is thought that the Hypo itself can produce inflammatory cytokines in response to peripheral infection causing further inflammation (272). Our result supports this and is also in concordance with increased infectious burden resulting in higher inflammation in a healthy population (97) but in contrast to reports demonstrating that increased peripheral infection results in increased neuroinflammation in AD (6, 92). Nonetheless it provides evidence of an altered

neuroinflammatory response in AD rats. It is important to note that infection is carried out prior to extensive AD-like pathology in these animals. It has been suggested that AD pathology burden in AD primes microglia leading to excessive activation with disease progression (87) and exacerbated responses to systemic infection (6). Hence, the reduced inflammatory response observed in these rats as a result of peripheral infection may be a compensatory or protective mechanism to dampen inflammation as it increases with pathology burden.

Altered [^{18}F]DPA-714 uptake as an effect of gene

Increases in microglial activation in the CC and in the HC are reported at 6 months (36% and 44% respectively) in the TgF344-AD rat by Cohen *et al* (114) and continue to increase with age (66% in the CC and 72% in the HC by 16 months). Here we observe a significant increases in [^{18}F]DPA-714 uptake in the CC at 6 months and a trend for increased values at 12 months of the TG rats. Increased [^{18}F]DPA-714 uptake was observed in the HC of TG rats at 12 but not 6 months of age, indicating that the early increases in the CC but not the HC were high enough to be detected by TSPO PET in this study. Increases in the HC (165) and cortex (169) using TSPO imaging have previously been reported in the APP_{swe}×$PS1_{\Delta e9}$ mouse model with the same mutations as are expressed in this rat model as well as in other APP associated models (117, 166, 167). In addition increased neuroinflammation has been found with PET in a tau model of AD prior to NFT deposition (168). In Chapter 3 an increase in [^{18}F]DPA-714 uptake of the TC was observed. An increase in this region was also found in this study. [^{18}F]DPA-714 uptake was increased at 6 months, but after Bonferroni correction it did not remain significant. However, at 12 months of age we see a highly significant effect of gene in this region with increased values seen in the TG groups compared to the WT, mirroring the results seen in this region in chapter 3. Increases in [^{18}F]DPA-714 uptake were also observed in the TH and MC at 6 months of age but this effect was lost by 12 months.

Age effects on [^{18}F]DPA-714 uptake

Changes in neuroinflammation as assessed by [^{18}F]DPA-714 PET were observed as an effect of age. Age had a significant overall increasing effect on [^{18}F]DPA-714 NUV_{cb} values in the FC, SC, HC, Hypo, Str and TH. These results indicate that increasing

neuroinflammation in these regions is observed as an effect of normal aging and is in agreement with previous reports describing increased microglia in normal aging (165). This in also in concordance with the increases in these regions with age reported in chapter 3. A significant age × group interaction was found in the TC with differences seen in [^{18}F]DPA-714 NUV_{cb} values of non-infected and infected groups, which is in line with the trend for an infection × gene interaction seen at 12 months. Similarly a group effect was seen in addition to an age effect in the TH. This group effect can be explained by the TG rats displaying increased basal [^{18}F]DPA-714 NUV_{cb} values at 6 months in this region.

Altered NAA and mI levels in 6 month old TgF344-AD rats

Increased mI levels were observed in the TH of TG rats at 6 months of age, which is in line with the significant effect of increased [^{18}F]DPA-714 uptake in TGs observed in this region at 6 months. Increased mI was also observed in the HC, where increased microglial and astrocyte activation has been shown *ex vivo* (114), however no effect was detectable in this region with TSPO PET imaging. mI is a putative indicator of gliosis and further evidence is needed to support its association with glia cells, however gliosis a process including activation of both microglia and astrocytes. The lack of consistency with TSPO PET imaging suggests that mI levels may be indicative of early maladaptive glial responses that include astrocyte as well as microglial activity. Hence, the increases in microglia alone are not enough to demonstrate effects on [^{18}F]DPA-714 uptake at this age, whereas the increases with age result in increased DPA-714 uptake in this region at 12 months. On the other hand no effects were seen on mI in the Ctx despite observing increased inflammation via PET in the MC at 6 months of age and it is possible that mI may be associated with pathology burden rather than inflammation as explained earlier. However the cellular microglial and astrocyte activation in this region has not been investigated using *ex vivo* techniques as of yet. Increased mI in the HC and regions of the cortex have been reported in the APP_{swe}×$PS1_{de9}$ mouse model (203, 205) other amyloid based models (201, 202, 204) as well as tau AD models (211). No effects on mI were found in the TG_{2576} model (209). Similarly, a study by Jansen *et al* in APP_{swe}×$PS1_{de9}$ mouse model reported no differences in mI at any age, with decreases in NAA the only metabolite alteration observed (206). In contrast, we report increased NAA levels in TG animals in this study.

Altered metabolite profile as an effect of infection

Infection differently effected mI levels WT and TG in the Hypo. A significant infection × gene interaction was observed in this region resulting in significantly increased mI levels in TG_NI compared to WT_NI. However the mI levels between WT_I and TG_I were not significantly different due to infection causing an increase in mI levels in WT rats and a decrease in TG rats. This antagonistic effect with infection hides the mI differences seen between WT and TG rats and highlights the importance of understanding the effects of co-morbidities on disease and putative diagnostic or progressive markers. This mirrors the increased neuroinflammation with infection in the WT group and the decreased neuroinflammation in the TG group with infection seen in the Hypo with TSPO imaging and suggests that AD animals have an underactive inflammatory response to peripheral infection at this age. However, this is also in contrast to the increased mI levels observed in APP_{swe}×$PS1_{\Delta e9}$ by Pardon *et al* (226), although it is worth noting that this study only investigated metabolite effects in the hippocampus and after 1, 2, 3 and 4 hours post-infection and did not investigate other regions or long-term effects. Despite getting an increase in mI in TGs and not in WTs with peripheral infection they observed increased microglial activation in WT but not TG mice suggesting that mI may not be a good indicator of increases in gliosis. This view has been shared by others and mI has been found to be associated with plaque burden rather than microglial activation in human post-mortem tissue (185). However, the time-points investigated in this study are prior to known heavy plaque or NFT deposition, therefore the microglia may not be sufficiently primed to elicit an exacerbated neuroinflammatory response to peripheral infection. A significant effect of gene and a borderline significant effect of infection ($p=0.0506$) was seen in NAA levels in the same region, with increased NAA seen in TG rat groups which were higher in infected groups. It is possible that prior to heavy pathology burden TG rats may have a reduced neuroinflammatory response and increased neuronal density as a protective or compensatory mechanism. Further investigation is needed to clarify whether mI is a reliable marker for gliosis or not.

A significant effect of infection was seen on tCho levels in the Ctx at 12 months causing an increase on tCho levels in both WT and TG groups. Similarly, a trend for decreased Cr levels with infection was observed in both TG and WT groups. However, this is in contrast to the metabolite alterations observed in APP_{swe}×$PS1_{de9}$ mice in response to

peripheral LPS challenge (226). Pardon *et al* reported a decrease in tCho in both WT and TG mice regardless of infection, whereas we found infection to significantly increased tCho levels observed in the Ctx of both WT and TG groups. They also reported Cr increases as an effect of infection in TG group. In contrast we observed a trend for decreased hippocampal Cr levels in the WT and TG infected rats compared to non-infected animals.

Altered metabolite profile as a result of gene at 12 months

At 12 months of age increased levels of NAA and Glu were observed in the Hypo of TG rat groups compared to the WT rat groups. This result was unexpected as decreased NAA and Glu levels have previously been reported in AD models (201-203, 205-207, 209). Reductions in NAA have been reported in the APP_{swe}×$PS1_{de9}$ model both prior to and after extensive pathology. In contrast, increased tCho levels were identified in TG rats in the Hypo, although tCho alterations in mouse models are not conclusive with some reporting increases (215) and some report no changes (204, 206, 207). Increased mI was seen in as an effect of gene in the Hypo, however no differences were seen in mI levels in the HC or CC despite significant increases in *ex vivo* microglial and astrocyte reported at this age by Cohen *et al.* and increases observed in [^{18}F]DPA-714 PET in these regions in this study.

Age effects on metabolite profile

A significant effect of aging was seen on NAA levels in the HC, TH and Ctx suggesting a normal effect of aging in these regions. However, a significant interaction was seen for NAA levels in the TH and Ctx. A significant decrease in NAA was seen in both TG groups in the TH suggesting that the aging effect of the strain is exacerbated in the TG animals. This is in agreement with the accelerated NAA we observed in the TG mice in Chapter 2. Similarly a significant decrease was only seen in the TG_I group in the Ctx suggesting that NAA loss is accelerated in this group. Nonetheless, decreased NAA is seen as an effect of normal aging in this strain also. This is in agreement with previous reports depicting decreased NAA as an effect of normal aging in humans (273-275). A significant age × group interaction was also seen on tCho levels in the Ctx, with increasing levels in the WT_I and decreased levels in all other groups which further supports the effect of

infection we see at 12 months and suggests that infection is causing a differential effect of aging in this group.

Regional alterations were seen in Cr levels with age. Reduced Cr was observed in HC whereas increased Cr levels were seen in the Ctx in all groups except TG_I. Similarly, Glu and tCho levels were increased as an effect of age in all groups in the TH, Hypo and Ctx. Increased Glu Cho and Cr levels were previously reported in both the AD TG McGill-R-Thy1-APP rats as well as WT rats from 3 to 9 months of age (60). Increased Cho and Cr levels have also been shown in healthy subjects with age (273, 275), indicating an effect of normal aging in these rat strains. Increases were also seen in Taur levels with age. No group effects or interactions were seen for any of these effects therefore they are indicative of normal aging in Fisher rats.

Limitations

A limitation to this study is the lack of *ex vivo* confirmation of microglial and astroglial activation as well as neuronal integrity markers in regions other than the HC and CC reported by Cohen et al. In addition, *ex vivo* confirmation is needed at 12 months of age to confirm imaging results observed in this study.

Conclusion

Here we report accelerated cognitive decline after re-current UTI infection in TG animals. We demonstrate increases in [^{18}F]DPA-714 PET that are in agreement with increased microglial activation markers previously reported in these regions and report evidence for peripheral infection resulting in differential effects in Hypo of WT and TG rats at ages prior to known extensive plaque and NFT deposition. We also report direct effects of infection resulting in increased NAA and tCho levels and a trend for reduced [^{18}F]DPA-714 uptake in the TC and Cr in the Ctx. Surprisingly, no significant effects of infection on [^{18}F]DPA-714 PET or metabolite profile were identified in the HC or Ctx, which could account for the accelerated cognitive decline observed in the NOR. Nonetheless, we can conclude that infection induces cognitive decline in 12 month old TG rats. Moreover, peripheral infection can induce overall changes as well as resulting in

different regional antagonistic responses in WT compared to TG rats. However, a simple model in which TG rats develop a hyperimmunogenic response to infection compared to WT is not supported by our data, which indicate a more complex interaction. We can also conclude that PET and MRS can be used to discriminate between WT and TG rats at an age that is before high pathology burden.

Acknowledgements

This research was supported by the European Union's Seventh Framework Programme (FP7/2007-2013) under grant agreement n°HEALTH-F2-2011-278850 (INMiND). The authors wish to thank all the personnel of the WMIC, especially Dr Michael Fairclough, Ms. Lidan Christie, Mr Michael Green, Mr Jamil Gregory, Ms. Carol Brough and Ms. Gemma Chapman for facilitating the study.

Chapter5. General Discussion

5.1 Overall Summary of Findings

The first aim of this thesis was to identify neuroinflammatory and metabolite changes using non-invasive imaging modalities PET and MRS that could discriminate between normal aging in WT animals and disease in TG animals. This was also supported by the investigation of cognitive decline in these animals. Secondly we aimed to further characterise a relatively new model of AD (TgF344-AD rat) that has been reported to develop all the characteristic pathology found in human AD. To do this we carried out longitudinal characterisation in the APP_{swe}×$PS1_{dE9}$ mouse model and characterisation of early time-points in the new TgF344-AD rat. Thirdly, we aimed to investigate the effects of peripheral inflammation on these markers in the TgF344-AD model using recurrent UTI. Hence this project allowed us to investigate the contribution of neuroinflammatory and metabolite alterations to AD progression but also assess the ability of the non-invasive imaging methods PET and MRS to detect these changes. From this project we can conclude the following:

- Increased neuroinflammation (as assessed by [^{18}F]DPA-714 PET) was seen as an effect of age in the rodents, however specific regional differences allowed discrimination between TG and WT animals. Increases in the hippocampus and cortex were seen in the APP_{swe}×$PS1_{de9}$ mouse, and increases in the thalamus and hypothalamus were seen in the TgF344-AD rat.

- No metabolites were significantly different in any region between WT and TG animals with only aging resulting in altered NAA, Glu, tCho and Taur levels, however gene × age interactions suggest that the aging effect seen on NAA levels exacerbated in both the mouse and rat TG animals.

- Peripheral infection prior to known extensive pathology resulted in accelerated cognitive decline in the TgF344-AD rat but not in WT animals. Peripheral infection also resulted in opposing effects on hypothalamic [^{18}F]DPA-714 PET

and metabolite profile in TG and WT animals, with infection causing increases in neuroinflammation and mI levels in WT rats but decreases in TG rats. This resulted in WT and TG infected animals displaying similar levels and masked the gene effect seen with [^{18}F]DPA-714 uptake in this region. This result highlights the importance of investigating possible confounding co-morbidities on biomarkers of disease.

- [^{18}F]DPA-714 PET and MRS were able to detect neuroinflammatory and metabolite alterations non-invasively in WT and TG rodents.

5.2 Detailed Discussion of Results

5.2.1 [^{18}F]DPA-714 PET and mI as markers of Neuroinflammation

To assess the contribution of neuroinflammation in AD it is implicit to have a marker that is not only highly specific for neuroinflammation but can also be measured non-invasively with good sensitivity. This is particularly important when investigating a disease such as AD that appears to be associated with complex regional changes in neuroinflammation. TSPO PET has been used both clinically and pre-clinically to look at inflammatory changes in conditions such as stroke and has been used to test the efficacy of anti-inflammatory treatments (reviewed by Boutin *et al* (148)). Inflammation is overt and localised in stroke; however changes in AD are thought to be more subtle in comparison. TSPO represents a good marker for assessing neuroinflammation as expression is low in the healthy CNS and is restricted mainly to microglia, and to a lesser extent astrocytes (132). However, upon inflammatory conditions microglia proliferate and TSPO expression is upregulated, therefore providing a marker that is amplified and directly related to increased neuroinflammation. Strong correlation has been shown between TSPO PET results *in vivo* and TSPO staining, microglial activation and autoradiography *ex vivo* (117, 141, 166). In support of this, in Chapter 2 we demonstrated age dependent increases in TSPO and CD11b expression *ex vivo* in the hippocampus and cortex of $APP_{swe}\times PS1_{\Delta e9}$ mice that was not visible in the WT animals confirming increased TSPO expression with increased microglia staining. This was reinforced by increases in hippocampal and cortical [^{18}F]DPA-714 uptake in TG compared to WT mice at all ages, however this increase was not significant until 18 months. If we refer to the *ex vivo* results we can see increased microglial and TSPO expression beginning at 6 months in TG when compared to WT and increasing with age. There is substantial microglial activation detected by immunohistochemistry at 12 months of age in this model when compared to WT mice but this increase is not significant with PET. These results suggest that TSPO based PET can detect increases in neuroinflammation, however the current tracer is not sensitive enough to detect changes at the same rate as seen *ex vivo*. Other studies have also found increases in microglial activation and TSPO expression *ex vivo* at earlier time-points than is detectable in *vivo* with TSPO PET (141, 166). Other smaller more subtle increases are also missed by PET, for example in James *et al.* a small increase was seen in the choroid plexus using autoradiography that was not detected *in vivo (166)*. However, in Chapter 2 as well

as in other mouse studies we are also limited by the small size of the mouse brain and the resolution of our PET scanner (~1.6mm), which meant that regions had to be pooled in order to accurately quantify uptake. By moving to the TgF344-AD rat model of AD in Chapter 3 and 4 we were able to investigate more brain structures with TSPO PET and changes were seen as early as 6 months of age in the TgF344-AD. In Chapter 4 significantly increased [^{18}F]DPA-714 uptake in TG compared to WT mice was observed in the cingulate cortex, which has previously been shown to display age dependent increased microglia and astrocyte activation (114), and further supporting the specificity of TSPO as a marker for increased neuroinflammation. On the other hand increased microglia and astrocytes have been reported in this model in the hippocampus at 6 months using immunohistochemistry (114) but we did not see any differences with PET in this region at the ages investigated in this thesis. In addition, in Chapter 3 when looking longitudinally at [^{18}F]DPA-714 uptake in 6 and 12 month old rats there was a small increase in the cingulate cortex and hippocampus but it was not significant. A significant increase was seen in the temporal cortex, however *ex vivo* analysis has not been reported in this region yet. These results suggest that although TSPO PET is a valid imaging marker for assessing neuroinflammation *in vivo* and can be used to help better understand inflammatory processes in many neurological diseases including AD, more sensitive tracers are needed to detect increases in inflammation at a cellular level. [^{18}F]DPA-714 was chosen in this project as it has been previously found to result in a higher signal to noise ratio, binding and bio-distribution than [^{11}C]PK11195 (153, 154), however development of more advanced tracers that are more sensitive to subtle inflammatory changes would greatly benefit this field. Another major disadvantage in TSPO imaging is that TSPO might not fully discriminate between different activation states of microglia (149). We do not know if the microglia detected by TSPO PET imaging are M1 or M2 activated or somewhere in between. TSPO is also found on macrophages therefore we cannot differentiate between resident inflammatory cells or infiltration of peripheral macrophages using TSPO PET. Although TSPO can give us an overall picture of increased/decreased neuroinflammation it limits the information we can achieve using this method. Multimodal approaches are needed to get a better understanding of the mechanisms at play hence we also employed MRS in this study.

In this project we observed an age dependent increase in neuroinflammation in the hippocampus and cortex of the APP_{swe}×$PS1_{\Delta E9}$ mouse model and in the temporal cortex of TgF344-AD rats, as shown by increased [^{18}F]DPA-714 uptake. However, no significant effects were seen on mI at any age in either TG model. This lack of concordance between mI and TSPO PET results, questions the association between mI and gliosis. Although mI is a putative marker of gliosis, in this study as well as in others (185, 226) we did not find consistent agreement of mI and increased neuroinflammation. Murray *et al* investigated metabolite profiles of probable AD patients *ante-mortem* and investigated the tissue *post-mortem* (185). This study reported no correlation of mI levels with microglial or astroglial markers supporting the theory that mI levels are not directly related to neuroinflammation. Moreover they reported a significant correlation between mI and plaque load but not NFT load suggesting that mI might be a good indicator of amyloid pathology. Increased mI has also been found to be associated with increased uptake of [^{18}F]Flutemetamol as well as being higher in people with a genetic risk (amyloid mutation) for AD and Aβ42-positive healthy controls prior to disease development (276). Therefore increased mI is reported prior to AD development and it is possible this is due to increased amyloid and not inflammation. In support of this it has been shown that mI can interact with amyloid aggregates and it has been shown that pre-incubation of Aβ with mI created stable aggregates and prevented Aβ induced toxicity (277). mI is known to be increased in Down's Syndrome a condition that also results in increased amyloid and risk of AD in later life (278-280). People with Down's syndrome have a duplicate of chromosome 21 which contains the gene for APP as well as the gene for the sodium/mI co-transporter. On the other hand inflammation is known to increase with amyloid pathology and activated microglia are known to surround amyloid plaques. Some studies have reported an increase in mI in parallel to increases in microglial and astrocyte activation. Chen *et al* found that there was increased mI at 3 months of age in the APP_{swe}×$PS1_{\Delta e9}$ mouse (205), which does not develop plaque deposition until 6 months but did reveal increased GFAP staining in TG compared to WT at this age. Therefore it is possible that the increases in GFAP previously reported in the TgF344-AD (114) rat are not sufficient enough to be detected by MRS. In Chapter 4 we observed changes in mI that mirrored changes in [^{18}F]DPA-714 uptake as a result of peripheral infection, however this is the only evidence of agreement and may just be that peripheral infection effects these markers in the same way but does not necessarily mean that they are related. Nonetheless, increased mI levels have been

associated with cognitive decline both in human (280) and in mouse models of AD (210). Moreover mI can differentiate AD from other forms of dementia suggesting that it is an AD-specific marker (193, 200). In agreement of this, Forster *et al* found increased mI in TASTPM mice however this was not age dependent and suggests that it may be a marker of AD but not of AD severity (210). Therefore high mI levels remain to be an important marker of AD, however further investigation is needed to clarify its' role in disease.

5.2.2 Altered Neuroinflammation and Metabolite Profile in normal Aging and AD

It has become evident that both neuroinflammation and neuronal dysfunction have a significant role to play in AD pathogenesis, however little is known about their exact contribution. As a result, multi-modal techniques have been exploited in this project to permit the investigation of these factors. The results presented in this thesis are in support of this. In Chapter 2 we report significant age dependent increases in neuroinflammation as assessed by [^{18}F]DPA-714 PET in regions associated with pathology in in the APP_{swe}×$PS1_{\Delta e9}$ mouse model of AD. A significant increase in neuroinflammation was seen in the hippocampal and cortical ROI of 18 month old TG mice that was not seen in age matched WT mice. These results were confirmed by increased immunostaining for microglial and astroglial markers. In agreement with this we also see a significant decrease in NAA from 6 to 18 months in the TG mice that was not significant in the WT mice. Reduced NAA is suggestive of neuronal dysfunction and although we did not observe any differences in neuronal or synaptic markers using *ex vivo* methods in this study. Alterations in NAA suggest dysfunction at a biochemical level in this model and are consistently reported in AD (194, 200) and with disease progression in AD animal models (201-204). Decreased NAA levels have been previously reported in the $APP_{swe}xPS1_{\Delta e9}$ mouse, however the ages of this becoming apparent is inconsistent. Decreased NAA levels have been reported as early as 5 months (203, 205) but were not evident until 12 (206) or 16 (201) months in this strain by other studies. An explanation for the inconsistencies reported in this mouse model could be down to factors such as different n numbers, analysis software, field strengths, voxel position and size and whether results were repeated measures or not.

In Chapter 3 we show increased neuroinflammation prior to known extensive plaque or NFT load in the TgF344-AD rat implicating neuroinflammation as a key player in the early stages of AD development. Significantly increased [^{18}F]DPA-714 PET uptake was observed in the thalamus of TG compared to WT rats at 6 months of age. *Ex vivo* analysis of pathology and glial cell activation in this region has not been previously reported and therefore should be carried out to confirm this result. Nonetheless it implicates early neuroinflammation in disease pathogenesis in this model. By 12 months of age both groups displayed similar uptake in this region due to an increase in the WTs with age that was not seen in the TGs. A significant increase was also seen in TG rats in the hypothalamus at 12 months of age providing further means of discriminating WT and TG rats via neuroinflammatory status. When investigating metabolite profile in these animals we observed a decrease in NAA with age in the hippocampus and thalamus but no significant differences were found between WT and TG rats. However a significant increase in Glu levels was seen from 6 to 12 months in the hypothalamus of TG rats that was not seen in the WT rats. This is in contrast to decreased levels reported in AD and AD models. An explanation for this may be that TG rats have higher levels at a young age which may change with pathology burden and disease progression. However it may also be that the hypothalamus has not been investigated previously and this region may be affected differently in AD. Although the thalamus and hypothalamus are not typically investigated in AD there are reports suggesting their involvement in AD such as the presence of AD pathological hallmarks, decreased grey matter volume, and decreased glucose consumption (258, 262, 271, 272). Furthermore, the hippocampus, a region that is highly affected in AD, is thought to be involved in the regulation of the hypothalamic-pituitary-axis, which in turn is thought to be associated with LTP and new memory formation. It has been suggested that prolonged dysregulation of the axis may contribute to the memory deficits seen in AD (281). Hence, further investigation into neuroinflammatory alterations and other abnormalities in these regions is warranted.

It is important to note that the increased neuroinflammation and alterations seen in metabolites such as NAA and Glu are known to also occur in normal aging. We report increased neuroinflammation and reductions in NAA with age in both the mouse and rat models of AD used in this study, suggesting these effects are also a part of normal aging. This highlights an important issue in AD research as some characteristics such as

decreased NAA are also markers of aging and disease. Although they may be exacerbated in disease, it presents challenges in their identification. Therefore when investigating AD or other diseases that affect an older population, it is imperative to know the difference between normal aging and disease related changes. This highlights the need for more longitudinal studies to identify robust and highly specific AD-like patterns of change that can be distinguished from normal aging. This can be achieved by investigating neuroinflammatory and metabolite alterations in the same animals at multiple time-points with disease progression rather than investigating the effect in old AD animals using single time-point studies.

5.2.3 Contribution of Peripheral Inflammation to AD Pathology

In the clinic, patients have a variety of different co-morbidities which may impact upon the progression of disease. As neuroinflammation is a key characteristic in AD pathogenesis and has been shown to be influenced by peripheral infection, we aimed to test the effects of UTI on CNS inflammation, metabolite profile and cognitive ability. UTI began prior to known extensive pathology load or cognitive decline (as shown in Chapter 3). No overall effect of infection was observed in any region with [^{18}F]DPA-714 PET, however we did observe an infection × gene interaction in the hypothalamus. This resulted in peripheral infection causing increased neuroinflammation in the WT rats and decreased neuroinflammation in the TG rats. This result was not expected as previous reports have shown increased infectious burden to result in elevated pro-inflammatory cytokines which are known to initiate hypothalamic inflammation after infection and during chronic disease (271, 272). One explanation for this may be that inflammatory processes in TG animals are preserved prior to extensive pathology. With increasing pathology burden, microglia become primed and neuroinflammation is elevated. At this stage systemic inflammation may drive pro-inflammatory processes. On the other hand this highlights how comorbidities can hide underlying disease effects. In Chapter 3 we observed increased [^{18}F]DPA-714 uptake in the hypothalamus in the TG compared to the WT at 12 months, however in Chapter 4 this effect is masked by the antagonistic effect of infection between groups resulting in WT-infected and TG-infected having similar levels of neuroinflammation in this region. We see the same effect on mI levels in this region but, as discussed previously, whether this is associated directly with neuroinflammation or rather

with AD pathology remains to be confirmed. Nonetheless, mI has been suggested to be a discriminating marker of AD from healthy aging, therefore it is important to recognise the impact of comorbidities on its expression. A significant effect of infection was seen on tCho levels in the cortex with increased tCho observed with UTI in both WT and TG. Choline containing compounds are associated with cell membrane turnover therefore increases in tCHo is suggestive of either increased levels of precursors or breakdown products of membranes (187). tCho has been shown to increase in disease and suggests dysfunction. Here we show direct tCho alteration as an effect of infection alone (no influence of gene) supporting the idea that peripheral infection can alter brain metabolites. In addition we also see a significant effect on cognitive ability in the TgF344-AD rat, with infection causing cognitive decline at 12 months that was not seen without UTI or in the WT group. Moreover, we show that only two doses of a common UTI can significantly alter these measurements. Considering this, it is imperative to better understand the effects of peripheral infection on AD and other neurological disorders. The effects of multiple simultaneous comorbidities and lifelong recurrent infections in patients may explain why many clinical studies are contradictive. This confounding effects make it more difficult to discriminate between specific effects of AD pathology and consequences of complex comorbidities. Further research into how this rat model and other models of AD respond to different types of systemic infection or other type of comorbidities like obesity, diabetes, at different time-points is needed to comprehend the contribution of peripheral infection to AD.

5.2.4 Advantages of a Rat Model of AD

The main advantage of using the new TgF344-AD model is that it has been reported to develop all the pathological characteristics seen in clinical AD including NFT pathology and neuronal loss despite only expressing amyloid mutations. In fact the TgF344-AD rat expresses the same mutations as the APP_{swe}×$PS1_{\Delta e9}$ mouse, which does not develop significant tau pathology. Although some amyloid based mouse models have been reported to develop increased p-tau, they do not develop aggregates that resemble NFTs (247, 248) and it is likely that endogenous mouse tau is not capable of developing NFT-like aggregates. Tau pathology can be expressed in a mouse model by introducing a human tau mutation such as is seen in the 3×Tg mouse which expresses both amyloid and

tau mutations. However the problem with this transgene is that no tau mutations are found in AD and although it creates pathology that is similar to AD, it does not exist in AD. Using a model that more fully represents the clinical situation by spontaneously generate NFTs provides a means for a better understanding of the pathological processes leading to disease development and progression. Currently only one paper characterises the TgF344-AD rat at 6, 16 and 26 months. Cohen *et al* demonstrate increased p-tau and $A\beta_{40}$ by 6 months and widespread NFT and plaque pathology as well as neuronal loss by 16 months. Age dependant increases in both microglial and astroglial activation was also reported at 6 months prior to extensive pathology burden using *ex vivo* methods. Increased NI has been found in to be early event in AD as well as being present in MCI. However time-points in between 6 and 16 months have not been characterised in this model. As early biomarkers of AD are essential for disease management and better diagnosis time-points in between 6 and 16 months should be investigated. Considering this, the TgF344-AD appears to be a good model to investigate the role of neuroinflammation in AD, particularly in early time-points allowing the investigation of early markers that predict AD development.

In terms of neuroimaging the biggest advantage of having a rat model is the increased brain size. In Chapter 2, we were limited by the small size of the mouse brain and the resolution of our PET scanner (~1.6mm). This also limited the regions we could analyse as the hippocampus in the mouse brain is approximately 3mm in length (282), therefore the number of voxels that would include the hippocampus would be very low as well as being slightly different depending on different placement of the animals within the scanner. This would result in inaccurate quantification of this region; hence we pooled the hippocampus and cortex as one larger ROI. This permits more accurate measurement of a larger ROI; however it also masks the individual effects of these regions. Therefore, in terms of imaging it is better to investigate specific regional differences in an animal model with a larger brain such as the rat. The hippocampus of a rat is approximately 7mm in length (283) and therefore allows the investigation of individual regions using PET. Similarly, the larger brain size of the rat is beneficial when investigating metabolite profile using MRS. In mice, we could use only a single minimal $3x3x3mm^3$ voxel covering the hippocampus but incorporating the most dorsal part of the thalamus to get a sufficient signal to noise ratio needed for quantification of metabolites within a reasonable time-

frame, whereas in rats we could use multiple voxels individually addressing a single brain structure while still acquiring improved spectra.

It is worth noting that a limitation that we observed in this rat model was the increased anxiety behaviour displayed by the Fisher strain. This was even more prominent in the TG rats and resulted in reduced exploration and mobility compared to other less anxious models (253, 254). This increased anxiety like behaviour created difficulties when assessing the NOR as they were observed to display low exploration times, hence the NOR test had to be adapted to a time and light percentage that was found to increase rat exploration time in the arena. Extensive handling by the tester only was carried out prior to every behavioural time-point to reduce this anxiety. Although the rats' anxiety did not prevent them from performing the NOR test, the low exploration times made it difficult to probe cognitive behaviour. However, it was noticed that with further generations bred in our facility the anxiety was reduced. Therefore it would be suggested for further use to breed a colony for a minimum of year to reduce any anxiety and reduce the confound of anxiety in behavioural tests or to back-cross the model with a less anxious strain.

5.3 Future Work

The TgF344-AD rat shows great promise for pre-clinical AD research particularly neuroimaging. However, as little is known about this model future work should focus on further characterising it at different ages. In Chapter 3 and 4 we demonstrated increased neuroinflammation in the temporal cortex. This region was not assessed by *Cohen et al.* (254) and therefore *ex vivo* techniques such as immunohistochemistry should be employed to assess pathology and neuroinflammatory load in this region. In addition, *ex vivo* analysis should be carried out in all relevant regions at 12 months of age to confirm imaging results and characterise the model further. It would also be interesting to characterise and correlate the plasma and tissue cytokine and chemokine expression after peripheral infection in this model to get a better picture of the systemic and CNS pro-/anti-inflammatory profiles in the WT and TG rats in response to infection. Furthermore, later time-points (e.g. 18 months of age) should be investigated to characterise how neuroinflammation changes with disease progression. In term of investigating the impact of peripheral infection, it

would be interesting to see the effects of infection at a later age when significant pathology is present in this model. It would also be beneficial to investigate the cytokine and chemokine expression in the brain tissue and peripheral plasma of these rats after recurrent UTI.

5.4 Final Remarks

This project demonstrates that neuroinflammation and metabolite alterations can successfully discriminate between AD-like disease and normal aging. Moreover, this can be done in a non-invasive manner that is highly translatable to the clinic. We report that [^{18}F]DPA-714PET is sufficient to allow significant discrimination between WT and TG rodents and hence is a viable marker for assessing neuroinflammation in AD. The results in this study are in line with increased neuroinflammation as a driver of disease in AD. However, future work needs to be focussed on either developing more sensitive detection methods or wider use of rat models of AD to allow improved regional quantification of neuroinflammation and neurodegeneration.

References

1. ARUK. 10 Things you need to know about dementia prevelance. Available at http://wwwalzheimersresearchukorg/wp-content/uploads/2015/05/2-10-things-prevalence-2016pdf. 2016.

2. WHO WHO. Dementia Fact sheet no362. 2012.

3. ARUK. 10 Things you need to know about impact of dementia on people, carers and the economy. Available at http://wwwalzheimersresearchukorg/wp-content/uploads/2015/05/3-10-things-impact-2016pdf. 2016.

4. Liu L, Chan C. The role of inflammasome in Alzheimer's disease. Ageing Res Rev. 2014;15:6-15.

5. Heneka MT, Carson MJ, El Khoury J, Landreth GE, Brosseron F, Feinstein DL, et al. Neuroinflammation in Alzheimer's disease. Lancet Neurol. 2015;14(4):388-405.

6. Holmes C, Cunningham C, Zotova E, Woolford J, Dean C, Kerr S, et al. Systemic inflammation and disease progression in Alzheimer disease. Neurology. 2009;73(10):768-74.

7. Neumann H, Daly MJ. Variant TREM2 as risk factor for Alzheimer's disease. The New England journal of medicine. 2013;368(2):182-4.

8. Hayes A, Thaker U, Iwatsubo T, Pickering-Brown SM, Mann DMA. Pathological relationships between microglial cell activity and tau and amyloid beta protein in patients with Alzheimer's disease. Neurosci Lett. 2002;331(3):171-4.

9. Cagnin A, Brooks DJ, Kennedy AM, Gunn RN, Myers R, Turkheimer FE, et al. In-vivo measurement of activated microglia in dementia. Lancet. 2001;358(9280):461-7.

10. Edison P, Archer HA, Gerhard A, Hinz R, Pavese N, Turkheimer FE, et al. Microglia, amyloid, and cognition in Alzheimer's disease: An [11C](R)PK11195-PET and [11C]PIB-PET study. Neurobiology of disease. 2008;32(3):412-9.

11. Nuzzo D, Picone P, Caruana L, Vasto S, Barera A, Caruso C, et al. Inflammatory Mediators as Biomarkers in Brain Disorders. Inflammation. 2014;37(3):639-48.

12. Braak H, Braak E. Neuropathological stageing of Alzheimer-related changes. Acta Neuropathol. 1991;82(4):239-59.

13. Serrano-Pozo A, Frosch MP, Masliah E, Hyman BT. Neuropathological alterations in Alzheimer disease. Cold Spring Harb Perspect Med. 2011;1(1):a006189.

14. Hardy J, Allsop D. Amyloid deposition as the central event in the aetiology of Alzheimer's disease. Trends Pharmacol Sci. 1991;12(10):383-8.

15. Hardy J, Selkoe DJ. The amyloid hypothesis of Alzheimer's disease: progress and problems on the road to therapeutics. Science. 2002;297(5580):353-6.

16. Selkoe DJ, Hardy J. The amyloid hypothesis of Alzheimer's disease at 25 years. EMBO Mol Med. 2016;8(6):595-608.

17. Zheng H, Koo EH. Biology and pathophysiology of the amyloid precursor protein. Molecular neurodegeneration. 2011;6(1):27.

18. Lista S, O'Bryant SE, Blennow K, Dubois B, Hugon J, Zetterberg H, et al. Biomarkers in Sporadic and Familial Alzheimer's Disease. Journal of Alzheimer's disease : JAD. 2015;47(2):291-317.

19. Schenk D, Barbour R, Dunn W, Gordon G, Grajeda H, Guido T, et al. Immunization with amyloid- attenuates Alzheimer-disease-like pathology in the PDAPP mouse. Nature. 1999;400(6740):173.

20. Schenk D. Amyloid- immunotherapy for Alzheimer's disease: the end of the beginning. Nature reviews Neuroscience. 2002;3(10):824-8.

21. Orgogozo J, Gilman S, Dartigues J, Laurent B, Puel M, Kirby L, et al. Subacute meningoencephalitis in a subset of patients with AD after AB42 immunization. Neurology. 2003;61(1):46-54.

22. Gilman S, Koller M, Black R, Jenkins L, Griffith S, Fox N, et al. Clinical effects of Abeta immunization (AN1792) in patients with AD in an interrupted trial. Neurology. 2005;64(9):1553-62.

23. Nicoll JA, Wilkinson D, Holmes C, Steart P, Markham H, Weller RO. Neuropathology of human Alzheimer disease after immunization with amyloid-beta peptide: a case report. Nature medicine. 2003;9(4):448-52.

24. Serrano-Pozo A, William CM, Ferrer I, Uro-Coste E, Delisle MB, Maurage CA, et al. Beneficial effect of human anti-amyloid-beta active immunization on neurite morphology and tau pathology. Brain : a journal of neurology. 2010;133(Pt 5):1312-27.

25. Levites Y, Das P, Price RW, Rochette MJ, Kostura LA, McGowan EM, et al. Anti-Abeta42- and anti-Abeta40-specific mAbs attenuate amyloid deposition in an Alzheimer disease mouse model. The Journal of clinical investigation. 2006;116(1):193-201.

26. Salloway S, Sperling R, Gilman S, Fox M, FRCP, N C., Blennow K, Raskind M, et al. A phase 2 multiple ascending dose trial of bapineuzumab in mild to moderate Alzheimer disease. Neurology. 2009;73(24):2061.

27. O Rinne J, Brooks DJ, Rossor MN, Fox NC, Bullock R, Klunk WE, et al. 11C-PiB PET assessment of change in fibrillar amyloid-β load in patients with Alzheimer’s disease treated with bapineuzumab: a phase 2, double-blind, placebo-controlled, ascending-dose study. Lancet Neurology. 2010;9(4):363-72.

28. Waragai M, Okamura N, Furukawa K, Tashiro M, Furumoto S, Funaki Y, et al. Comparison study of amyloid PET and voxel-based morphometry analysis in mild cognitive impairment and Alzheimer's disease. Journal of the neurological sciences. 2009;285(1-2):100-8.

29. Berg L, McKeel DWJ, Miller JP, Storandt M, Rubin EH, Morris JC, et al. Clinicopathologic studies in cognitively healthy aging and Alzheimer's disease: relation of histologic markers to dementia severity, age, sex, and apolipoprotein E genotype. Arch Neurol. 1998;55(3):326-35.

30. McLean CA, Cherny RA, Fraser FW, Fuller SJ, Smith MJ, Beyreuther K, et al. Soluble pool of Abeta amyloid as a determinant of severity of neurodegeneration in Alzheimer's disease. Ann Neurol. 1999;46(6):860-6.

31. Lue LF, Kuo YM, Roher AE, Brachova L, Shen Y, Sue L, et al. Soluble Amyloid beta Peptide Concentration as a Predictor of Synaptic Change in Alzheimer's Disease. The American journal of pathology. 1999;155(3):853-62.

32. Zussy C, Brureau A, Keller E, Marchal S, Blayo C, Delair B, et al. Alzheimer's Disease Related Markers, Cellular Toxicity and Behavioral Deficits Induced Six Weeks after Oligomeric Amyloid-beta Peptide Injection in Rats. PloS one. 2013;8(1):e53117.

33. Mitani Y, Yarimizu J, Saita K, Uchino H, Akashiba H, Shitaka Y, et al. Differential effects between gamma-secretase inhibitors and modulators on cognitive function in amyloid precursor protein-transgenic and nontransgenic mice. The Journal of neuroscience : the official journal of the Society for Neuroscience. 2012;32(6):2037-50.

34. Mitani Y, Yarimizu J, Akashiba H, Shitaka Y, Ni K, Matsuoka N. Amelioration of cognitive deficits in plaque-bearing Alzheimer's disease model mice through selective reduction of nascent soluble Abeta42 without affecting other Abeta pools. Journal of neurochemistry. 2012.

35. Lane RF, Shineman DW, Steele JW, Lee LB, Fillit HM. Beyond amyloid: the future of therapeutics for Alzheimer's disease. Advances in pharmacology. 2012;64:213-71.

36. Busche MA, Chen X, Henning HA, Reichwald J, Staufenbiel M, Sakmann B, et al. Critical role of soluble amyloid-β for early hippocampal hyperactivity in a mouse model of Alzheimer's disease. Proc Natl Acad Sci U S A. 2012;109(22):8740-5.

37. Iqbal K, Liu F, Gong CX, I. G-I. Tau in Alzheimer Disease and Related Tauopathies. Curr Alzheimer Res. 2010a;7(8):656-64.

38. Maccioni RB, Farias G, Morales I, Navarrete L. The revitalized tau hypothesis on Alzheimer's disease. Archives of medical research. 2010;41(3):226-31.

39. Iqbal K, Wang X, Blanchard J, Liu F, Gong CX, Grundke-Iqbal I. Alzheimer's disease neurofibrillary degeneration: pivotal and multifactorial. Biochemical Society transactions. 2010b;38(4):962-6.

40. Braak E, Braak H, Mandelkow EM. A sequence of cytoskeleton changes related to the formation of neurofibrillary tangles and neuropil threads.
. Acta Neuropathol. 1994;87(6):554-67.

41. Ghoshal N. Tau Conformational Changes Correspond to Impairments of Episodic Memory in Mild Cognitive Impairment and Alzheimer's Disease. Experimental Neurology. 2002;177(2):475-93.

42. Maccioni RB, Lavados M, Guillon M, Mujica C, Bosch R, Farias G, et al. Anomalously phosphorylated tau and Abeta fragments in the CSF correlates with cognitive impairment in MCI subjects. Neurobiology of aging. 2006;27(2):237-44.

43. Hampel H, Bürger K, Pruessner JC, Zinkowski R, DeBernardis J, Kerkman D, et al. Correlation of Cerebrospinal Fluid Levels of Tau Protein Phosphorylated at Threonine 231 With Rates of Hippocampal Atrophy in Alzheimer Disease. Arch Neurol. 2005;62(5):770-3.

44. Spires-Jones TL, Kopeikina KJ, Koffie RM, de Calignon A, Hyman BT. Are tangles as toxic as they look? Journal of molecular neuroscience : MN. 2011;45(3):438-44.

45. Santacruz K, Lewis J, Spires T, Paulson J, Kotilinek L, Ingelsson M, et al. Tau suppression in a neurodegenerative mouse model improves memory function. Science. 2005;309(5733):476-81.

46. Berger Z, Roder H, Hanna A, Carlson A, Rangachari V, Yue M, et al. Accumulation of pathological tau species and memory loss in a conditional model of tauopathy. The Journal of neuroscience : the official journal of the Society for Neuroscience. 2007;27(14):3650-62.

47. Lee VM, Goedert M, Trojanowski JQ. Neurodegenerative tauopathies. Annu Rev Neurosci. 2001;24:1121-59.

48. Valles AS, Borroni MV, Barrantes FJ. Targeting brain alpha7 nicotinic acetylcholine receptors in Alzheimer's disease: rationale and current status. CNS Drugs. 2014;28(11):975-87.

49. Raskind MA, Peskind ER, Wessel T, Yuan W. Galantamine in AD: A 6-month randomized, placebo-controlled trial with a 6-month extension. Neurology. 2000;54(12):2261-8.

50. Hynd MR, Scott HL, Dodd PR. Glutamate-mediated excitotoxicity and neurodegeneration in Alzheimer's disease. Neurochem Int. 2004;45(5):583-95.

51. Navarro A, Boveris A. Brain mitochondrial dysfunction in aging, neurodegeneration, and Parkinson's disease. Frontiers in aging neuroscience. 2010;2.

52. Valko M, Leibfritz D, Moncol J, Cronin MT, Mazur M, Telser J. Free radicals and antioxidants in normal physiological functions and human disease. The international journal of biochemistry & cell biology. 2007;39(1):44-84.

53. Keller JN, Mark RJ, Bruce AJ, Blanc E, Rothstein JD, Uchida K, et al. 4-Hydroxynonenal, an aldehydic product of membrane lipid peroxidation, impairs glutamate transport and mitochondrial function in synaptosomes. Neuroscience. 1997;80(3):685-96.

54. van Waarde A, Ramakrishnan NK, Rybczynska AA, Elsinga PH, Ishiwata K, Nijholt IM, et al. The cholinergic system, sigma-1 receptors and cognition. Behavioural brain research. 2011;221(2):543-54.

55. Mishina M, Ohyama M, Ishi iK, Kitamura S, Kimura Y, Oda K, et al. Low density of sigma1 receptors in early Alzheimer's disease. Ann Nucl Med. 2008;22(3):151-6.

56. Marrazzo A, Caraci F, Salinaro ET, Su TP, Copani A, Ronsisvalle G. Neuroprotective effects of sigma-1 receptor agonists against beta-amyloid-induced toxicity. Neuroreport. 2005;16(11):1223-6.

57. Villard V, Espallergues J, Keller E, Vamvakides A, Maurice T. Anti-amnesic and neuroprotective potentials of the mixed muscarinic receptor/sigma 1 (sigma1) ligand ANAVEX2-73, a novel aminotetrahydrofuran derivative. J Psychopharmacol. 2011;25(8):1101-17.

58. Meunier J, Ieni J, Maurice T. The anti-amnesic and neuroprotective effects of donepezil against amyloid beta25-35 peptide-induced toxicity in mice involve an interaction with the sigma1 receptor. British journal of pharmacology. 2006;149(8):998-1012.

59. Rissman RA, De Blas AL, Armstrong DM. GABA(A) receptors in aging and Alzheimer's disease. Journal of neurochemistry. 2007;103(4):1285-92.

60. Nilsen LH, Melo TM, Saether O, Witter MP, Sonnewald U. Altered neurochemical profile in the McGill-R-Thy1-APP rat model of Alzheimer's disease: a longitudinal in vivo 1 H MRS study. Journal of neurochemistry. 2012;123(4):532-41.

61. Town T, Nikolic V, Tan J. The microglial "activation" continuum: from innate to adaptive responses. Journal of neuroinflammation. 2005;2:24.

62. Gomez-Nicola D, Perry VH. Microglial Dynamics and Role in the Healthy and Diseased Brain: A Paradigm of Functional Plasticity. The Neuroscientist : a review journal bringing neurobiology, neurology and psychiatry. 2014.

63. Wood PL. CNS marcophages in Neurodegeneration. Neuroinflammation: Mechanisms and Management, Textbook. 1998:1-29.

64. Haga S, Akai K, Ishii T. Demonstration of microglial cells in and around senile (neuritic) plaques in the Alzheimer brain. An immunohistochemical study using a novel monoclonal antibody. . Acta Neuropath. 1989; 77(6): 569-75.

65. Weitz TM, Town T. Microglia in Alzheimer's Disease: It's All About Context. International journal of Alzheimer's disease. 2012;2012:314185.

66. Paranjape GS, Gouwens LK, Osborn DC, Nichols MR. Isolated amyloid-beta(1-42) protofibrils, but not isolated fibrils, are robust stimulators of microglia. ACS chemical neuroscience. 2012;3(4):302-11.

67. Kim EK, Choi EJ. Pathological roles of MAPK signaling pathways in human diseases. Biochim Biophys Acta. 2010;1802(4):396-405.

68. Lee KS, Chung JH, Choi TK, Suh SY, Oh BH, Hong CH. Peripheral Cytokines and Chemokines in Alzheimer's Disease. Dementia and geriatric cognitive disorders. 2009;28:281-7.

69. Rubio-Perez JM, Morillas-Ruiz JM. A review: inflammatory process in Alzheimer's disease, role of cytokines. TheScientificWorldJournal. 2012;2012:756357.

70. Forlenza OV, Diniz BS, Talib LL, Mendonca VA, Ojopi EB, Gattaz WF, et al. Increased serum IL-1beta level in Alzheimer's disease and mild cognitive impairment. Dementia and geriatric cognitive disorders. 2009;28(6):507-12.

71. Kitazawa M, Cheng D, Tsukamoto MR, Koike MA, Wes PD, Vasilevko V, et al. Blocking IL-1 signaling rescues cognition, attenuates tau pathology, and restores neuronal beta-catenin pathway function in an Alzheimer's disease model. Journal of immunology. 2011;187(12):6539-49.

72. Yardan T, Erenler AK, Baydin A, Aydin K, Cokluk C. Usefulness of S100B protein in neurological disorders. J Pak Med Assoc. 2011;61(3):276-81.

73. Craft JM, Watterson DM, Van Eldik LJ. Human Amyloid b-Induced Neuroinflammation is an Early Event in Neurodegeneration. Glia. 2006;53:484-90.

74. Rachal Pugh C, Fleshner M, Watkins LR, Maier SF, Rudy JW. The immune system and memory consolidation: a role for the cytokine IL-1beta. Neurosci Biobehav Rev. 2005;25(1):29-41.

75. Schneider H, Pitossi F, Balschun D, Wagner A, del Rey A, Besedovsky HO. A neuromodulatory role of interleukin-1beta in the hippocampus. Proc Natl Acad Sci U S A. 1998;95(13):7778-83.

76. Chakrabarty P, Tianbai L, Herring A, Ceballos-Diaz C, Das P, Golde TE. Hippocampal expression of murine IL-4 results in exacerbation of amyloid deposition. Mol Neurodegener. 2012;7(36).

77. Kimelberg HK, Nedergaard M. Functions of astrocytes and their potential as therapeutic targets. Neurotherapeutics : the journal of the American Society for Experimental NeuroTherapeutics. 2010;7(4):338-53.

78. Elsayed M, Magistretti PJ. A New Outlook on Mental Illnesses: Glial Involvement Beyond the Glue. Front Cell Neurosci. 2015;9:468.

79. Torgner L, Kvamme E. Synthesis of transmitter glutamate and glial-neuron interrelationship. Mol chem neuopathol. 1990;12(1):11-7.

80. Sidoryk-Wegrzynowicz M, Wegrzynowicz M, Lee E, Bowman AB, Aschner M. Role of astrocytes in brain function and disease. Toxicologic pathology. 2011;39(1):115-23.

81. Dringen R, Pfeiffer B, Hamprecht B. Synthesis of the antioxidant glutathione in neurons: supply by astrocytes of CysGly as precursor for neuronal glutathione. The Journal of neuroscience : the official journal of the Society for Neuroscience. 1999;19(2):562-9.

82. Berk M, Ng F, Dean O, Dodd S, Bush AI. Glutathione: a novel treatment target in psychiatry. Trends in pharmacological sciences. 2008;29(7):346-51.

83. Nagele RG, D'Andrea MR, Lee H, Venkataraman V, Wang HY. Astrocytes accumulate Aβ42 and give rise to astrocytic amyloid plaques in Alzheimer disease brains. Brain research. 2003;971(2):197-209.

84. Olabarria M, Noristani HN, Verkhratsky A, Rodriguez JJ. Concomitant astroglial atrophy and astrogliosis in a triple transgenic animal model of Alzheimer's disease. Glia. 2010;58(7):831-8.

85. Chow SK, Yu D, Macdonald CL, Buibas M, Silva GA. Amyloid beta-peptide directly induces spontaneous calcium transients, delayed intercellular calcium waves and gliosis in rat cortical astrocytes. ASN neuro. 2010;2(1):e00026.

86. Nagele RG, Wegiel J, Venkataraman V, Imaki H, Wang KC, Wegiel J. Contribution of glial cells to the development of amyloid plaques in Alzheimer's disease. Neurobiology of aging. 2004;25(5):663-74.

87. Perry VH, Holmes C. Microglial priming in neurodegenerative disease. Nat Rev Neurol. 2014;10(4):217-24.

88. Goldeck D, Witkowski JM, Fulop T, Pawelec G. Peripheral Immune Signatures in Alzheimer Disease. Curr Alzheimer Res. 2016;13(7):739-49.

89. Bauer K, Schwarzkopf L, Graessel E, Holle R. A claims data-based comparison of comorbidity in individuals with and without dementia. BMC Geriatr. 2014;14:10.

90. Denes A, Thornton P, Rothwell NJ, Allan SM. Inflammation and brain injury: acute cerebral ischaemia, peripheral and central inflammation. Brain Behav Immun. 2010;24(5):708-23.

91. Lastra G, Sowers JR. Obesity and cardiovascular disease: role of adipose tissue, inflammation, and the renin-angiotensin-aldosterone system. Horm Mol Biol Clin Investig. 2013;15(2):49-57.

92. Holmes C, El-Okl M, Williams AL, Cunningham C, Wilcockson D, Perry VH. Systemic infection, interleukin 1beta, and cognitive decline in Alzheimer's disease. Journal of neurology, neurosurgery, and psychiatry. 2003;74(6):788-9.

93. Vlad SC, Miller DR, Kowall NW, Felson DT. Protective effects of NSAIDs on the development of Alzheimer disease. Neurology. 2008;70(19):1672-7.

94. Cunningham C. Microglia and neurodegeneration: the role of systemic inflammation. Glia. 2013;61(1):71-90.

95. Trollor JN, Smith E, Baune BT, Kochan NA, Campbell L, Samaras K, et al. Systemic inflammation is associated with MCI and its subtypes: the Sydney Memory and Aging Study. Dementia and geriatric cognitive disorders. 2010;30(6):569-78.

96. Bu XL, Yao XQ, Jiao SS, Zeng F, Liu YH, Xiang Y, et al. A study on the association between infectious burden and Alzheimer's disease. Eur J Neurol. 2015;22(12):1519-25.

97. Wright CB, Gardener H, Dong C, Yoshita M, DeCarli C, Sacco RL, et al. Infectious Burden and Cognitive Decline in the Northern Manhattan Study. J Am Geriatr Soc. 2015;63(8):1540-5.

98. Kitazawa M, Oddo S, Yamasaki TR, Green KN, LaFerla FM. Lipopolysaccharide-induced inflammation exacerbates tau pathology by a cyclin-dependent kinase 5-mediated pathway in a transgenic model of Alzheimer's disease. The Journal of neuroscience : the official journal of the Society for Neuroscience. 2005;25(39):8843-53.

99. Lee JW, Lee YK, Yuk DY, Choi DY, Ban SB, Oh KW, et al. Neuro-inflammation induced by lipopolysaccharide causes cognitive impairment through enhancement of beta-amyloid generation. Journal of neuroinflammation. 2008;5:37.

100. Krstic D, Madhusudan A, Doehner J, Vogel P, Notter T, Imhof C, et al. Systemic immune challenges trigger and drive Alzheimer-like neuropathology in mice. Journal of neuroinflammation. 2012;9:151.

101. McManus RM, Higgins SC, Mills KH, Lynch MA. Respiratory infection promotes T cell infiltration and amyloid-beta deposition in APP/PS1 mice. Neurobiology of aging. 2014;35(1):109-21.

102. Games D, Adams D, Alessandrini R, Barbour R, Berthelette P, Blackwell C, et al. Alzheimer-type neuropathology in transgenic mice overexpressing V717F beta-amyloid precursor protein. Nature. 1995;373(6514):523-7.

103. Webster SJ, Bachstetter AD, Van Eldik LJ. Comprehensive behavioral characterization of an APP/PS-1 double knock-in mouse model of Alzheimer's disease. Alzheimers Res Ther. 2013;5(3):28.

104. Sturchler-Pierrat C, Abramowski D, Duke M, Wiederhold KH, Mistl C, Rothacher S, et al. Two amyloid precursor protein transgenic mouse models with Alzheimer disease-like pathology. Proceedings of the National Academy of Sciences of the United States of America. 1997;94(24):13287-92.

105. Holcomb L, Gordon MN, McGowan E, Yu X, Benkovic S, Jantzen P, et al. Accelerated Alzheimer-type phenotype in transgenic mice carrying both mutant amyloid precursor protein and presenilin 1 transgenes. Nat Med. 1998;4(1):97-100.

106. Rockenstein E, Mallory M, Mante M, Sisk A, Masliaha E. Early formation of mature amyloid-beta protein deposits in a mutant APP transgenic model depends on levels of Abeta(1-42). Journal of neuroscience research. 2001;66(4):573-82.

107. Jankowsky JL, Fadale DJ, Anderson J, Xu GM, Gonzales V, Jenkins NA, et al. Mutant presenilins specifically elevate the levels of the 42 residue beta-amyloid peptide in vivo: evidence for augmentation of a 42-specific gamma secretase. Hum Mol Genet. 2004;13(2):159-70.

108. Garcia-Alloza M, Robbins EM, Zhang-Nunes SX, Purcell SM, Betensky RA, Raju S, et al. Characterization of amyloid deposition in the APPswe/PS1dE9 mouse model of Alzheimer disease. Neurobiology of disease. 2006;24(3):516-24.

109. Howlett DR, Richardson JC, Austin A, Parsons AA, Bate ST, Davies DC, et al. Cognitive correlates of Abeta deposition in male and female mice bearing amyloid precursor protein and presenilin-1 mutant transgenes. Brain research. 2004;1017(1-2):130-6.

110. Mastrangelo MA, Bowers WJ. Detailed immunohistochemical characterization of temporal and spatial progression of Alzheimer's disease-related pathologies in male triple-transgenic mice. BMC Neurosci. 2008;9:81.

111. Echeverria V, Ducatenzeiler A, Alhonen L, Janne J, Grant SM, Wandosell F, et al. Rat transgenic models with a phenotype of intracellular Abeta accumulation in hippocampus and cortex. Journal of Alzheimer's disease : JAD. 2004;6(3):209-19.

112. Folkesson R, Malkiewicz K, Kloskowska E, Nilsson T, Popova E, Bogdanovic N, et al. A transgenic rat expressing human APP with the Swedish Alzheimer's disease mutation. Biochem Biophys Res Commun. 2007;358(3):777-82.

113. Leon WC, Canneva F, Partridge V, Allard S, Ferretti MT, DeWilde A, et al. A novel transgenic rat model with a full Alzheimer's-like amyloid pathology displays pre-plaque intracellular amyloid-beta-associated cognitive impairment. Journal of Alzheimer's disease : JAD. 2010;20(1):113-26.

114. Cohen RM, Rezai-Zadeh K, Weitz TM, Rentsendorj A, Gate D, Spivak I, et al. A transgenic Alzheimer rat with plaques, tau pathology, behavioral impairment, oligomeric abeta, and frank neuronal loss. The Journal of neuroscience : the official journal of the Society for Neuroscience. 2013;33(15):6245-56.

115. Saha GB. Basics of PET Imaging. Physics, Chemistry and Regulations. Springer. 2004(Chp 1):1-18.

116. Mosconi L. Brain glucose metabolism in the early and specific diagnosis of Alzheimer's disease. FDG-PET studies in MCI and AD. European journal of nuclear medicine and molecular imaging. 2005;32(4):486-510.

117. Brendel M, Probst F, Jaworska A, Overhoff F, Korzhova V, Albert NL, et al. Glial Activation and Glucose Metabolism in a Transgenic Amyloid Mouse Model: A Triple-Tracer PET Study. Journal of nuclear medicine : official publication, Society of Nuclear Medicine. 2016;57(6):954-60.

118. Poisnel G, Herard AS, El Tannir El Tayara N, Bourrin E, Volk A, Kober F, et al. Increased regional cerebral glucose uptake in an APP/PS1 model of Alzheimer's disease. Neurobiology of aging. 2012;33(9):1995-2005.

119. Kuntner C, Kesner AL, Bauer M, Kremslehner R, Wanek T, Mandler M, et al. Limitations of small animal PET imaging with [18F]FDDNP and FDG for quantitative studies in a transgenic mouse model of Alzheimer's disease. Molecular imaging and

biology : MIB : the official publication of the Academy of Molecular Imaging. 2009;11(4):236-40.

120. Deleye S, Waldron AM, Richardson JC, Schmidt M, Langlois X, Stroobants S, et al. The Effects of Physiological and Methodological Determinants on 18F-FDG Mouse Brain Imaging Exemplified in a Double Transgenic Alzheimer Model. Mol Imaging. 2016;15.

121. Waldron AM, Wintmolders C, Bottelbergs A, Kelley JB, Schmidt ME, Stroobants S, et al. In vivo molecular neuroimaging of glucose utilization and its association with fibrillar amyloid-beta load in aged APPPS1-21 mice. Alzheimers Res Ther. 2015;7(1):76.

122. Herholz K, Salmon E, Perani D, Baron JC, Holthoff V, Frölich L, et al. Discrimination between Alzheimer Dementia and Controls by Automated Analysis of Multicenter FDG PET. NeuroImage. 2002;17(1):302-16.

123. Lister-James J, Pontecorvo MJ, Clark C, Joshi AD, Mintun MA, Zhang W, et al. Florbetapir f-18: a histopathologically validated Beta-amyloid positron emission tomography imaging agent. Seminars in nuclear medicine. 2011;41(4):300-4.

124. Choi SR, Golding G, Zhuang Z, Zhang W, Lim N, Hefti F, et al. Preclinical properties of 18F-AV-45: a PET agent for Abeta plaques in the brain. Journal of nuclear medicine : official publication, Society of Nuclear Medicine. 2009;50(11):1887-94.

125. Sabri O, Seibyl J, Rowe C, Barthel H. Beta-amyloid imaging with florbetaben. Clin Transl Imaging. 2015;3(1):13-26.

126. Quigley H, Colloby SJ, O'Brien JT. PET imaging of brain amyloid in dementia: a review. Int J Geriatr Psychiatry. 2011;26(10):991-9.

127. Klunk WE, Engler H, Nordberg A, Wang Y, Blomqvist G, Holt DP, et al. Imaging Brain Amyloid in Alzheimer's Disease with Pittsburgh Compound-B. Ann Neurol. 2004;55(3):306-19.

128. Forsberg A, Engler H, Almkvist O, Blomquist G, Hagman G, Wall A, et al. PET imaging of amyloid deposition in patients with mild cognitive impairment. Neurobiology of aging. 2008;29(10):1456-65.

129. Klunk WE, Lopresti BJ, Ikonomovic MD, Lefterov IM, Koldamova RP, Abrahamson EE, et al. Binding of the positron emission tomography tracer Pittsburgh compound-B reflects the amount of amyloid-beta in Alzheimer's disease brain but not in transgenic mouse brain. The Journal of neuroscience : the official journal of the Society for Neuroscience. 2005;25(46):10598-606.

130. Villemagne VL, Klunk WE, Mathis CA, Rowe CC, Brooks DJ, Hyman BT, et al. Abeta Imaging: feasible, pertinent, and vital to progress in Alzheimer's disease. European journal of nuclear medicine and molecular imaging. 2012;39(2):209-19.

131. Brown RC, Papadopoulos V. Role of the peripheral-type benzodiazepine receptor in adrenal and brain steroidogenesis. Int Rev Neurobiol. 2001;46:117-1143.

132. Scarf AM, Kassiou M. The translocator protein. Journal of nuclear medicine : official publication, Society of Nuclear Medicine. 2011;52(5):677-80.

133. Papadopoulos V, Lecanu L, Brown RC, Han Z, Yao ZX. Peripheral-type benzodiazepine receptor in neurosteroid biosynthesis, neuropathology and neurological disorders. Neuroscience. 2006;138(3):749-56.

134. Ryu JK, Choi HB, McLarnon JG. Peripheral benzodiazepine receptor ligand PK11195 reduces microglial activation and neuronal death in quinolinic acid-injected rat striatum. Neurobiology of disease. 2005;20(2):550-61.

135. Leaver KR, Reynolds A, Bodard S, Guilloteau D, Chalon S, Kassiou M. Effects of translocator protein (18 kDa) ligands on microglial activation and neuronal death in the quinolinic-acid-injected rat striatum. ACS chemical neuroscience. 2012;3(2):114-9.

136. Ferzaz B, Brault E, Bourliaud G, Robert JP, Poughon G, Claustre Y, et al. SSR180575 (7-Chloro-N,N,5-trimethyl-4-oxo-3-phenyl-3,5- dihydro-4H-pyridazino[4,5-b]indole-1-acetamide), a Peripheral Benzodiazepine Receptor Ligand, Promotes Neuronal Survival and Repair. J Pharmacol Exp Ther. 2002;301(3):1067-78.

137. Veiga S, Azcoitia I, Garcia-Segura LM. Ro5-4864, a peripheral benzodiazepine receptor ligand, reduces reactive gliosis and protects hippocampal hilar neurons from kainic acid excitotoxicity. Journal of neuroscience research. 2005;80(1):129-37.

138. Barron AM, Garcia-Segura LM, Caruso D, Jayaraman A, Lee JW, Melcangi RC, et al. Ligand for translocator protein reverses pathology in a mouse model of Alzheimer's disease. The Journal of neuroscience : the official journal of the Society for Neuroscience. 2013;33(20):8891-7.

139. Banati RB. Visualising microglial activation in vivo. Glia. 2002;40(2):206-17.

140. Benavides J, Cornu P, Dennis T, Dubois A, Hauw JJ, MacKenzie ET, et al. Imaging of human brain lesions with an omega 3 site radioligand. Annals of neurology. 1988;24(6):708-12.

141. Venneti S, Lopresti BJ, Wang G, Hamilton RL, Mathis CA, Klunk WE, et al. PK11195 labels activated microglia in Alzheimer's disease and in vivo in a mouse model using PET. Neurobiology of aging. 2009;30(8):1217-26.

142. Yokokura M, Mori N, Yagi S, Yoshikawa E, Kikuchi M, Yoshihara Y, et al. In vivo changes in microglial activation and amyloid deposits in brain regions with hypometabolism in Alzheimer's disease. European journal of nuclear medicine and molecular imaging. 2011;38(2):343-51.

143. Wiley CA, Lopresti BJ, Venneti S, Price J, Klunk WE, DeKosky ST, et al. Carbon 11-labeled Pittsburgh Compound B and carbon 11-labeled (R)-PK11195 positron emission tomographic imaging in Alzheimer disease. Archives of neurology. 2009;66(1):60-7.

144. Schuitemaker A, Kropholler MA, Boellaard R, van der Flier WM, Kloet RW, van der Doef TF, et al. Microglial activation in Alzheimer's disease: an (R)-[(1)(1)C]PK11195 positron emission tomography study. Neurobiology of aging. 2013;34(1):128-36.

145. Okello A, Edison P, Archer HA, Turkheimer FE, Kennedy J, Bullock R, et al. Microglial activation and amyloid deposition in mild cognitive impairment: a PET study. Neurology. 2009;72(1):56-62.

146. Hommet C, Mondon K, Camus V, Ribeiro MJ, Beaufils E, Arlicot N, et al. Neuroinflammation and beta amyloid deposition in Alzheimer's disease: in vivo quantification with molecular imaging. Dementia and geriatric cognitive disorders. 2014;37(1-2):1-18.

147. Fan Z, Okello AA, Brooks DJ, Edison P. Longitudinal influence of microglial activation and amyloid on neuronal function in Alzheimer's disease. Brain : a journal of neurology. 2015;138(Pt 12):3685-98.

148. Boutin H, Pinborg LH. TSPO imaging in stroke: from animal models to human subjects. Clinical Translational Imaging. 2015;3:423-35.

149. Varrone A, Lammertsma AA. Imaging of neuroinflammation: TSPO and beyond. Clinical Translational Imaging. 2015;3(6):389-90.

150. Suridjan I, Rusjan PM, Voineskos AN, Selvanathan T, Setiawan E, Strafella AP, et al. Neuroinflammation in healthy aging: a PET study using a novel Translocator Protein 18kDa (TSPO) radioligand, [(18)F]-FEPPA. NeuroImage. 2014;84:868-75.

151. Fujimura Y, Ikoma Y, Yasuno F, Suhara T, Ota M, Matsumoto R, et al. Quantitative analyses of 18F-FEDAA1106 binding to peripheral benzodiazepine receptors in living human brain. Journal of nuclear medicine : official publication, Society of Nuclear Medicine. 2006;47(1):43-50.

152. Boutin H, Chauveau F, Thominiaux C, Gregoire MC, James ML, Trebossen R, et al. 11C-DPA-713: a novel peripheral benzodiazepine receptor PET ligand for in vivo imaging of neuroinflammation. Journal of nuclear medicine : official publication, Society of Nuclear Medicine. 2007;48(4):573-81.

153. Boutin H, Prenant C, Maroy R, Galea J, Greenhalgh AD, Smigova A, et al. [18F]DPA-714: direct comparison with [11C]PK11195 in a model of cerebral ischemia in rats. PloS one. 2013;8(2):e56441.

154. Chauveau F, Van Camp N, Dolle F, Kuhnast B, Hinnen F, Damont A, et al. Comparative evaluation of the translocator protein radioligands 11C-DPA-713, 18F-DPA-714, and 11C-PK11195 in a rat model of acute neuroinflammation. Journal of nuclear medicine : official publication, Society of Nuclear Medicine. 2009;50(3):468-76.

155. Doorduin J, Klein HC, Dierckx RA, James M, Kassiou M, de Vries EF. [11C]-DPA-713 and [18F]-DPA-714 as new PET tracers for TSPO: a comparison with [11C]-(R)-PK11195 in a rat model of herpes encephalitis. Molecular imaging and biology : MIB : the official publication of the Academy of Molecular Imaging. 2009;11(6):386-98.

156. Boutin H, Murray K, Pradillo J, Maroy R, Smigova A, Gerhard A, et al. (18)F-GE-180: a novel TSPO radiotracer compared to (11)C-R-PK11195 in a preclinical model of stroke. European journal of nuclear medicine and molecular imaging. 2015;42(3):503-11.

157. Dickens AM, Vainio S, Marjamaki P, Johansson J, Lehtiniemi P, Rokka J, et al. Detection of microglial activation in an acute model of neuroinflammation using PET and radiotracers 11C-(R)-PK11195 and 18F-GE-180. Journal of nuclear medicine : official publication, Society of Nuclear Medicine. 2014;55(3):466-72.

158. Dolle F, Luus C, Reynolds A, Kassiou M. Radiolabelled molecules for imaging the translocator protein (18 kDa) using positron emission tomography. Current medicinal chemistry. 2009;16(22):2899-923.

159. Fujita M, Imaizumi M, Zoghbi SS, Fujimura Y, Farris AG, Suhara T, et al. Kinetic analysis in healthy humans of a novel positron emission tomography radioligand to image the peripheral benzodiazepine receptor, a potential biomarker for inflammation. NeuroImage. 2008;40(1):43-52.

160. Owen DR, Yeo AJ, Gunn RN, Song K, Wadsworth G, Lewis A, et al. An 18-kDa translocator protein (TSPO) polymorphism explains differences in binding affinity of the PET radioligand PBR28. Journal of cerebral blood flow and metabolism : official journal of the International Society of Cerebral Blood Flow and Metabolism. 2012;32(1):1-5.

161. Owen DR, Howell OW, Tang SP, Wells LA, Bennacef I, Bergstrom M, et al. Two binding sites for [3H]PBR28 in human brain: implications for TSPO PET imaging of neuroinflammation. Journal of cerebral blood flow and metabolism : official journal of the International Society of Cerebral Blood Flow and Metabolism. 2010;30(9):1608-18.

162. Kreisl WC, Lyoo CH, McGwier M, Snow J, Jenko KJ, Kimura N, et al. In vivo radioligand binding to translocator protein correlates with severity of Alzheimer's disease. Brain : a journal of neurology. 2013;136(Pt 7):2228-38.

163. Yasuno F, Kosaka J, Ota M, Higuchi M, Ito H, Fujimura Y, et al. Increased binding of peripheral benzodiazepine receptor in mild cognitive impairment-dementia converters measured by positron emission tomography with [(1)(1)C]DAA1106. Psychiatry research. 2012;203(1):67-74.

164. Rapic S, Backes H, Viel T, Kummer MP, Monfared P, Neumaier B, et al. Imaging microglial activation and glucose consumption in a mouse model of Alzheimer's disease. Neurobiology of aging. 2013;34(1):351-4.

165. Liu B, Le KX, Park MA, Wang S, Belanger AP, Dubey S, et al. In Vivo Detection of Age- and Disease-Related Increases in Neuroinflammation by 18F-GE180 TSPO MicroPET Imaging in Wild-Type and Alzheimer's Transgenic Mice. The Journal of neuroscience : the official journal of the Society for Neuroscience. 2015;35(47):15716-30.

166. James ML, Belichenko NP, Nguyen TV, Andrews LE, Ding Z, Liu H, et al. PET imaging of translocator protein (18 kDa) in a mouse model of Alzheimer's disease using N-(2,5-dimethoxybenzyl)-2-18F-fluoro-N-(2-phenoxyphenyl)acetamide. Journal of nuclear medicine : official publication, Society of Nuclear Medicine. 2015;56(2):311-6.

167. Ji B, Maeda J, Sawada M, Ono M, Okauchi T, Inaji M, et al. Imaging of peripheral benzodiazepine receptor expression as biomarkers of detrimental versus beneficial glial responses in mouse models of Alzheimer's and other CNS pathologies. The Journal of neuroscience : the official journal of the Society for Neuroscience. 2008;28(47):12255-67.

168. Yoshiyama Y, Higuchi M, Zhang B, Huang SM, Iwata N, Saido TC, et al. Synapse loss and microglial activation precede tangles in a P301S tauopathy mouse model. Neuron. 2007;53(3):337-51.

169. Serriere S, Tauber C, Vercouillie J, Mothes C, Pruckner C, Guilloteau D, et al. Amyloid load and translocator protein 18 kDa in APPswePS1-dE9 mice: a longitudinal study. Neurobiology of aging. 2015;36(4):1639-52.

170. Maeda J, Ji B, Irie T, Tomiyama T, Maruyama M, Okauchi T, et al. Longitudinal, quantitative assessment of amyloid, neuroinflammation, and anti-amyloid treatment in a living mouse model of Alzheimer's disease enabled by positron emission tomography. The Journal of neuroscience : the official journal of the Society for Neuroscience. 2007;27(41):10957-68.

171. McRobbie DW, Moore EA, Graves MJ, Prince MR. MRI from Picture to Proton. Cambridge University Press. 2007;second edition(Chp 8):137-66.

172. De Graaf RA. In vivo NMR spectroscopy. Principles and Techniques. John Wiley and sons Ltd. 2007(Second edition):20-5.

173. McRobbie DW, Moore EA, Graves MJ, Prince MR. MRI from Picture to Proton. Cambridge University Press. 2007; second edition:109-10.

174. Weishaupt D, Kochli, V. D., Marineck, B. How does MRI work? An introduction to the physics and function of magnetic resonance imaging. Chapter1 Spin and nuckear magnetic resonoance phenomeneon. Springer. 2006.

175. Westman E, Wahlund LO, Foy C, Poppe M, Cooper A, Murphy D, et al. Magnetic resonance imaging and magnetic resonance spectroscopy for detection of early Alzheimer's disease. Journal of Alzheimer's disease : JAD. 2011;26 Suppl 3:307-19.

176. Juottonen K, Laakso MP, Partanen K, Soininen H. Comparative MR analysis of the entorhinal cortex and hippocampus in diagnosing Alzheimer disease. AJNR Am J Neuroradiol. 1999;20(1):139-44.

177. Scahill RI, Fox NC. Longitudinal imaging in dementia. The British journal of radiology. 2007;80 Spec No 2:S92-8.

178. Freeman R. Magnetic Resonance in Chemistry and Medicine. Oxford University Press. 2003:88-104.

179. Freeman R. Magnetic Resonance in Chemistry and Medicine. Oxford University Press. 2003;Chp 8 105-18.

180. McRobbie DW, Moore EA, Graves MJ, Prince MR. MRI from picture to proton. Cambridge University Press. 2007;Second edition(Chp 15):306-24.

181. Haase A, Frahm J, Hanicke W, Matthaei D. 1H NMR chemical shift selective (CHESS) imaging. Phys Med Biol. 1985;30(4):341-4.

182. Griffey RH, Flamig DP. VAPOR for Solvent-Supressed, Short-Echo, Volume-Localized Proton Spectroscopy. Journal of Magnetic Resonance. 1990;88:161-6.

183. Birken DL, Oldendorf WH. N-acetyl-L-aspartic acid: a literature review of a compound prominent in 1H-NMR spectroscopic studies of brain. Neurosci Biobehav Rev. 1989;13(1):23-31.

184. Brand A, Richter-Landsberg C, Leibfritz D. Multinuclear NMR studies on the energy metabolism of glial and neuronal cells. Dev Neurosci. 1993;15(3-5):289-98.

185. Murray ME, Przybelski SA, Lesnick TG, Liesinger AM, Spychalla A, Zhang B, et al. Early Alzheimer's disease neuropathology detected by proton MR spectroscopy. The Journal of neuroscience : the official journal of the Society for Neuroscience. 2014;34(49):16247-55.

186. Almeida LS, Salomons GS, Hogenboom F, Jakobs C, Schoffelmeer AN. Exocytotic release of creatine in rat brain. Synapse. 2006;60(2):118-23.

187. Govindaraju V, Young K, Maudsley AA. Proton NMR chemical shifts and coupling constants for brain metabolites. NMR Biomed. 2000;13(3):129-53.

188. Gharibani PM, Modi J, Pan C, Menzie J, Ma Z, Chen PC, et al. The mechanism of taurine protection against endoplasmic reticulum stress in an animal stroke model of cerebral artery occlusion and stroke-related conditions in primary neuronal cell culture. Adv Exp Med Biol. 2013;776:241-58.

189. Louzada PR, Paula Lima AC, Mendonca-Silva DL, Noel F, De Mello FG, Ferreira ST. Taurine prevents the neurotoxicity of beta-amyloid and glutamate receptor agonists: activation of GABA receptors and possible implications for Alzheimer's disease and other neurological disorders. FASEB J. 2004;18(3):511-8.

190. Parnetti L, Tarducci R, Presciutti O, Lowenthal DT, Pippi M, Palumbo B, et al. Proton magnetic resonance spectroscopy can differentiate Alzheimer's disease from normal aging. Mech Ageing Dev. 1997;97(1):9-14.

191. Kantarci K. 1H magnetic resonance spectroscopy in dementia. The British journal of radiology. 2007;80 Spec No 2:S146-52.

192. Shinno H, Inagaki T, Miyaoka T, Okazaki S, Kawamukai T, Utani E, et al. A decrease in N-acetylaspartate and an increase in myoinositol in the anterior cingulate gyrus are associated with behavioral and psychological symptoms in Alzheimer's disease. Journal of the neurological sciences. 2007;260(1-2):132-8.

193. Shiino A, Watanabe T, Shirakashi Y, Kotani E, Yoshimura M, Morikawa S, et al. The profile of hippocampal metabolites differs between Alzheimer's disease and subcortical ischemic vascular dementia, as measured by proton magnetic resonance spectroscopy. Journal of cerebral blood flow and metabolism : official journal of the International Society of Cerebral Blood Flow and Metabolism. 2012;32(5):805-15.

194. Foy CM, Daly EM, Glover A, O'Gorman R, Simmons A, Murphy DG, et al. Hippocampal proton MR spectroscopy in early Alzheimer's disease and mild cognitive impairment. Brain topography. 2011;24(3-4):316-22.

195. Rose SE, de Zubicaray GI, Wang D, Galloway GJ, Chalk JB, Eagle SC, et al. A 1H MRS study of probable Alzheimer's disease and normal aging: implications for longitudinal monitoring of dementia progression. Magn Reson Imaging. 1999;17(2):291-9.

196. Watanabe T, Shiino A, Akiguchi I. Absolute quantification in proton magnetic resonance spectroscopy is useful to differentiate amnesic mild cognitive impairment from Alzheimer's disease and healthy aging. Dementia and geriatric cognitive disorders. 2010;30(1):71-7.

197. Targosz-Gajniak MG, Siuda JS, Wicher MM, Banasik TJ, Bujak MA, Augusciak-Duma AM, et al. Magnetic resonance spectroscopy as a predictor of conversion of mild cognitive impairment to dementia. Journal of the neurological sciences. 2013;335(1-2):58-63.

198. Kantarci K, Petersen RC, Przybelski SA, Weigand SD, Shiung MM, Whitwell JL, et al. Hippocampal volumes, proton magnetic resonance spectroscopy metabolites, and cerebrovascular disease in mild cognitive impairment subtypes. Archives of neurology. 2008;65(12):1621-8.

199. Hattori N, Abe K, Sakoda S, Sawada T. Proton MR spectroscopic study at 3 Tesla on glutamate/glutamine in Alzheimer's disease. Neuroreport. 2002;13(1):183-6.

200. Griffith HR, den Hollander JA, Okonkwo OC, O'Brien T, Watts RL, Marson DC. Brain metabolism differs in Alzheimer's disease and Parkinson's disease dementia. Alzheimers Dement. 2008;4(6):421-7.

201. Marjanska M, Curran GL, Wengenack TM, Henry PG, Bliss RL, Poduslo JF, et al. Monitoring disease progression in transgenic mouse models of Alzheimer's disease with proton magnetic resonance spectroscopy. Proceedings of the National Academy of Sciences of the United States of America. 2005;102(33):11906-10.

202. Jack CR, Jr., Marjanska M, Wengenack TM, Reyes DA, Curran GL, Lin J, et al. Magnetic resonance imaging of Alzheimer's pathology in the brains of living transgenic mice: a new tool in Alzheimer's disease research. The Neuroscientist : a review journal bringing neurobiology, neurology and psychiatry. 2007;13(1):38-48.

203. Chen SQ, Cai Q, Shen YY, Wang PJ, Teng GJ, Zhang W, et al. Age-related changes in brain metabolites and cognitive function in APP/PS1 transgenic mice. Behav Brain Res. 2012;235(1):1-6.

204. Oberg J, Spenger C, Wang FH, Andersson A, Westman E, Skoglund P, et al. Age related changes in brain metabolites observed by 1H MRS in APP/PS1 mice. Neurobiology of aging. 2008;29(9):1423-33.

205. Chen SQ, Wang PJ, Ten GJ, Zhan W, Li MH, Zang FC. Role of myo-inositol by magnetic resonance spectroscopy in early diagnosis of Alzheimer's disease in APP/PS1 transgenic mice. Dementia and geriatric cognitive disorders. 2009;28(6):558-66.

206. Jansen D, Zerbi V, Janssen CI, Dederen PJ, Mutsaers MP, Hafkemeijer A, et al. A longitudinal study of cognition, proton MR spectroscopy and synaptic and neuronal pathology in aging wild-type and AbetaPPswe-PS1dE9 mice. PloS one. 2013;8(5):e63643.

207. Xu W, Zhan Y, Huang W, Wang X, Zhang S, Lei H. Reduction of hippocampal N-acetyl aspartate level in aged APP(Swe)/PS1(dE9) transgenic mice is associated with degeneration of CA3 pyramidal neurons. Journal of neuroscience research. 2010;88(14):3155-60.

208. von Kienlin M, Kunnecke B, Metzger F, Steiner G, Richards JG, Ozmen L, et al. Altered metabolic profile in the frontal cortex of PS2APP transgenic mice, monitored throughout their life span. Neurobiology of disease. 2005;18(1):32-9.

209. Dedeoglu A, Choi JK, Cormier K, Kowall NW, Jenkins BG. Magnetic resonance spectroscopic analysis of Alzheimer's disease mouse brain that express mutant human APP shows altered neurochemical profile. Brain research. 2004;1012(1-2):60-5.

210. Forster D, Davies K, Williams S. Magnetic resonance spectroscopy in vivo of neurochemicals in a transgenic model of Alzheimer's disease: a longitudinal study of metabolites, relaxation time, and behavioral analysis in TASTPM and wild-type mice. Magnetic resonance in medicine : official journal of the Society of Magnetic Resonance in Medicine / Society of Magnetic Resonance in Medicine. 2013;69(4):944-55.

211. Yang D, Xie Z, Stephenson D, Morton D, Hicks CD, Brown TM, et al. Volumetric MRI and MRS provide sensitive measures of Alzheimer's disease neuropathology in inducible Tau transgenic mice (rTg4510). NeuroImage. 2011;54(4):2652-8.

212. Forster DM, James MF, Williams SR. Effects of Alzheimer's disease transgenes on neurochemical expression in the mouse brain determined by (1)H MRS in vitro. NMR in biomedicine. 2011;25(1):52-8.

213. Esteras N, Alquezar C, Bartolome F, Antequera D, Barrios L, Carro E, et al. Systematic evaluation of magnetic resonance imaging and spectroscopy techniques for imaging a transgenic model of Alzheimer's disease (AbetaPP/PS1). Journal of Alzheimer's disease : JAD. 2012;30(2):337-53.

214. Marjanska M, Weigand SD, Preboske G, Wengenack TM, Chamberlain R, Curran GL, et al. Treatment effects in a transgenic mouse model of Alzheimer's disease: a magnetic resonance spectroscopy study after passive immunization. Neuroscience. 2014;259:94-100.

215. Choi JK, Carreras I, Aytan N, Jenkins-Sahlin E, Dedeoglu A, Jenkins BG. The effects of aging, housing and ibuprofen treatment on brain neurochemistry in a triple transgene Alzheimer's disease mouse model using magnetic resonance spectroscopy and imaging. Brain research. 2014;1590:85-96.

216. Choi JK, Jenkins BG, Carreras I, Kaymakcalan S, Cormier K, Kowall NW, et al. Anti-inflammatory treatment in AD mice protects against neuronal pathology. Experimental neurology. 2010;223(2):377-84.

217. Mhatre SD, Tsai CA, Rubin AJ, James ML, Andreasson KI. Microglial malfunction: the third rail in the development of Alzheimer's disease. Trends Neurosci. 2015;38(10):621-36.

218. Halliday G, Robinson SR, Shepherd C, Kril J. Alzheimer's disease and inflammation: a review of cellular and therapeutic mechanisms. Clin Exp Pharmacol Physiol. 2000;27(1-2):1-8.

219. Haga S, Akai K, Ishii T. Demonstration of microglial cells in and around senile (neuritic) plaques in the Alzheimer brain. An immunohistochemical study using a novel monoclonal antibody. Acta Neuropath. 1989;77(6):569-75.

220. Varnum MM, Ikezu T. The classification of microglial activation phenotypes on neurodegeneration and regeneration in Alzheimer's disease brain. Archivum immunologiae et therapiae experimentalis. 2012;60(4):251-66.

221. Swardfager W, Lanctot K, Rothenburg L, Wong A, Cappell J, Herrmann N. A meta-analysis of cytokines in Alzheimer's disease. Biological psychiatry. 2010;68(10):930-41.

222. Westin K, Buchhave P, Nielsen H, Minthon L, Janciauskiene S, Hansson O. CCL2 is associated with a faster rate of cognitive decline during early stages of Alzheimer's disease. PloS one. 2012;7(1):e30525.

223. Song C, Zhang Y, Dong Y. Acute and subacute IL-1beta administrations differentially modulate neuroimmune and neurotrophic systems: possible implications for neuroprotection and neurodegeneration. Journal of neuroinflammation. 2013;10:59.

224. Lee Y, Oliynyk S, Jung JC, Han JJ, Oh S. Administration of glucosylceramide ameliorated the memory impairment in aged mice. Evid Based Complement Alternat Med. 2013;2013:824120.

225. James ML, Fulton RR, Vercoullie J, Henderson DJ, Garreau L, Chalon S, et al. DPA-714, a new translocator protein-specific ligand: synthesis, radiofluorination, and pharmacologic characterization. Journal of nuclear medicine : official publication, Society of Nuclear Medicine. 2008;49(5):814-22.

226. Pardon MC, Yanez Lopez M, Yuchun D, Marjanska M, Prior M, Brignell C, et al. Magnetic Resonance Spectroscopy discriminates the response to microglial stimulation of wild type and Alzheimer's disease models. Sci Rep. 2016;6:19880.

227. Klunk WE, Panchalingam K, Moossy J, McClure RJ, Pettegrew JW. N-acetyl-L-aspartate and other amino acid metabolites in Alzheimer's disease brain: a preliminary proton nuclear magnetic resonance study. Neurology. 1992;42(8):1578-85.

228. Ennaceur A, Delacour J. A new one-trial test for neurobiological studies of memory in rats. 1: Behavioral data. Behav Brain Res. 1988;31(1):47-59.

229. Maroy R, Boisgard R, Comtat C, Frouin V, Cathier P, Duchesnay E, et al. Segmentation of rodent whole-body dynamic PET images: an unsupervised method based on voxel dynamics. IEEE Trans Med Imaging. 2008;27(3):342-54.

230. Maroy R, Boisgard R, Comtat C, Jego B, Fontyn Y, Jan S, et al. Quantitative organ time activity curve extraction from rodent PET images without anatomical prior. Med Phys. 2010;37(4):1507-17.

231. Johnson GA, Badea A, Brandenburg J, Cofer G, Fubara B, Liu S, et al. Waxholm space: an image-based reference for coordinating mouse brain research. NeuroImage. 2010;53(2):365-72.

232. Bottomley PA. Spatial localization in NMR spectroscopy in vivo. Ann N Y Acad Sci. 1987;508:333-48.

233. Gruetter R. Automatic, localized in vivo adjustment of all first- and second-order shim coils. Magnetic resonance in medicine : official journal of the Society of Magnetic Resonance in Medicine / Society of Magnetic Resonance in Medicine. 1993;29(6):804-11.

234. van den Boogaart A, van Ormondt D, Pijnappel WWF, de Beer R, Ala Korpel M. Removal of the residual water resonance from 1H magnetic resonance spectra. . Mathematics of Signal Processing III. 1994;Clarendon Press: Oxford:175-95.

235. Ratiney H, Sdika M, Coenradie Y, Cavassila S, van Ormondt D, Graveron-Demilly D. Time-domain semi-parametric estimation based on a metabolite basis set. NMR Biomed. 2005;18(1):1-13.

236. Nagakura A, Shitaka Y, Yarimizu J, Matsuoka N. Characterization of cognitive deficits in a transgenic mouse model of Alzheimer's disease and effects of donepezil and memantine. Eur J Pharmacol. 2013;703(1-3):53-61.

237. Kumar A, Muzik O, Shandal V, Chugani D, Chakraborty P, Chugani HT. Evaluation of age-related changes in translocator protein (TSPO) in human brain using (11)C-[R]-PK11195 PET. Journal of neuroinflammation. 2012;9:232.

238. Yokokura M, Terada T, Bunai T, Nakaizumi K, Takebayashi K, Iwata Y, et al. Depiction of microglial activation in aging and dementia: Positron emission tomography with [11C]DPA713 versus [11C](R)PK11195. Journal of cerebral blood flow and metabolism : official journal of the International Society of Cerebral Blood Flow and Metabolism. 2016.

239. Gulyas B, Vas A, Toth M, Takano A, Varrone A, Cselenyi Z, et al. Age and disease related changes in the translocator protein (TSPO) system in the human brain: positron emission tomography measurements with [11C]vinpocetine. NeuroImage. 2011;56(3):1111-21.

240. Forster DM, James MF, Williams SR. Effects of Alzheimer's disease transgenes on neurochemical expression in the mouse brain determined by (1)H MRS in vitro. NMR Biomed. 2012;25(1):52-8.

241. Kantarci K, Weigand SD, Petersen RC, Boeve BF, Knopman DS, Gunter J, et al. Longitudinal 1H MRS changes in mild cognitive impairment and Alzheimer's disease. Neurobiology of aging. 2007;28(9):1330-9.

242. van Groen T, Kiliaan AJ, Kadish I. Deposition of mouse amyloid beta in human APP/PS1 double and single AD model transgenic mice. Neurobiology of disease. 2006;23(3):653-62.

243. Turkheimer FE, Edison P, Pavese N, Roncaroli F, Anderson AN, Hammers A, et al. Reference and target region modeling of [11C]-(R)-PK11195 brain studies. Journal of nuclear medicine : official publication, Society of Nuclear Medicine. 2007;48(1):158-67.

244. Sturchler-Pierrat C, Staufenbiel M. Pathogenic mechanisms of Alzheimer's disease analyzed in the APP23 transgenic mouse model. Ann N Y Acad Sci. 2000;920:134-9.

245. Webster SJ, Bachstetter AD, Nelson PT, Schmitt FA, Van Eldik LJ. Using mice to model Alzheimer's dementia: an overview of the clinical disease and the preclinical behavioral changes in 10 mouse models. Front Genet. 2014;5:88.

246. Arendash GW, King DL, Gordon MN, Morgan D, Hatcher JM, Hope CE, et al. Progressive, age-related behavioral impairments in transgenic mice carrying both mutant amyloid precursor protein and presenilin-1 transgenes. Brain research. 2001;891(1-2):42-53.

247. Kurt MA, Davies DC, Kidd M, Duff K, Howlett DR. Hyperphosphorylated tau and paired helical filament-like structures in the brains of mice carrying mutant amyloid precursor protein and mutant presenilin-1 transgenes. Neurobiology of disease. 2003;14(1):89-97.

248. Radde R, Bolmont T, Kaeser SA, Coomaraswamy J, Lindau D, Stoltze L, et al. Abeta42-driven cerebral amyloidosis in transgenic mice reveals early and robust pathology. EMBO Rep. 2006;7(9):940-6.

249. Orgogozo JM, Gilman S, Dartigues JF, Laurent B, Puel M, Kirby LC, et al. Subacute meningoencephalitis in a subset of patients with AD after Abeta42 immunization. Neurology. 2003;61(1):46-54.

250. Flood DG, Lin YG, Lang DM, Trusko SP, Hirsch JD, Savage MJ, et al. A transgenic rat model of Alzheimer's disease with extracellular Abeta deposition. Neurobiology of aging. 2009;30(7):1078-90.

251. File SE, Hyde JR. Can social interaction be used to measure anxiety? Br J Pharmacol. 1978;62(1):19-24.

252. Schwarz AJ, Danckaert A, Reese T, Gozzi A, Paxinos G, Watson C, et al. A stereotaxic MRI template set for the rat brain with tissue class distribution maps and co-registered anatomical atlas: application to pharmacological MRI. NeuroImage. 2006;32(2):538-50.

253. Bert B, Fink H, Huston JP, Voits M. Fischer 344 and wistar rats differ in anxiety and habituation but not in water maze performance. Neurobiol Learn Mem. 2002;78(1):11-22.

254. Ramos A, Berton O, Mormede P, Chaouloff F. A multiple-test study of anxiety-related behaviours in six inbred rat strains. Behav Brain Res. 1997;85(1):57-69.

255. Ringman JM, Liang LJ, Zhou Y, Vangala S, Teng E, Kremen S, et al. Early behavioural changes in familial Alzheimer's disease in the Dominantly Inherited Alzheimer Network. Brain : a journal of neurology. 2015;138(Pt 4):1036-45.

256. Kreisl WC, Lyoo CH, Liow JS, Wei M, Snow J, Page E, et al. (11)C-PBR28 binding to translocator protein increases with progression of Alzheimer's disease. Neurobiology of aging. 2016;44:53-61.

257. Davies CA, Mann DM, Sumpter PQ, Yates PO. A quantitative morphometric analysis of the neuronal and synaptic content of the frontal and temporal cortex in patients with Alzheimer's disease. Journal of the neurological sciences. 1987;78(2):151-64.

258. Ishii M, Iadecola C. Metabolic and Non-Cognitive Manifestations of Alzheimer's Disease: The Hypothalamus as Both Culprit and Target of Pathology. Cell Metab. 2015;22(5):761-76.

259. Loskutova N, Honea RA, Brooks WM, Burns JM. Reduced limbic and hypothalamic volumes correlate with bone density in early Alzheimer's disease. Journal of Alzheimer's disease : JAD. 2010;20(1):313-22.

260. Baron JC, Chetelat G, Desgranges B, Perchey G, Landeau B, de la Sayette V, et al. In vivo mapping of gray matter loss with voxel-based morphometry in mild Alzheimer's disease. NeuroImage. 2001;14(2):298-309.

261. Cross DJ, Anzai Y, Petrie EC, Martin N, Richards TL, Maravilla KR, et al. Loss of olfactory tract integrity affects cortical metabolism in the brain and olfactory regions in aging and mild cognitive impairment. Journal of nuclear medicine : official publication, Society of Nuclear Medicine. 2013;54(8):1278-84.

262. Karas GB, Burton EJ, Rombouts SA, van Schijndel RA, O'Brien JT, Scheltens P, et al. A comprehensive study of gray matter loss in patients with Alzheimer's disease using optimized voxel-based morphometry. NeuroImage. 2003;18(4):895-907.

263. Perry VH, Cunningham C, Holmes C. Systemic infections and inflammation affect chronic neurodegeneration. Nature reviews Immunology. 2007;7(2):161-7.

264. Ray S, Britschgi M, Herbert C, Takeda-Uchimura Y, Boxer A, Blennow K, et al. Classification and prediction of clinical Alzheimer's diagnosis based on plasma signaling proteins. Nat Med. 2007;13(11):1359-62.

265. Marsland AL, Gianaros PJ, Abramowitch SM, Manuck SB, Hariri AR. Interleukin-6 covaries inversely with hippocampal grey matter volume in middle-aged adults. Biological psychiatry. 2008;64(6):484-90.

266. Cunningham C, Campion S, Lunnon K, Murray CL, Woods JF, Deacon RM, et al. Systemic inflammation induces acute behavioral and cognitive changes and accelerates neurodegenerative disease. Biological psychiatry. 2009;65(4):304-12.

267. Cunningham C, Wilcockson DC, Campion S, Lunnon K, Perry VH. Central and systemic endotoxin challenges exacerbate the local inflammatory response and increase neuronal death during chronic neurodegeneration. The Journal of neuroscience : the official journal of the Society for Neuroscience. 2005;25(40):9275-84.

268. Niraula A, Sheridan JF, Godbout JP. Microglia Priming with Aging and Stress. Neuropsychopharmacology. 2016.

269. Oliveria SA, Liperoti R, L'Italien G, Pugner K, Safferman A, Carson W, et al. Adverse events among nursing home residents with Alzheimer's disease and psychosis. Pharmacoepidemiol Drug Saf. 2006;15(11):763-74.

270. Natalwala A, Potluri R, Uppal H, Heun R. Reasons for hospital admissions in dementia patients in Birmingham, UK, during 2002-2007. Dementia and geriatric cognitive disorders. 2008;26(6):499-505.

271. McCusker RH, Kelley KW. Immune-neural connections: how the immune system's response to infectious agents influences behavior. J Exp Biol. 2013;216(Pt 1):84-98.

272. Dwarkasing JT, Marks DL, Witkamp RF, van Norren K. Hypothalamic inflammation and food intake regulation during chronic illness. Peptides. 2016;77:60-6.

273. Ding XQ, Maudsley AA, Sabati M, Sheriff S, Schmitz B, Schutze M, et al. Physiological neuronal decline in healthy aging human brain - An in vivo study with MRI and short echo-time whole-brain (1)H MR spectroscopic imaging. NeuroImage. 2016;137:45-51.

274. Yang ZY, Yue Q, Xing HY, Tan QY, Sun HQ, Gong QY, et al. A quantitative analysis of (1)H-MR spectroscopy at 3.0 T of three brain regions from childhood to middle age. The British journal of radiology. 2015;88(1052):20140693.

275. Angelie E, Bonmartin A, Boudraa A, Gonnaud PM, Mallet JJ, Sappey-Marinier D. Regional differences and metabolic changes in normal aging of the human brain: proton MR spectroscopic imaging study. AJNR Am J Neuroradiol. 2001;22(1):119-27.

276. Voevodskaya O, Sundgren PC, Strandberg O, Zetterberg H, Minthon L, Blennow K, et al. Myo-inositol changes precede amyloid pathology and relate to APOE genotype in Alzheimer disease. Neurology. 2016;86(19):1754-61.

277. McLaurin J, Golomb R, Jurewicz A, Antel JP, Fraser PE. Inositol stereoisomers stabilize an oligomeric aggregate of Alzheimer amyloid beta peptide and inhibit abeta -induced toxicity. J Biol Chem. 2000;275(24):18495-502.

278. Shonk T, Ross BD. Role of increased cerebral myo-inositol in the dementia of Down syndrome. Magnetic resonance in medicine : official journal of the Society of Magnetic Resonance in Medicine / Society of Magnetic Resonance in Medicine. 1995;33(6):858-61.

279. Huang W, Alexander GE, Daly EM, Shetty HU, Krasuski JS, Rapoport SI, et al. High brain myo-inositol levels in the predementia phase of Alzheimer's disease in adults with Down's syndrome: a 1H MRS study. Am J Psychiatry. 1999;156(12):1879-86.

280. Beacher F, Simmons A, Daly E, Prasher V, Adams C, Margallo-Lana ML, et al. Hippocampal myo-inositol and cognitive ability in adults with Down syndrome: an in vivo proton magnetic resonance spectroscopy study. Arch Gen Psychiatry. 2005;62(12):1360-5.

281. Pomara N, Greenberg WM, Branford MD, Doraiswamy PM. Therapeutic implications of HPA axis abnormalities in Alzheimer's disease: review and update. Psychopharmacol Bull. 2003;37(2):120-34.

282. Paxinos G, Franklin KBJ. The Mouse Brain in Stereotaxic Coordinates. Elsevier Academic Press. 2001;2nd Edition.

283. Paxinos. G, C W. Paxinos and Watson's The Rat Brain in Stereotaxic Coordinates,. Elsevier Academic Press. 2014;7th Edition.